The Dissertation Committee for Ran Cheng
certifies that this is the approved version of the following dissertation:

Aspects of Antiferromagnetic Spintronics

Committee:

Qian Niu, Supervisor

Gregory A. Fiete, Co-supervisor

Linda Reichl

Lorenzo A. Sadun

Allan H. MacDonald

Maxim Tsoi

Aspects of Antiferromagnetic Spintronics

by

Ran Cheng, B.S.

DISSERTATION

Presented to the Faculty of the Graduate School of

The University of Texas at Austin

in Partial Fulfillment

of the Requirements

for the Degree of

DOCTOR OF PHILOSOPHY

THE UNIVERSITY OF TEXAS AT AUSTIN

August 2014

Dedicated to those who had sacrificed their lives for the dignity of human being, the world peace, and the pursuit of truth.

Acknowledgments

Over the years of my pursuit of physics, I have been fortunate enough to be inspired by so many talented mentors. Their valuable guidance on both my career and life could never be overemphasized. Of all of those whom I indebted to, I especially wish to thank my advisor, Professor Qian Niu. He is always nice to everyone including me even I came up with a silly question. At Austin and overseas, discussion with Qian is quite enjoyable, relax, and on a walk-in base. Although rumor says that Qian's group is sort of paper machine, I never have such feeling. Instead, I always feel the opposite. He is more than stringent on every detail, and never allow me to swallow any fancy idea without a careful practice. I had spent three years on my first paper, during which Qian had helped me overcoming numerous critical moments. Being a student of Qian's group is not just a luck, but is something I really take pride of. Probably as all former members of this group may experienced, I have developed the "Niu-style" over constant inquiries, which offers a subtle joy that has no substitute.

Until 2012, I was not quite familiar with spintronics, it was Arne Brataas and Jiang Xiao who guided me through. I would say that they are my co-supervisors. Jiang and I collaborated on the spin pumping project for one year, during which I have received very detailed guidance in the calculation-

s, which would otherwise be impossible from an advisor. I met Arne on the Newspin2 conference at TAMU, he invited me to visit his group about one year after, which marked the waypoint of my graduate research. In the following months after the visit with Arne, I had been exposed to many cutting-edge studies in the community. Among those, what deserves special mentioning is the visit to Japan, where I had made crucial discussions with Sadamichi Maekawa, Gerrit Bauer, Eiji Saitoh, and Teruo Ono.

During the first two years of my graduate study, Professor Gregory A. Fiete had played a crucial role in teaching me many of the modern issues of condensed matter physics, especially the topological properties of strongly correlated systems. The nonlinear sigma model used in the dissertation is one of the those critical knowledge harvested from his class.

During my early days of academic life, Biao Wu and Ying Wu had propelled me a lot. Without their kind help, I would have no chance to be admitted to the University of Texas at Austin and every exciting moment afterwards would be impossible.

I acknowledge great helps and discussions with the Cologne group led by Achim Rosch, where I had a short but impressive stay and received warm reception by the Sitte's family and Robert Bamler. Karin Everschor-Sitte has given many detailed suggestions on my first project.

I am grateful to my colleague Xiao Li, who has shared office and apartment with me for many years. We had collaborated during early years but

unfortunately the work failed to be published at the end. It was probably for this reason that we finally choose different research topics. Everett Y. You is the very genius who inspires me continuously in condensed matter physics, he is always knowledgeable enough to give pertinent and insightful comments on any question I asked, even when the problem is out of his field.

With gratefulness, I would like to thank my great course instructors for educating me the laws of physics. Among them I especially acknowledge important discussions with Linda Reichl, Gennady Shvets, and Allan H. MacDonald. Linda had offered me a real rewarding class on statistical mechanics, Gennady had supervised me on a research-level project, and Allan had given many valuable advices on my research. During my final year, Maxim Tsoi has provided substantial advice on my research from an experimentalist's view.

Last but not the least, I acknowledge fruitful discussions with Erlend Tveten, Alireza Qaiumzadeh, Oleg Tretiakov, Jun'ichi Ieda, Mamoru Matsuo, Nato Nagaosa, Clement Wong, Yaroslav Tserkovnyak, and Mark Stiles during my travels outside Austin. I also thank important discussions, either formally or informally, with Di Xiao, Cheng Wang, Shengyuan Yang, Yang Gao, Bangguo Xiong, Zhenhua Qiao, Jimmy Zhu, and Lifa Zhang.

Aspects of Antiferromagnetic Spintronics

Publication No. _____

Ran Cheng, Ph.D.
The University of Texas at Austin, 2014

Supervisor: Qian Niu, Co-supervisor: Gregory A. Fiete

Spintronics is the study of mutual dependence of magnetization and electron transport, which forms a complementary picture in ferromagnetic (FM) materials. Recently, spintronics based on antiferromagnetic (AF) materials has been suggested. However, a systematic study is not yet available, and a complementary picture of the AF dynamics with electron transport is highly desired. By developing a microscopic theory, we predict the occurrence of spintronic phenomena both in bulk AF texture and on the interface of AF with normal metals. For the bulk, we find that the electron dynamics becomes adiabatic when the local staggered field is varying slowly over space and time, by which the spin-motive force and the reactive spin-transfer torque (STT) are derived as reciprocal effects. While the former generates a pure spin voltage across the texture, the latter can be used to drive AF domain wall and trigger spin wave excitation with lower current densities compared to FM materials. For the interface, by calculating how electrons scatter off a normal metal -antiferromagnet heterostructure, we derive the pumped spin and staggered

spin currents in terms of the staggered order parameter, the magnetization, and their rates of change; the reactions of an incident spin current on the antiferromagnet is derived as STTs. These effects are applicable to both compensated and uncompensated interfaces with a similar order of magnitude. In contrast to FM materials, the direction of spin pumping is controlled by the circular polarization of driving microwave; and conversely, the chirality of AF spin wave is tunable by the direction of spin accumulation.

Table of Contents

List of Figures

List of Tables

Chapter 1

Introduction

1.1 Motivation and Outline

Spintronics is the study of mutual dependence of electron transport and magnetization dynamics, which initially stemmed from the field of magnetism and has evolved into a large area in condensed matter physics today. Studies on spintronics has stimulated numerous possibilities in device design and engineering, information science, nano-technology, and more importantly, the fundamental physics. Despite that conduction electrons and local magnetization are coupled through an exchange interaction, phenomena arising from this simple physics are yet manifold.

Nowadays, people have paid substantial amount of efforts on improving the functioning of magnetic materials targeting at a strong and robust control by electrical means. However, main stream studies all focus on ferromagnetic materials with non-zero macroscopic magnetization. Few attentions have been paid to its intimate counterpart – antiferromagnet, which admits vanishing magnetization where the magnetic ordering is characterized by the staggered field. For a long time, antiferromagnet plays merely a subsidiary role in magnetic materials, while its potential application has been overlooked. For

example, an antiferromagnetic layer is used to pin the ferromagnetic layer in a spin-valve unit, where it provides auxiliary support to the device but has no active role in information storage.

However, by a series of fundamental explorations, we claim that antiferromagnetic materials are not only useful in processing information (such as spin current generation), but also exhibit relatively easier control under current-induced torques compared to ferromagnet. At the very beginning, the story started from an effort to generalize the Berry phase physics that are well established in ferromagnetic metals to a more fancy version incorporating degenerate bands, namely, the non-Abelian Berry phase. While the initial motivation is pretty mathematical, successive discoveries with specific predictions have becoming the principle impetus for later investigations.

In this dissertation, I present a full story of the arduous yet rewarding ways towards antiferromagnetic spintronics. The dissertation naturally breaks up into two categories, the bulk spintronics and the interface spintronics. I am aiming at a complementary picture between electron transport (spin current) and the dynamics of the background staggered field. Chapter two and three are devoted to the two complementary aspects in the bulk, with the implicit assumption that the system is infinite. Chapter four and five, on the other hand, explore the two reciprocal processes on a normal metal/antiferromagnet heterostructure where only interfacial physics is considered. The entire topic of antiferromagnetic spintronics is concluded in Chapter six. A common thread of our discussion is *the Berry phase formalism within linear response*.

The following sections of the present chapter introduce some basic notions and necessary background required to understand the topics of the dissertation. Without sacrificing rigorousness, I will try to emphasis the physical picture and motivations more than mathematical tricks.

1.2 Magnetization Dynamics

The journey of spintronics starts from the magnetization dynamics. The ferromagnetic ordering is characterized by the magnetization $\boldsymbol{M}$, which consists of both local magnetic moments and itinerant electron spins. Well below the Curie temperature, fluctuations of $\boldsymbol{M}$ is negligible and we are able to describe its dynamics by a classical equation known as the Landau-Lifshitz Equation [60] that can be written simply as

$$\frac{\partial \boldsymbol{M}}{\partial t} = \gamma \boldsymbol{H}_{_{eff}} \times \boldsymbol{M}, \tag{1.1}$$

where γ is the gyro-magnetic ratio, and $\boldsymbol{H}_{_{eff}}$ is the *effective* magnetic field including the external magnetic field, the exchange field, the anisotropy, and the demagnetization. Eq. (1.1) is just the macroscopic version of the Bloch equation for a single spin. Besides a precession about the effective field, it can hardly provide much further information.

Interesting physics steps in when the damping effect is taken into account. Regardless of the microscopic mechanism, the damping effect always drag the precessing magnetization towards its equilibrium position, *i.e.*, the direction of the effective field. So in a phenomenological manner, we can write

down the modified version of Eq. (1.1) as

$$\frac{\partial \boldsymbol{M}}{\partial t} = \gamma \boldsymbol{H}_{_{eff}} \times \boldsymbol{M} + \frac{\alpha}{M_s} \boldsymbol{M} \times \frac{\partial \boldsymbol{M}}{\partial t}, \tag{1.2}$$

where α is a dimensionless constant that determines the strength of damping, and M_s is the saturation magnetization. At low temperatures, M_s is nearly constant thus only the orientation of $\boldsymbol{M}$ can change. Eq. (1.2) is usually known as the Landau-Lifshitz-Gilbert equation (LLG).

As most keen learners may quest, is it able to combine the $\frac{\partial \boldsymbol{M}}{\partial t}$ terms on both sides of Eq. (1.2) into a single term? Of course yes. By a straightforward manipulation, the LLG is recast into a more suggestive form

$$(1 + \frac{\alpha^2}{M_s^2}) \frac{\partial \boldsymbol{M}}{\partial t} = \gamma \boldsymbol{H}_{_{eff}} \times \boldsymbol{M} + \gamma \frac{\alpha}{M_s} \boldsymbol{M} \times (\boldsymbol{H}_{_{eff}} \times \boldsymbol{M}). \tag{1.3}$$

It is clear from the right hand side of Eq. (1.3) that the precessional torque and the damping torque are perpendicular to each other. Meanwhile, they are both linear in the effective field. When written in this way, the damping is known as the Landau-Lifshitz damping. Eq. (1.3) is particularly important in studying the linear response property of the magnetic system.

1.3 Path Integral and Spin Berry phase

Semi-classical dynamics is suffice to describe the itinerant and the localized electrons in a unified fashion, which will be characterized by a universal Lagrangian in the following sections. To this end, a crucial ingredient known as the Berry's phase is introduced in the path integral formalism.

1.3.1 Single Spin

As is well-known in ordinary quantum mechanics, the path integral is a weighted sum of all possible routes of quantum evolution in terms of the exponential of action. For spin dynamics, however, we need to define an unambiguous "path" before constructing path integral. Following references [3, 30,91], let us consider a spin-S representation of the SU(2) group. Denote $|0\rangle = |S, S\rangle$ as the state of highest possible spin projection along the quantization axis. Now define the state $|\boldsymbol{n}\rangle$ labeled by the unit vector $\boldsymbol{n}$ upon a unitary transformation from $|S, S\rangle$,

$$|\boldsymbol{n}\rangle = e^{i\theta(\boldsymbol{n}_0\times\boldsymbol{n})\cdot\boldsymbol{S}}|S, S\rangle, \tag{1.4}$$

where $\boldsymbol{n}_0$ is a unit vector along the quantization axis, θ is the co-latitude of $\boldsymbol{n}$, namely $\boldsymbol{n}_0 \cdot \boldsymbol{n} = \cos\theta$. And S_i (i=1,2,3) are the three generators of SU(2) in the spin-S representation; for $S = 1/2$, they are just Pauli matrices.

The state $|\boldsymbol{n}\rangle$ can be expanded in a complete basis of the spin-S irreducible representation $\{|S, M\rangle\}$, where M is an integer that $-S \leq M \leq S$ and labels the eigenvalue of S_3,

$$S_3|S, M\rangle = M|S, M\rangle, \tag{1.5a}$$

$$\boldsymbol{S}^2|S, M\rangle = S(S+1)|S, M\rangle. \tag{1.5b}$$

The expansion coefficients are the matrices $D^{(s)}(\boldsymbol{n})_{MS}$ defined by

$$|\boldsymbol{n}\rangle = \sum_{M=-S}^{S} D^{(s)}(\boldsymbol{n})_{MS}|S, M\rangle, \tag{1.6}$$

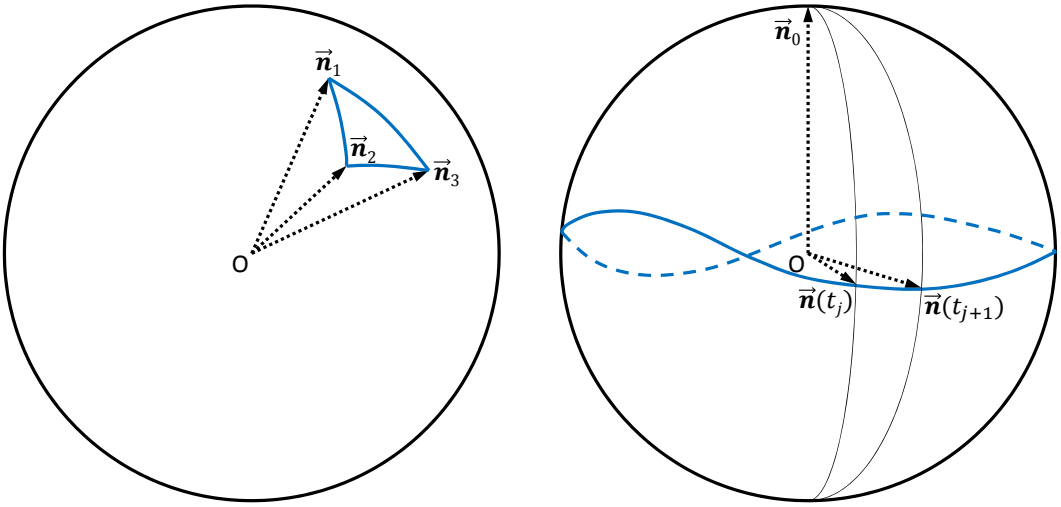

Figure 1.1: Left: the spherical triangle is constructed by connecting vertices at $\boldsymbol{n}_1$, $\boldsymbol{n}_2$, and $\boldsymbol{n}_3$ by great arcs. Right: a closed path is divided by N steps, with each single time slice defining a spherical triangle.

which do NOT form a group but respect the algebra

$$D^{(S)}(\boldsymbol{n}_1)D^{(S)}(\boldsymbol{n}_2) = D^{(S)}(\boldsymbol{n}_3)e^{i\Phi(\boldsymbol{n}_1,\boldsymbol{n}_2,\boldsymbol{n}_3)S_3}, \tag{1.7}$$

where $\boldsymbol{n}_1$, $\boldsymbol{n}_2$, and $\boldsymbol{n}_3$ are three arbitrary unit vectors on the unit sphere. And $\Phi(\boldsymbol{n}_1, \boldsymbol{n}_2, \boldsymbol{n}_3)$ is the area of the spherical triangle subtended by $\boldsymbol{n}_1$, $\boldsymbol{n}_2$, and $\boldsymbol{n}_3$, as shown in Fig. 1.1.

Since there is no distinction between interior and exterior of a closed path on the sphere (or closed manifold in general), the area of a spherical triangle is only determined up to a 4π ambiguity. Since the eigenvalues of S_3 equals M, which is either an integer or a half-integer, this phase ambiguity has no physical consequence since

$$e^{i4\pi M} = 1, \quad \text{regardless of } M. \tag{1.8}$$

The inner product of two spin coherent states $|\boldsymbol{n}_1\rangle$ and $|\boldsymbol{n}_2\rangle$ is

$$\begin{aligned}\langle \boldsymbol{n}_1|\boldsymbol{n}_2\rangle &= \langle 0|D^{(S)\dagger}(\boldsymbol{n}_1)D^{(S)}(\boldsymbol{n}_2)|0\rangle \\ &= e^{i\Phi(\boldsymbol{n}_1,\boldsymbol{n_2},\boldsymbol{n}_0)S}\left[\frac{1+\boldsymbol{n}_1\cdot\boldsymbol{n}_2}{2}\right]^S,\end{aligned} \tag{1.9}$$

and the diagonal elements of the SU(2) generators $\boldsymbol{S}$ is $\langle \boldsymbol{n}|\boldsymbol{S}|\boldsymbol{n}\rangle = S\boldsymbol{n}$. Now we resort to the path integral in the imaginary time; the evolution operator is denoted by $Z = \mathrm{tr}e^{iHT} = \mathrm{tr}e^{-\beta H}$, where T is the period of evolution. We split the imaginary time by N slices that $\beta = N\delta t$. As $N \to \infty$ ($\delta t \to 0$), the exponentiated operators at adjacent times become commutative, so

$$Z = \mathrm{tr}e^{-\beta H} = \lim_{N\to\infty}[e^{-\delta t H}]^N. \tag{1.10}$$

Now insert a bunch of resolution of identity

$$\hat{I} = \int d\mu(\boldsymbol{n})|\boldsymbol{n}\rangle\langle\boldsymbol{n}|, \tag{1.11}$$

$$d\mu(\boldsymbol{n}) = \left(\frac{2S+1}{4\pi}\right)d^3\boldsymbol{n}\delta(\boldsymbol{n}^2-1), \tag{1.12}$$

between each adjacent time step, we obtain

$$\begin{aligned}Z &= \lim_{N\to\infty}\left(\prod_{j=1}^{N}\int d\mu(\boldsymbol{n}_j)\right)\left(\prod_{j=1}^{N}\langle\boldsymbol{n}(t_j)|e^{-\delta t H}|\boldsymbol{n}(t_{j+1})\rangle\right) \\ &= \lim_{N\to\infty}\left(\prod_{j=1}^{N}\int d\mu(\boldsymbol{n}_j)\right)\left(\prod_{j=1}^{N}[\langle\boldsymbol{n}(t_j)|\boldsymbol{n}(t_{j+1})\rangle - \delta t\langle\boldsymbol{n}(t_j)|H|\boldsymbol{n}(t_{j+1})\rangle]\right),\end{aligned} \tag{1.13}$$

and $\boldsymbol{n}(t_0) = \boldsymbol{n}(t_{N+1})$ is assumed to close the path on the sphere. By virtue of Eq. (1.9), we know

$$\langle\boldsymbol{n}(t_j)|\boldsymbol{n}(t_{j+1})\rangle = e^{i\Phi(\boldsymbol{n}(t_j),\boldsymbol{n}(t_{j+1}),\boldsymbol{n}_0)S}\left[\frac{1+\boldsymbol{n}(t_j)\cdot\boldsymbol{n}(t_{j+1})}{2}\right]^S, \tag{1.14}$$

and to the lowest order in δt, we have

$$\frac{\langle \boldsymbol{n}(t_j)|H|\boldsymbol{n}(t_{j+1})\rangle}{\langle \boldsymbol{n}(t_j)|\boldsymbol{n}(t_{j+1})\rangle} = \langle \boldsymbol{n}(t_j)|H|\boldsymbol{n}(t_j)\rangle + \mathcal{O}(\delta t). \tag{1.15}$$

By inserting Eq. (1.14) and (1.15) into Eq. (1.13), we obtain the path integral formally as

$$Z = \lim_{N\to\infty} \int \mathcal{D}\boldsymbol{n} e^{-S_E[\boldsymbol{n}]}, \tag{1.16}$$

where $\mathcal{D}\boldsymbol{n} = \prod_{j=1}^{N} d\mu(\boldsymbol{n}(t_j))$ and the effective action is

$$S_E[\boldsymbol{n}] = -iS\sum_{j=1}^{N} \Phi(\boldsymbol{n}(t_j), \boldsymbol{n}(t_{j+1}), \boldsymbol{n}_0) - S\sum_{j=1}^{N} \ln\left[\frac{1+\boldsymbol{n}(t_j)\cdot\boldsymbol{n}(t_{j+1})}{2}\right] + \sum_{j=1}^{N}\langle \boldsymbol{n}(t_j)|H|\boldsymbol{n}(t_j)\rangle. \tag{1.17}$$

The first term of Eq. (1.17) leads to a sum over possible trajectories weighted by the phase factor $e^{iS\mathcal{A}[\boldsymbol{n}]}$, where

$$\mathcal{A}[\boldsymbol{n}] = \lim_{N\to\infty} \sum_{j=1}^{N} \Phi(\boldsymbol{n}(t_j), \boldsymbol{n}(t_{j+1}), \boldsymbol{n}_0) \tag{1.18}$$

is the area of the spherical triangle depicted in the right panel of Fig. 1.1. A way to express the area in terms of $\boldsymbol{n}$ requires a special mathematical trick where the path $\boldsymbol{n}(t)$ is *continuously* but *arbitrarily* mapped to a series of paths by $\boldsymbol{n}(t) \mapsto \boldsymbol{n}(t,\tau)$. As illustrated by Fig. 1.2, when the parameter τ varies from 0 to 1, the path deforms continuously from the real path to the north pole, *i.e.*, $\boldsymbol{n}(t,0) = \boldsymbol{n}(t)$ and $\boldsymbol{n}(t,1) = \boldsymbol{n}_0$. For any $0 < \tau < 1$, the deformed path satisfies the closed path condition that $\boldsymbol{n}(0,\tau) = \boldsymbol{n}(\beta,\tau)$. Due to the

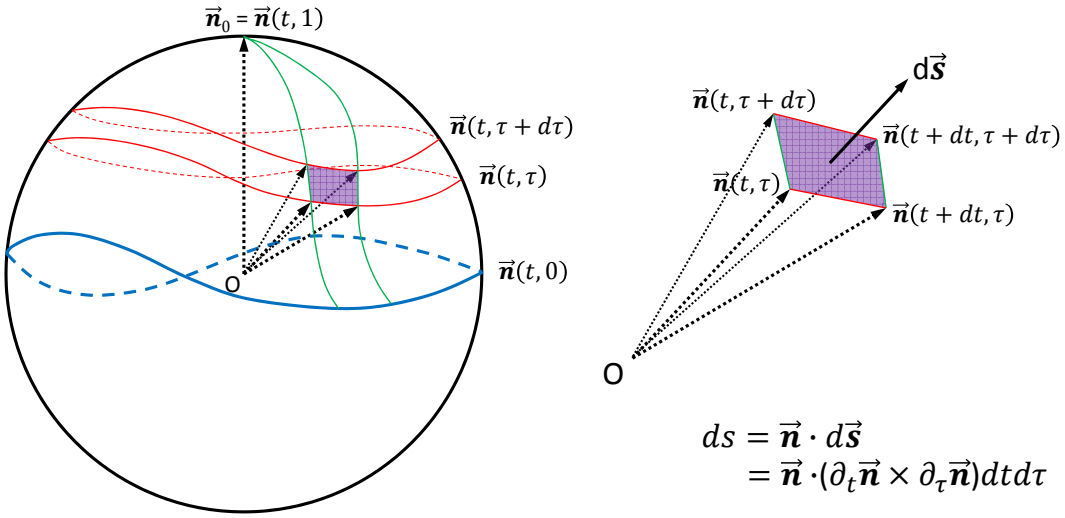

Figure 1.2: $\boldsymbol{n}(t)$ with $t \in [0, \beta]$ defines a closed path (blue curve) on the sphere. $\tau \in [0, 1]$ maps the path continuous towards the north pole (red curves) with $\boldsymbol{n}(t, 0) = \boldsymbol{n}(t)$ and $\boldsymbol{n}(t, 1) = \boldsymbol{n}_0$. For $\forall\tau$, $\boldsymbol{n}(0, \tau) = \boldsymbol{n}(\beta, \tau)$. Grids are formed by varying both t and τ, which defines the differential area ds.

arbitrariness of the mapping, curves of equal-t and equal-τ are not orthogonal, thus the differential area is expressed by the mixed product

$$ds = \boldsymbol{n} \cdot (\partial_t \boldsymbol{n} \times \partial_\tau \boldsymbol{n}) dt d\tau, \tag{1.19}$$

which is pictures in Fig. 1.2. Consequently, the area on the sphere enclosed by the path becomes

$$\mathcal{A}[\boldsymbol{n}] = \int_0^1 d\tau \int_0^\beta dt \boldsymbol{n}(t,\tau) \cdot [\partial_t \boldsymbol{n}(t,\tau) \times \partial_\tau \boldsymbol{n}(t,\tau)] \equiv \mathcal{S}_{WZ}[\boldsymbol{n}], \tag{1.20}$$

which is known as the Wess-Zumino term or spin Berry phase. It worths emphasizing that the area is subject to a 4π ambiguity, which has no physical consequence. Specifically, if we choose the lower cap of the path with the south pole, it works as well in defining the effective action.

By taking the continuum limit $N \to \infty$, the final form of the effective action in the imaginary time representation is written as

$$S_E[\boldsymbol{n}] = -iS\mathcal{S}_{WZ}[\boldsymbol{n}] + \frac{S\delta t}{4}\int_0^\beta dt|\partial_t \boldsymbol{n}(t)|^2 + \int_0^\beta H(t), \tag{1.21}$$

where $H(t) = \langle \boldsymbol{n}(t)|H|\boldsymbol{n}(t)\rangle$. The second term of Eq. (1.21) amounts to a small mass of a particle moving on a sphere. However, it vanishes as $\delta t \to 0$, and we will ignore it in the following discussions.

1.3.2 Many Spin Systems

It is a simple but non-trivial generalization of the spin path integral from single spin to multiple spin systems. Assume that spins are interacting through the Heisenberg Hamiltonian

$$H = J\sum_{<\boldsymbol{r},\boldsymbol{r}'>} \boldsymbol{S}(\boldsymbol{r})\cdot\boldsymbol{S}(\boldsymbol{r}'), \tag{1.22}$$

where $< ... >$ implies summation over nearest neighboring sites. Now turn back to the real time representation with $t \to it$ and $\beta \to iT$, we obtain the path integral $Z = \int \mathcal{D}\boldsymbol{n} e^{iS_M[\boldsymbol{n}]}$ with the action

$$S_M[\boldsymbol{n}] = S\sum_{\boldsymbol{r}} \mathcal{S}_{WZ}[\boldsymbol{n}(\boldsymbol{r})] - JS^2\int_0^T dt \sum_{<\boldsymbol{r},\boldsymbol{r}'>} \boldsymbol{n}(\boldsymbol{r},t)\cdot\boldsymbol{n}(\boldsymbol{r}',t). \tag{1.23}$$

This action can describe both ferromagnetic and antiferromagnetic systems according to the sign of J. Setting the variational derivative of the action to zero, *i.e.*, $\delta_{\boldsymbol{n}} S_M[\boldsymbol{n}] = 0$, gives the local dynamics of the system, which is the basic tool we will adopt in the next two chapters. Especially, the variation of

the Wess-Zumino (or Berry phase) term can be extracted out from Eq. (1.20),

$$\delta \mathcal{S}_{WZ}[\boldsymbol{n}] = \delta \boldsymbol{n} \cdot (\boldsymbol{n} \times \partial_t \boldsymbol{n}), \tag{1.24}$$

where the functional variation is fulfilled by the deformation along τ in the neighborhood of the given path $\boldsymbol{n}(t)$.

1.4 Effective Lagrangian

In the preceding section we have formulated the magnetization dynamics in terms of the path integral, at the heart of which is the effective Lagrangian as a functional of the order parameter. To describe the magnetization dynamics and the electron dynamics in a uniform fashion, we also need to characterize the conduction electrons by a proper Lagrangian. We first formulate in a purely general context the dynamics of a quantum system subjects to a time-dependent Hamiltonian that varies adiabatically. In the next section, the formalism is applied to obtain the semi-classical electron dynamics and is generalized to incorporate degenerate bands.

Consider a quantum Hamiltonian that depends on time through some parameter $H = H(\boldsymbol{r}(t))$. At each instant of time, the Hamiltonian fosters a complete set of eigenstates $\{|\psi_j(\boldsymbol{r}(t))\rangle\}$ that is also parametrically depends on $\boldsymbol{r}(t)$. Now the wave vector of the system is expanded by the eigenstates

$$|\Psi\rangle = \sum_j c_j |\psi_j(\boldsymbol{r}(t))\rangle, \tag{1.25}$$

where $c_j = |c_j| e^{i\theta_j}$ is complex and respects the normalization $\sum_j |c_j|^2 = 1$. The Schrödinger equation is equivalent to the variation over $|\Psi\rangle$ from the universal

Lagrangian $L = \langle\Psi|(i\partial_t - H)|\Psi\rangle$ ($\hbar = 1$). Insert Eq. (1.25) into the Lagrangian, and consider the orthogonal-normalization condition of eigenstates $\langle\psi_i(\boldsymbol{r}(t))|\psi_j(\boldsymbol{r}(t))\rangle = \delta_{ij}$ (for $\forall\ t$), we obtain

$$\begin{aligned} L =& \frac{1}{2} i\partial_t \left(\sum_j |c_j|^2 \right) - \sum_i |c_j|^2 \dot{\theta}_j \\ &+ i \sum_{ij} |c_i||c_j| e^{i(\theta_j - \theta_i)} \dot{\boldsymbol{r}} \cdot \langle\psi_i(\boldsymbol{r})|\boldsymbol{\nabla}\psi_j(\boldsymbol{r})\rangle - \sum_j |c_j|^2 E_j(\boldsymbol{r}), \end{aligned} \tag{1.26}$$

where $\boldsymbol{\nabla}$ is the gradient over $\boldsymbol{r}$, and $E_i(\boldsymbol{r})$ is defined by the eigen-equation

$$H(\boldsymbol{r})|\psi_j(\boldsymbol{r})\rangle = E_j(\boldsymbol{r})|\psi_j(\boldsymbol{r})\rangle. \tag{1.27}$$

The first term of Eq. (1.26) vanishes due to normalization. The third term is a little bit tricky. Assume that the eigenvalues $\{E_i\}$ are all non-degenerate, and $\boldsymbol{r}(t)$ changes with time sufficiently slowly, then the phase factor $e^{i(\theta_j - \theta_i)}$ for $i \neq j$ rotates on the complex plane by a large number of circles while $\langle\psi_i(\boldsymbol{r})|\nabla\psi_j(\boldsymbol{r})\rangle$ has only undergone a slight change. When we take a time average over one period of phase oscillation, all terms are nearly zero except the diagonal terms with $i = j$. Therefore, to the lowest order in the deviation due to the weak time dependence of $\boldsymbol{r}(t)$, we can keep only $i = j$ terms in the summation. This is known as the adiabatic approximation. Denote $I_j = |c_j|^2$, and define the Berry's connection on the j-th level as

$$\boldsymbol{\mathcal{A}}_j(\boldsymbol{r}) \equiv i\langle\psi_j(\boldsymbol{r})|\boldsymbol{\nabla}\psi_j(\boldsymbol{r})\rangle, \tag{1.28}$$

the adiabatic Lagrangian is written as

$$L = \sum_j I_j[-\dot{\theta}_j + \dot{\boldsymbol{r}} \cdot \boldsymbol{\mathcal{A}}_j(\boldsymbol{r}) - E_j(\boldsymbol{r})]. \tag{1.29}$$

Since the system is labeled by three set of parameters $\{I_j\}$, $\{\theta_j\}$ and $\boldsymbol{r} = \{R_1, R_2, \cdots\}$, the quantum evolution is described by the Euler-Lagrangian equations in terms of the three set of parameters, which can be directly obtained from Eq. (1.29). These equations of motion should be equivalent to the Schrödinger equation in the adiabatic limit.

(1) $\frac{\partial L}{\partial \theta_j} - \frac{\partial}{\partial t}\left(\frac{\partial L}{\partial \dot{\theta}_j}\right) = 0$ gives $\dot{I}_j = 0$ or I_j =constant, which means that the probability of the system to be in any eigenstate remains invariant. This is consistent with the adiabatic assumption.

(2) $\frac{\partial L}{\partial I_j} - \frac{\partial}{\partial t}\left(\frac{\partial L}{\partial \dot{I}_j}\right) = 0$ gives the dynamics of the phase angle

$$\dot{\theta}_j = \dot{\boldsymbol{r}} \cdot \boldsymbol{\mathcal{A}}_j(\boldsymbol{r}) - E_j(\boldsymbol{r}). \tag{1.30}$$

After integrated over time, Eq. (1.30) becomes

$$\theta_j(t) = \int d\boldsymbol{r} \cdot \boldsymbol{\mathcal{A}}_j(\boldsymbol{r}) - \int dt E_j(\boldsymbol{r}), \tag{1.31}$$

where we should note that dt has been canceled in the first term. Thus it only depends on the geometry of the path of $\boldsymbol{r}$ in the parameter space, but does not depend on the rate of change of $\boldsymbol{r}(t)$ at any instant of time. For a closed path C in the parameter space, this geometric term becomes

$$\oint_C d\boldsymbol{r} \cdot \boldsymbol{\mathcal{A}}_j(\boldsymbol{r}) = \iint_{\text{enclosure } C} d\boldsymbol{s} \cdot \boldsymbol{\nabla} \times \boldsymbol{\mathcal{A}}_j(\boldsymbol{r}) \tag{1.32}$$

by the Stokes' theorem. The curl $\boldsymbol{\mathcal{B}}_j(\boldsymbol{r}) = \boldsymbol{\nabla} \times \boldsymbol{\mathcal{A}}_j(\boldsymbol{r})$ is known as the Berry curvature, which amounts to a fictitious magnetic field in the parameter space. By straightforward algebra, it can be expressed as

$$\boldsymbol{\mathcal{B}}_j = \text{Im} \sum_{i \neq j} \frac{\langle \psi_j | \boldsymbol{\nabla} H | \psi_i \rangle \times \langle \psi_i | \boldsymbol{\nabla} H | \psi_j \rangle}{(E_i - E_j)^2}. \tag{1.33}$$

The flux of the magnetic field determines the geometric phase (or Berry's phase) of the system. Although the derivation up to now requires that the eigenstates are non-degenerate, a non-zero geometric phase usually originates from the magnetic flux of a fictitious monopole that locates at the degenerate point. What should be bear in mind is that the actual evolution of the system can never touch the degenerate point in order to respect the adiabatic approximation, but the degenerate point itself must exist somewhere in the parameter space.

(3) Before varying with respect to $\boldsymbol{r}$, the physical origin of $\boldsymbol{r}$ has to be resolved. This is often realized by the quantum-classical hybrid system [143] where $\boldsymbol{r}$ plays the role of classical position. For example, in the prototype Born-Oppenheimer problem, the mass of the nuclei far exceeds that of the electron, thus it is a good approximation to treat the nuclei motion as classical while keeping the quantum description of the electron dynamics. So the entire atom is regarded as a quantum-classical hybrid system, and $\boldsymbol{r}$ is the position of the nuclei. To this end, we need to add the kinetic term of the classical part to the Lagrangian: $L_{tot} = L + \frac{1}{2}M\dot{\boldsymbol{r}}^2$, where M represents the mass of the classical particle. Then $\frac{\partial L_{tot}}{\partial \boldsymbol{r}} - \frac{\partial}{\partial t}\left(\frac{\partial L_{tot}}{\partial \dot{\boldsymbol{r}}}\right) = 0$ gives

$$M\ddot{\boldsymbol{r}} = \dot{\boldsymbol{r}} \times \boldsymbol{\mathcal{B}}(\boldsymbol{r}) - \boldsymbol{\nabla} E(\boldsymbol{r}), \tag{1.34}$$

where $\boldsymbol{\mathcal{B}}(\boldsymbol{r}) = \sum_j I_j \boldsymbol{\mathcal{B}}_j(\boldsymbol{r})$ is the total (fictitious) magnetic field and $E(\boldsymbol{r}) = \sum_j I_j E_j(\boldsymbol{r})$ is the average energy of the system. The first term of Eq. (1.34) is a Lorentz force due to the magnetic field, which is known as the geometric

force. The second term of Eq. (1.34) is known as the Born-Oppenheimer force. They represent two different back-actions that the quantum subsystem exerts on the classical subsystem. Typically the former is much smaller than the latter and is often neglected. However, in the following discussions, the Born-Oppenheimer force is zero, thus the geometric force is crucial and is used to interpret the spin-transfer torques.

What has been demonstrated above is the simplest case of the adiabatic dynamics. If the Hamiltonian depends on time both through $\boldsymbol{r}(t)$ and explicitly, $H = H(t, \boldsymbol{r}(t))$, the eigenstate and eigenvalues are $|\psi_j(t, \boldsymbol{r}(t))\rangle$ and $E_j(t, \boldsymbol{r}(t))$, respectively. In this case, besides the vector potential defined in Eq. (1.28), we can also define a scalar potential

$$\phi_j(t, \boldsymbol{r}) \equiv i\langle\psi_j(t, \boldsymbol{r})|\partial_t\psi_j(t, \boldsymbol{r})\rangle, \tag{1.35}$$

which gives rise to an electric component to the Berry curvature

$$\boldsymbol{\mathcal{E}}(t, \boldsymbol{r}) = \partial_t\boldsymbol{\mathcal{A}}(t, \boldsymbol{r}) - \boldsymbol{\nabla}\phi(t, \boldsymbol{r}), \tag{1.36}$$

where $\phi(t, \boldsymbol{r}) = \sum_j I_j\phi_j(t, \boldsymbol{r})$ and $\boldsymbol{\mathcal{A}}(t, \boldsymbol{r}) = \sum_j I_j\boldsymbol{\mathcal{A}}_j(t, \boldsymbol{r})$. As a result, The dynamics of slow variables Eq. (1.34) becomes

$$M\ddot{\boldsymbol{r}} = \boldsymbol{\mathcal{E}}(t, \boldsymbol{r}) + \dot{\boldsymbol{r}} \times \boldsymbol{\mathcal{B}}(t, \boldsymbol{r}) - \boldsymbol{\nabla}E(t, \boldsymbol{r}). \tag{1.37}$$

As a matter of fact, the electric and magnetic fields can be recast in a unified description by virtue of the joint space-time coordinate $r_\mu \equiv (t, \boldsymbol{r})$ with $\mu = 0, 1, 2, 3, \cdots$. Regarding the effective speed of light as 1, the scalar and vector

potentials can be written in a single gauge potential $\mathcal{A}_\mu \equiv (\phi, \boldsymbol{\mathcal{A}})$, upon which we are able to define the electromagnetic field

$$\mathcal{F}_{\mu\nu} = \partial_\mu \mathcal{A}_\nu - \partial_\nu \mathcal{A}_\mu, \tag{1.38}$$

which is an antisymmetric tensor that $\mathcal{F}_{\mu\nu} = -\mathcal{F}_{\nu\mu}$.

The appearance of the artificial electromagnetic field in the parameter space can be easily understood in the language of gauge invariance. In the adiabatic approximation, the system does not make transitions between different energy levels, thus the dynamics refers only to the phase evolution of each individual eigenstates. As a result, an arbitrary phase change $|\psi_j\rangle \to e^{i\chi_j(r_\mu)}|\psi_j\rangle$ yields the effective Lagrangian

$$L = I_j[-\dot{\theta}_j + \dot{r}_\mu \mathcal{A}_\mu - E_j] \tag{1.39}$$

invariant, where summation over repeated indexes is implied from now on unless otherwise stated. This is known as the emergent $U(1)$ gauge invariance under the adiabatic approximation, which guarantees the appearance of the artificial electromagnetic field $\mathcal{F}_{\mu\nu}$ in the dynamics of slow variables, in exactly the same sense as how a charged particle is coupled to the real electromagnetic field. The Bianchi identity of the antisymmetric tensor $\mathcal{F}_{\mu\nu}$ requires $\varepsilon_{\alpha\lambda\mu\nu}\partial_\lambda \mathcal{F}_{\mu\nu} = 0$ for $\forall\alpha$. This leads to the Faraday's law

$$\boldsymbol{\nabla} \times \boldsymbol{\mathcal{E}} + \partial_t \boldsymbol{\mathcal{B}} = 0, \tag{1.40}$$

which has important consequences on the electron transport in ferromagnets.

A prototype example is an electron moving in a magnetization texture that varies slowly in space and time. With a sufficiently strong exchange coupling, the electron spin will be locked into the direction of the local magnetization $\boldsymbol{m}(t, \boldsymbol{r})$. The precession of the electron spin then gives rise to a geometric phase in space time, producing an effective electromagnetic field depending on the gradient and time derivative of the magnetization

$$\boldsymbol{\mathcal{E}} = \frac{1}{2}\boldsymbol{m} \cdot (\partial_t \boldsymbol{m} \times \boldsymbol{\nabla} \boldsymbol{m}) = \frac{1}{2} \sin\alpha (\partial_t \alpha \boldsymbol{\nabla} \beta - \boldsymbol{\nabla} \alpha \partial_t \beta), \tag{1.41}$$

$$\boldsymbol{\mathcal{B}} = -\frac{1}{4} \varepsilon_{ijk} m_i \boldsymbol{\nabla} m_j \times \boldsymbol{\nabla} m_k = -\frac{1}{2} \sin\alpha \boldsymbol{\nabla} \alpha \times \boldsymbol{\nabla} \beta, \tag{1.42}$$

where $\alpha(\boldsymbol{r}, t)$ and $\beta(\boldsymbol{r}, t)$ are spherical angles specifying the direction of $\boldsymbol{m}$,

$$\boldsymbol{m} = \{\sin\alpha\cos\beta, \sin\alpha\sin\beta, \cos\alpha\}. \tag{1.43}$$

Eq. (1.41) and (1.42) are not restricted to magnetic systems, they are applicable to the general case whenever the spin of a particle follows adiabatically the background order parameter.

1.5 Semi-classical Dynamics of Electrons

Due to the spin degree of freedom, electron transport in magnetic materials is affected significantly by the dynamically coupled bands. The main stream approach towards a general description of electrons in such context involves the non-equilibrium Green's function, the linear response theory, and the effective gauge theory. While the first two are more rigorous and depend only on minimal assumptions, the effective gauge theory, on the other hand,

provides prevailing physical insights and mathematical clarity. More importantly, it unveils the hidden structure of geometry and topology that would otherwise be elusive.

Construction of an effective gauge theory on an arbitrary magnetic material is difficult. Nevertheless, by generalizing the effective Lagrangian introduced in the previous section, a theory can well be formulated in two limiting cases: degenerate bands and well-separated bands. In the vast majority of magnetic materials, the situation falls in either of the two categories. By adding the electron Lagrangian to the (magnetic) background Lagrangian, we are able to describe their dynamics in a unified way.

1.5.1 Case I: Degenerate Bands

We adopt the semi-classical description of a single conduction electron, where it is described by a wave packet that compromises the quantum uncertainty in real and momentum spaces. This is done in order to take advantage of classical concepts such as position, momentum, velocity, etc.

The wave packet formalism becomes a good approximation when one band (or a group of degenerate sub-bands) is separated from other bands by large energy gaps and the external fields are weak [16, 17, 101, 133]. The wave packet is a coherent sum of all Bloch states of that particular band in the first Brillouin zone (BZ) through a weighting function $w(\boldsymbol{k})$:

$$|W\rangle = \int_{BZ} \mathrm{d}\boldsymbol{k} w(\boldsymbol{k}) |u_n(\boldsymbol{k})\rangle, \tag{1.44}$$

where $|u_n(\boldsymbol{k})\rangle$ is the periodic part of the Bloch wave in the n-th band. The weighting function $w(\boldsymbol{k})$ is chosen in a way that the wave function exhibits Gaussian profile in both the real and the momentum spaces

$$\int \mathrm{d}^3 r \boldsymbol{r} |\langle \boldsymbol{r}|W\rangle|^2 = \boldsymbol{r}_c, \quad \int \mathrm{d}^3 k \boldsymbol{k} |w(\boldsymbol{k})|^2 = \boldsymbol{k}_c, \tag{1.45}$$

$\boldsymbol{r}_c$ and $\boldsymbol{k}_c$ are the center-of-mass position and center-of-mass momentum, respectively. According to the adiabatic theorem, if the background order parameter varies slowly in time and smoothly in space, the electron bands are adjusted to the local environment and transitions out of the degenerate group only contribute fast rotating factors that are averaged to zero (c.f. Eq. (1.29)). Therefore, the wave vector can be expanded within the degenerate group. Denote the joint space-time coordinate as $r_\mu \equiv (t, \boldsymbol{r}_c)$, so that the local Bloch Hamiltonian is $\mathcal{H} = \mathcal{H}(r_\mu)$, and the periodic parts of Bloch wave vectors are labeled by $|u_n(r_\mu, \boldsymbol{k})\rangle$. Without loss of generality, we focus on a doubly degenerate band where the two sub-bands are represented by a and b,

$$|W\rangle = \int \mathrm{d}^3 k w(\boldsymbol{k})[c_a|u_a(r_\mu, \boldsymbol{k})\rangle + c_b|u_b(r_\mu, \boldsymbol{k})\rangle], \tag{1.46}$$

where c_a and c_b reflect relative contributions from the two sub-bands. We group the two coefficients into a column vector $\tilde{c} = [c_a, c_b]^T$, known as the isospinor. The normalization condition $|c_a|^2 + |c_b|^2 = 1$ becomes $\tilde{c}^\dagger \tilde{c} = 1$. Similar to the derivation of Eq. (1.29), the effective Lagrangian of the wave packet on the doubly degenerate band is obtained [22]

$$\begin{aligned} \mathcal{L} &= \mathcal{L}(r_\mu, k_\mu, \tilde{c};\ \dot{r}_\mu, \dot{k}_\mu, \dot{\tilde{c}}) = \langle W|(i\frac{\partial}{\partial t} - \mathcal{H})|W\rangle \\ &= \varepsilon + \boldsymbol{k}_c \cdot \dot{\boldsymbol{r}}_c + i\tilde{c}^\dagger \dot{\tilde{c}} + \tilde{c}^\dagger (A^r_\mu \dot{r}_\mu + A^k_\mu \dot{k}_\mu)\tilde{c}, \end{aligned} \tag{1.47}$$

where $k_\mu = (0, \boldsymbol{k}_c)$ has no temporal component in contrast to $r_\mu = (t, \boldsymbol{r}_c)$, but it is still written this way just to simplify symbols. Different from the non-degenerate case in Eq. (1.28), the Berry connections here are 2×2 matrices and are functions of both r_μ and k_μ. The real space components are

$$\begin{aligned} A^r_\mu &= i \begin{bmatrix} \langle u_a|\partial^r_\mu|u_a\rangle, & \langle u_a|\partial^r_\mu|u_b\rangle \\ \langle u_b|\partial^r_\mu|u_a\rangle, & \langle u_b|\partial^r_\mu|u_b\rangle \end{bmatrix} \\ &= \tau_1(\mathcal{A}^r_\mu)^1 + \tau_2(\mathcal{A}^r_\mu)^2 + \tau_3(\mathcal{A}^r_\mu)^3, \end{aligned} \tag{1.48}$$

where in the second equality the 2×2 has been decomposed by three Pauli matrices representing the isospin. The isospin vector $\boldsymbol{\tau} \equiv \{\tau_1, \tau_2, \tau_3\}$ should not be confused with the real spin vector $\boldsymbol{\sigma} = \{\sigma_x, \sigma_y, \sigma_z\}$. Similarly, the momentum space components are

$$A^k_\mu = i \begin{bmatrix} \langle u_a|\partial^k_\mu|u_a\rangle, & \langle u_a|\partial^k_\mu|u_b\rangle \\ \langle u_b|\partial^k_\mu|u_a\rangle, & \langle u_b|\partial^k_\mu|u_b\rangle \end{bmatrix}, \tag{1.49}$$

which in general should not vanish if spin-orbit coupling terms are added to the original Hamiltonian. In existing literatures [22, 23, 69, 72, 149], the Berry connections on degenerate energy levels are introduced in the Hamiltonian form, but here the Lagrangian form is used to search for a unified description for both the electron transport and the magnetization dynamics.

To avoid cumbersome matrix products in the the following discussions, we now define the isospin vector

$$\begin{aligned} \mathfrak{C} &= \{c_1, c_2, c_3\} = \tilde{c}^\dagger \boldsymbol{\tau} \tilde{c} \\ &= \{2\mathrm{Re}(c_a c_b^*), -2\mathrm{Im}(c_a c_b^*), |c_a|^2 - |c_b|^2\}, \end{aligned} \tag{1.50}$$

with which the Berry connection A^r_μ can be expressed as a vector in the isospin vector space (the adjoint representation),

$$\boldsymbol{\mathcal{A}}^r_\mu = \frac{1}{2}\mathrm{Tr}[\boldsymbol{\tau} A^r_\mu] = \{(\mathcal{A}^r_\mu)^1,\ (\mathcal{A}^r_\mu)^2,\ (\mathcal{A}^r_\mu)^3\}, \tag{1.51}$$

where we have used $\frac{1}{2}\mathrm{Tr}[\tau_i\tau_j] = \delta_{ij}$. In a similar way, $\boldsymbol{\mathcal{A}}^k_\mu = \frac{1}{2}\mathrm{Tr}[\boldsymbol{\tau} A^k_\mu] = \{(\mathcal{A}^k_\mu)^1,\ (\mathcal{A}^k_\mu)^2,\ (\mathcal{A}^k_\mu)^3\}$. Eq. (1.47) becomes

$$\mathcal{L} = \varepsilon + k_\mu \dot{r}_\mu + i\tilde{c}^\dagger\dot{\tilde{c}} + \boldsymbol{\mathcal{C}}\cdot[\boldsymbol{\mathcal{A}}^r_\mu \dot{r}_\mu + \boldsymbol{\mathcal{A}}^k_\mu \dot{k}_\mu], \tag{1.52}$$

where the $i\tilde{c}^\dagger\dot{\tilde{c}}$ term cannot be expressed in terms of $\boldsymbol{\mathcal{C}}$ and $\dot{\boldsymbol{\mathcal{C}}}$, but this poses no problem in the following. Both Eqs. (1.47) and (1.52) are useful forms of the effective Lagrangian, they are sometimes known as the fundamental and adjoint representations, respectively.

Within the semi-classical description, the state of a conduction electron is completely determined by three parameters $(\boldsymbol{\mathcal{C}}, r_\mu, k_\mu)$. Thus the electron dynamics is represented by the equations of motion of $(\boldsymbol{\mathcal{C}}, r_\mu, k_\mu)$, which can be obtained from the Euler-Lagrange equations:

(1) $\delta\mathcal{L}/\delta\tilde{c} = 0$ on Eq. (1.47) gives

$$\dot{\tilde{c}} = i[A^r_\mu \dot{r}_\mu + A^k_\mu \dot{k}_\mu]\tilde{c} \tag{1.53a}$$

$$\dot{\tilde{c}}^\dagger = -i\tilde{c}^\dagger[A^r_\mu \dot{r}_\mu + A^k_\mu \dot{k}_\mu] \tag{1.53b}$$

then from $\boldsymbol{\mathcal{C}} = \tilde{c}^\dagger\boldsymbol{\tau}\tilde{c}$ we have,

$$\begin{aligned}\dot{\boldsymbol{\mathcal{C}}} &= \dot{\tilde{c}}^\dagger\boldsymbol{\tau}\tilde{c} + \tilde{c}^\dagger\boldsymbol{\tau}\dot{\tilde{c}} \\ &= i\dot{r}_\mu\tilde{c}^\dagger[\boldsymbol{\tau}A^r_\mu - A^r_\mu\boldsymbol{\tau}]\tilde{c} + i\dot{k}_\mu\tilde{c}^\dagger[\boldsymbol{\tau}A^k_\mu - A^k_\mu\boldsymbol{\tau}]\tilde{c}\end{aligned} \tag{1.54}$$

where $\boldsymbol{\tau} A_\mu$ terms are matrix products. In view of the decomposition Eq. (1.51), we take a specified component of Eq. (1.54),

$$\begin{aligned}\dot{\mathfrak{C}}_\alpha &= i\dot{r}_\mu(\mathcal{A}^r_\mu)^\beta \tilde{c}^\dagger(\tau_\alpha\tau_\beta - \tau_\beta\tau_\alpha)\tilde{c} + i\dot{k}_\mu(\mathcal{A}^k_\mu)^\beta \tilde{c}^\dagger(\tau_\alpha\tau_\beta - \tau_\beta\tau_\alpha)\tilde{c} \\ &= -2\varepsilon_{\alpha\beta\gamma}[(\mathcal{A}^r_\mu)^\beta \dot{r}_\mu + (\mathcal{A}^k_\mu)^\beta \dot{k}_\mu](\tilde{c}^\dagger\tau_\gamma\tilde{c}). \end{aligned} \tag{1.55}$$

When written in the iso-spin vector form, the above equation becomes

$$\dot{\mathfrak{C}} = 2\mathfrak{C} \times (\boldsymbol{\mathcal{A}}^r_\mu \dot{r}_\mu + \boldsymbol{\mathcal{A}}^k_\mu \dot{k}_\mu), \tag{1.56}$$

which can be regarded as the Bloch equation in the iso-spin space.

(2) $\delta\mathcal{L}/\delta r_\mu = 0$ on Eq. (1.52) requires some care. We note that

$$\frac{\partial \mathcal{L}}{\partial r_\mu} = \partial^r_\mu \varepsilon + \mathfrak{C} \cdot [(\partial^r_\mu \boldsymbol{\mathcal{A}}^r_\nu)\dot{r}_\nu + (\partial^r_\mu \boldsymbol{\mathcal{A}}^k_\nu)\dot{k}_\nu] \tag{1.57a}$$

$$\begin{aligned}\frac{\mathrm{d}}{\mathrm{d}t}\frac{\partial \mathcal{L}}{\partial \dot{r}_\mu} &= \dot{k}_\mu + (\dot{\mathfrak{C}} \cdot \boldsymbol{\mathcal{A}}^r_\mu + \mathfrak{C} \cdot \frac{\mathrm{d}}{\mathrm{d}t}\boldsymbol{\mathcal{A}}^r_\mu) \\ &= \dot{k}_\mu + 2[\dot{r}_\nu \mathfrak{C} \cdot (\boldsymbol{\mathcal{A}}^r_\nu \times \boldsymbol{\mathcal{A}}^r_\mu) + \dot{k}_\nu \mathfrak{C} \cdot (\boldsymbol{\mathcal{A}}^k_\nu \times \boldsymbol{\mathcal{A}}^r_\mu)] \\ &\quad + \mathfrak{C} \cdot [(\partial^r_\nu \boldsymbol{\mathcal{A}}^r_\mu)\dot{r}_\nu + (\partial^k_\nu \boldsymbol{\mathcal{A}}^r_\mu)\dot{k}_\nu] \end{aligned} \tag{1.57b}$$

where in the last line Eq. (1.56) has been used. Therefore, from

$$\frac{\delta \mathcal{L}}{\delta r_\mu} = \frac{\partial \mathcal{L}}{\partial r_\mu} - \frac{\mathrm{d}}{\mathrm{d}t}\frac{\partial \mathcal{L}}{\partial \dot{r}_\mu} = 0, \tag{1.58}$$

we obtain the equation of motion

$$\dot{k}_\mu = \partial^r_\mu \varepsilon + \mathfrak{C} \cdot [\boldsymbol{\Omega}^{rr}_{\mu\nu}\dot{r}_\nu + \boldsymbol{\Omega}^{rk}_{\mu\nu}\dot{k}_\nu], \tag{1.59}$$

where the Berry curvatures are defined as

$$\boldsymbol{\Omega}^{rr}_{\mu\nu} \equiv \partial^r_\mu \boldsymbol{\mathcal{A}}^r_\nu - \partial^r_\nu \boldsymbol{\mathcal{A}}^r_\mu + 2\boldsymbol{\mathcal{A}}^r_\mu \times \boldsymbol{\mathcal{A}}^r_\nu, \tag{1.60a}$$

$$\boldsymbol{\Omega}^{rk}_{\mu\nu} \equiv \partial^r_\mu \boldsymbol{\mathcal{A}}^k_\nu - \partial^k_\nu \boldsymbol{\mathcal{A}}^r_\mu + 2\boldsymbol{\mathcal{A}}^r_\mu \times \boldsymbol{\mathcal{A}}^k_\nu, \tag{1.60b}$$

they are antisymmetric tensors with permutations of r_μ and k_μ, and at the same time they are vectors in the isospin vector space – the internal space unique to non-Abelian gauge theory.

(3) $\delta\mathcal{L}/\delta k_\mu = 0$ on Eq. (1.52) follows quite similar procedures as above, and the equation of motion is

$$\dot{r}_\mu = -\partial^k_\mu \varepsilon - \boldsymbol{\mathcal{C}} \cdot [\boldsymbol{\Omega}^{kr}_{\mu\nu}\dot{r}_\nu + \boldsymbol{\Omega}^{kk}_{\mu\nu}\dot{k}_\nu], \tag{1.61}$$

where the Berry curvatures are

$$\boldsymbol{\Omega}^{kk}_{\mu\nu} \equiv \partial^k_\mu \boldsymbol{\mathcal{A}}^k_\nu - \partial^k_\nu \boldsymbol{\mathcal{A}}^k_\mu + 2\boldsymbol{\mathcal{A}}^r_\mu \times \boldsymbol{\mathcal{A}}^r_\nu, \tag{1.62a}$$

$$\boldsymbol{\Omega}^{kr}_{\mu\nu} \equiv \partial^k_\mu \boldsymbol{\mathcal{A}}^r_\nu - \partial^r_\nu \boldsymbol{\mathcal{A}}^k_\mu + 2\boldsymbol{\mathcal{A}}^k_\mu \times \boldsymbol{\mathcal{A}}^r_\nu, \tag{1.62b}$$

which, together with Eqs. (1.60), form a generalized matrix of Berry curvature jointing real space and BZ into a unified parameter space,

$$\tilde{\boldsymbol{\Omega}}_{\mu\nu} = \begin{bmatrix} \boldsymbol{\Omega}^{rr}_{\mu\nu} & \boldsymbol{\Omega}^{rk}_{\mu\nu} \\ \boldsymbol{\Omega}^{kr}_{\mu\nu} & \boldsymbol{\Omega}^{kk}_{\mu\nu} \end{bmatrix}. \tag{1.63}$$

Eqs. (1.59), (1.61), and Eq. (1.56) constitute the essential formula for the non-Abelian adiabatic dynamics:

$$\dot{\boldsymbol{\mathcal{C}}} = 2\boldsymbol{\mathcal{C}} \times (\boldsymbol{\mathcal{A}}^r_\mu \dot{r}_\mu + \boldsymbol{\mathcal{A}}^k_\mu \dot{k}_\mu), \tag{1.64a}$$

$$\dot{k}_\mu = \partial^r_\mu \varepsilon + \boldsymbol{\mathcal{C}} \cdot [\boldsymbol{\Omega}^{rr}_{\mu\nu}\dot{r}_\nu + \boldsymbol{\Omega}^{rk}_{\mu\nu}\dot{k}_\nu], \tag{1.64b}$$

$$\dot{r}_\mu = -\partial^k_\mu \varepsilon - \boldsymbol{\mathcal{C}} \cdot [\boldsymbol{\Omega}^{kr}_{\mu\nu}\dot{r}_\nu + \boldsymbol{\Omega}^{kk}_{\mu\nu}\dot{k}_\nu]. \tag{1.64c}$$

These equations will be frequently used in the following chapter to study the electron transport in an antiferromagnetic texture.

1.5.2 Case II: Well Separated Bands

In a ferromagnetic metal, the two spin eigenstates are well separated due to the large exchange coupling (typically s-d mixing) between conduction electron spins and local magnetization. The non-Abelian gauge theory developed previously is not applicable. Interestingly, when we regard the separation of spin eigenstates as much larger than the typical frequency of magnetization dynamics, the theory recovers in the opposite limit of adiabaticity (but a theory interpolating the two limits are not possible).

Set the wave vector as $|u\rangle = c_a|\uparrow(\boldsymbol{r}_c,t)\rangle + c_b|\downarrow(\boldsymbol{r}_c,t)\rangle$, where the $\boldsymbol{r}_c$ dependence originates from the local Hamiltonian. Similar to the previous case, the effective Lagrangian is

$$L = i\hbar\langle u|\frac{\mathrm{d}u}{\mathrm{d}t}\rangle + \hbar\boldsymbol{k}_c\cdot\dot{\boldsymbol{r}}_c - \langle u|H_{ex}|u\rangle. \tag{1.65}$$

Due to the orthogonality $\langle\uparrow\mid\downarrow\rangle = 0$, the energy term becomes $\langle u|H_{ex}|u\rangle = |c_a|^2\mathcal{E}_\uparrow + |c_b|^2\mathcal{E}_\downarrow$. The physical spin is defined as $\boldsymbol{s} = \langle u|\boldsymbol{\sigma}|u\rangle$, we known that $s_3 = |c_a|^2 - |c_b|^2$ and $|c_a|^2 + |c_b|^2 = 1$, thus we have the following:

$$\begin{aligned}\langle u|H_{ex}|u\rangle &= \frac{1+s_3}{2}\mathcal{E}_\uparrow + \frac{1-s_3}{2}\mathcal{E}_\downarrow \\ &= \frac{\mathcal{E}_\uparrow+\mathcal{E}_\downarrow}{2} + s_3\frac{\mathcal{E}_\uparrow-\mathcal{E}_\downarrow}{2} = \mathcal{E}_0 + \frac{1}{2}s_3\Delta.\end{aligned} \tag{1.66}$$

To compute the Berry connection term, we notice that

$$\begin{aligned}|\frac{\mathrm{d}u}{\mathrm{d}t}\rangle =& \dot{c}_a|\uparrow\rangle + \dot{c}_b|\downarrow\rangle + \\ & [c_a(\dot{\boldsymbol{r}}_c\cdot\nabla+\partial_t)|\uparrow\rangle + c_b(\dot{\boldsymbol{r}}_c\cdot\nabla+\partial_t)|\downarrow\rangle\ ,\end{aligned} \tag{1.67}$$

where $\nabla = \frac{\partial}{\partial \boldsymbol{r}_c}$. Multiply by $\langle u|$ we have

$$\begin{aligned}\langle u|\frac{\mathrm{d}u}{\mathrm{d}t}\rangle =&(c_a^*\dot{c}_a + c_b^*\dot{c}_b) \\ &+ |c_a|^2\langle\uparrow|\dot{\boldsymbol{r}}_c\cdot\nabla + \partial_t|\uparrow\rangle + c_a^*c_b\langle\uparrow|\dot{\boldsymbol{r}}_c\cdot\nabla + \partial_t|\downarrow\rangle \\ &+ |c_b|^2\langle\downarrow|\dot{\boldsymbol{r}}_c\cdot\nabla + \partial_t|\downarrow\rangle + c_ac_b^*\langle\downarrow|\dot{\boldsymbol{r}}_c\cdot\nabla + \partial_t|\uparrow\rangle. \end{aligned} \tag{1.68}$$

Now define the Berry connection (2×2) matrices

$$\boldsymbol{A}(\boldsymbol{r}_c,t) = i\hbar\begin{bmatrix}\langle\uparrow|\nabla|\uparrow\rangle & \langle\uparrow|\nabla|\downarrow\rangle \\ \langle\downarrow|\nabla|\uparrow\rangle & \langle\downarrow|\nabla|\downarrow\rangle\end{bmatrix}, \tag{1.69}$$

$$\Phi(\boldsymbol{r}_c,t) = i\hbar\begin{bmatrix}\langle\uparrow|\partial_t|\uparrow\rangle & \langle\uparrow|\partial_t|\downarrow\rangle \\ \langle\downarrow|\partial_t|\uparrow\rangle & \langle\downarrow|\partial_t|\downarrow\rangle\end{bmatrix}, \tag{1.70}$$

which play the roles of a vector potential and a scalar potential, respectively. From Eqs. (1.66), (1.68), (1.69), and (1.70) we obtain the effective Lagrangian,

$$L = i\hbar\eta^\dagger\dot{\eta} + \eta^\dagger[\dot{\boldsymbol{r}}_c\cdot\boldsymbol{A} + \Phi]\eta + \hbar\boldsymbol{k}_c\cdot\dot{\boldsymbol{r}}_c - \frac{1}{2}s_3\Delta - \mathcal{E}_0, \tag{1.71}$$

where $\eta = [c_a, c_b]^{\mathrm{T}}$ is the pseudo-spinor. Here we adopt a different notation to distinguished from the degenerate case, because the pseudo-spin here is identical to the physical spin, whereas the two may not be identical in the degenerate case.

The local spin wave functions are chosen to be

$$|\uparrow\rangle = \begin{bmatrix}e^{-i\frac{\phi}{2}}\cos\frac{\theta}{2} \\ e^{i\frac{\phi}{2}}\sin\frac{\theta}{2}\end{bmatrix}, \qquad |\downarrow\rangle = \begin{bmatrix}-e^{-i\frac{\phi}{2}}\sin\frac{\theta}{2} \\ e^{i\frac{\phi}{2}}\cos\frac{\theta}{2}\end{bmatrix}, \tag{1.72}$$

where θ and ϕ are spherical angles specifying the direction of local magnetization $\boldsymbol{M}(\boldsymbol{r},t)$, hence they are functions of space and time. Using Eq. (1.72), the

Berry connections (1.69) and (1.70) can be written in a unified 2×2 matrix,

$$\begin{aligned} \mathscr{A}(\boldsymbol{r}_c, t) &\equiv \dot{\boldsymbol{r}}_c \cdot \boldsymbol{A}(\boldsymbol{r}_c, t) + \Phi(\boldsymbol{r}_c, t) \\ &= \frac{\hbar}{2} \begin{bmatrix} \cos\theta\dot{\phi} & -\sin\theta\dot{\phi} - i\dot{\theta} \\ -\sin\theta\dot{\phi} + i\dot{\theta} & -\cos\theta\dot{\phi} \end{bmatrix}, \end{aligned} \tag{1.73}$$

where $\dot{\theta} = \dot{\boldsymbol{r}}_c \cdot \nabla\theta + \partial_t\theta$ and $\dot{\phi} = \dot{\boldsymbol{r}}_c \cdot \nabla\phi + \partial_t\phi$ are total time derivatives. It should be noted that the choice of Eq. (1.72) is not unique, which gives rise to the gauge freedom of the Berry potential.

1.6 Spin-transfer Torques

[1] When a current flows through a ferromagnetic metal, it becomes spin-polarized due to local exchange coupling between conduction electron spins and local magnetic moments. In turn, spin angular momentum is transferred to magnetization through the mechanism known as spin-transfer torque (STT) [8, 99, 148], which is a consequence of spin conservation. STT provides key mechanisms for numerous intriguing phenomena in ferromagnets, such as current-driven domain wall motion [7, 112], spin wave excitations [45, 59], *etc.*, which paves the way towards electrical writing in, e.g., STT-MRAM devices. In both fundamental studies and applications, STT-driven magnetization dynamics has aroused enormous attention in the past two decades [12, 88], and it is becoming the core issue of spintronics.

While STT has been widely studied in numerous publications, here

[1] The contents of this section are based on the article: R. Cheng and Q. Niu, *Microscopic derivation of spin-transfer torque in ferromagnets*, Phys. Rev. B **88**, 024422 (2013).

we present our own derivation using the Berry phase and effect Lagrangian formalism developed in the previous section. At present, STT is believed to be divided into adiabatic (reactive) and non-adiabatic (dissipative) contributions. While the former has been derived microscopically via different approaches [6,8,99], the latter has only been justified macroscopically through spin conservation [108,132,144] and Galilean invariance [4], whose microscopic origin is under intense debates. In many recent efforts, microscopic theories have been developed in generic ways [27, 31, 85, 106, 114] and in specific contexts [105, 107, 123, 125], but their coefficients do not lead to a consensus. Meanwhile, some others even cast doubt on the existence of the non-adiabatic STT [134]. From an experimental point of view, measurements of this torque are not in agreement [15, 42, 70], and the magnitude is sensitive to spin-orbit interaction [71] and impurity doping [58].

We adopt the s-d model where electron transport is mainly attributed to the itinerant s-band. It will be treated separately from the magnetization, which mostly originates from the localized d-band. The conduction electrons interact with the magnetization through the exchange coupling described by

$$H_{ex} = \frac{SJ_{ex}}{M_s} \boldsymbol{s} \cdot \boldsymbol{M}(\boldsymbol{r}, t), \tag{1.74}$$

where $\boldsymbol{s}$ is the (dimensionless) spin of a conduction electron, $|\boldsymbol{M}(\boldsymbol{r}, t)| = M_s$ is the saturation magnetization, and S denotes the magnitude of background spins. The coupling strength J_{ex} can be as large as an eV in transition metals and their alloys, so that if $\boldsymbol{M}(\boldsymbol{r}, t)$ varies slowly in space and time, conduction

electron spins will follow the background profile when the system is in thermal equilibrium, known as the adiabatic limit. However, when an external current is applied to the system, a small non-equilibrium spin accumulation $\delta\boldsymbol{m}$ transverse to local $\boldsymbol{M}(\boldsymbol{r},t)$ is induced. It is this $\delta\boldsymbol{m}$ that exerts STT on the background magnetization.

To compute $\delta\boldsymbol{m}$, we first study the spin response of an individual conduction electron to the background $\boldsymbol{M}(\boldsymbol{r},t)$ when current is applied. From Eq. (1.74), we know that *local* spin-up (majority) and spin-down (minority) bands are separated by a large gap $\Delta \equiv SJ_{ex} = \mathcal{E}_\downarrow - \mathcal{E}_\uparrow$, and the associated spin wave functions are denoted by $|\uparrow(\boldsymbol{r},t)\rangle$ and $|\downarrow(\boldsymbol{r},t)\rangle$, respectively. As stated in the previous section, the electron is described by a coherent wave packet centered at $(\boldsymbol{r}_c,\boldsymbol{k}_c)$ [19, 133]

$$|W\rangle = \int \mathrm{d}^3\boldsymbol{k}\ w(\boldsymbol{k})e^{i\boldsymbol{k}\cdot\boldsymbol{r}}|\boldsymbol{k}\rangle[c_a|\uparrow(\boldsymbol{r}_c,t)\rangle + c_b|\downarrow(\boldsymbol{r}_c,t)\rangle], \tag{1.75}$$

where $w(\boldsymbol{k})$ is a profile function that satisfies $\int \mathrm{d}\boldsymbol{k}\boldsymbol{k}|w(\boldsymbol{k})|^2 = \boldsymbol{k}_c$; $|\boldsymbol{k}\rangle$ is the periodic part of the *local* Bloch function; and c_a, c_b are superposition coefficients. Since $|\uparrow(\boldsymbol{r}_c,t)\rangle$ and $|\downarrow(\boldsymbol{r}_c,t)\rangle$ form a set of local spin bases with the quantization axis being $\boldsymbol{n}(\boldsymbol{r}_c,t) = \boldsymbol{M}(\boldsymbol{r}_c,t)/M_s$, we can construct a local frame moving with $\boldsymbol{M}(\boldsymbol{r}_c,t)$, where the coordinates are labeled by $\boldsymbol{n}$, $\hat{e}_\theta$, and $\hat{e}_\phi$ in Fig. 1.3. The electron spin expressed in this local frame reads

$$\begin{aligned}\boldsymbol{s} &= \{s_1,s_2,s_3\} = \eta^\dagger\boldsymbol{\sigma}\eta \\ &= \{2\mathrm{Re}(c_ac_b^*),\ -2\mathrm{Im}(c_ac_b^*),\ |c_a|^2 - |c_b|^2\},\end{aligned} \tag{1.76}$$

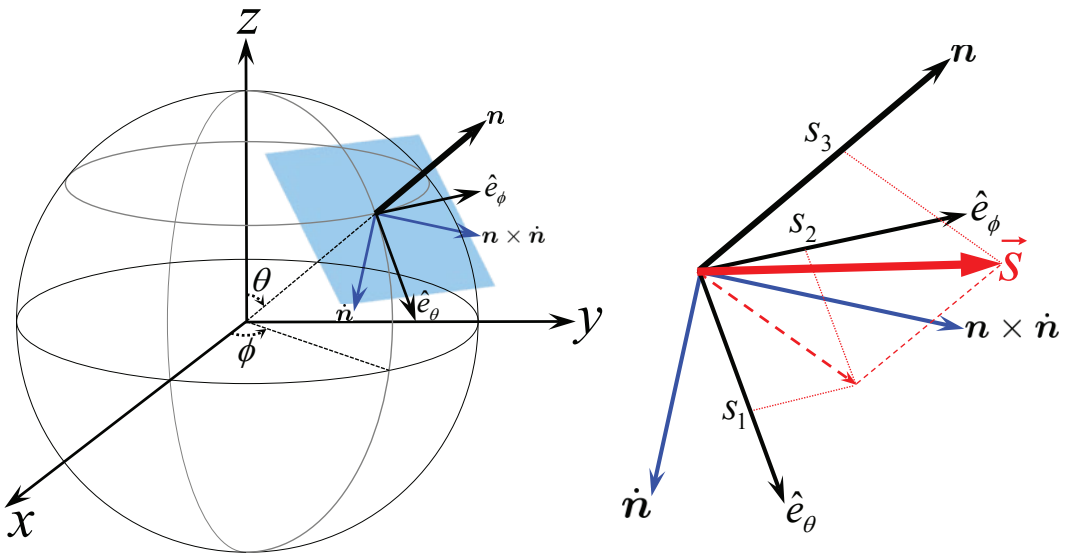

Figure 1.3: The eigenstates of Eq. (1.74) form a set of local spin bases, and define a local frame that moves with $\boldsymbol{n} = \boldsymbol{M}/M_s$. Components of the conduction electron spin $\boldsymbol{s}$ (red) in the local frame are denoted by s_1, s_2, and s_3. In the tangential plane with normal $\boldsymbol{n}$, we make a coordinate transformation from $\hat{e}_\theta$ and $\hat{e}_\phi$ to $\dot{\boldsymbol{n}}$ and $\boldsymbol{n}\times\dot{\boldsymbol{n}}$ so that everything expressed in the new basis is physical.

where $\boldsymbol{\sigma}$ is a vector of Pauli matrices, and $\eta = [c_a, c_b]^{\mathrm{T}}$ is regarded as the spin wave function in the local basis.

The equations of motion are obtained from the universal Lagrangian $L = \langle W|i\hbar\partial_t - H|W\rangle$ through the variational principle, which involves not only the dynamics of $\boldsymbol{r}_c$ and $\boldsymbol{k}_c$, but also the dynamics between the two (well separated) spin bands. The latter represents spin evolution with respect to the local magnetization $\boldsymbol{M}(\boldsymbol{r}, t)$ and exhibits fast rotating character due to the large gap Δ. As derived in Eq. (1.71), the effective Lagrangian is,

$$L = i\hbar\eta^\dagger\dot{\eta} + \eta^\dagger[\dot{\boldsymbol{r}}_c\cdot\boldsymbol{A} + \Phi]\eta + \hbar\boldsymbol{k}_c\cdot\dot{\boldsymbol{r}}_c - \frac{1}{2}s_3\Delta - \mathcal{E}_0, \tag{1.77}$$

where $\mathcal{E}_0 = \frac{1}{2}(\mathcal{E}_\uparrow(\boldsymbol{k}_c) + \mathcal{E}_\downarrow(\boldsymbol{k}_c))$, and the Berry connections are defined in Eq. (1.73). It is worth mentioning that freedom exists in the choice of local spin wave functions, which leads to free gauge choices of the Berry gauge connection. More graphically, a specified set of spin wave functions corresponds to a particular choice of local frame in Fig. 1.3, and the relative orientation of the local frame can be rotated about $\boldsymbol{n}$ by gauge transformations, thus is not physical. But everything will be expressed in terms of gauge invariant quantities in the end.

Decomposing the Berry potential $\mathscr{A}$ (Eq. (1.73)) in terms of Pauli matrices $\mathscr{A} = \sigma_i \mathcal{A}_i$ (adjoint representation), we have

$$\{\mathcal{A}_1, \mathcal{A}_2, \mathcal{A}_3\} = \frac{1}{2}\mathrm{Tr}[\boldsymbol{\sigma}\mathscr{A}] = \frac{1}{2}\{-\sin\theta\dot{\phi},\ \dot{\theta},\ \cos\theta\dot{\phi}\}, \tag{1.78}$$

where $\mathrm{Tr}[\sigma_i\sigma_j] = 2\delta_{ij}$ has been used. By taking the variational derivative of the Lagrangian with respect to η, we obtain the evolution of the spin wave function in the local frame,

$$i\hbar\dot{\eta} = i\hbar\frac{\mathrm{d}}{\mathrm{d}t}\begin{bmatrix} c_a \\ c_b \end{bmatrix} = -\mathscr{A}\begin{bmatrix} c_a \\ c_b \end{bmatrix} + \frac{\Delta}{2}\begin{bmatrix} c_a \\ -c_b \end{bmatrix}. \tag{1.79}$$

From Eq. (1.79) and its complex conjugate, we derive the spin dynamics in the local frame

$$\begin{aligned} i\hbar\frac{\mathrm{d}}{\mathrm{d}t}\boldsymbol{s} &= i\hbar\frac{\mathrm{d}}{\mathrm{d}t}(\eta^\dagger\boldsymbol{\sigma}\eta) = i\hbar(\dot{\eta}^\dagger\boldsymbol{\sigma}\eta + \eta^\dagger\boldsymbol{\sigma}\dot{\eta}) \\ &= (\eta^\dagger\mathscr{A}\boldsymbol{\sigma}\eta - \eta^\dagger\boldsymbol{\sigma}\mathscr{A}\eta) \\ &\quad + \frac{\Delta}{2}\left([-c_a^*, c_b^*]\boldsymbol{\sigma}\eta + \eta^\dagger\boldsymbol{\sigma}\begin{bmatrix} c_a \\ -c_b \end{bmatrix}\right). \end{aligned} \tag{1.80}$$

To transform Eq. (1.80) into a simple and elegant form, we should write it down component by component. The third component of Eq. (1.80) is

$$\begin{aligned} i\hbar\dot{s}_3 &= \eta^\dagger \mathcal{A}_i[\sigma_i, \sigma_3]\eta + \frac{\Delta}{2}(-|c_a|^2 - |c_b|^2 + |c_a|^2 + |c_b|^2) \\ &= -2i\hbar\eta\varepsilon_{3ij}\mathcal{A}_i\sigma_j\eta + 0 = 2i\hbar\varepsilon_{3ij}s_i\mathcal{A}_j, \end{aligned} \tag{1.81}$$

where ε_{ijk} is the total antisymmetric tensor. The first component reads

$$\begin{aligned} i\hbar\dot{s}_1 &= \eta^\dagger \mathcal{A}_i[\sigma_i, \sigma_1]\eta + \Delta(c_a c_b^* - c_a^* c_b) \\ &= -2i\hbar\eta\varepsilon_{1ij}\mathcal{A}_i\sigma_j\eta + 2i\Delta \mathrm{Im}[c_a c_b^*] \\ &= 2i\hbar\varepsilon_{1ij}s_i\mathcal{A}_j - i\Delta s_2, \end{aligned} \tag{1.82}$$

and the second component reads

$$\begin{aligned} i\hbar\dot{s}_2 &= \eta^\dagger \mathcal{A}_i[\sigma_i, \sigma_2]\eta + i\Delta(c_a c_b^* + c_a^* c_b) \\ &= -2i\hbar\eta\varepsilon_{2ij}\mathcal{A}_i\sigma_j\eta + 2i\Delta \mathrm{Re}[c_a c_b^*] \\ &= 2i\hbar\varepsilon_{2ij}s_i\mathcal{A}_j + i\Delta s_1. \end{aligned} \tag{1.83}$$

Now we are able to combine Eqs. (1.81), (1.82), (1.83) in a matrix form:

$$\begin{bmatrix} \dot{s}_1 \\ \dot{s}_2 \\ \dot{s}_3 \end{bmatrix} = \begin{bmatrix} 0 & \cos\theta\dot{\phi} - \dfrac{1}{\tau_{ex}} & -\dot{\theta} \\ -\cos\theta\dot{\phi} + \dfrac{1}{\tau_{ex}} & 0 & -\sin\theta\dot{\phi} \\ \dot{\theta} & \sin\theta\dot{\phi} & 0 \end{bmatrix} \begin{bmatrix} s_1 \\ s_2 \\ s_3 \end{bmatrix}, \tag{1.84}$$

where $\tau_{ex} = \hbar/\Delta$ is defined as the exchange time.

Eq. (1.84) describes the coherent spin dynamics in the local frame moving with $\boldsymbol{M}(\boldsymbol{r}_c, t)$. However, spin relaxation as a non-coherent process should

also be taken into account. In real materials spin relaxation is very case dependent, but regardless of the underlying mechanism, it adds a term $-\frac{1}{\tau_{sf}}(\boldsymbol{s}-\boldsymbol{s}_{eq})$ to Eq. (1.84), where τ_{sf} is the mean spin-flip time and $\boldsymbol{s}_{eq}=\{0,0,1(-1)\}$ is the local equilibrium spin configuration for the majority (minority) band $\mathcal{E}_{\uparrow}(\mathcal{E}_{\downarrow})$. Eq. (1.84) should be solved numerically in general, but an approximation can be made based upon the following considerations: the large gap Δ results in an extremely small τ_{ex} (typically of the order of $10^{-14}\sim 10^{-15}s$). Thus on the time scale marked by τ_{ex}, the change of magnetization is negligible, *i.e.*, magnitudes of $\partial_t\boldsymbol{M}$ and $(\dot{\boldsymbol{r}}_c\cdot\nabla)\boldsymbol{M}$ are much smaller than M_s/τ_{ex}. To this end, we define two small parameters $\varepsilon_1=\tau_{ex}\sin\theta\dot{\phi}$ and $\varepsilon_2=\tau_{ex}\dot{\theta}$ which satisfy $\sqrt{\varepsilon_1^2+\varepsilon_2^2}=\hbar|\dot{\boldsymbol{M}}|/(M_s\Delta)\ll 1$. On the same time scale, variations of ε_1 and ε_2 are even higher order small quantities, thus it is a good approximation to treat ε_1 and ε_2 as constants, by which Eq. (1.84) becomes a set of first order differential equations with a constant coefficient matrix. As a result, it can be solved analytically. Given the initial condition $\boldsymbol{s}=\boldsymbol{s}_{eq}$, the solution of Eq. (1.84) for the majority band is obtained, which, when maintaining up to the lowest order in $\varepsilon_{1,2}$, becomes the following:

$$s_1(t)=\frac{\varepsilon_1-\xi\varepsilon_2}{1+\xi^2}-\frac{e^{-\xi\tilde{t}}}{1+\xi^2}[\varepsilon_1(\cos\tilde{t}+\xi\sin\tilde{t})+\varepsilon_2(\sin\tilde{t}-\xi\cos\tilde{t})], \tag{1.85a}$$

$$s_2(t)=-\frac{\xi\varepsilon_1+\varepsilon_2}{1+\xi^2}-\frac{e^{-\xi\tilde{t}}}{1+\xi^2}[\varepsilon_1(\sin\tilde{t}-\xi\cos\tilde{t})-\varepsilon_2(\cos\tilde{t}+\xi\sin\tilde{t})], \tag{1.85b}$$

$$s_3(t)=1+\frac{e^{-\xi\tilde{t}}}{1+\xi^2}(\varepsilon_1^2+\varepsilon_2^2)[\cos\tilde{t}+\xi\sin\tilde{t}], \tag{1.85c}$$

where $\tilde{t}=t/\tau_{ex}$ is the scaled time, and $\xi=\tau_{ex}/\tau_{sf}$ (this is usually known as the β parameter in the literature).

As stated above, magnetization dynamics occurs on a time scale T much larger than τ_{ex}, thus the number $N = T/\tau_{ex} \gg 1$. This allows us to take a time average of the electron spin by defining $\langle s_i \rangle = \frac{1}{T}\int_0^T s_i(t)\mathrm{d}t$. Then all time dependent terms in Eq. (1.85) will be negligible, because according to the following expressions

$$\begin{aligned}\frac{1}{T}\int_0^T \mathrm{d}t\ e^{-\xi\tilde{t}}\cos\tilde{t} &= \frac{\xi + e^{-N\xi}(\sin N - \xi\cos N)}{N(1+\xi^2)} \\ &< \frac{1}{N}\left[\frac{\xi+\sqrt{1+\xi^2}}{1+\xi^2}\right] \leq \frac{1}{N}\frac{3\sqrt{3}}{4}, \end{aligned} \tag{1.86a}$$

$$\begin{aligned}\frac{1}{T}\int_0^T \mathrm{d}t\ e^{-\xi\tilde{t}}\sin\tilde{t} &= \frac{1 - e^{-N\xi}(\xi\sin N + \cos N)}{N(1+\xi^2)} \\ &< \frac{1}{N}\left[\frac{1+\sqrt{1+\xi^2}}{1+\xi^2}\right] \leq \frac{2}{N}, \end{aligned} \tag{1.86b}$$

no matter how large ξ is, their upper bounds are suppressed $1/N$ as $N \gg 1$. As a result, only the time-independent terms of Eq. (1.85) will survive after the time averaging,

$$\langle s_1 \rangle = \frac{\varepsilon_1 - \xi\varepsilon_2}{1+\xi^2}, \quad \langle s_2 \rangle = -\frac{\xi\varepsilon_1 + \varepsilon_2}{1+\xi^2}, \quad \langle s_3 \rangle = 1. \tag{1.87a}$$

If we write the spin as $\boldsymbol{s} = \boldsymbol{s}_{eq} + \delta\boldsymbol{s}$, then $\delta\boldsymbol{s} = \langle s_1\rangle\hat{e}_\theta + \langle s_2\rangle\hat{e}_\phi$. For the minority band, Eq. (1.87) only differs by an overall minus sign. To express $\delta\boldsymbol{s}$ in terms of gauge invariant quantities, we need to make a coordinate transformation that amounts to a rotation of basis in the tangential plane depicted in Fig. 1.3. In matrix form, it is

$$\begin{bmatrix} \dot{\boldsymbol{n}} \\ \boldsymbol{n}\times\dot{\boldsymbol{n}} \end{bmatrix} = \frac{\Omega}{\tau_{ex}}\begin{bmatrix} \varepsilon_2 & \varepsilon_1 \\ -\varepsilon_1 & \varepsilon_2 \end{bmatrix}\begin{bmatrix} \hat{e}_\theta \\ \hat{e}_\phi \end{bmatrix}, \tag{1.88}$$

where $\Omega = |\dot{\boldsymbol{n}}|$. Then we obtain

$$\begin{aligned}\delta \boldsymbol{s}_{\uparrow,\downarrow} &= \mp\frac{\tau_{ex}}{1+\xi^2}[\boldsymbol{n}\times\dot{\boldsymbol{n}} + \xi\dot{\boldsymbol{n}}] \\ &= \mp\frac{\tau_{ex}}{1+\xi^2}[\boldsymbol{n}\times\frac{\partial \boldsymbol{n}}{\partial t} + \xi\frac{\partial \boldsymbol{n}}{\partial t} + \boldsymbol{n}\times(\dot{\boldsymbol{r}}_c\cdot\nabla)\boldsymbol{n} + \xi(\dot{\boldsymbol{r}}_c\cdot\nabla)\boldsymbol{n}], \end{aligned} \tag{1.89}$$

where $\dot{\boldsymbol{n}} = \partial_t \boldsymbol{n} + (\dot{\boldsymbol{r}}_c\cdot\nabla)\boldsymbol{n}$ has been used and $\dot{\boldsymbol{r}}_c = -\frac{\partial \mathcal{E}_{\uparrow,\downarrow}}{\hbar\partial \boldsymbol{k}_c}$ is the center of mass velocity. The local non-equilibrium spin accumulation is obtained

$$\delta\boldsymbol{m} = \mu_B \int \mathrm{d}\mathcal{E}[\mathscr{D}_\uparrow(\mathcal{E})g_\uparrow(\mathcal{E})\delta\boldsymbol{s}_\uparrow + \mathscr{D}_\downarrow(\mathcal{E})g_\downarrow(\mathcal{E})\delta\boldsymbol{s}_\downarrow], \tag{1.90}$$

where μ_B is the Bohr magneton, $\mathscr{D}_{\uparrow,\downarrow}(\mathcal{E})$ is the density of states, and $g_{\uparrow,\downarrow}(\mathcal{E})$ represents the distribution function. In a weak electric field $\boldsymbol{E}$ and zero temperature, we have $g_{\uparrow,\downarrow}(\mathcal{E}) = f_{0\uparrow,\downarrow}(\mathcal{E}) + e\tau_{0\uparrow,\downarrow}\boldsymbol{E}\cdot\frac{\partial \mathcal{E}_{\uparrow,\downarrow}}{\hbar\partial \boldsymbol{k}_c}\frac{\partial f_{0\uparrow,\downarrow}}{\partial \mathcal{E}}$ where $f_{0\uparrow,\downarrow}(\mathcal{E})$ is the Fermi distribution function without electric field and $\tau_{0\uparrow,\downarrow}$ is the relaxation time. It should be noted that when the mean spin-flip time τ_{sf} is assumed to be independent of energy, it is equivalent to introducing it either in solving the Boltzmann equation or in Eq. (1.84), and we have chosen the latter. Our target now is to relate $\delta\boldsymbol{m}$ to the charge current

$$\boldsymbol{j}_e = -\frac{e}{\hbar}\int \delta\mathcal{E}\left[\mathscr{D}_\uparrow(\mathcal{E})g_\uparrow(\mathcal{E})\frac{\partial \mathcal{E}_\uparrow}{\partial \boldsymbol{k}_c} + \mathscr{D}_\downarrow(\mathcal{E})g_\downarrow(\mathcal{E})\frac{\partial \mathcal{E}_\downarrow}{\partial \boldsymbol{k}_c}\right].$$

Regarding Eq. (1.89) and Eq. (1.90), terms involving electric field $\boldsymbol{E}$ and $\tau_{0\uparrow,\downarrow}$ can be expressed in terms of $\boldsymbol{j}_e$. After some simple algebra, we obtain

$$\begin{aligned}\delta\boldsymbol{m} = \frac{\tau_{ex}}{1+\xi^2}\Bigg[&-\frac{n_0}{M_s^2}\boldsymbol{M}\times\frac{\partial \boldsymbol{M}}{\partial t} - \frac{\xi n_0}{M_s}\frac{\partial \boldsymbol{M}}{\partial t} \\ &+\frac{\mu_B P}{eM_s^2}\boldsymbol{M}\times(\boldsymbol{j}_e\cdot\nabla)\boldsymbol{M} + \frac{\xi\mu_B P}{eM_s}(\boldsymbol{j}_e\cdot\nabla)\boldsymbol{M}\Bigg], \end{aligned} \tag{1.91}$$

where $P = (n_\uparrow^F - n_\downarrow{}^F)/(n_\uparrow^F + n_\downarrow{}^F)$ is the spin polarization with $n_{\uparrow(\downarrow)}^F$ being the electron density of the two bands at the Fermi level, and

$$n_0 = \mu_B \int \mathrm{d}\mathcal{E}[\mathscr{D}_\uparrow(\mathcal{E}) f_{0\uparrow}(\mathcal{E}) - \mathscr{D}_\downarrow(\mathcal{E}) f_{0\downarrow}(\mathcal{E})]$$

is the local equilibrium spin density of conduction electrons, which represents the s-band contribution to the total magnetization. For the s-d model, the magnetization is mainly attributed to the d-band electrons, thus the ratio n_0/M_s should be very small. For example, in typical ferromagnetic metals (Fe, Co, Ni and their alloys), $n_0/M_s \sim 10^{-2}$. Eq. (1.91) reproduces Eq. (8) in Ref. [144], but the above derivation is purely microscopic, and the four terms of Eq. (1.91) can be traced back to the four terms in Eq. (1.89), respectively.

From Eq. (1.74), the STT exerted on the background magnetization $\boldsymbol{M}(\boldsymbol{r}, t)$ is $\boldsymbol{T} = (1/\tau_{ex} M_s)\delta\boldsymbol{m} \times \boldsymbol{M}$, which should be added to the LLG derived in Eq. (1.2). The final form of magnetization dynamics becomes

$$\begin{aligned} \frac{\partial \boldsymbol{M}}{\partial t} = {} & \tilde{\gamma} \mathrm{H}_{eff} \times \boldsymbol{M} + \frac{\tilde{\alpha}}{M_s} \boldsymbol{M} \times \frac{\partial \boldsymbol{M}}{\partial t} \\ & + \frac{1}{1+\eta} \left[(\boldsymbol{u} \cdot \nabla)\boldsymbol{M} - \xi \frac{\boldsymbol{M}}{M_s} \times (\boldsymbol{u} \cdot \nabla)\boldsymbol{M} \right], \end{aligned} \tag{1.92}$$

where $\boldsymbol{u} = P\boldsymbol{j}_e \mu_B / e M_s (1 + \xi^2)$ is the effective electron velocity, and $\eta = (n_0/M_s)/(1 + \xi^2)$ is a dimensionless factor. The renormalized gyro-magnetic ratio and Gilbert damping parameter are

$$\tilde{\gamma} = \frac{\gamma}{1+\eta}, \quad \tilde{\alpha} = \frac{1}{1+\eta}[\alpha + \eta\xi], \tag{1.93}$$

where the renormalization originates from the first two terms of Eq. (1.89) (or Eq. (1.91)), and they are determined by the local equilibrium spin density n_0

which exists even in the absence of current. Eqs. (1.92) and (1.93) confirm the results macroscopic theory derived from spin conservation [144].

Our microscopic derivation relies on two assumptions: local equilibrium can be defined, and $\boldsymbol{M}$ is nearly constant on the time scale marked by τ_{ex}. The former requires diffusive transport which is usually the case in transition metals and their alloys; the latter, however, is only true when the characteristic length of the texture l (*e.g.*, the domain wall width) satisfies $l \gg v_F \tau_{ex}$ where v_F is the Fermi velocity, otherwise the solution Eqs. (1.85) and (1.87) are invalid. In a recent experiment [15], people measured the non-adiabatic torque on very narrow domain walls ($1 \sim 10$nm) and found disagreement with Eq. (1.92). A rough estimate using $v_F \sim 3 \times 10^5$m/s and $\Delta \sim 1$eV tells us that $v_F \tau_{ex}$ is of the order of many angstroms, thus a domain wall of a few nm wide cannot be considered as $l \gg v_F \tau_{ex}$. In that case, our local solution is no longer a good approximation, because the time-dependent terms in Eq. (1.85) become important and the averaging in Eq. (1.87) is no longer good. As a result, STT may exhibit non-local behavior and also oscillatory patterns in space.

The parameter ξ determines the relative strength of the non-adiabatic torque with respect to the adiabatic torque. It is very material dependent and tunable in many different ways [58, 71]. But according to Eq. (1.86) and Eq. (1.87), the result is valid *regardless* of the value of ξ; only $N = T/\tau_{ex} \gg 1$ is sufficient to guarantee the negligence of the time dependent terms of Eq. (1.85). This can be used to explain a recent experiment in which ξ is as large as 1 [71], while the observed domain wall velocity is still fitted using the form of

Eq. (1.92). However, we should mention that large ξ is usually accompanied by large spin-orbit coupling, which brings about spin-orbit torque in addition to the non-adiabatic torque [66, 77]. This is an important issue that draws people's attention very recently, but goes beyond the scope of our discussion.

In another experiment, ξ is enhanced by increasing impurity doping (which decreases τ_{sf}), but the damping is basically not affected [58]. This can be easily understood through Eq. (1.93): since $n_0/M_s \sim 10^{-2}$ is very small within the s-d model description, η is a small quantity, hence $\tilde{\alpha}$ could only be slightly renormalized even if ξ has a sizable change.

A final remark concerns the spin motive force [138, 139] $\boldsymbol{E}_{SMF} = \frac{\hbar}{2e}\boldsymbol{n} \cdot (\partial_t \boldsymbol{n} \times \nabla \boldsymbol{n})$, which is small but should be taken into consideration in a strict sense. As a result, the electric field should be replaced by the effective field $\boldsymbol{E}_{eff} = \boldsymbol{E} + \boldsymbol{E}_{SMF}$ in deriving Eq. (1.91) from Eqs. (1.89) and (1.90). This creates an additional contribution to the renormalized $\tilde{\alpha}$, which has been studied recently via a quite different route [145].

Chapter 2

Electron Transport in Antiferromagnets

[1] Interplay between current and magnetization is an essential issue underpinning the field of spintronics [148], which consists of two reciprocal problems: control of current through magnetization with a known configuration, and its converse, *i.e.*, control of magnetization dynamics via applied current. In ferromagnetic (FM) materials with slowly varying spin texture $\boldsymbol{m}(\boldsymbol{r}, t)$ over space and time, these issues can be solved by assuming that conduction electron spins always follow the background texture profile, known as the adiabatic approximation [9, 16, 17, 101, 133]. The microscopic basis underlying adiabaticity is the strong exchange coupling $H = -J\sigma \cdot \boldsymbol{m}(\boldsymbol{r}, t)$ between conduction electron spins and local magnetic moments, through which spin mistracking with the background causes large energy penalty and becomes highly unfavorable [138, 139].

Under the adiabatic approximation, the current – magnetization interaction is recast into an emergent electrodynamics, in which its reciprocal influence boils down to a simple electromagnetic problem. Specifically, by diagonalizing the local exchange Hamiltonian via local unitary transformation,

[1] The contents of this chapter are based on the article: R. Cheng and Q. Niu, *Electron dynamics in slowly varying antiferromagnetic texture*, Phys. Rev. B **86**, 245118 (2012).

fictitious electric and magnetic fields are generated that significantly affect the orbital dynamics of the electron [5, 124, 138, 139]

$$E_i = \frac{1}{2}\boldsymbol{m}\cdot(\partial_t\boldsymbol{m}\times\partial_i\boldsymbol{m}) = \frac{1}{2}\sin\theta(\partial_t\theta\partial_i\phi - \partial_i\theta\partial_t\phi), \tag{2.1}$$

$$B_i = -\frac{1}{4}\varepsilon_{ijk}\boldsymbol{m}\cdot(\partial_j\boldsymbol{m}\times\partial_k\boldsymbol{m}) = -\frac{1}{2}\varepsilon_{ijk}\sin\theta\partial_j\theta\partial_k\phi, \tag{2.2}$$

where $\theta(\boldsymbol{r},t)$ and $\phi(\boldsymbol{r},t)$ are spherical angles specifying the direction of $\boldsymbol{m}$. As a consequence, the influence of background texture is represented by an effective Lorentz force $\boldsymbol{F} = s\hbar(\boldsymbol{E} + \dot{\boldsymbol{r}}\times\boldsymbol{B})$ exerted on the conduction electrons, where $s = +1(-1)$ denotes the spin-up (-down) bands. The electric and magnetic components of the Lorentz force are responsible for the spin motive force [1, 5, 28, 41, 96, 124, 136, 138, 139] and the topological Hall effect [14, 57, 74, 140], respectively. In turn, the back-reaction of the Lorentz force provides an interpretation to the current-induced spin torque exerted on magnetic texture [6, 48, 115, 132, 141]. In a formal language, the adiabaticity induces an effective gauge interaction $\mathcal{L}_{\rm int} = j_\mu\mathcal{A}_\mu$ as introduced by the previous chapter, where j_μ acquires a gauge charge according to $s = \pm 1$, and $\mathcal{A}_\mu = \mathcal{A}_\mu(\boldsymbol{m}, \partial\boldsymbol{m})$ is the effective electromagnetic potential representing the space-time dependence of the texture. Variation over the current $\delta\mathcal{L}_{\rm int}/\delta j_\mu = 0$ yields the effective Lorentz force; and variation over the magnetization $\delta\mathcal{L}_{\rm int}/\delta\boldsymbol{m} = 0$ produces the spin-transfer torque. In this way, the reciprocal relation of the current-magnetization interaction is manifested.

However, the above picture apparently fails in antiferromagnetic (AF) materials where neighboring magnetic moments are antiparallel. Conduction

electrons are not able to adjust their spins with the local moments that alter orientation on atomic scale. Nevertheless, the staggered order parameter $\boldsymbol{n} = (\boldsymbol{M}_A - \boldsymbol{M}_B)/2M_s$ can be slowly varying over space-time, where $\boldsymbol{M}_A$ and $\boldsymbol{M}_B$ are the alternating local moments and M_s denotes their magnitudes. A natural question is whether a slowly varying staggered order still renders adiabatic dynamics of conduction electrons in some other sense. This is desired knowledge for studying spin transport in AF materials, especially the quest for current-magnetization interaction as that for FM materials.

In spite of recent theoretical [39, 40, 76, 102, 103, 131, 135] and experimental [44, 122, 128] progress, this problem has never been addressed microscopically. But at the same time, AF materials are believed to be promising candidates for new thrusts of spintronics [64], partly due to their enhanced anisotropy, robustness against external magnetic perturbations, and vanishingly small demagnetization, which bring prevailing advantages for device design and engineering control.

In this chapter, we develop the effective electron dynamics in a bulk AF texture with slowly-varying time dependence and smooth spatial modulation by applying the non-Abelian Berry phase theory [22, 23, 69, 72, 149] on energy bands that are doubly degenerate. The physics of adiabaticity in AF materials is found to be an internal dynamics between degenerate bands which can be attributed to a SU(2) Berry curvature. When translating into spin dynamics, the adiabaticity no more indicates spin alignment with the background, but a totally new evolution principle [Eq. (2.19)]. Aside from spin dynamics, the

orbital motion of conduction electrons is coupled to two different gauge fields: one leads to the non-Abelian generalization of the effective Lorentz force; the other results in an anomalous velocity that is truly new and unique to AF systems. With comparisons to FM materials, this chapter provides a general framework on how a given textured AF background affects the dynamics of conduction electrons [18]. The other side of the story, *i.e.*, back-reaction of current on the AF background, will be discussed in the next chapter.

2.1 Band Structure

Consider an AF system on a bipartite lattice with local magnetic moments labeled by alternating $\boldsymbol{M}_A$ and $\boldsymbol{M}_B$. The spin of a conduction electron couples to the local moments by the exchange interaction $J(\boldsymbol{M}/M_s)\cdot\boldsymbol{\sigma}$, where $\boldsymbol{\sigma}$ denotes the spin operator of the conduction electron, and $\boldsymbol{M}$ flips sign on neighboring A and B sublattice sites. In spite of antiparallel of neighboring moments, the staggered order parameter $\boldsymbol{n} = (\boldsymbol{M}_A - \boldsymbol{M}_B)/2M_s$ usually varies slowly over space and time, and we can treat it as a continuous function $\boldsymbol{n}(\boldsymbol{r}, t)$. Accordingly, the conduction electron is described by a nearest-neighbor tight-binding Hamiltonian locally defined around $\boldsymbol{n}(\boldsymbol{r}, t)$:

$$\mathcal{H}(\boldsymbol{n}(\boldsymbol{r}, t)) = \begin{bmatrix} -J\boldsymbol{n}\cdot\boldsymbol{\sigma} & \gamma(\boldsymbol{k}) \\ \gamma^*(\boldsymbol{k}) & J\boldsymbol{n}\cdot\boldsymbol{\sigma} \end{bmatrix} \tag{2.3}$$

where $\gamma(\boldsymbol{k}) = -t\sum_{\boldsymbol{\delta}} e^{i\boldsymbol{k}\cdot\boldsymbol{\delta}}$ is the hopping term with $\boldsymbol{\delta}$ connecting nearest neighboring $A-B$ sites (we set $\hbar = 1$). The exchange J can have multiple origins such as Hund's coupling or s-d mixing, but it does not matter too much in

the exchange limit. In general J can be negative, but we assume a positive J throughout this paper.

The local band structure can be easily solved as $\pm\varepsilon(\boldsymbol{k})$ with $\varepsilon(\boldsymbol{k}) = \sqrt{J^2 + |\gamma(\boldsymbol{k})|^2}$, and in the adiabatic limit we neglect transitions between ε and $-\varepsilon$. Each of the two bands are doubly degenerate, and without loss of generality we will focus on the lower band $-\varepsilon$ with the two sub-bands labeled by A and B, whose wave functions are $|\psi_a\rangle = e^{i\boldsymbol{k}\cdot\boldsymbol{r}}|u_a\rangle$ and $|\psi_b\rangle = e^{i\boldsymbol{k}\cdot\boldsymbol{r}}|u_b\rangle$. The Bloch waves consist of the spatial part and the spin part

$$|u_a\rangle = |A(\boldsymbol{k})\rangle|\uparrow(\boldsymbol{r},t)\rangle; \quad |u_b\rangle = |B(\boldsymbol{k})\rangle|\downarrow(\boldsymbol{r},t)\rangle \tag{2.4}$$

where $\boldsymbol{k}$ is understood as the *local* lattice momentum as the Hamiltonian maintains local periodicity around $(\boldsymbol{r},t)$. The position dependence all come from the local spin eigenstates

$$|\uparrow(\boldsymbol{r},t)\rangle = \begin{bmatrix} e^{-i\frac{\phi}{2}}\cos\frac{\theta}{2} \\ e^{i\frac{\phi}{2}}\sin\frac{\theta}{2} \end{bmatrix}; \quad |\downarrow(\boldsymbol{r},t)\rangle = \begin{bmatrix} -e^{-i\frac{\phi}{2}}\sin\frac{\theta}{2} \\ e^{i\frac{\phi}{2}}\cos\frac{\theta}{2} \end{bmatrix} \tag{2.5}$$

where $\theta = \theta(\boldsymbol{r},t)$ and $\phi = \phi(\boldsymbol{r},t)$ are the spherical angles specifying the orientation of $\boldsymbol{n}(\boldsymbol{r},t)$. The choice of phase factors in Eq. (2.5) is not unique, but this freedom does not alter our final results.

The periodic parts are spinors in the pseudo-spin space furnished by the $A-B$ sublattices. They are

$$|A(\boldsymbol{k})\rangle = \frac{1}{\sqrt{(\varepsilon(\boldsymbol{k})+J)^2 + |\gamma(\boldsymbol{k})|^2}} \begin{bmatrix} -(\varepsilon(\boldsymbol{k})+J) \\ \gamma(\boldsymbol{k})^* \end{bmatrix}, \tag{2.6a}$$

$$|B(\boldsymbol{k})\rangle = \frac{1}{\sqrt{(\varepsilon(\boldsymbol{k})-J)^2 + |\gamma(\boldsymbol{k})|^2}} \begin{bmatrix} J-\varepsilon(\boldsymbol{k}) \\ \gamma(\boldsymbol{k})^* \end{bmatrix}, \tag{2.6b}$$

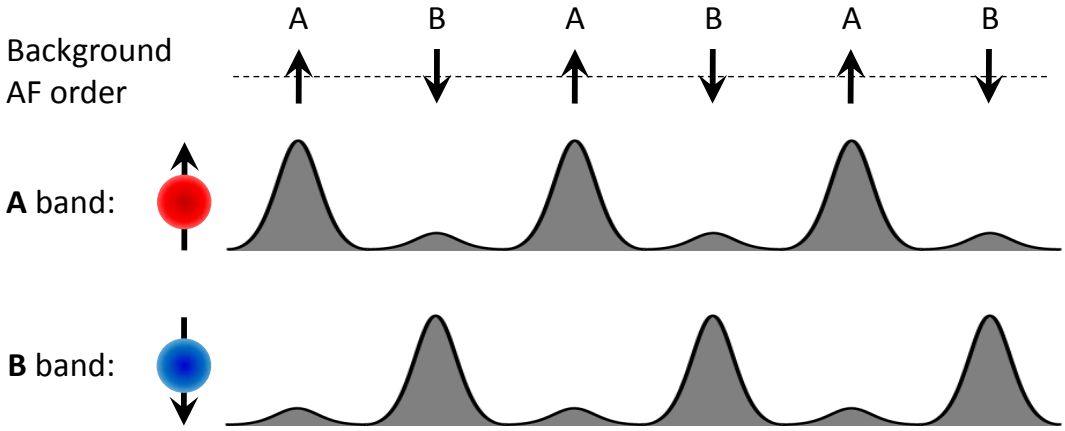

Figure 2.1: A schematic view of Bloch waves in the lower band. Sub-band A means a local spin up electron has a larger probability on the A sites and a smaller probability on the B sites; sub-band B means the opposite case. They are degenerate in energy and their wave functions have a finite overlap depending on the ratio of J/ε.

which exhibit opposite spatial patterns schematically illustrated in Fig. 2.1. While $\langle\psi_a|\psi_b\rangle = 0$ due to the orthogonality of local spin eigenstates, $\langle A(\boldsymbol{k})|B(\boldsymbol{k})\rangle$ does not vanish, and we define this overlap as

$$\xi(\boldsymbol{k}) = \langle A(\boldsymbol{k})|B(\boldsymbol{k})\rangle = \frac{|\gamma(\boldsymbol{k})|}{\sqrt{J^2 + |\gamma(\boldsymbol{k})|^2}} = \frac{\sqrt{\varepsilon^2 - J^2}}{\varepsilon}, \tag{2.7}$$

which is a key parameter in our theory and $\xi < 1$. It reaches maximum at the Brillouin zone (BZ) center and vanishes at the BZ boundary. From Eq. (2.7) we know $\xi(\boldsymbol{k})$ is a system parameter determined by the band structure, and it is constant since the energy conservation $\dot{\varepsilon} = 0$ requires $\dot{\xi} = 0$. If J tends to infinity, the overlap $\xi(\boldsymbol{k})$ will vanish and the two subbands will be effectively decoupled, by which the system will become a simple combination of two independent FM subsystems.

2.2 Equations of Motion

With the wave functions derived in the previous section, we are able to construct the effective gauge theory to study the electron dynamics. Since the band is degenerate, the non-Abelian formalism must be invoked. The electron wave packet introduced in Section 1.5.1 is

$$|W(r_\mu)\rangle = \int \mathrm{d}^3k w(\boldsymbol{k})[c_a|A(\boldsymbol{k})\rangle|\uparrow(r_\mu)\rangle + c_b|B(\boldsymbol{k})\rangle|\downarrow(r_\mu)\rangle], \tag{2.8}$$

which defines the center-of-mass position by $\boldsymbol{r}_c = \langle W|\boldsymbol{r}|W\rangle$, the center-of-mass momentum by $\boldsymbol{k}_c = \int \mathrm{d}\boldsymbol{k}\boldsymbol{k}|w(\boldsymbol{k})|^2$, and the isospin vector $\boldsymbol{\mathcal{C}}$ by Eq. (1.50). The electron dynamics is characterized by the equations of motion of the three parameters $\boldsymbol{k}_c$, $\boldsymbol{r}_c$, and $\boldsymbol{\mathcal{C}}$, *i.e.*, which have been derived as Eq. (1.64).

By substituting the wave functions into Eq. (1.48) and Eq. (1.49), we obtain the Berry connections in terms of θ, ϕ, and ξ

$$\begin{aligned} A^r_\mu =& \frac{1}{2}\begin{bmatrix} \cos\theta\partial_\mu\phi & \xi(-i\partial_\mu\theta - \sin\theta\partial_\mu\phi) \\ \xi(i\partial_\mu\theta - \sin\theta\partial_\mu\phi) & -\cos\theta\partial_\mu\phi \end{bmatrix} \\ =& \frac{1}{2}[-\tau_1\xi\sin\theta\partial_\mu\phi + \tau_2\xi\partial_\mu\theta + \tau_3\cos\theta\partial_\mu\phi], \end{aligned} \tag{2.9}$$

and $A^k_\mu = 0$. The vanishing of A^k_μ can be attributed to the omission of spin-orbit coupling in the Hamiltonian.

The evolution of the iso-spin $\boldsymbol{\mathcal{C}}$ represents dynamics between the A and B sub-bands, which defines an internal degree of freedom unique to antiferromagnets. As explained in section 1.5.1, $\boldsymbol{\mathcal{C}}$ itself is not gauge invariant and is unmeasurable. However, it is ultimately related to the physical spin $\boldsymbol{s}$ which has unambiguous observable effect.

2.2.1 Spin and Iso-spin

With the wave-packet $|W(r_\mu)\rangle$ (we have omitted the subscript c for simplicity), the physical spin is defined as

$$\boldsymbol{s} = \langle W(r_\mu)|\boldsymbol{\sigma}|W(r_\mu)\rangle, \tag{2.10}$$

which respects gauge invariance. From Eqs. (1.50), (2.5), (2.8), and (2.10), we know the components of $\boldsymbol{s}$ in the *lab* frame after some tedious algebra,

$$s_x = c_3 \sin\theta\cos\phi + \xi[c_1\cos\theta\cos\phi - c_2\sin\phi], \tag{2.11a}$$

$$s_y = c_3 \sin\theta\sin\phi + \xi[c_1\cos\theta\sin\phi + c_2\cos\phi], \tag{2.11b}$$

$$s_z = c_3\cos\theta - \xi c_1\sin\theta. \tag{2.11c}$$

where ξ is defined in Eq. (2.7).

On the other hand, the iso-spin $\boldsymbol{\mathcal{C}}$ is defined by (1.50). Throughout the dissertation, the gauge resides in the choice of local spin eigenstates, which are obtained by acting $U(\boldsymbol{r},t) = e^{-i\sigma_z\phi/2}e^{-i\sigma_y\theta/2}e^{-i\sigma_z\chi/2}$ on the eigenstates of σ_z. While $\theta(\boldsymbol{r},t)$ and $\phi(\boldsymbol{r},t)$ are physical, $\chi(\boldsymbol{r},t)$ is not and can be chosen arbitrarily; the gauge is fixed by setting $\chi = 0$. With this special gauge choice, $\boldsymbol{\mathcal{C}}$ can be pictured as a vector in the local frame extended by $\boldsymbol{\theta}$, $\boldsymbol{\phi}$, and $\boldsymbol{n}$, as depicted Fig. 2.2: $\boldsymbol{\mathcal{C}} = c_1\boldsymbol{\theta} + c_2\boldsymbol{\phi} + c_3\boldsymbol{n}$, and components of the real spin $\boldsymbol{s}$ in this *local* frame are

$$s_1 = s_x\cos\theta\cos\phi + s_y\cos\theta\sin\phi - s_z\sin\theta = \xi c_1 \tag{2.12a}$$

$$s_2 = -s_x\sin\phi + s_y\cos\phi = \xi c_2 \tag{2.12b}$$

$$s_3 = s_x\sin\theta\cos\phi + s_y\sin\theta\sin\phi + s_z\cos\theta = c_3 \tag{2.12c}$$

where Eqs. (2.11) have been used, and we obtain the important relation,

$$\boldsymbol{s} = \xi(c_1\boldsymbol{\theta} + c_2\boldsymbol{\phi}) + c_3\boldsymbol{n}. \tag{2.13}$$

Equation (2.13) indicates two important properties: (i) $\mathcal{C}$ is coplanar with $\boldsymbol{n}$ and $\boldsymbol{s}$, which is specific to the particular gauge $\chi = 0$; (ii) while the isospin vector is constrained on the unit sphere $c_1^2 + c_2^2 + c_3^2 = 1$, the physical spin satisfies $\frac{s_1^2+s_2^2}{\xi^2} + s_3^2 = 1$, which constrains the tip of $\boldsymbol{s}$ on an prolate spheroid with semi-major axis being $\boldsymbol{n}(\boldsymbol{r}, t)$ and semi-minor axis on its equator having length ξ (Fig. 2.2, right panel).

For arbitrary gauge with $\chi \neq 0$, it is easy to show that we always have $s_3 = c_3$ and $s_1^2 + s_2^2 = \xi^2(c_1^2 + c_2^2)$, but the angles between $s_{1,2}$ and $c_{1,2}$ will be different, *i.e.*, $\mathcal{C}$ will not be coplanar with $\boldsymbol{n}$ and $\boldsymbol{s}$.

We mention that the iso-spin is different from the pseudo-spin furnished by the $A - B$ sublattices. Iso-spin refers to the superposition coefficients c_a and c_b. Only in the limit $\xi \to 0$ where $|A\rangle$ and $|B\rangle$ are orthogonal, iso-spin and pseudo-spin become equivalent. But in such a limit, the two are also equivalent to the physical spin.

2.2.2 Geometric Evolution of Spin

We know that in ferromagnet, electron spin is locked to the orientation of the local magnetization, thus $\boldsymbol{s}$ is actually a slaved variable. As a consequence, the spin evolution is a geometric map from space-time to the Bloch sphere. In the AF texture, however, iso-spin dynamics results in spin

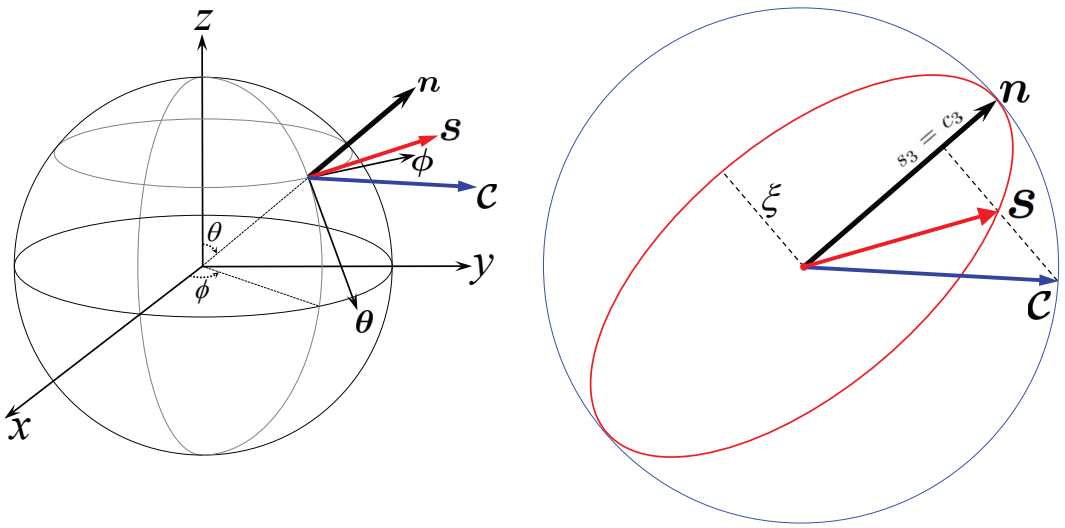

Figure 2.2: Left panel: the isospin vector $\mathcal{C}$ (blue arrow) in the local frame: $\mathcal{C} = c_1\boldsymbol{\theta} + c_2\boldsymbol{\phi} + c_3\boldsymbol{n}$, where $\boldsymbol{\theta}$ and $\boldsymbol{\phi}$ are spherical unit vectors. Right panel: In our particular gauge, $\mathcal{C}$ (blue) is coplanar with $\boldsymbol{n}$ and $\boldsymbol{s}$ (red). The tip of $\mathcal{C}$ moves on a unit sphere, whereas tip of $\boldsymbol{s}$ is constrained on the ellipsoid whose semi-major axis is $\boldsymbol{n}$ and semi-minor axis having length ξ.

mistracking with the background, is the spin evolution still geometrical?

To derive the spin dynamics, we first substitute Eq. (1.51) into Eq. (1.56) with the Berry connection given by Eq. (2.9), and note that

$$\dot{\theta} = \dot{r}_\mu \partial_\mu \theta = \partial_t \theta + \dot{\boldsymbol{r}}_c \cdot \nabla\theta, \ \text{(same for } \phi) \tag{2.14}$$

we obtain the iso-spin dynamics

$$\frac{\mathrm{d}}{\mathrm{d}t}\begin{bmatrix} c_1 \\ c_2 \\ c_3 \end{bmatrix} = \begin{bmatrix} 0 & \cos\theta\dot{\phi} & -\xi\dot{\theta} \\ -\cos\theta\dot{\phi} & 0 & -\xi\sin\theta\dot{\phi} \\ \xi\dot{\theta} & \xi\sin\theta\dot{\phi} & 0 \end{bmatrix}\begin{bmatrix} c_1 \\ c_2 \\ c_3 \end{bmatrix}. \tag{2.15}$$

Then, we notice that in the laboratory frame, the spin components are related to the iso-spin by Eq. (2.11). Take the total time derivative over each

component of $\boldsymbol{s}$, for example,

$$\begin{aligned}\dot{s}_x &= \dot{c}_3 \sin\theta\cos\phi + c_3(\cos\theta\cos\phi\dot{\theta} - \sin\theta\sin\phi\dot{\phi}) \\ &\quad + \xi[\dot{c}_1\cos\theta\cos\phi - c_1(\sin\theta\cos\phi\dot{\theta} + \cos\theta\sin\phi\dot{\phi})] \\ &\quad - \xi[\dot{c}_2\sin\phi + c_2\cos\phi\dot{\phi}] \\ &= c_3(1-\xi^2)(\cos\theta\cos\phi\dot{\theta} - \sin\theta\sin\phi\dot{\phi}) \\ &= c_3(1-\xi^2)\dot{n}_x \end{aligned} \tag{2.16}$$

where in deriving the second equality Eq. (2.15) has been used. In a similar manner, we obtain the other two components

$$\dot{s}_y = c_3(1-\xi^2)\dot{n}_y, \quad \dot{s}_z = c_3(1-\xi^2)\dot{n}_z. \tag{2.17}$$

To eliminate c_3 in the above equations, we reverse Eqs. (2.11) and obtain,

$$c_3 = s_x\sin\theta\cos\phi + s_y\sin\theta\sin\phi + s_z\cos\theta = \boldsymbol{s}\cdot\boldsymbol{n} \tag{2.18}$$

then from Eqs. (2.16) and (2.17), we obtain a simple and elegant equation of motion for the physical spin,

$$\dot{\boldsymbol{s}} = (1-\xi^2)(\boldsymbol{s}\cdot\boldsymbol{n})\dot{\boldsymbol{n}}, \tag{2.19}$$

where the $\boldsymbol{s}$ dependence on the right hand side is important.

As dt can be eliminated from Eq. (2.19), we claim that the spin evolution is geometrical given that $\boldsymbol{n}(\boldsymbol{r}, t)$ is a function of space-time. The motion of $\boldsymbol{s}$ can be decomposed into a superposition of two motions: one strictly follows $\boldsymbol{n}$ (for stationary $\mathcal{C}$) and the other represents mistracking with $\boldsymbol{n}$ (for

dynamical $\mathfrak{C}$), where the latter originates from dynamics between the A and B sub-bands and is unique to AF materials. It is worth emphasizing that the mistracking between $\boldsymbol{s}$ and $\boldsymbol{n}$ has nothing to do with any non-adiabatic process, but is entirely due to the non-Abelian nature of the problem.

From Eq. (2.19), we can generalize Eq. (2.13) to a gauge-invariant form, which will be useful in the following discussions. Since

$$\mathrm{d}\boldsymbol{s} = (1-\xi^2)(\boldsymbol{s}\cdot\boldsymbol{n})\mathrm{d}\boldsymbol{n}, \tag{2.20}$$

the dot product with $\boldsymbol{n}$ on both sides yields

$$\boldsymbol{n}\cdot\mathrm{d}\boldsymbol{s} = (1-\xi^2)(\boldsymbol{s}\cdot\boldsymbol{n})\frac{1}{2}\mathrm{d}(\boldsymbol{n}^2) = 0, \tag{2.21}$$

where $\boldsymbol{n}^2 = 1$ has been considered. Eq. (2.21) gives us the relation

$$\mathrm{d}(\boldsymbol{n}\cdot\boldsymbol{s}) = \boldsymbol{s}\cdot\mathrm{d}\boldsymbol{n}. \tag{2.22}$$

On the other hand, dot product with $\boldsymbol{s}$ on both sides of Eq. (2.20) gives,

$$\mathrm{d}(\boldsymbol{s}^2) = 2(1-\xi^2)(\boldsymbol{s}\cdot\boldsymbol{n})(\boldsymbol{s}\cdot\mathrm{d}\boldsymbol{n}) = (1-\xi^2)\mathrm{d}(\boldsymbol{s}\cdot\boldsymbol{n})^2 \tag{2.23}$$

From Pythagorean theorem we know that $\boldsymbol{s}^2 = (\boldsymbol{s}\cdot\boldsymbol{n})^2 + (\boldsymbol{s}\times\boldsymbol{n})^2$, then take derivative on both sides, regarding Eq. (2.23), we arrive at

$$\xi^2\mathrm{d}(\boldsymbol{s}\cdot\boldsymbol{n})^2 = -\mathrm{d}(\boldsymbol{s}\times\boldsymbol{n})^2. \tag{2.24}$$

Assume the initial condition to be $(\boldsymbol{s}\cdot\boldsymbol{n})|_0 = 1$, the above equation can be integrated into

$$(\boldsymbol{s}\cdot\boldsymbol{n})^2 + \frac{(\boldsymbol{s}\times\boldsymbol{n})^2}{\xi^2} = s_3^2 + \frac{s_1^2+s_2^2}{\xi^2} = 1, \tag{2.25}$$

which describes a three dimensional prolate spheroid. While Eq. (2.13) applies only the our special gauge $\chi = 0$, Eq. (2.25) is valid in arbitrary gauge.

To appreciate the geometric property of the spin evolution and to better compare it with the ferromagnetic case, let us consider a simple example illustrated by Fig. 2.3: $\boldsymbol{n}(t)$ is varying round a cone of constant semiangle θ in the laboratory frame, which can be realized in a spin wave. According to Eq. (2.19), we know that $\mathrm{d}s_z = 0$ due to $\mathrm{d}n_z = 0$, thus, the tip of $\boldsymbol{s}$ should stay in the bottom plane of the cone. On the other hand, we learn from Eq. (2.25) that the tip is constrained on the spheroid that moves with the instantaneous $\boldsymbol{n}(t)$. Therefore, the actual orbit traversed by the tip is contained in the intersection of the two constraints. Through some straightforward geometric analysis, we know that $\boldsymbol{s}$ is bounded between the $\boldsymbol{n}$ cone and an inner cone whose semiangle depends on ξ. Figure 2.3 depicts the actual orbits of $\boldsymbol{s}$ for three different ξ's: they all exhibit precession and nutation, which can be easily read out from the bird's eye view. Remarkably, the motion of $\boldsymbol{s}$ falls into two topologically distinct classes separated by the critical condition

$$\xi_c^2 = \frac{\cos^2\theta}{(1+\cos^2\theta)}, \tag{2.26}$$

which corresponds to the case where the inner cone angle shrunk to zero (the middle panel of Fig. 2.3). In a real spin wave, θ is nearly zero, thus $\xi_c \approx 1/\sqrt{2}$. For real materials, we expect $t \leq J$, thus from Eq. (2.7) we know that for a partially filled band, ξ is always smaller than $1/\sqrt{2}$. Therefore, the $\xi < \xi_c$ phase is more realistic. In section 2.3, we will provide further physical insights on how the value of ξ affects the topology of spin evolution.

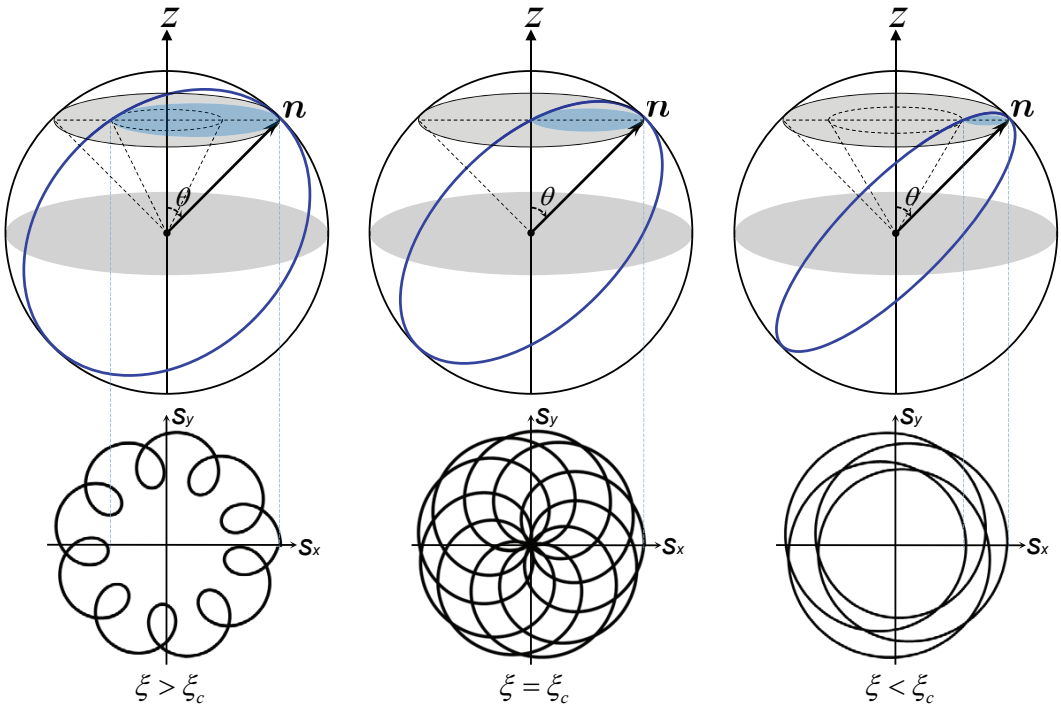

Figure 2.3: Spin evolutions for three different ξ's when $\boldsymbol{n}(t)$ is moving round a cone with constant angle θ from the z axis. Upper panels: the tip of $\boldsymbol{s}$ respects two constraints: it stays both on the cone's bottom (small gray slab) and on the spheroid described by Eq. (2.25) (blue ellipsoid), thus the vector $\boldsymbol{s}$ is confined in between two cones with different semiangles. Lower panels: orbits of the tip from bird's eye view. The topology of the orbits is separated into two classes (left and right) by the critical case (middle) where the inner cone's semiangle shrunk to zero. Orbits may not commensurate with $\boldsymbol{n}$.

Now, the physical picture of adiabatic spin evolution is clear: as the background order parameter $\boldsymbol{n}(\boldsymbol{r}, t)$ moves slowly in space-time, the prolate spheroid moves with it. The motion of physical spin $\boldsymbol{s}$ is a superposition of the relative motion on the spheroid and the motion of the spheroid itself. The overall motion of $\boldsymbol{s}$ described by Eq. (2.19) is purely geometrical as $\mathrm{d}t$ can be eliminated on both sides, as a result, a given path of $\boldsymbol{n}$ uniquely determines a path of $\boldsymbol{s}$ on the spheroid which is independent of the Hamiltonian.

A further remark: it seems surprising that the magnitude of $\boldsymbol{s}$ varies on the spheroid since $\xi \leq 1$, but how can the physical spin have a non-constant magnitude? We answer this question by studying the *reduced* density matrix for the spin degree of freedom. It is a 2×2 matrix and can be written as $\rho_s = \frac{1}{2}(1+\boldsymbol{a}\cdot\boldsymbol{\sigma})$, thus the expectation value of physical spin is $\boldsymbol{s} = \mathrm{Tr}[\rho_s \boldsymbol{\sigma}] = \boldsymbol{a}$. Now since $s^2 \leq 1$, thus $a^2 \leq 1$, and what follows is $\mathrm{Tr}\rho_s^2 \leq \mathrm{Tr}\rho_s$, which suggests that the electron is *effectively* in a mixed spin state. This can be attributed to the entanglement of spin and sublattice degrees of freedom, specifically, because $s_3 = c_3$, we are able to infer the spin projection along $\boldsymbol{n}$ by measuring the probability difference on neighboring $A - B$ sites (vice versa). The entanglement provides us with partial information of spin orientation from the knowledge of sublattice, this destroys full coherence of the spin states.

2.2.3 Dynamics in Momentum Space

In correspondence with the novel spin dynamics, the orbital dynamics of an individual electron also becomes nontrivial, which is attributed to the

non-Abelian Berry curvatures. In this section and the following section, we derive the orbital dynamics of a single conduction electron in momentum space (BZ) and real space, respectively.

From Eq. (1.51) the real-space curvature becomes

$$\begin{aligned}\boldsymbol{\Omega}^{rr}_{\mu\nu} &\equiv \partial^r_\mu \boldsymbol{\mathcal{A}}^r_\nu - \partial^r_\nu \boldsymbol{\mathcal{A}}^r_\mu + 2\boldsymbol{\mathcal{A}}^r_\mu \times \boldsymbol{\mathcal{A}}^r_\nu \\ &= \{0, 0, (\xi^2-1)\frac{1}{2}\sin\theta(\partial^r_\mu\theta\partial^r_\nu\phi - \partial^r_\nu\theta\partial^r_\mu\phi)\} \\ &= \{0,\ 0,\ (\xi^2-1)\frac{1}{2}\boldsymbol{n}\cdot(\partial^r_\mu\boldsymbol{n}\times\partial^r_\nu\boldsymbol{n})\}, \end{aligned} \tag{2.27}$$

where $\boldsymbol{n} = \{\sin\theta\cos\phi, \sin\theta\sin\phi, \cos\theta\}$ is the local order parameter. We see that only the third component is non-zero in our particular gauge marked by $\chi = 0$. But one can check that in any gauge with $\chi \neq 0$, the first two components do not vanish. However, the third component is actually gauge invariant and it has the form of Skyrmion density.

The cross components can be obtained in a similar way,

$$\begin{aligned}\boldsymbol{\Omega}^{rk}_{\mu\nu} = -\boldsymbol{\Omega}^{kr}_{\nu\mu} &= \partial^r_\mu \boldsymbol{\mathcal{A}}^k_\nu - \partial^k_\nu \boldsymbol{\mathcal{A}}^r_\mu + 2\boldsymbol{\mathcal{A}}^r_\mu \times \boldsymbol{\mathcal{A}}^k_\nu \\ &= \frac{1}{2}\{\partial^k_\nu\xi\sin\theta\partial^r_\mu\phi,\ -\partial^k_\nu\xi\partial^r_\mu\theta,\ 0\}, \end{aligned} \tag{2.28}$$

where again the first two components are changeable subject to gauge transformations, whereas the third is gauge invariant. Moreover, due to $\boldsymbol{\mathcal{A}}^k_\mu = 0$, the BZ space Berry curvature $\boldsymbol{\Omega}^{kk}_{\mu\nu}$ vanishes and it will be no more mentioned in the following.

Before deriving the equations of motion, special attention should be paid on the fact that gauge fields (Berry curvatures) in non-Abelian theory

are *not* gauge invariant, but gauge covariant. It is the isospin *scalars* $\boldsymbol{\mathcal{C}} \cdot \boldsymbol{\Omega}_{\mu\nu}$ that respect gauge invariance. Specifically, as we make a gauge transformation on the wave functions $|\psi_a\rangle$ and $|\psi_b\rangle$, change of $\boldsymbol{\Omega}$ just compensates that of $\boldsymbol{\mathcal{C}}$.

By substituting Eqs. (2.27) and (2.28) into Eq. (1.59), regarding that k_μ has only spatial but no temporal components, we arrive at,

$$\begin{aligned}
\dot{\boldsymbol{k}}_c &= \frac{1}{2} c_3 (\xi^2 - 1) \boldsymbol{n} \cdot (\nabla \boldsymbol{n} \times \dot{\boldsymbol{n}}) + \frac{1}{2} \dot{\xi} [c_1 \sin\theta \nabla\phi - c_2 \nabla\theta] \\
&= \frac{1}{2} \boldsymbol{n} \cdot \{\nabla \boldsymbol{n} \times [(\xi^2 - 1)(\boldsymbol{s} \cdot \boldsymbol{n}) \dot{\boldsymbol{n}}]\} \\
&= -\frac{1}{2} \boldsymbol{n} \cdot (\nabla \boldsymbol{n} \times \dot{\boldsymbol{s}})
\end{aligned} \tag{2.29}$$

where $\dot{\xi} = 0$ and Eq. (2.19) have been used. We also have ignored $\partial_\mu^r \varepsilon$ term in Eq. (2.29) since the band structure is only a function of $\boldsymbol{k}$ and is independent of space-time in the adiabatic approximation. To make better comparisons with the spin motive force [5, 41, 124, 136, 138] and the topological Hall effect [14, 57, 74, 140] widely studied in FM materials, we also derive another suggestive form of Eq. (2.29). Take an arbitrary component i of Eq. (2.29),

$$\begin{aligned}
\dot{k}_i &= \frac{1}{2} c_3 (\xi^2 - 1) \sin\theta (\partial_i \theta \dot{\phi} - \dot{\theta} \partial_i \phi) \\
&= \frac{1}{2} c_3 (\xi^2 - 1) \sin\theta \{[\partial_i \theta \partial_t \phi - \partial_t \theta \partial_i \phi] + [\partial_i \theta (\dot{r}_j \partial_j \phi) - (\dot{r}_j \partial_j \theta) \partial_i \phi]\} \\
&= \frac{1}{2} c_3 (\xi^2 - 1) \{\sin\theta [\partial_i \theta \partial_t \phi - \partial_t \theta \partial_i \phi] + \sin\theta \varepsilon_{ijk} \varepsilon_{klm} \dot{r}_j \partial_l \theta \partial_m \phi\},
\end{aligned} \tag{2.30}$$

where $\dot{\theta} = \partial_t \theta + \dot{r}_i \partial_i \theta$ (the same for $\dot{\phi}$) and the identity $\varepsilon_{ijk}\varepsilon_{klm} = \delta_{il}\delta_{jm} - \delta_{im}\delta_{jl}$ have been used. Eq. (2.30) can be written in a concise way as,

$$\dot{\boldsymbol{k}} = (1 - \xi^2)(\boldsymbol{s} \cdot \boldsymbol{n})(\boldsymbol{E} + \dot{\boldsymbol{r}} \times \boldsymbol{B}), \tag{2.31}$$

where the gauge fields are defined as

$$\boldsymbol{E} = \frac{1}{2}\sin\theta(\partial_t\theta\nabla\phi - \nabla\theta\partial_t\phi), \tag{2.32}$$

$$\boldsymbol{B} = -\frac{1}{2}\sin\theta(\nabla\theta\times\nabla\phi), \tag{2.33}$$

which are exactly the same as their counterparts in ferromagnets. Also as in ferromagnets, it is easy to check that Eqs. (2.32) and (2.33) satisfy the Faraday's relation $\nabla\times\boldsymbol{E} + \frac{\partial\boldsymbol{B}}{\partial t} = 0$.

However, quite different from the ferromagnetic case, the gauge charge $\boldsymbol{s}\cdot\boldsymbol{n}$ in Eq. (2.31) is not just a constant, but involves internal dynamics. In other words, the orbital motion is accompanied by a time-dependent gauge charge which should be determined by solving the coupled dynamics of spin and orbit all together. Moreover, the factor ξ^2 results from the non-commutative term $2\boldsymbol{\mathcal{A}}^r_\mu\times\boldsymbol{\mathcal{A}}^r_\nu$ in Eq. (1.60a); it also reflects the coupling between spin and orbital dynamics.

The parameter $\xi\in(0,1)$ plays a key role here: in the $\xi\to 1$ limit, $1-\xi^2$ vanishes thus from Eqs. (2.19) and (2.31) we get null results $\dot{\boldsymbol{s}} = 0$ and $\dot{\boldsymbol{k}} = 0$. In the other limit where $\xi\to 0$, the solution of Eq. (2.19) reduces to $\boldsymbol{s} = \pm\boldsymbol{n}$ if initial condition is $\boldsymbol{s}(0) = \pm\boldsymbol{n}(0)$, and Eq. (2.31) reduces to the conventional Lorentz force equation, by which the system loses the non-Abelian feature and behaves as two decoupled ferromagnetic sub-systems. It deserves attention that in real AF materials, both A and B sub-bands host majority carriers, but they are subject to effective Lorentz forces of opposite directions, which may lead to non-trivial spin transport via Mott scattering.

2.2.4 Dynamics in Real Space

From Eq. (1.61) and Eq. (2.28), we have

$$\dot{\boldsymbol{r}} = -\partial_{\boldsymbol{k}}\varepsilon + \frac{1}{2}\partial_{\boldsymbol{k}}\xi(c_1 \sin\theta\dot{\phi} - c_2\dot{\theta}). \tag{2.34}$$

To get a gauge-independent equation, we need to eliminate $c_{1,2}$ in terms of the physical spin. Regarding Eq. (2.13) and $\dot{\boldsymbol{n}} = \dot{\theta}\boldsymbol{\theta} + \sin\theta\dot{\phi}\boldsymbol{\phi}$, we have

$$\boldsymbol{n}\cdot(\boldsymbol{s}\times\dot{\boldsymbol{n}}) = \xi(c_1\sin\theta\dot{\phi} - c_2\dot{\theta}), \tag{2.35}$$

thus Eq. (2.34) becomes

$$\dot{\boldsymbol{r}} = -\partial_{\boldsymbol{k}}\varepsilon - \frac{1}{2}(\boldsymbol{s}\times\boldsymbol{n})\cdot\dot{\boldsymbol{n}}\partial_{\boldsymbol{k}}\ln\xi, \tag{2.36}$$

where the last term on the right hand side represents a spin-dependent anomalous velocity. Moreover, from Eq. (2.7) we know

$$\partial_{\boldsymbol{k}}\ln\xi = \frac{1-\xi^2}{\xi^2}\frac{\partial_{\boldsymbol{k}}\varepsilon}{\varepsilon}, \tag{2.37}$$

thus the direction of the anomalous velocity $\frac{1}{2}(\boldsymbol{s}\times\boldsymbol{n})\cdot\dot{\boldsymbol{n}}\partial_{\boldsymbol{k}}\ln\xi$ is the same as the group velocity: it simply represents the modification of the group velocity due to presence of background AF texture.

With the anomalous velocity, the orbital dynamics exhibits *effective* spin-orbit coupling. We stress that this is unique to bulk AF textures and has nothing to do with the anomalous velocity widely studied in ferromagnets or quantum Hall systems. Mathematically, the anomalous velocity originates from the $\boldsymbol{\Omega}^{kr}_{\mu\nu}$ curvature that joints real space with BZ, the importance of

Ferromagnetic texture	Antiferromagnetic texture
$\boldsymbol{s} = \boldsymbol{n}$	$\dot{\boldsymbol{s}} = (1-\xi^2)(\boldsymbol{s}\cdot\boldsymbol{n})\dot{\boldsymbol{n}}$
$\dot{\boldsymbol{k}} = \boldsymbol{E} + \dot{\boldsymbol{r}} \times \boldsymbol{B}$	$\dot{\boldsymbol{k}} = (1-\xi^2)(\boldsymbol{s}\cdot\boldsymbol{n})(\boldsymbol{E} + \dot{\boldsymbol{r}} \times \boldsymbol{B})$
$\dot{\boldsymbol{r}} = -\partial_{\boldsymbol{k}}\varepsilon$	$\dot{\boldsymbol{r}} = -\partial_{\boldsymbol{k}}\varepsilon - \frac{1}{2}(\boldsymbol{s}\times\boldsymbol{n})\cdot\dot{\boldsymbol{n}}\ \partial_{\boldsymbol{k}}\ln\xi$

Table 2.1: Comparison of effective electron dynamics in ferromagnetic and antiferromagnetic textures. In the former, spin dynamics is trivial, and a Lorentz force is induced in the orbital motion. In the latter, spin dynamics is non-trivial due to the mixture of degenerate sub-bands, and the orbital dynamics is subject to a Lorentz force as well as an anomalous velocity that are spin-dependent.

which has been overlooked before. For better comparison, we summarize the fundamental electron dynamics of FM and AFM textures in Table 2.1.

A further point should be added is that in the most general case, the effective Lagrangian Eq. (1.47) should also contain a term representing self-rotation of the wave packet $-\mathrm{Im}[\tilde{c}_i\langle\partial^r_\mu u_i|(\varepsilon-\mathcal{H})|\partial^r_\mu u_j\rangle\tilde{c}_j]$, but after some sophisticated manipulations one can show that this term vanishes for quit similar reasons as the vanishing of $\boldsymbol{\Omega}^{kk}_{\mu\nu}$.

2.3 ‘t Hooft-Polyakov Monopole

In section 2.2.2, we have shown that the spin evolution is geometrical even though there is no exact tracking of electron spin and the background. Associated with this geometric motion, a SU(2) Berry phase $\mathcal{P}\exp[-i\int\boldsymbol{\mathcal{A}}^r_\mu\cdot\boldsymbol{\tau}\mathrm{d}r_\mu]$ is accumulated along the electron trajectory [69, 72, 149], which can be regarded as the (non-Abelian) gauge flux of a ‘t Hooft-Polyakov monopole [43, 97] at the center of the unit sphere spanned by $\boldsymbol{n}$. This is in analogy to the

$U(1)$ Dirac monopole associated the Abelian Berry phase of the electron wave function in ferromagnets.

To study the monopole, we turn to a different coordinate system. By assigning a variable magnitude to $\boldsymbol{n}$, we define the dimensionless order parameter $\boldsymbol{R} \equiv R\boldsymbol{n} = \frac{J}{t}\boldsymbol{n}$. Then the Berry connection can be equivalently defined in the $\boldsymbol{R}$ space, which relates to the original one by $A_\mu \mathrm{d}r_\mu = A_i \mathrm{d}R_i$ with

$$A_i = i \begin{bmatrix} \langle \uparrow | \partial_i | \uparrow \rangle & \xi \langle \uparrow | \partial_i | \downarrow \rangle \\ \xi \langle \downarrow | \partial_i | \uparrow \rangle & \langle \downarrow | \partial_i | \downarrow \rangle \end{bmatrix}, \tag{2.38}$$

where $\xi = |\tilde{\gamma}|/\sqrt{R^2 + |\tilde{\gamma}|^2}$ is also a function of R, and $|\tilde{\gamma}| = \sum_{\boldsymbol{\delta}} e^{i\boldsymbol{k}\cdot\boldsymbol{\delta}}$ depends on the position in BZ. Written in spherical coordinates, components of Eq. (2.38) are $A_{\mathfrak{R}} = 0$,

$$A_\theta = \frac{\xi}{2R} \begin{bmatrix} 0 & -i \\ i & 0 \end{bmatrix}, \quad \text{and } A_\phi = \frac{1}{2R} \begin{bmatrix} \cot\theta & -\xi \\ -\xi & -\cot\theta \end{bmatrix} \tag{2.39}$$

To see the monopole, we should further make a singular gauge transformation on the potential,

$$\begin{aligned} A'_\theta &= S A_\theta S^\dagger + i \frac{1}{R} S \partial_\theta S^\dagger \\ &= i \frac{(1 - \xi(R))}{2R} \begin{bmatrix} 0 & e^{-i\phi} \\ -e^{i\phi} & 0 \end{bmatrix} \qquad (2.40a) \\ A'_\phi &= S A_\phi S^\dagger + i \frac{1}{R \sin\theta} S \partial_\phi S^\dagger \\ &= \frac{(1 - \xi(R))}{2R} \begin{bmatrix} -\sin\theta & e^{-i\phi}\cos\theta \\ e^{i\phi}\cos\theta & \sin\theta \end{bmatrix} \qquad (2.40b) \end{aligned}$$

with the unitary matrix being

$$S = \begin{bmatrix} e^{-i\phi/2}\cos\frac{\theta}{2} & -e^{-i\phi/2}\sin\frac{\theta}{2} \\ e^{i\phi/2}\sin\frac{\theta}{2} & e^{i\phi/2}\cos\frac{\theta}{2} \end{bmatrix}. \tag{2.41}$$

Finally, expressing the gauge potential in Cartesian coordinates, we obtain

$$A_x = A'_\theta \cos\theta\cos\phi - A'_\phi \sin\phi = \frac{(1-\xi)}{2R^2}\begin{bmatrix} y & iz \\ -iz & -y \end{bmatrix}, \tag{2.42a}$$

$$A_y = A'_\theta \sin\phi + A'_\phi \cos\phi = \frac{(1-\xi)}{2R^2}\begin{bmatrix} -x & z \\ z & x \end{bmatrix}, \tag{2.42b}$$

$$A_z = A'_\theta \sin\theta = \frac{(1-\xi)}{2R^2}\begin{bmatrix} 0 & -y-ix \\ -y+ix & 0 \end{bmatrix}, \tag{2.42c}$$

they are nothing but the "hedgehog" gauge potential of a 't Hooft -Polyakov monopole at $\boldsymbol{R} = 0$,

$$A'_i = \frac{1-\xi(\mathcal{R})}{2R^2}\varepsilon_{ijk}R_j\sigma_k, \tag{2.43}$$

where $R_i = \{x, y, z\}$ and σ_i's are Pauli matrices. The radial profile of Eq. (2.43) is determined by the factor $1-\xi(R)$. For fixed nonzero $\tilde{\gamma}$, $1-\xi(R)$ tends to 1 as $R \to \infty$, and $1-\xi(R) \sim R^2$ as $R \to 0$, which cancels the R^2 in the denominator thus the gauge potential is *regular* at origin. The form and behaviors of Eq. (2.43) are all the same as the gauge potential proposed by Sonner and Tong for realizing artificial 't Hooft-Polyakov monopole [100]. In fact, our parameter ξ can be understood as the $f(B)$ factor in Ref. [100], they both reflect the overlap of (partial) wave functions from doubly degenerate bands. However, at BZ boundary $\tilde{\gamma}$ is zero, thus $\xi = 0$ regardless of R. In this case, Eq. (2.43) becomes the gauge potential of a Wu-Yang monopole and the origin $\boldsymbol{R} = 0$ becomes singular.

We can also define the associated Higgs field as

$$\phi_H \equiv \begin{bmatrix} \langle A|\sigma_3|A\rangle & \langle A|\sigma_3|B\rangle \\ \langle B|\sigma_3|A\rangle & \langle B|\sigma_3|B\rangle \end{bmatrix} = \sqrt{1-\xi^2}\ \sigma_3, \tag{2.44}$$

which is the pseudo-spin polarization of the AF systems. It describes the extent to which the conduction electrons with opposite spins are spatially separated on alternating A and B sites. In other words, it represents how much those electrons respect the staggered order. Upon the same gauge transformation with matrix (2.41), we have

$$\phi_H \to \phi'_H = S\phi_H S^\dagger = \frac{\boldsymbol{R}\cdot\boldsymbol{\sigma}}{\sqrt{|\tilde{\gamma}|^2 + r^2}} = \boldsymbol{\Phi}_H \cdot \boldsymbol{\sigma}. \tag{2.45}$$

The SU(2) gauge field associated with Eq. (2.38) is broken into an Abelian magnetic field due to the *effective* Higgs mechanism,

$$F_{ij} = \partial_i(\boldsymbol{\Phi}\cdot\boldsymbol{A}_j) - \partial_j(\boldsymbol{\Phi}\cdot\boldsymbol{A}_i) + 2\boldsymbol{\Phi}\cdot(\partial_i\boldsymbol{\Phi}\times\partial_j\boldsymbol{\Phi}), \tag{2.46}$$

$$B_i = \frac{1}{2}\varepsilon_{ijk}F_{jk} = \frac{R_i}{2R^3}, \tag{2.47}$$

where $\boldsymbol{\Phi} = \boldsymbol{\Phi}_H/|\boldsymbol{\Phi}_H|$. Eq. (2.47) is the magnetic field of a Dirac monopole.

An unsolved issue is the Bogomol'nyi relation [43, 97]. For the non-Abelian gauge field $\Omega_{ij} = \partial_i A_j - \partial_j A_i - i[A_i, A_j]$, and the covariant derivative $\mathcal{D}_i = \partial_i - i[A_i,\ ]$, it is straightforward to derive

$$\Omega_{ij} = \frac{1}{2}\varepsilon_{ijk}[\mathcal{D}_k\phi_H - \frac{|\tilde{\gamma}| + \sqrt{|\tilde{\gamma}|^2 + R^2}}{(|\tilde{\gamma}| + R^2)^{3/2}}\sigma_k]. \tag{2.48}$$

If not were the last term, Eq. (2.48) reproduces the Bogomol'nyi relation. One can show that only for a profile function $\xi(R) = 2R/\sinh(R)$ (the case of a true 't Hooft-Polyakov monopole) that the last term vanishes. While our $\xi(R)$ asymptotically resembles $2R/\sinh(R)$, it gives a different profile for finite R. As a result, the last term in Eq. (2.48) vanishes only when $R \to \infty$.

To close the argument of the above two sections, we summarize the coupled dynamics of spin and orbit as follows:

$$\dot{\boldsymbol{s}} = (1-\xi^2)(\boldsymbol{s}\cdot\boldsymbol{n})\dot{\boldsymbol{n}}, \tag{2.49a}$$

$$\dot{\boldsymbol{k}} = -\frac{1}{2}\boldsymbol{n}\cdot(\nabla\boldsymbol{n}\times\dot{\boldsymbol{s}}), \tag{2.49b}$$

$$\dot{\boldsymbol{r}} = -\partial_{\boldsymbol{k}}\varepsilon - \frac{1}{2}(\boldsymbol{s}\times\boldsymbol{n})\cdot\dot{\boldsymbol{n}}\;\partial_{\boldsymbol{k}}\ln\xi, \tag{2.49c}$$

where $\dot{\boldsymbol{n}} = \partial_t\boldsymbol{n} + (\dot{\boldsymbol{r}}\cdot\nabla)\boldsymbol{n}$, and we have omitted subscript c of $\boldsymbol{r}_c$ and $\boldsymbol{k}_c$ for convenience of following discussions. Equations. (2.49) are the fundamental equations of motion of a conduction electron in a slowly-varying AF texture, which are represented by joint evolutions of three variables $(\boldsymbol{s},\boldsymbol{k},\boldsymbol{r})$.

In real materials with impurities, equations (2.49) are valid so long as spin coherence length is as large as, if not more than, the typical width of the texture. While this is quite true in ferromagnetic materials, its validity in AF materials awaits experimental verification. At extremely low temperatures, spin-flip scattering is dominated by magnetic impurities which can be made negligibly small in clean samples. Besides, spin-independent scattering processes (*e.g.*, electron-phonon scattering) do not destroy our essential conclusions if $\dot{\boldsymbol{r}}$ is understood as the drift velocity of carriers. We mention that AF spintronics is an emerging field where very little is known. While it shares some similarities with the established ferromagnetic spintronics, it is not always correct to copy ideas from ferromagnetic systems.

2.4 Domain Wall Magnetoresistance

Consider a spiraling AF texture sandwiched by two ferromagnetic layers, see Fig. 2.4. This magnetic structure has been realized in Co/FeMn/Py trilayers in a recent experiment [137], where the ferromagnetic order of Co layer is nearly fixed but that of Py can be rotated by external magnetic field. The AF order is dragged into a spiral due to the exchange bias effect on the AF/F interfaces. The layer thickness of FeMn is roughly $10 \sim 20$ nm and can be made even larger, which far exceeds the lattice constant thus adiabatic approximation is valid; Meanwhile, typical spin coherence length is larger than the layer thickness at low temperatures so that spin evolution is governed by Eq. (2.19).

When an electron flows from top to bottom with applied current, the top ferromagnetic layer polarizes its spin so that it enters the A sub-band across the interface. According to Eq. (2.19), the physical spin orientation of the electron after passing through the AF layer is rotated by $\Pi = \pi - \arctan[\xi \tan \xi\pi]$ if $\xi < \frac{1}{2}$, and $\Pi = -\arctan[\xi \tan \xi\pi]$ is $\xi > \frac{1}{2}$. This is a topological result that only depends on the initial and final directions of $\boldsymbol{n}$, but is *independent* of the texture's profile detail. When $\xi \to 0$, Π reduces to π, which means the electron spin follows $\boldsymbol{n}$ and remains in the A sub-band, thus it flows into the bottom ferromagnetic layer with a lower resistance; in the $\xi \to 1$ limit, Π vanishes and the electron completely evolves into the B sub-band thus experiencing a higher resistance. For an arbitrary ξ and an arbitrary total rotation of the spiral denoted by Φ, the electron will partially evolve into

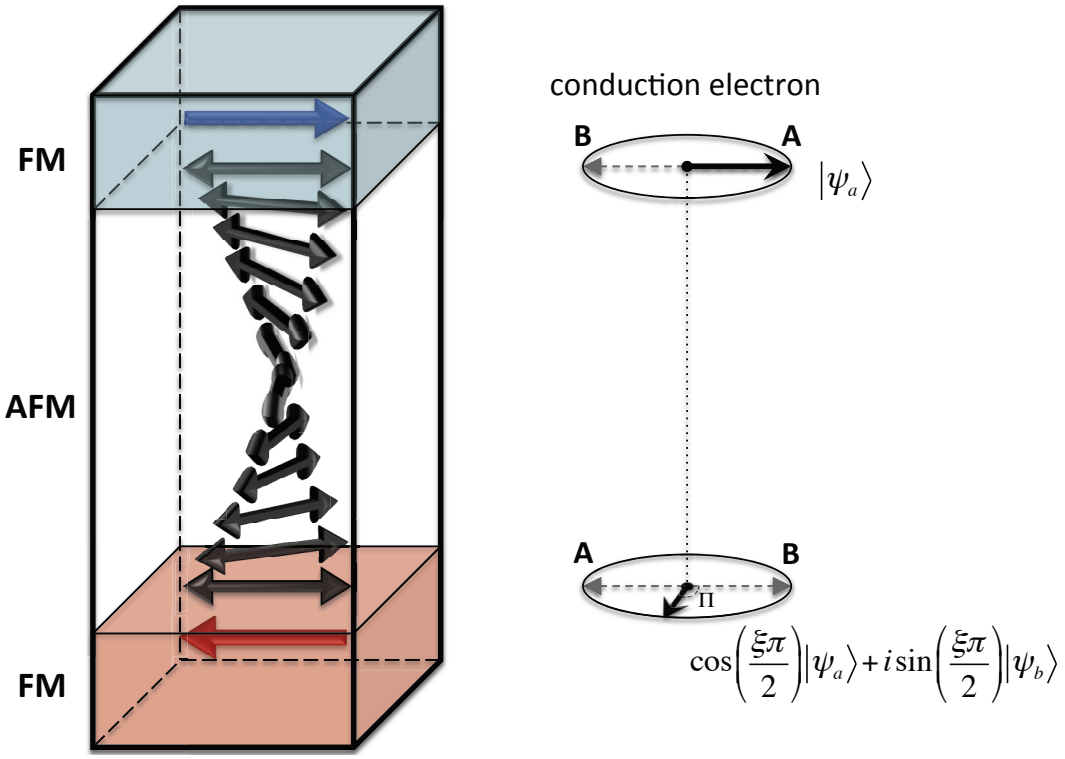

Figure 2.4: Left: F/AF/F trilayer with opposite ferromagnetic orientations on two sides. The black double arrows represent the A-B sublattices of the AF layer, which is dragged into a spiraling texture due to exchange bias on the interfaces. Right: incoming electrons only enter the A sub-band due to the upper ferromagnetic polarizer, the out-going electrons partially occupy the B sub-band depending on the value of ξ.

the B sub-band with the wave function $\cos(\xi\Phi/2)|\psi_a\rangle + i\sin(\xi\Phi/2)|\psi_b\rangle$, thus the total resistance is

$$\rho = \rho_0 + \frac{1}{2}\Delta\rho[1 - \cos(\xi\Phi)], \tag{2.50}$$

where ρ_0 is the intrinsic resistance of the AF texture itself, which depends monotonously but not too much on Φ. $\Delta\rho$ represents the magnetoresistance of the spin valve which is determined by material details of the two ferromagnetic layers and is independent of Φ. If Φ is increased beyond π, ρ will reach a maximum at $\Phi_m = \pi/\xi$ and then reduces. The resistance maximum, if observed, serves as an experimental verification of Eq. (2.19). Moreover, measuring Φ_m also enables us to find ξ without calculating the band structure.

We remark that the above results survive in the presence of diffusive processes so long as spin-flip scattering is ignored. The reason is that spin-independent scattering only deflects $\boldsymbol{k}$-space orbit, whereas the $\boldsymbol{s}$ dynamics is determined by the variation of $\boldsymbol{n}$ that is blind to $\boldsymbol{k}$ in one dimension. In addition, FeMn is a non-collinear antiferromagnet that has more than two sub-lattices. To test our theory unambiguously, we can replace FeMn by the collinear IrMn which is feasible for current technique. Moreover, we are aware of the experiment [10, 11] where the spiraling AF texture exhibits spatial *periodic* patterns, it provides a better way of realizing large $\Phi's$.

An experimental complication may arise from irregularities on the interface. Small grains are hard to avoid, which may reduce the effect predicted under a perfect assumption.

2.5 Proposed Experiment

The induced gauge fields Eq. (2.32) can be detected via similar technique as the spin-motive force experiment based on ferromagnetic materials. We learn from previous discussions a key property that the electron transport of an AF metal resembles that of a ferromagnet when ξ is small. In other words, when the spatial overlap of the two degenerate subbands is small, the AF can indeed be regarded as two ferromagnetic subsystems. The parameter ξ is a measure of how well the independence of the two subsystems is kept. From Eqs. (2.49), we see that the electron transport in AF just respects the rule $1 + 1 = 2(1 - \xi^2)$. The reduction by ξ^2 originates from the non-commutative or the non-Abelian feature of inter-sub-band dynamics.

In a recent experiment [136], a comb shaped permalloy is fabricated, where the shape anisotropy breaks the resonance condition of the material into two well-separated frequencies. When one of the two eigen-frequencies is being excited by external microwaves, the material exhibits both spatial texture and time variation. A careful look at the resonance geometry tells us that the spin-motive force is generated across the two leads, which results in a voltage drop that can be detected easily, see Fig. 2.5 (upper panel).

We propose a similar experiment to measure the effective electrical component of the non-Abelian Berry curvature in Eq. (2.32). As illustrated in the lower panel of Fig. 2.5, we replace the normal metal leads made up of AuPd in Ref. [136] by heavy metals with strong spin-orbit coupling, such as Pt or Au. When the left part of the antiferromagnet (*e.g.*, FeF_2 [79]) is driven

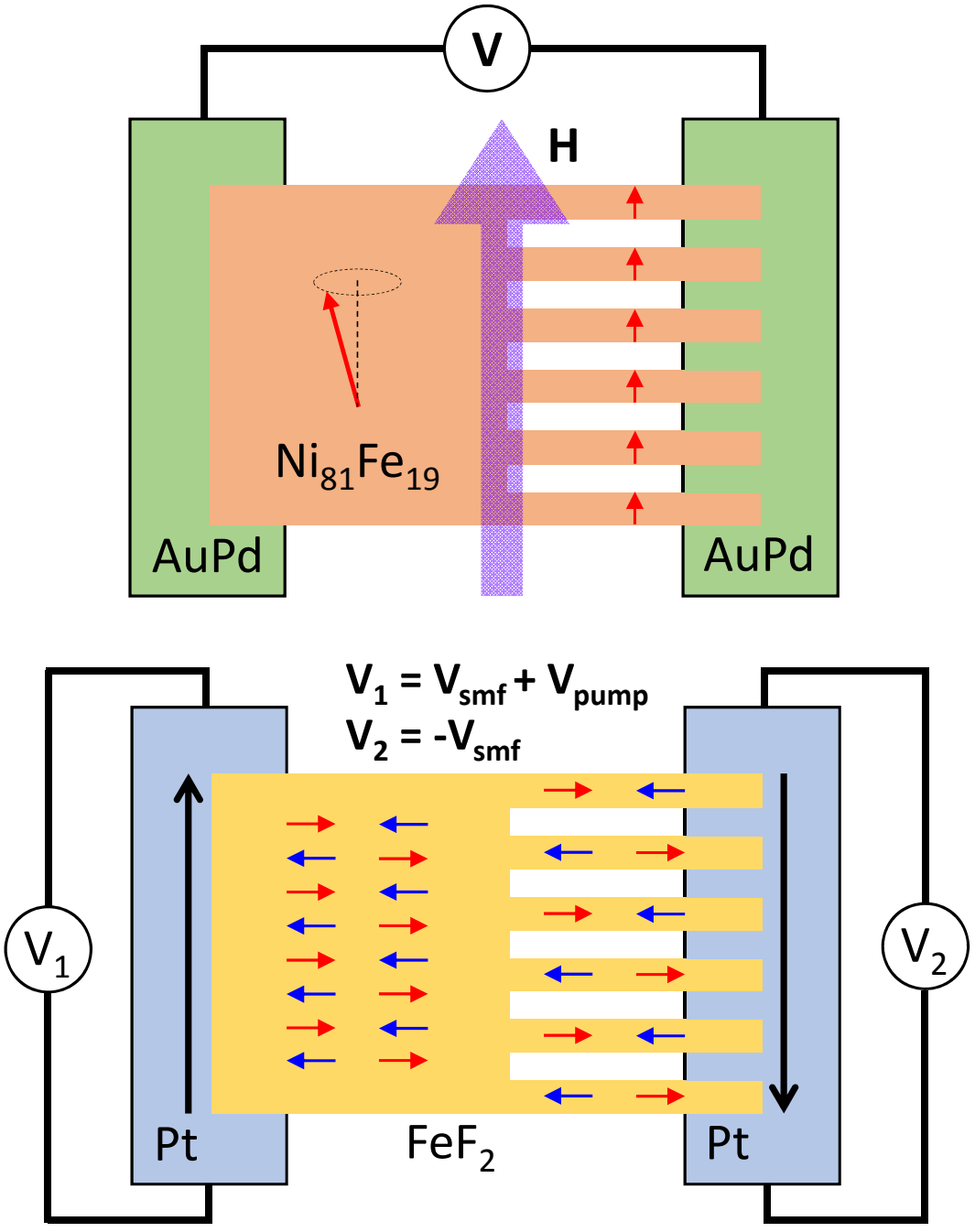

Figure 2.5: Schematics of spin-motive force experiments based on ferromagnet (upper panel) and antiferromagnet (lower panel).

into resonance (see details in the next chapter), electrons of opposite spins drift to different leads. Consequently, no charge voltage is generated between the two leads. Nevertheless, the spin-motive force in the antiferromagnet leads to a *pure spin voltage* between the two sides. When the spin accumulation is injected into the Pt leads on both sides, it generates two opposite transverse charge voltages as indicated by the black arrows in Fig. 2.5. This is due to the inverse spin Hall effect – a frequently used technique to measure spin injection. In this geometry, we can monitor either V_1 or V_2.

However, when the left part of the antiferromagnet is resonating with the microwave, the measured voltage V_1 also includes the contribution from spin-pumping. The spin-pumping effect on the N/AF interface is studied in great detail in the next chapter; here we only need to note that it is an interface effect independent of the bulk. So the difference between the magnitudes of V_1 and V_2 gives the contribution of spin-pumping. If the antiferromagnet is insulating, $V_1 = V_{pump}$ and $V_2 \approx 0$ since the spin-motive force only exists in metals and is a pure bulk effect.

Closing remarks. In this chapter, we find that a slowly varying AF texture renders adiabatic dynamics of conduction electrons, which are described by three coupled equations of motion [Eqs. (2.49)]. Quite different from the ferromagnetic case, the adiabaticity in AF materials does not imply strict alignment between conduction electron spins and the profile of background texture. Instead, the adiabatic spin evolution is a superposition of a motion following the background order plus a motion on a prolate spheroid

attached to the local order, where the latter originates from internal dynamics between degenerate bands. The overall motion of the spin is still geometric; it can be attributed to the accumulation of a SU(2) non-Abelian Berry phase originating from the gauge flux of an effective 't Hooft-Polyakov monopole in the parameter space.

The corresponding orbital dynamics shares some similarities with ferromagnetic materials in that the $\boldsymbol{k}$-space dynamics can be described by an effective Lorentz force equation. However, two prominent differences in the orbital dynamics distinguish an AF system from its ferromagnetic counterpart: first, the gauge charge is dynamical rather than constant, by which spin and orbital motions no longer separate; second, the group velocity is renormalized by a spin-dependent anomalous velocity, which is quite different from what has been studied before.

Theory developed in this chapter lays the foundation for charge and spin transports in textured AF systems, which will be applied to real materials in the future. The validity of the theory needs to be tested experimentally since available data on AF spintronic materials are very rare. This chapter solves only the first half of the whole story; the other half, *i.e.*, the converse effect regarding the back-reaction of current on background AFM order, is discussed in the following chapter.

Chapter 3

Staggered Field Dynamics

[1]This chapter solves the reciprocal phenomenon of the electron transport studied in the previous chapter. By varying the effective system Lagrangian that incorporates the conduction electrons and the background antiferromagnet, we derive the current-induced dynamics of the staggered field from a microscopic point of view. The formalism in this chapter is valid in the long wave length limit, *i.e.*, the pitch of spatial modulation of the background texture far exceeds the lattice spacing.

3.1 Nonlinear Sigma Model

The dynamics of an AF system can be described, in principle, by the Heisenberg Hamiltonian. However, solving the AF Heisenberg model is usually elusive and requires special computational technique. This motivates people to search for effective models that captures the essential physics while providing mathematical clarity.

In the continuum limit, the long wave-length (low energy) dynamics of

[1]The contents of this chapter are partly based on the article: R. Cheng and Q. Niu, *Dynamics of antiferromagnets driven by spin current*, Phys. Rev. B, **89**, 081105(R) (2014).

an AF system is effectively characterized by the nonlinear sigma model [3,30, 37,38,91,119], which was initially proposed to interpret the alternating gapped and gapless behavior of one dimensional quantum Heisenberg AF chain with respect to the spin magnitude of local moments. Here, we will not digress too much into this picture, but instead introduce necessary mathematical tools that are used in the following sections.

As shown in Section 1.3, the action of a local magnetic moment includes an exchange term and a WZ term. Consider a one dimensional AF chain with $J > 0$ and a total number of N atoms,

$$\mathcal{S} = s \sum_{j=1}^{N} \mathcal{S}_{WZ}[\boldsymbol{m}(j)] - Js^2 \int_0^T \mathrm{d}t \sum_{j=1}^{N} \boldsymbol{m}(j,t) \cdot \boldsymbol{m}(j+1,t), \tag{3.1}$$

where s denotes the magnitude of local spins. The staggered AF chain requires that $\boldsymbol{m}(j) = (-1)^j \boldsymbol{n}(j)$, by which the exchange term becomes ferromagnetic. However, the WZ term distinguishes it from a true ferromagnet. The action written in terms of the staggered order parameter is

$$\mathcal{S}[\boldsymbol{n}] = s \sum_{j=1}^{N} (-1)^j \mathcal{S}_{WZ}[\boldsymbol{n}(j)] - \frac{Js^2}{2} \int_0^T \mathrm{d}t \sum_{j=1}^{N} [\boldsymbol{n}(j,t) - \boldsymbol{n}(j+1,t)]^2, \tag{3.2}$$

and the WZ term can be further expressed as

$$s \sum_{j=1}^{N} (-1)^j \mathcal{S}_{WZ}[\boldsymbol{n}(j)] = s \sum_{r=1}^{N/2} \left(\mathcal{S}_{WZ}[\boldsymbol{n}(2r)] - \mathcal{S}_{WZ}[\boldsymbol{n}(2r-1)] \right). \tag{3.3}$$

In view of $\boldsymbol{n} \cdot \boldsymbol{m} = 0$ and $n^2 + m^2 = 1$, we decompose the staggered field $\boldsymbol{n}$ in terms of its unit normal $\boldsymbol{N}$ and a small oscillatory part:

$$\boldsymbol{n}(j) = \boldsymbol{N}(j) \sqrt{1 - |\boldsymbol{m}(j)|^2} + (-1)^j a_0 \boldsymbol{m}(j), \tag{3.4}$$

where a_0 is the lattice constant. To the lowest order,

$$\begin{aligned}\boldsymbol{n}(2r)-\boldsymbol{n}(2r-1) &= \boldsymbol{N}(2r)-\boldsymbol{N}(2r-1)+a_0[\boldsymbol{m}(2r)+\boldsymbol{m}(2r-1)] \\ &= a_0[\partial_x\boldsymbol{N}(2r)+2\boldsymbol{m}(2r)]+h.o., \end{aligned} \tag{3.5}$$

so that the WZ term Eq. (3.3) becomes

$$\begin{aligned} s\sum_{j=1}^{N}(-1)^j\mathcal{S}_{WZ}[\boldsymbol{n}(j)] &= s\sum_{r=1}^{N/2}\int_0^T \mathrm{d}t\delta\boldsymbol{n}(2r,t)\cdot[\boldsymbol{n}(2r,t)\times\partial_t\boldsymbol{n}(2r,t)] \\ &\approx sa_0\sum_{r=1}^{N/2}\int_0^T \mathrm{d}t[\partial_x\boldsymbol{N}(2r)+2\boldsymbol{m}(2r)]\cdot[\boldsymbol{N}(2r,t)\times\partial_t\boldsymbol{N}(2r,t)], \end{aligned} \tag{3.6}$$

where $\delta S_{WZ}=\int \mathrm{d}t\delta\boldsymbol{n}\cdot(\boldsymbol{n}\times\partial_t\boldsymbol{n})$ has been used. In the continuum limit ($a_0\to 0$), we can further simplify the WZ term as

$$\begin{aligned} & s\sum_{j=1}^{N}(-1)^j\mathcal{S}_{WZ}[\boldsymbol{n}(j)] \\ &\qquad \approx \frac{s}{2}\int \mathrm{d}t\mathrm{d}x[\boldsymbol{N}\cdot(\partial_t\boldsymbol{N}\times\partial_x\boldsymbol{N})+2\boldsymbol{m}\cdot(\boldsymbol{N}\times\partial_t\boldsymbol{N})]. \end{aligned} \tag{3.7}$$

Similarly, the exchange term becomes $\frac{Js^2a_0}{2}\int \mathrm{d}t\mathrm{d}x[(\partial_x\boldsymbol{N})^2+4\boldsymbol{m}^2]$. Thus the effective Lagrangian density consists of four terms

$$\begin{aligned}\mathcal{L}(\boldsymbol{N},\boldsymbol{m}) = s\boldsymbol{m}\cdot(\boldsymbol{N}\times\partial_t\boldsymbol{N}) &- 2a_0Js^2\boldsymbol{m}^2 \\ &-\frac{a_0Js^2}{2}(\partial_x\boldsymbol{N})^2+\frac{s}{2}\boldsymbol{N}\cdot(\partial_t\boldsymbol{N}\times\partial_x\boldsymbol{N}), \end{aligned} \tag{3.8}$$

and the action is understood as $\mathcal{S}[\boldsymbol{N},\boldsymbol{m}]=\int \mathrm{d}t\mathrm{d}x\mathcal{L}(\boldsymbol{N},\boldsymbol{m})$. To obtain the effective dynamics in terms of $\boldsymbol{N}$ alone, we integrate out the small canting field $\boldsymbol{m}(x,t)$, and define the effective action by

$$\int \mathcal{D}\boldsymbol{N}\mathcal{D}\boldsymbol{m}e^{-\mathcal{S}[\boldsymbol{N},\boldsymbol{m}]}=\int \mathcal{D}\boldsymbol{N}\delta(N^2-1)e^{-\mathcal{S}_{\mathrm{eff}}[\boldsymbol{N}]}, \tag{3.9}$$

where the integration over $\boldsymbol{m}$ is a Gaussian integral and can be performed analytically. In the new action $\mathcal{S}_{\text{eff}}[\boldsymbol{N}] = \int \mathrm{d}t\mathrm{d}x\mathcal{L}_{\text{eff}}(\boldsymbol{N})$, the effective Lagrangian density reads

$$\mathcal{L}_{\text{eff}}(\boldsymbol{N}) = \frac{1}{2g}\left[\frac{1}{c}(\partial_t \boldsymbol{N})^2 - c(\partial_x \boldsymbol{N})^2\right] + \frac{s}{4}\varepsilon_{\mu\nu}\boldsymbol{N}\cdot(\partial_\mu \boldsymbol{N}\times\partial_\nu \boldsymbol{N}), \qquad (3.10)$$

where $c = 2a_0 sJ/\hbar$ is the spin wave velocity, and $g = 2\sqrt{d}/\hbar s$. The last term is a topological term in the sense that it does NOT depend on the metric of space-time, but is only determined by the total antisymmetric tensor $\varepsilon_{\mu\nu}$. Eq. (3.10) can be easily generalized into higher dimensions, where $(\partial_x \boldsymbol{N})^2$ is replaced by $|\nabla \boldsymbol{N}|^2$ [38, 91, 119, 129, 142].

The subtle physics underlying Eq. (3.10) is: the staggered field renders the canceling of Berry phase of neighboring spins if $\boldsymbol{N}$ is homogeneous in space. However, when $\boldsymbol{N}$ has smooth spatial modulation, a term $\partial_x \boldsymbol{N}$ is induced by the Berry phase which does not cancel. In other word, the cancellation of WZ term $\boldsymbol{m}\cdot(\partial_\mu \boldsymbol{m}\times\partial_\nu \boldsymbol{m})$ of individual moments is accompanied by the introduction of the term $\boldsymbol{N}\cdot(\partial_\mu \boldsymbol{N}\times\partial_\nu \boldsymbol{N})$ that governs the large scale variation of the texture. The nonlinear sigma model (NLSM) described by Eq. (3.10) has many equivalent forms, such as the CP^1 model that has been widely studied in high energy physics [3, 91, 119]. A strict proof of the equivalence between NLSM and the CP^1 model is provided in Appendix A.

While the topological term substantially changes the low energy excitations through *global* effect, it does not affect *local* dynamics of the staggered field, thus in the following sections we will not discuss it any more.

3.2 Staggered Field Dynamics

Many recent experiments [84, 122, 128] and numerical simulations [49, 131, 135] indicate that AF materials exhibit current-induced effects with similar orders of magnitude, if not stronger than, as those in ferromagnets. Those pioneering investigations ushered the field of AF spintronics [64] and propelled AF materials as promising candidates for real applications. From a theoretical point of view, AF dynamics driven by charge current has been studied both phenomenologically [39, 120] and microscopically [40, 76, 102, 103]. In the former, both adiabatic torque by ac current and non-adiabatic torque by dc current are predicted, but an adiabatic effect in the dc limit is absent; in the latter, adiabatic torque is generated by dc current, but the result includes only second-order derivatives in space and time. Case becomes rather unclear when turning to spin current, which can be realized by attaching a ferromagnetic polarizer to the system. This problem has only been explored phenomenologically [32–34] and no microscopic study is yet available. Even in the phenomenological model, it is the induced ferromagnetic moments on top of the AF background that respond to the spin current, which is a higher order effect that drives the AF staggered order *indirectly*. Is a spin current able to drive the staggered order *directly* without the participation of induced ferromagnetic moments?

Equipped with the effective gauge theory on the adiabatic electron dynamics studied in the preceding chapters, we answer this question in a reciprocal sense of the electron dynamics.

3.2.1 Reaction of A Single Electron

The interaction term $\mathcal{L}_{int}$ is constructed by summing over contributions from individual electrons: $\mathcal{L}_{int} = \sum_\lambda \int \mathrm{d}^d\boldsymbol{k} L_\lambda(\boldsymbol{k}) f_\lambda(\boldsymbol{k})$, where $L_\lambda(\boldsymbol{k})$ is the Lagrangian of an electron with momentum $\boldsymbol{k}$ in band λ, and $f_\lambda(\boldsymbol{k})$ is the distribution function. As was shown in the Chapter one and Ref. [18, 20], a slowly-varying $\boldsymbol{n}(\boldsymbol{r}, t)$ in space-time admits an effective gauge theory, which is described by the single electron Lagrangian

$$L_e = \frac{\hbar}{2}\dot{r}_\mu[-c_1\xi\sin\theta\partial_\mu\varphi + c_2\xi\partial_\mu\theta + c_3\cos\theta\partial_\mu\varphi], \tag{3.11}$$

where $c_i = \tilde{c}^\dagger\tau_i\tilde{c}$ is the iso-spin component, and $\mu = \{t, \boldsymbol{r}\} = \{t, x, y, z\}$ labels the spacetime. The 4-velocity $\dot{r}_\mu \equiv \{0, \dot{\boldsymbol{r}}\} = \{0, \boldsymbol{v}_e\}$, where $\boldsymbol{v}_e = \boldsymbol{v}_e(\boldsymbol{k}) = \frac{1}{\hbar}\frac{\partial\varepsilon}{\partial\boldsymbol{k}}$ is the electron group velocity. Now, the reaction of the electron on the background is calculated through the variational derivative

$$\frac{\delta L_e}{\delta\boldsymbol{n}} = \frac{\delta L_e}{\delta\theta}\hat{\theta} + \frac{1}{\sin\theta}\frac{\delta L_e}{\delta\varphi}\hat{\varphi}, \tag{3.12}$$

where the components in spherical coordinates are

$$\begin{aligned}\frac{\delta L_e}{\delta\theta} &= \frac{\partial L_e}{\partial\theta} - \partial_\mu\left[\frac{\partial L_e}{\partial(\partial_\mu\theta)}\right] \\ &= -\frac{\hbar}{2}\dot{r}_\mu[\xi c_1\cos\theta\partial_\mu\varphi + c_3\sin\theta\partial_\mu\varphi] - \frac{\hbar}{2}\xi\dot{r}_\mu\left[\frac{\partial c_2}{\partial\theta}\partial_\mu\theta + \frac{\partial c_2}{\partial\varphi}\partial_\mu\varphi\right],\end{aligned} \tag{3.13a}$$

$$\begin{aligned}\frac{\delta L_e}{\delta\varphi} &= \frac{\partial L_e}{\partial\varphi} - \partial_\mu\left[\frac{\partial L_e}{\partial(\partial_\mu\varphi)}\right] \\ &= \frac{\hbar}{2}\xi\dot{r}_\mu\left[\left(\frac{\partial c_1}{\partial\theta}\partial_\mu\theta + \frac{\partial c_1}{\partial\varphi}\partial_\mu\varphi\right) + c_1\cos\theta\partial_\mu\theta\right] \\ &\qquad - \frac{\hbar}{2}\dot{r}_\mu\left[\left(\frac{\partial c_3}{\partial\theta}\partial_\mu\theta + \frac{\partial c_3}{\partial\varphi}\partial_\mu\varphi\right)\cos\theta - c_3\sin\theta\partial_\mu\theta\right].\end{aligned} \tag{3.13b}$$

To proceed, we need to relate c_i to θ and φ. Resorting to the dynamics between a and b sub-bands, which is obtained by varying the system Lagrangian with respect to $c_{1,2,3}$ in Chapter One, we have the following relations:

$$\mathrm{d}c_1 = c_2 \cos\theta \mathrm{d}\varphi - \xi c_3 \mathrm{d}\theta \tag{3.14a}$$

$$\mathrm{d}c_2 = -c_1 \cos\theta \mathrm{d}\varphi - \xi c_3 \sin\theta \mathrm{d}\varphi \tag{3.14b}$$

$$\mathrm{d}c_3 = \xi(c_1 \mathrm{d}\theta + c_2 \sin\theta\varphi) \tag{3.14c}$$

these equations enable us to take partial derivatives of $c_{1,2,3}$ with respect to the two spherical angles θ and φ,

$$\frac{\partial c_1}{\partial\theta} = -\xi c_3, \quad \frac{\partial c_1}{\partial\varphi} = c_2\cos\theta, \tag{3.15}$$

$$\frac{\partial c_2}{\partial\theta} = 0, \qquad \frac{\partial c_2}{\partial\varphi} = -c_1\cos\theta - \xi c_3 \sin\theta, \tag{3.16}$$

$$\frac{\partial c_3}{\partial\theta} = \xi c_1, \qquad \frac{\partial c_3}{\partial\varphi} = \xi c_2 \sin\theta. \tag{3.17}$$

Substituting them into Eq. (3.13a) and Eq. (3.13b) ends up with two simple and elegant expressions,

$$\frac{\delta L_e}{\delta\theta} = -\frac{\hbar}{2}(1-\xi^3)c_3\sin\theta\partial_\mu\varphi, \quad \frac{\delta L_e}{\delta\varphi} = \frac{\hbar}{2}(1-\xi^3)c_3\sin\theta\partial_\mu\theta, \tag{3.18}$$

hence the variational derivative Eq. (3.12) finally becomes

$$\begin{aligned}\frac{\delta L_e}{\delta \boldsymbol{n}} &= \frac{\hbar}{2}(1-\xi^2)c_3\dot{r}_\mu[-\sin\theta\partial_\mu\varphi\hat{\theta} + \partial_\mu\theta\hat{\varphi}] = \frac{\hbar}{2}(1-\xi^2)(\boldsymbol{s}\cdot\boldsymbol{n})\dot{r}_\mu(\boldsymbol{n}\times\partial_\mu\boldsymbol{n}), \\ &= \pm\frac{\hbar}{2}(1-\xi^2)\boldsymbol{n}\times\left[\partial_t\boldsymbol{n} + (\boldsymbol{v}_e\cdot\nabla)\boldsymbol{n}\right],\end{aligned} \tag{3.19}$$

where $+(-)$ is for the a (b) sub-band. In deriving the second step, we have used $c_3 = s_3 = \boldsymbol{s}\cdot\boldsymbol{n}$ (see Eq. (2.12c)).

3.2.2 Spin Diffusion

To derive the reaction of a spin current, we need to sum up all individual electrons. However, when an ensemble of electrons are injected into the AF texture, a serious problem arises: spin polarization of the current will relax due to spin-flip scattering. Recall the spatial overlap between the two degenerate bands Eq.(2.7)

$$\xi(\boldsymbol{k}) = \langle A(\boldsymbol{k}) | B(\boldsymbol{k}) \rangle = \frac{|\gamma(\boldsymbol{k})|}{\sqrt{J^2 + |\gamma(\boldsymbol{k})|^2}} = \frac{\sqrt{\varepsilon^2 - J^2}}{\varepsilon}, \tag{3.20}$$

which is determined by the ratio of t/J and the position of Fermi level. In AF metals, the exchange coupling is as large as that in ferromagnetic metals, $J \sim 1\text{eV}$, which is supposed to be larger than t. If the Fermi level lies in the middle of either the upper band or the lower band: $\xi_F^2 \sim 20\%$ for $J = 2t$, and $\xi_F^2 < 1\%$ for $J = 10t$, thus $\xi^2 \in (0, \xi_F^2)$ is restricted to a small range close to zero. The smallness of ξ^2 leads to two important consequences:

(1) Coherent dynamics between a and b sub-bands is suppressed. The semi-classical evolution of the physical spin of an electron wave packet respects $\mathrm{d}\boldsymbol{s} = (1 - \xi^2)(\boldsymbol{s} \cdot \boldsymbol{n})\mathrm{d}\boldsymbol{n}$. When $\xi^2 \ll 1$, we have demonstrated in Section 2.2.2 that $\boldsymbol{s}$ tends to following $\boldsymbol{n}$, thus $\boldsymbol{s} \cdot \boldsymbol{n} \approx$ constant in the absence of spin relaxation. In other word, if an electron initially belongs to one of the two sub-bands, it will stay there forever and will not hop to the other unless spin-flip scattering is introduced.

(2) Spin-flip scattering due to impurities is also highly suppressed. An attached ferromagnetic polarizer injects spin imbalance into a metal with no

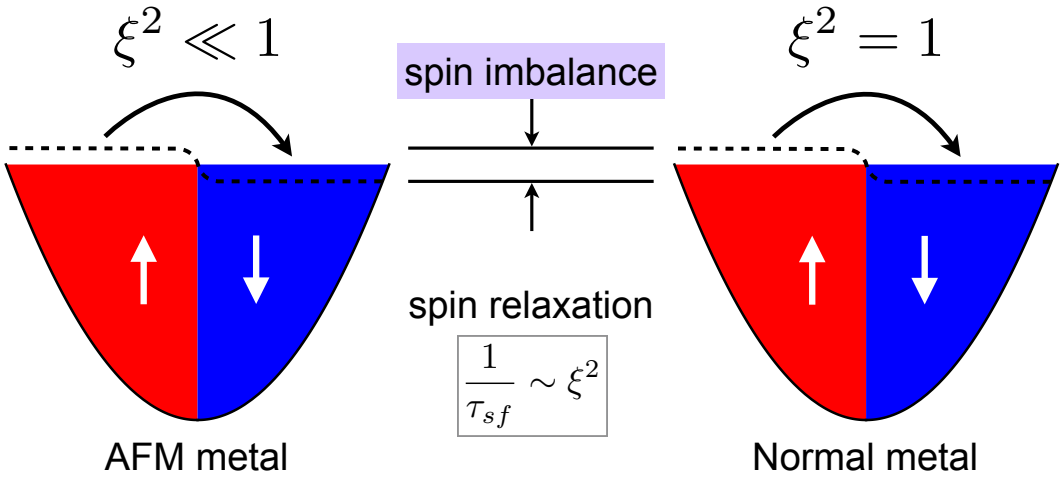

Figure 3.1: While opposite (local) spin orientations are locked with different spatial patterns in an AF metal, no such difference is present in a normal metal. As a result, normal metals have effectively $\xi^2 = 1$. Since spin relaxation rate is proportional to ξ^2, AF metals have relatively longer spin diffusion lengths.

macroscopic magnetization when current is applied. This spin imbalance will relax through many different mechanisms, for example, spin-orbital coupling, spin-dependent impurity scattering, *etc.* In normal metals, spin relaxation rate is proportional to $|\langle\uparrow|H_{sf}|\downarrow\rangle|^2$ where H_{sf} is the spin-flip Hamiltonian. In AF metals, however, opposite spin orientations are associated with different spatial wave functions, thus the spin relaxation rate should be

$$\begin{aligned}\frac{1}{\tau_{sf}} \sim |\langle u_a|H_{sf}|u_b\rangle|^2 &= |\langle A| \otimes \langle\uparrow|H_{sf}|\downarrow\rangle \otimes |B\rangle|^2 \\ &= \xi^2 |\langle\uparrow|H_{sf}|\downarrow\rangle|^2. \end{aligned} \tag{3.21}$$

Given the same H_{sf} and the same density of states around the Fermi energy, spin relaxation rate in an AF metal will be much smaller than that in a normal metal, because it is suppressed by the smallness of ξ^2, see Fig. 3.1 for

an illustration. As a result, **AF metals are good spin-preservers**, which seems to be counter-intuitive without solving the band structure.

In fact, we can regard the normal metal as a special case of AF metal with $\xi = 1$. This is because $\xi \to 1$ only when $J \to 0$; without J, conduction electrons are not able to distinguish A and B sub-lattices thus they cannot see the AF background. Based on the above analysis, we assume the spin diffusion length to be sufficiently large that exceeds the system size.

Similar to the treatment of a F/N interface, we solve the spin diffusion equation [65, 104] for a F/AF interface assuming perfect alignment between the ferromagnetic polarizer and the staggered order parameter (can be realized by exchange bias effect)

$$\nabla^2(\mu_\uparrow - \mu_\downarrow) = \frac{1}{\lambda^2}(\mu_\uparrow - \mu_\downarrow). \tag{3.22}$$

Here, λ denotes the spin diffusion length, $\mu_\uparrow$ and $\mu_\downarrow$ are the electrochemical potentials of local spin up and spin down bands.

We should note that *for the left (right) case of Fig. 3.2, $\mu_\uparrow$ ($\mu_\downarrow$) is identified with μ_a on the AF side.* Let us focus on the left case, the associated current is $j_{\uparrow,\downarrow} = \frac{\sigma_{\uparrow,\downarrow}}{e}\frac{\partial}{\partial z}\mu_{\uparrow,\downarrow}$, where $\sigma_{\uparrow,\downarrow}$ represents the conductivity. By taking the continuity and boundary conditions

$$\mu^F_{\uparrow,\downarrow}(0) = \mu^{AF}_{\uparrow,\downarrow}(0), \tag{3.23}$$

$$j^F_{\uparrow,\downarrow}(0) = j^{AF}_{\uparrow,\downarrow}(0), \tag{3.24}$$

$$\mu_\uparrow(\pm\infty) = \mu_\downarrow(\pm\infty), \tag{3.25}$$

we obtain the spin current and the potential drop on the interface

$$j_s = j_\uparrow(0) - j_\downarrow(0) = \mathcal{P} j_c \frac{1}{1+\beta(1-\mathcal{P}^2)}, \tag{3.26}$$

$$\begin{aligned}\Delta\mu &= \frac{1}{2}\left[\mu_\uparrow^F(0) + \mu_\downarrow^F(0) - (\mu_\uparrow^{AF}(0) + \mu_\downarrow^{AF}(0))\right] \\ &= \mathcal{P}^2 j_c \frac{e\lambda_{AF}}{\sigma_{AF}[1+\beta(1-\mathcal{P}^2)]},\end{aligned} \tag{3.27}$$

where $\mathcal{P} = \frac{\sigma_\uparrow^F - \sigma_\downarrow^F}{\sigma_\uparrow^F + \sigma_\downarrow^F}$ is the conductivity polarization of the polarizer. The parameter $\beta = \frac{\lambda_{AF}}{\lambda_F}\frac{\sigma_F}{\sigma_{AF}}$, where $\sigma_F = \sigma_\uparrow^F + \sigma_\downarrow^F$ and $\sigma_{AF} = \sigma_\uparrow^{AF} + \sigma_\downarrow^{AF}$, is a factor that limits the injection efficiency of spin current. If the ferromagnetic polarizer is half metallic ($\mathcal{P} \sim 1$), β will not be a problem. However, there is no *direct* experimental evidence on λ_{AF}, but as explained just now, the AF background enforces a strong coupling between conduction electron spin and sublattice, thus spin-flip must be accompanied by sub-lattice transition (in fact, sub-band transition), the probability of which is quadratic in ξ (see Eq. (3.21)). As a result, λ_{AF} is substantially enlarged.

For current purpose, we just estimate λ_{AF} by typical spin diffusion length of normal metals, and assume $\sigma_{AF} \sim \sigma_F$. As a result, $\beta \sim 100$ and $\frac{\mathcal{P}^2}{1+\beta(1-\mathcal{P}^2)} \sim 0.01$ for $\mathcal{P} \sim 0.7$. The accumulation of spin density on the interface is $\rho_s = \mathcal{N}(\varepsilon_F)\Delta\mu$, where $\mathcal{N}(\varepsilon_F)$ is the density of states at the Fermi energy. For system size much smaller than λ_{AF}, ρ_s preserves through the entire system, so does j_s. We define the effective electron velocity as

$$v_s = \frac{j_s}{e\rho_s} = \frac{\sigma_{AF}}{e^2\mathcal{N}(\varepsilon_F)\lambda_{AF}\mathcal{P}}, \tag{3.28}$$

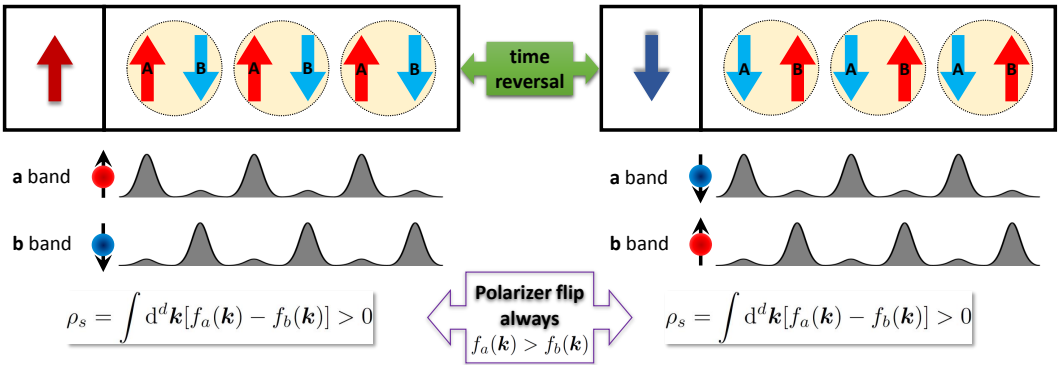

Figure 3.2: Magnetic moment of A sublattice is pinned along the polarizer. Under time reversal operation, not only AF moments flip sign, but the orientation of the polarizer switches also. Therefore, ρ_s defined in Eq. (3.29) is kept the same, *i.e.*, the polarizer always populate the a-subband. For specific wave functions of a and b subbands, see Section 2.1.

which is a system parameter independent of j_c. In typical AF metals with collinear order [52, 121], $\mathcal{N}(\varepsilon_F)$ is roughly $0.2 \sim 0.5$ states/(eV $\cdot$ atom), $\sigma_{AF} \sim 2.5 \times 10^4$ S/cm at room temperature, thus v_s is of order 10^5 cm/s. As $\sigma_{AF} \sim T$, and λ_{AF} increases with decreasing temperature, v_s can reach $10^6 \sim 10^7$ cm/s around 10K. The above results can be easily generalized to d dimensions.

3.2.3 Equations of Motion

Assume the polarizer pins the magnetic moment of A-sublattice through the exchange bias effect. Microscopically, the spin and the spin current densities **with respect to the local staggered order** (or equivalently, the polarizer direction, see Fig. 3.2) are defined as

$$\rho_s = \int \mathrm{d}^d\boldsymbol{k}[f_a(\boldsymbol{k}) - f_b(\boldsymbol{k})], \qquad \boldsymbol{j}_s = \int \mathrm{d}^d\boldsymbol{k}[f_a(\boldsymbol{k}) - f_b(\boldsymbol{k})]\boldsymbol{v}_e(\boldsymbol{k}), \tag{3.29}$$

where f_a and f_b are distribution functions of the two sub-bands. The $\mathcal{L}_{int}$ we seek is constructed by summing over each individual electron: $\mathcal{L}_{int} = \sum_{\lambda=a,b} \int \mathrm{d}^d \boldsymbol{k} L_\lambda(\boldsymbol{k}) f_\lambda(\boldsymbol{k})$. Regarding Eq. (3.19) and (3.29), and approximate ξ by its value at Fermi energy ξ_F (at low temperatures), we obtain

$$\begin{aligned} \frac{\delta \mathcal{L}_{int}}{\delta \boldsymbol{n}} &= \sum_{\lambda=a,b} \int \mathrm{d}^d \boldsymbol{k} \frac{\delta L_\lambda}{\delta \boldsymbol{n}} f_\lambda(\boldsymbol{k}) \\ &= \frac{\hbar}{2}(1-\xi_F^2)\boldsymbol{n} \times [\rho_s \frac{\partial \boldsymbol{n}}{\partial t} + (\boldsymbol{j}_s \cdot \nabla)\boldsymbol{n}], \end{aligned} \tag{3.30}$$

where attention should be paid that the sign of ρ_s and $\boldsymbol{j}_s$ is determined with respect to $\boldsymbol{n}$, not a global axis.

We are ready to derive the current-induced staggered field dynamics. The total Lagrangian for the system is

$$L = \int \mathrm{d}^d r \mathcal{L} = \int \mathrm{d}^d r (\mathcal{L}_n + \mathcal{L}_{int}), \tag{3.31}$$

with d being the dimensionality. $\mathcal{L}_n$ describes the AF background, which is derived as the NLSM in the Section 3.1. In the exchange limit, $\boldsymbol{n} \approx 1$ thus we replace the unit vector $\boldsymbol{N}$ by the staggered field $\boldsymbol{n}$ in Eq. (3.10). As we only care about the local dynamics, the topological term is ignored,

$$\mathcal{L}_n = \frac{1}{2g}[\frac{1}{c}(\partial_t \boldsymbol{n})^2 - c|\nabla \boldsymbol{n}|^2 - \frac{\omega_0^2}{c}\boldsymbol{n}_\perp^2], \tag{3.32}$$

where the coupling constant $g = 2\sqrt{d}a_0^{d-1}/\hbar s$; how it scales with the lattice constant a_0 depends sensitively on the dimensionality d. The last term in Eq. (3.32) describes the uniaxial anisotropy, where $\boldsymbol{n}_\perp$ includes components of

$\boldsymbol{n}$ perpendicular to the easy axis. Variation over the total Lagrangian density $\mathcal{L} = \mathcal{L}_n + \mathcal{L}_{int}$ with respect to $\boldsymbol{n}$ is

$$\begin{aligned}\frac{\delta\mathcal{L}}{\delta\boldsymbol{n}} &= \frac{\partial\mathcal{L}}{\partial\boldsymbol{n}} - \frac{\mathrm{d}}{\mathrm{d}t}\frac{\partial\mathcal{L}}{\partial\dot{\boldsymbol{n}}} - \nabla\cdot\frac{\partial\mathcal{L}}{\partial(\nabla\boldsymbol{n})} \\ &= \frac{-\hbar s}{2\sqrt{d}a_0^{d-1}c}(\partial_t^2\boldsymbol{n} - c^2\nabla^2\boldsymbol{n} + \omega_0^2\boldsymbol{n}_\perp) \\ &\qquad + \frac{2}{\hbar}(1-\xi_F^2)\boldsymbol{n}\times(\rho_s\partial_t + \boldsymbol{j}_s\cdot\nabla)\boldsymbol{n}. \end{aligned} \tag{3.33}$$

To account for the Gilbert damping, the Rayleigh's dissipation function $R = \int \mathrm{d}^d r\mathcal{R} = \alpha\int \mathrm{d}^d r\ \dot{\boldsymbol{n}}^2$ should be added; to enforce the constraint $\boldsymbol{n}^2 = 1$, the full variational equation should satisfy

$$\int \mathrm{d}^d r\delta\boldsymbol{n}\cdot\boldsymbol{n}\times\left[\frac{\partial\mathcal{R}}{\partial\dot{\boldsymbol{n}}} + \frac{\partial}{\partial t}\frac{\partial\mathcal{L}}{\partial\dot{\boldsymbol{n}}} + \nabla\cdot\frac{\partial\mathcal{L}}{\partial(\nabla\boldsymbol{n})} - \frac{\partial\mathcal{L}}{\partial\boldsymbol{n}}\right] = 0. \tag{3.34}$$

With these considerations, we finally obtain

$$\boldsymbol{n}\times[\partial_t^2\boldsymbol{n} - c^2\nabla^2\boldsymbol{n} + \omega_0^2\boldsymbol{n}_\perp] + \tilde{\alpha}\boldsymbol{n}\times\partial_t\boldsymbol{n} + \mathcal{G}(\rho_s\partial_t + \boldsymbol{j}_s\cdot\nabla)\boldsymbol{n} = 0, \tag{3.35}$$

where $\mathcal{G} = ca_0^{d-1}\sqrt{d}(1-\xi_F^2)/s$ and $\tilde{\alpha} = 2\alpha c\sqrt{d}a_s^{d-1}/\hbar s$. Eq. (3.35) is the central result of this section. Though similar to the adiabatic torque in ferromagnets, the term $\boldsymbol{j}_s\cdot\nabla\boldsymbol{n}$ does not behave as a torque, it is a driving force since the AF dynamics is second order in time derivative. Therefore, we interpret the last two terms as spin forcing terms.

It worths special attention that ρ_s defined in Eq. (3.29) is <u>even</u> under time reversal operation, it represents spin imbalance (in number density) with respect to the staggered field (or the polarizer), which is illustrated in Fig. 3.2. Under time reversal operation, $\boldsymbol{n}$ flips, but the polarizer is also reversed, thus

ρ_s is kept the same. In contrast, $\boldsymbol{j}_s$ is odd under time reversal operation. As a consequence, all terms in Eq. (3.35) respect the same time reversal symmetry except the Gilbert damping term. This is consistent with our starting point – electron dynamics is restricted to the adiabatic limit. All effects derived from it should be adiabatic and non-dissipative.

3.2.4 Charge Current v.s. Spin Current

We learn from previous discussions that only spin current produces adiabatic effect in the dc limit within first order space-time derivative, the three properties have been taken advantages of all together. In contrast, although a pure charge current is able to drive the staggered field dynamics of an antiferromagnet, either one of the three properties must be lost. Specifically, a pure charge current can generate: (i) non-adiabatic effect in the dc limit within first order [39, 120]; (ii) adiabatic effect via high frequency ac current within first order [39, 120]; (iii) adiabatic effect in the dc limit at second order space-time derivative [102, 103]. As a consequence, a charge current is usually less powerful in driving an AF system compared to a spin current.

In ferromagnets, the non-adiabatic torque is typically two orders of magnitude smaller than the adiabatic torque, but it is yet more important because of the inability of driving a domain wall by the adiabatic torque [7, 12, 108, 112, 144]. In antiferromagnet, however, the situation is completely different thanks to the second order time derivative of Eq. (3.35). As will become clear in the next section, we are able to harness the adiabatic torque

Reference	Approach	Driving	Result
[40, 76]	Green's function	charge current	numerical
[102, 103]	linear response	charge current	$\partial_t[\boldsymbol{n}\times(\boldsymbol{j}_c\cdot\nabla)\boldsymbol{n}]$, $\nabla^2\boldsymbol{n}$ $\boldsymbol{n}\cdot[\partial_t\boldsymbol{n}\times(\boldsymbol{j}_c\cdot\nabla)\boldsymbol{n}]\boldsymbol{n}$
[39, 120]	phenomenology	charge current	adiabatic $\boldsymbol{n}\times(\frac{\mathrm{d}\boldsymbol{j}_c}{\mathrm{d}t}\cdot\nabla)\boldsymbol{n}$ non-adiabatic $\boldsymbol{n}\times(\boldsymbol{j}_c\cdot\nabla)\boldsymbol{n}$
[33, 34]	phenomenology	spin current	(no texture) $\boldsymbol{n}\times(\boldsymbol{n}\times\boldsymbol{p})$
[18, 20]	Gauge theory	spin current	adiabatic $(\rho_s\partial_t+\boldsymbol{j}_s\cdot\nabla)\boldsymbol{n}$

Table 3.1: Comparison of current-induced forcing terms studied in different publications. All deal with AF metals with spatial texture except Ref. [33,34].

and exert substantial control of an AF system by spin currents.

Nevertheless, it is quite useful to clarify the effects of charge current studied in various publications. We compare results from existing literatures in Tab. 3.1, where the vector direction has been manipulated to be addable to the right-hand side of Eq. (3.35).

3.3 Domain Wall Dynamics

Due to the absence of dipolar interaction, formation of an AF domain wall (DW) requires two pinning ferromagnets (along the easy axis) at the ends. The pinning originates from exchange bias effect on the interface between the ferromagnetic polarizer and the AF material [53, 68, 75]. Consider the DW of 180 degree depicted in Fig. 3.3. Such a configuration can be achieved by first growing two pinning ferromagnetic layers on a homogeneous AF metal, then rotating one of them to the opposite direction. Though not in exact agreement with theoretical prediction [82,83], it has been realized experimentally in many

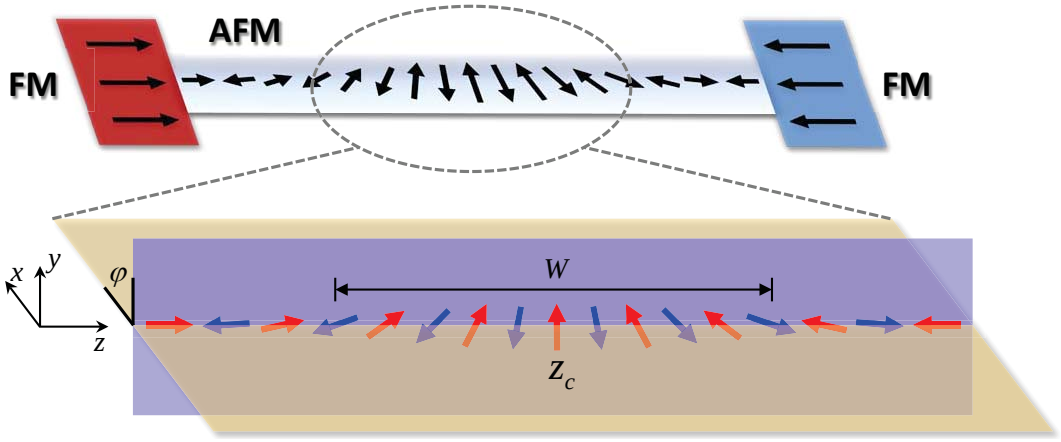

Figure 3.3: Schematic view of a setup of AF DW between two pinning ferromagnets at its ends. DW dynamics is described by two collective coordinates, the center position z_c and the canting angle φ. The DW width W is approximately invariant during the motion.

different contexts [10, 11, 137].

As a compromise between exchange interaction and anisotropy, the DW assumes a soliton profile [82, 83]. When the DW is moving, we describe it by the Walker's ansatz [95]:

$$\varphi(z,t) = \varphi(t); \quad \tan\frac{\theta(z,t)}{2} = \exp\left[\frac{z - z_c(t)}{W(t)}\right], \tag{3.36}$$

where φ and θ are spherical angles specifying the local orientation of $\boldsymbol{n}(\boldsymbol{r},t)$. The first equation states that $\boldsymbol{n}$-vectors at different positions are kept coplanar and have a common canting angle. The second equation implies that the DW remains a soliton shape except that its width $W(t)$ varies with time and that the DW moves as a whole with an instantaneous center position $z_c(t)$. Eq. (3.36) enables us to compute the total Lagrangian as a function of three parameters z_c, φ, and W, known as the collective coordinates [109].

3.3.1 Collective Coordinates

Ignore an overall constant $\frac{-\hbar S}{2\sqrt{d}a_0^{d-1}c}$ (as it does not affect the equation of motion), the effective Lagrangian density reads

$$\mathcal{L} = (\partial_t \boldsymbol{n})^2 - c^2(\partial_z \boldsymbol{n})^2 - \omega_0^2 \boldsymbol{n}_\perp^2 + 2\mathcal{G}\cos\theta(\rho_s \partial_t \varphi + j_s \partial_z \varphi). \tag{3.37}$$

Regarding $\boldsymbol{n}(\boldsymbol{r}, t) = \{\sin\theta\cos\varphi, \sin\theta\sin\varphi, \cos\theta\}$, we have

$$(\partial_t \boldsymbol{n})^2 = (\partial_t \theta)^2 + \sin^2\theta(\partial_t \theta)^2, \tag{3.38}$$

$$(\partial_z \boldsymbol{n})^2 = (\partial_z \theta)^2 + \sin^2\theta(\partial_z \theta)^2, \tag{3.39}$$

and $\boldsymbol{n}_\perp^2 = \sin^2\theta$. From the Walker's ansatz

$$\varphi(z,t) = \varphi(t); \quad \theta(z,t) = 2\arctan\left\{\exp\left[\frac{z - z_c(t)}{W(t)}\right]\right\}, \tag{3.40}$$

we are able to derive the following expressions,

$$\partial_z \theta = \frac{1}{W}\cosh^{-1}(\frac{z - z_c}{W}), \tag{3.41}$$

$$\partial_t \theta = \left[-\frac{\dot{z}_c}{W} - \frac{z - z_c}{W^2}\dot{W}\right]\cosh^{-1}(\frac{z - z_c}{W}), \tag{3.42}$$

$$\sin\theta = \cosh^{-1}(\frac{z - z_c}{W}), \tag{3.43}$$

$$\cos\theta = -\tanh(\frac{z - z_c}{W}), \tag{3.44}$$

thus the total Lagrangian $L = \int \mathrm{d}^d r \mathcal{L}$ becomes

$$\begin{aligned} L = &\left(\frac{\dot{z}_c^2}{W^2} + \dot{\varphi}^2 - \frac{c^2}{W^2} - \omega_0^2 + \frac{2\mathcal{G}}{W} j_s \varphi\right) \int_{-\infty}^{\infty} \frac{\mathrm{d}z}{\cosh^2[\frac{z - z_c}{W}]} \\ &- 2\mathcal{G}\rho_s \dot{\varphi} \int_{-\infty}^{\infty} \mathrm{d}z \tanh[\frac{z - z_c}{W}] + \frac{\dot{W}^2}{W^4} \int_{-\infty}^{\infty} \frac{\mathrm{d}z\ (z - z_c)^2}{\cosh^2[\frac{z - z_c}{W}]}, \end{aligned} \tag{3.45}$$

where we have performed an integration by part in deriving the term containing j_s. This mathematical trick is the same as that in tackling with a ferromagnetic domain wall. To evaluate Eq. (3.45), we notice that

$$\int_{-\infty}^{\infty} \mathrm{d}z \tanh[\frac{z-z_c}{W}] = \lim_{N\to\infty} \int_{-N}^{N} \mathrm{d}z \tanh[\frac{z-z_c}{W}]$$
$$= W \lim_{N\to\infty} \ln \frac{e^{(N-z_c)/W} + e^{(z_c-N)/W}}{e^{(N+z_c)/W} + e^{-(N+z_c)/W}} = -2z_c, \qquad (3.46)$$

and similarly, we also have

$$\int_{-\infty}^{\infty} \frac{\mathrm{d}z}{\cosh^2[\frac{z-z_c}{W}]} = 2W, \quad \text{and} \quad \int_{-\infty}^{\infty} \frac{\mathrm{d}z\ (z-z_c)^2}{\cosh^2[\frac{z-z_c}{W}]} = \frac{1}{6}\pi^2 W^3. \qquad (3.47)$$

Not bothering with an overall factor of 2, we obtain

$$L = \frac{\dot{z}_c^2}{W} + W\dot{\varphi}^2 + 2\mathcal{G}(\rho_s z_c \dot{\varphi} + j_s \varphi) - \frac{c^2}{W} - \omega_0^2 W + \frac{\pi^2}{12}\frac{\dot{W}^2}{W}, \qquad (3.48)$$

which is a functional of three collective coordinates z_c, φ, and W. It worths noting that the last three terms of Eq. (3.48) only depend on the variable $W(t)$, they determine the change of the domain wall width along its motion. The Rayleigh's dissipation function can be evaluated in a similar way,

$$R = \frac{\tilde{\alpha}}{2}\int_{-\infty}^{\infty} \mathrm{d}z[\dot{\theta}^2 + \sin^2\theta\dot{\varphi}^2] = \tilde{\alpha}\left(\frac{\dot{z}_c^2}{W} + W\dot{\varphi}^2\right), \qquad (3.49)$$

which has the same form as the first two terms in Eq. (3.48).

Before calculating the DW velocity, we first explore the dynamics of $W(t)$, which is obtained by $\frac{\partial L}{\partial W} - \frac{\mathrm{d}}{\mathrm{d}t}\left(\frac{\partial L}{\partial \dot{W}}\right) - \frac{\partial R}{\partial \dot{W}} = 0$:

$$\frac{c^2 - \dot{z}_c^2}{W^2} - (\omega_0^2 - \dot{\varphi}^2) + \frac{\pi^2}{12}\left(\frac{\dot{W}^2}{W^2} - \frac{2\ddot{W}}{W}\right) = 0. \qquad (3.50)$$

In the absence of spin current, all time derivatives in the above equation vanish, which gives us an initial condition $W(0) = c/\omega_0$. Considering what will become clear at the end of this section that the domain wall motion respects $\dot{z}_c \ll c$ and $\dot{\varphi} \ll \omega_0$, Eq. (3.50) becomes

$$\frac{c^2}{W^2} - \omega_0^2 + \frac{\pi^2}{12}\left(\frac{\dot{W}^2}{W^2} - \frac{2\ddot{W}}{W}\right) = 0. \tag{3.51}$$

We scale W by its initial value $W(0)$ and time by ω_0^{-1}. Define dimensionless variables $\tilde{t} \equiv \omega_0 t$ and $x(\tilde{t}) \equiv W(\tilde{t})/W(0)$, we obtain

$$\ddot{x} - \frac{\dot{x}^2}{2x} + \frac{6}{\pi^2}(x - \frac{1}{x}) = 0, \quad \text{with} \quad x(0) = 1. \tag{3.52}$$

For arbitrary initial value of $\dot{x}(0)$, Eq. (3.52) can be solved as

$$x(\tilde{t}) = 2\mathcal{X}_0\sqrt{1+\mathcal{X}_0^2}\sin\left(\frac{2\sqrt{3}}{\pi}\tilde{t} + \arccos\sqrt{\frac{1}{1+\mathcal{X}_0^2}}\right) + (1+2\mathcal{X}_0^2), \tag{3.53}$$

where $\mathcal{X}_0 = \frac{\pi\dot{x}(0)}{4\sqrt{3}}$. Since $\tilde{t}$ registers the passage of time on an extremely small scale ($\omega_0 \sim 100$ GHz, it amounts to only 10 ps), during which the variation of the width is negligible, so we know $\dot{x}(\tilde{t}) \to 0$. If we take $\dot{x}(0) = 0$, then $\mathcal{X}_0 = 0$ and the solution becomes $x(\tilde{t}) = 1$, which means the domain wall width $W(t) = W(0) = c/\omega_0$ is **a constant of motion**. Even for a small nonzero $\dot{x}(0)$, the solution $x(\tilde{t})$ only slightly oscillates around 1. As a matter of fact, if we regard $\dot{W}$ and $\ddot{W}$ in Eq. (3.50) as higher order terms and omit them, we immediately arrive at

$$W^2 = \frac{c^2 - \dot{z}_c^2}{\omega_0^2 - \dot{\varphi}^2} \approx \frac{c^2}{\omega_0^2}, \quad \text{for} \quad \dot{z}_c \ll c \text{ and } \dot{\varphi} \ll \omega_0. \tag{3.54}$$

That W is nearly constant allows us to disregard the last three terms in Eq. (3.48), by which we are left with only two dynamical variables z_c and φ, and the effective Lagrangian now reads

$$L = \frac{\dot{z}_c^2}{W} + W\dot{\varphi}^2 + 2\mathcal{G}(\rho_s z_c \dot{\varphi} + j_s \varphi). \tag{3.55}$$

Eq. (3.55) is the first central result of this section.

3.3.2 Domain Wall Velocity

When the domain wall is regarded as a particle, its velocity stands for the rate of change of its center. By taking variational derivatives with respect to z_c and φ, *i.e.*,

$$\frac{\partial L}{\partial z_c} - \frac{\mathrm{d}}{\mathrm{d}t}\left(\frac{\partial L}{\partial \dot{z}_c}\right) - \frac{\partial R}{\partial \dot{z}_c} = 0, \tag{3.56a}$$

$$\frac{\partial L}{\partial \varphi} - \frac{\mathrm{d}}{\mathrm{d}t}\left(\frac{\partial L}{\partial \dot{\varphi}}\right) - \frac{\partial R}{\partial \dot{\varphi}} = 0, \tag{3.56b}$$

we obtain the equations of motion of the DW:

$$\ddot{z}_c + \tilde{\alpha}\dot{z}_c = \rho_s \mathcal{G} W \dot{\varphi}, \tag{3.57a}$$

$$\ddot{\varphi} + \tilde{\alpha}\dot{\varphi} = \frac{\rho_s \mathcal{G}}{W}(v_s - \dot{z}_c), \tag{3.57b}$$

which can be solved analytically. We scale the parameters as

$$V_{DW} \equiv \frac{\dot{z}_c}{v_s}, \qquad V = \frac{v_s}{\tilde{\alpha} W}, \qquad \Omega \equiv \frac{\dot{\varphi}}{\alpha}, \qquad G = \frac{\rho_s \mathcal{G}}{\tilde{\alpha}}, \quad \text{and} \quad \tilde{t} \equiv \tilde{\alpha} t, \tag{3.58}$$

(note: $\tilde{t}$ here is different as that in demonstrating $W(t)$ dynamics just now) by which Eqs. (3.57a) and (3.57b) become

$$\dot{V}_{DW} + V_{DW} = \frac{G}{V}\Omega, \tag{3.59}$$

$$\dot{\Omega} + \Omega = GV(1 - V_{DW}), \tag{3.60}$$

where dot indicates derivative with respect to $\tilde{t}$. The above two equations are coupled dynamics of the dimensionless variables V_{DW} and Ω. We can decouple them by eliminating either Ω or V_{DW},

$$\ddot{V}_{\rm DW} + 2\dot{V}_{\rm DW} + (G^2+1)V_{\rm DW} = G^2, \tag{3.61}$$

$$\ddot{\Omega} + 2\dot{\Omega} + (G^2+1)\Omega = GV, \tag{3.62}$$

they are equivalent to underdamped harmonic oscillators driven by constant forces. For the initial condition $V_{\rm DW}(0) = 0$, the solution of Eq. (3.61) is

$$V_{\rm DW} = \frac{G^2 - Ge^{-\tilde{t}}[G\cos G\tilde{t} + \sin G\tilde{t}]}{1+G^2}, \tag{3.63}$$

which is plotted in Fig. 3.4 for two different G's. As $\tilde{t} \to \infty$, $V_{\rm DW}$ terminates at $V_{\rm DW}(\infty) = G^2/(1+G^2)$. As mentioned before, ρ_s is proportional to the current density j_c, and so is G. Therefore, $V_{\rm DW}(\infty)$ is quadratic in j_c for small current and approaches v_s as a limit at extremely large current. However, the DW velocity may not saturate at v_s when effects due to pure charge current are considered [39, 120].

Regarding pure spin current effect alone, we estimate for typical collinear AF metals, such as IrMn and PdMn [52,121]. The core spin is $2 \sim 4\ \mu_B$; c is of order 10^5 cm/s; a is $3.6 \sim 3.8$ Å; the damping rate is similar to ferromagnetic metals thus $\tilde{\alpha} \sim 10^9\ s^{-1}$. For a current density of 10^5 A/cm^2, G is somewhere between 0.1 and 1, thus the DW is driven up to 10^4 cm/s. As a comparison, the same DW velocity in ferromagnets requires 10^8 A/cm^2, which means that an AF DW is easier to drive. However, if the polarizer is not half metallic, for

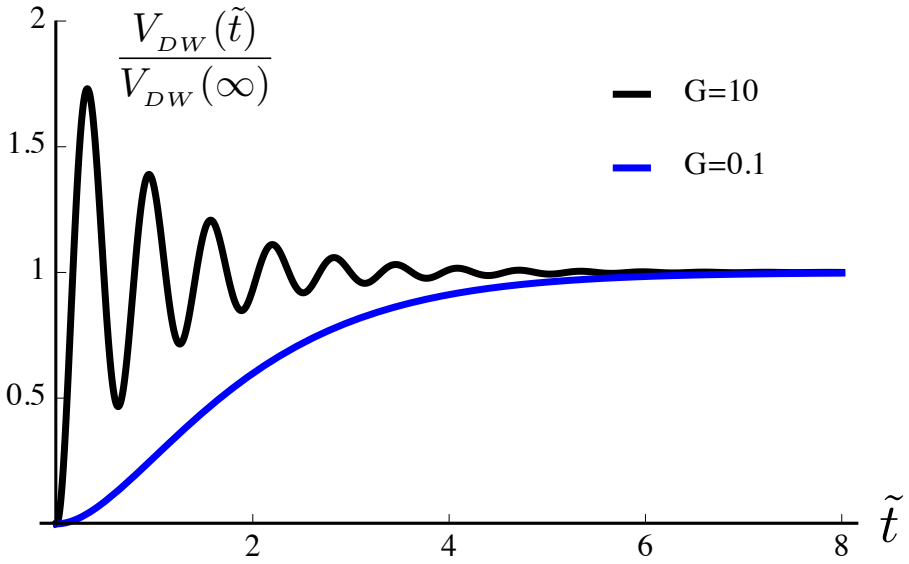

Figure 3.4: Scaled DW velocity plotted as a function of time, for $G = 0.1$ and $G = 10$, respectively. V_{DW} exhibits damped oscillations with the terminal value $V_{DW}(\infty) = G^2/(1 + G^2)$.

example, with a polarization of 0.7, the required current density will be raised up to roughly 10^7 A/cm^2.

To close the argument, three remarks are in order. (i) The solution of Eq. (3.62) gives similar result as Eq. (3.63), which indicates that no matter how slow the DW center moves, it is always accompanied by the precession of φ. This is in sharp contrast to the DW dynamics in ferromagnets, where precession only occurs after the Walker's break-down. What removes the Walker's break-down here is the absence of demagnetization due to vanishing net magnetization. (ii) Our theory is based on the adiabatic electron dynamics, thus $\mathcal{G}(\rho_s\partial_t + \boldsymbol{j}_s \cdot \nabla)\boldsymbol{n}$ only includes the adiabatic effect of spin current. While *only* non-adiabatic torque determines the terminal velocity of a ferromagnetic D-

W [7,12,108,112,144], the AF DW here is driven to a steady motion by *purely* adiabatic forcing, the transfer efficiency of which is usually much higher than that of non-adiabatic effects. This is responsible for why an AF DW is more movable. (iii) When a DW is passing by, local moments will be dragged away from the easy axis, which result in a change of anisotropic magnetoresistance along the transverse direction; this effect is found to be sufficiently large to observe in recent experiments [67, 84, 126]. Thus we have a feasible way to monitor the AF DW motion.

We provide a final remark on the DW behavior at $t \to \infty$, where the terminal velocity and the terminal rotation rate are

$$\dot{z}_c(\infty) = v_s \left(\frac{G^2}{1+G^2} \right), \qquad \dot{\varphi}(\infty) = \frac{v_s}{GW} \left(\frac{G^2}{1+G^2} \right), \tag{3.64}$$

respectively. We make a rough estimate on the change of DW width at $t \to \infty$: for $j_c \sim 10^5$ A/cm^2, $G^2/(1+G^2) \sim 0.1$, thus $(v_s/c)^2 \sim 1\%$ and $(\dot{\varphi}/\omega_0)^2 \sim 1\%$. Regarding Eq. (3.54), we know $W(\infty)$ only differs from $W(0)$ by roughly 1%. A careful calculation shows that

$$\frac{W(\infty)}{W(0)} = \sqrt{1 + \left(\frac{v_s}{c} \right)^2 \cdot \frac{G^2(1-G^2)}{(1+G^2)^2}}. \tag{3.65}$$

If $G < 1$, the DW width expands; If $G > 1$, the DW width shrinks. We know that $v_s/c \sim 1$, thus for the case $G \gg 1$ (extremely large current density), W cannot be considered as nearly constant! But for our estimations just now, the system is within $G < 1$ region, where $\frac{G^2(1-G^2)}{(1+G^2)^2} \leq \frac{1}{8}$, thus $W(\infty)$ differs from $W(0)$ at most by 10%. It can also be shown in a straightforward manner that charge current does not significantly alter W either.

3.4 Spin Wave Instability

Injection of spin current significantly modifies spin wave excitations in antiferromagnets. We take the ansatz $\boldsymbol{n} = \hat{\boldsymbol{e}} + \boldsymbol{n}_\perp e^{i(\boldsymbol{k}\cdot\boldsymbol{r}-\omega t)}$, where $\boldsymbol{n}_\perp$ is a small deviation ($|\boldsymbol{n}_\perp| \ll 1$) perpendicular to the easy axis $\hat{\boldsymbol{e}}$. It is worth mentioning that the relative motion between $\boldsymbol{m}_A$ and $\boldsymbol{m}_B$ within a unit cell [the dynamics of $\boldsymbol{m} = (\boldsymbol{m}_A + \boldsymbol{m}_B)/2$ with the constraint $\boldsymbol{m}\cdot\boldsymbol{n} = 0$] seems to have been ignored, but in fact it has been *resolved* into the dynamics of $\boldsymbol{n}$ described by Eq. (3.32). Substituting the above ansatz into Eq. (3.35),

$$(-\omega^2 + c^2k^2 + \omega_0^2)\boldsymbol{n}\times\boldsymbol{n}_\perp - i\omega\tilde{\alpha}\boldsymbol{n}\times\boldsymbol{n}_\perp + \rho_s\mathcal{G}(-i\omega + i\boldsymbol{v}_s\cdot\boldsymbol{k})\boldsymbol{n}_\perp = 0, \quad (3.66)$$

write it in matrix form and set its determinant zero

$$\begin{vmatrix} \omega^2 - c^2k^2 - \omega_0^2 + i\tilde{\alpha}\omega & i\rho_s\mathcal{G}(\omega - \boldsymbol{v}_s\cdot\boldsymbol{k}) \\ -i\rho_s\mathcal{G}(\omega - \boldsymbol{v}_s\cdot\boldsymbol{k}) & \omega^2 - c^2k^2 - \omega_0^2 + i\tilde{\alpha}\omega \end{vmatrix} = 0, \quad (3.67)$$

we obtain the eigen-equation

$$(\omega^2 - \omega_0^2 - c^2k^2) + i\tilde{\alpha}\omega \pm \rho_s\mathcal{G}(\omega - \boldsymbol{v}_s\cdot\boldsymbol{k}) = 0. \quad (3.68)$$

where $+$ $(-)$ refers to the case where the direction of the A (B) sublattice is pinned along the ferromagnetic polarizer. The solution of Eq. (3.68) is

$$\omega = \frac{1}{2}\left[-i\tilde{\alpha} \pm \rho_s\mathcal{G} \right. \\ \left. [\pm]\sqrt{-\tilde{\alpha}^2 + (\rho_s\mathcal{G})^2 + 4(\omega_0^2 + c^2k^2) \mp 4(\rho_s\mathcal{G})\boldsymbol{v}_s\cdot\boldsymbol{k} \mp i2\tilde{\alpha}\rho_s\mathcal{G}}\right], \quad (3.69)$$

where $[\pm]$ is independent and has no connection to other $\pm$ and $\mp$. Eq. (3.69) is elusive and sophisticated, so we discuss separately the case of uniform precession and spin waves with finite wave length.

3.4.1 Mode of Uniform Precession

First consider the macrospin model that the system precesses as a whole ($k = 0$). In this case, we solve ω as a function of ρ_s. In expanding Eq. (3.69), we notice that $\omega_0 \gg \tilde{\alpha}$. Keeping up to the lowest order in $\tilde{\alpha}$,

$$\omega = \frac{1}{2}\left[-i\tilde{\alpha} \pm \rho_s \mathcal{G}[\pm]\left(\sqrt{(\rho_s\mathcal{G})^2 + 4\omega_0^2} + i\tilde{\alpha}\frac{\rho_s\mathcal{G}}{\sqrt{(\rho_s\mathcal{G})^2 + 4\omega_0^2}}\right) + h.o.\right]. \tag{3.70}$$

Its real part reads

$$\mathrm{Re}[\omega] = \frac{1}{2}\left[\pm\rho_s\mathcal{G}[\pm]\sqrt{(\rho_s\mathcal{G})^2 + 4\omega_0^2}\right], \tag{3.71}$$

where the two $\pm$ are independent. The first $+(-)$ sign represents that the polarizer pins the A (B) sublattice. Eq. (3.71) is plotted in Fig. 3.5; we see that the frequency difference $\Delta\omega$ for opposite polarizer orientations is proportional to the spin density ρ_s. An estimation for IrMn and PdMn [52,121] is as follows: with $j_c \sim 10^7$ A/cm^2, $\Delta\omega = \rho_s\mathcal{G}$ reaches 100 GHz, which is comparable to the anisotropy gap ω_0. Such an appreciable difference can be easily measured by AF resonance (see Section 4.1).

We should note that in the presence of a spin current, the two branches with $\mathrm{Re}[\omega] < 0$ experience enhanced damping, whereas branches with $\mathrm{Re}[\omega] > 0$ exhibits reduced damping. Since for finite ω_0, we always have $\frac{\rho_s\mathcal{G}}{\sqrt{(\rho_s\mathcal{G})^2+4\omega_0^2}} < 1$, the current-induced anti-damping will never be able to overcome the intrinsic Gilbert damping. Thus spin wave instability driven by spin current is impossible for the uniform precession mode.

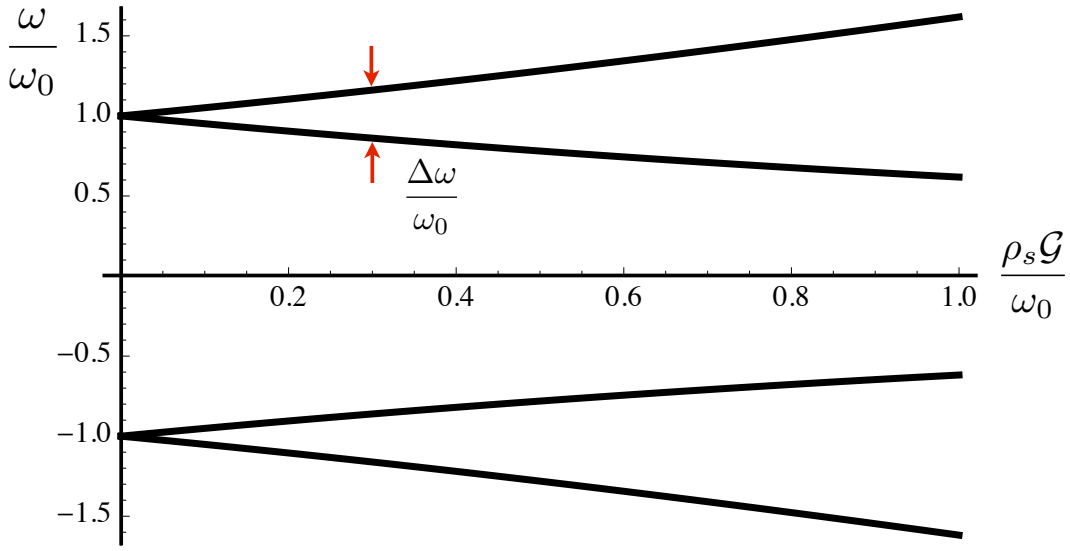

Figure 3.5: Spin wave spectrum (at zero k) as a function of spin injection. As to whether the A or B sublattice is pinned along the polarizer, there is a sizable difference in the AF resonance frequency represented by $\Delta\omega$.

3.4.2 Mode of Finite Wave Length

As the current density is increased, the imaginary part of $\omega(k)$ changes sign at a threshold, where the instability occurs. As a result, spin waves at certain frequencies become unstable, *i.e.*, magnons are emitted by the fast moving electrons.

In this section, we only consider spin wave excitations in the longitudinal direction of the electron flow, thus $\boldsymbol{v}_s \cdot \boldsymbol{k} = \pm v_s k$. To guarantee that the instability occurs for $v_s > 0$, we must take $\boldsymbol{v}_s \cdot \boldsymbol{k} = -v_s k$ (see Eq. (3.75) below). Namely, $\boldsymbol{v_s}$ should be (anti-)parallel to $\boldsymbol{k}$ for the $-(+)$ sign. Denote

$$y \equiv -\tilde{\alpha}^2 + (\rho_s \mathcal{G})^2 + 4(\omega_0^2 + c^2 k^2) - 4(\rho_s \mathcal{G}) v_s k, \tag{3.72}$$

the solution Eq. (3.69) then becomes

$$\omega = \frac{1}{2}\left[-i\tilde{\alpha} \pm \rho_s \mathcal{G}[\pm]\sqrt{y \mp i2\tilde{\alpha}\rho_s\mathcal{G}}\right]. \tag{3.73}$$

As we vary the current density, y may flip sign, so we split the cases into $y > 0$ and $y < 0$ and discuss separately.

(1) If $y > 0$, $[\pm]\sqrt{y - i2\tilde{\alpha}\rho_s\mathcal{G}}$ is plotted by the red and blue points in Fig. 3.6–panel (a); $[\pm]\sqrt{y + i2\tilde{\alpha}\rho_s\mathcal{G}}$ is plotted in Fig. 3.6–panel (b). Only red points correspond to positive imaginary values, which are able to compete with the damping $-i\tilde{\alpha}$, and lead to the instability. The blue points, on the other hand, correspond to the modes experiencing enhanced damping, which do not concern us here. The critical condition is marked by $\left|\mathrm{Im}\left[\sqrt{y \mp i2\tilde{\alpha}\rho_s\mathcal{G}}\right]\right| = \tilde{\alpha}$, which gives the same result for both (a) and (b):

$$[y^2 + 4\tilde{\alpha}^2(\rho_s\mathcal{G})^2]^{\frac{1}{4}} \sin\left[\frac{1}{2}\arctan\left(\frac{2\tilde{\alpha}\rho_s\mathcal{G}}{y}\right)\right] = \tilde{\alpha}. \tag{3.74}$$

Using $\sin\frac{\theta}{2} = \sqrt{\frac{1-\cos\theta}{2}}$, the above equation gives $\sqrt{y^2 + 4\tilde{\alpha}^2(\rho_s\mathcal{G})^2} = y + 2\tilde{\alpha}^2$, which simplifies to $y + \tilde{\alpha}^2 = (\rho_s\mathcal{G})^2$. In view of Eq. (3.72), we have

$$(\rho_s\mathcal{G})v_s k = c^2k^2 + \omega_0^2, \tag{3.75}$$

define $k_0 \equiv \omega_0/c$, the threshold spin current density is thus obtained,

$$j_s = \rho_s v_s = \frac{\omega_0 c}{\mathcal{G}}\left[\frac{k}{k_0} + \frac{k_0}{k}\right]. \tag{3.76}$$

(2) If $y < 0$, it is just a similar job as above. $[\pm]\sqrt{y \mp i2\tilde{\alpha}\rho_s\mathcal{G}}$ are plotted in panels (c) and (d) of Fig. 3.6. Again, the $[\pm]$ sign is marked by red and blue

points. The critical condition in this case becomes

$$[y^2 + 4\tilde{\alpha}^2(\rho_s \mathcal{G})^2]^{\frac{1}{4}} \sin\left[\frac{\pi}{2} - \frac{1}{2}\arctan\left(\frac{2\tilde{\alpha}\rho_s \mathcal{G}}{|y|}\right)\right] = \tilde{\alpha}, \tag{3.77}$$

which leads to $\sqrt{y^2 + 4\tilde{\alpha}^2(\rho_s \mathcal{G})^2} + |y| = 2\tilde{\alpha}^2$. Since $|y| = -y$, it gives the same result (Eq. (3.76)) as case (1).

The threshold condition Eq. (3.76) is associated with a specified wave number k. At $k = k_0$, the threshold reaches a minimum $j_s^{min} = \frac{2\omega_0}{\mathcal{G}} c$, which marks the most unstable mode. For this particular mode, the wave length is estimated to be $\lambda_0 \sim 10^2$ nm for IrMn and PdMn [52, 121]. Since λ_0 is much larger than the lattice spacing of the two materials, the adiabatic assumption at the beginning is guaranteed.

For IrMn and PdMn, we also estimate that the threshold current density is of order 10^7 A/cm^2. Again, this value will be much higher if the polarizer is not half metallic. But we stress that the instability solved above is a phenomenon peculiar to spin current injection. If the polarizer is completely removed, $\mathcal{G}$ will vanish and $j_s^{\text{crit.}}$ will go to infinity, by which the instability will disappear. In fact, pure charge current leads to a Doppler shift of the spin wave velocity [40, 76, 102, 103]; it is not able to trigger an instability of the same sense. Furthermore, it is pretty remarkable that $\tilde{\alpha}$ does not appear in Eq. (3.76), though the instability is physically due to the overcoming of damping by the spin current.

To better understand the physical picture of the instability, especially how the excited spin wave propagate, we are also in need of the real part of

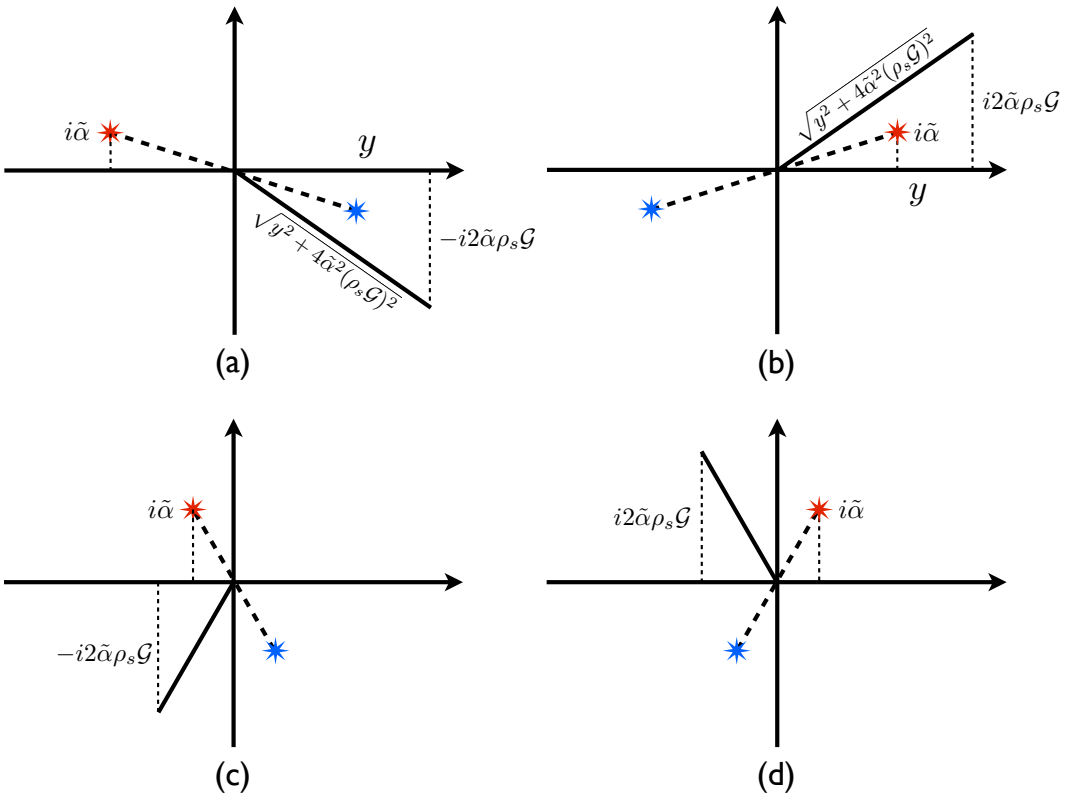

Figure 3.6: In all four panels, red points have positive imaginary parts that just cancel the damping, while blue points enhance the damping. (a) $y > 0$, $\boldsymbol{v}_s$ parallel to $\boldsymbol{k}$, plot for $[\pm]\sqrt{y - i2\tilde{\alpha}\rho_s\mathcal{G}}$; (b) $y > 0$, $\boldsymbol{v}_s$ anti-parallel to $\boldsymbol{k}$, plot for $[\pm]\sqrt{y + i2\tilde{\alpha}\rho_s\mathcal{G}}$; (c) $y < 0$, $\boldsymbol{v}_s$ parallel to $\boldsymbol{k}$, plot for $[\pm]\sqrt{y - i2\tilde{\alpha}\rho_s\mathcal{G}}$; (d) $y < 0$, $\boldsymbol{v}_s$ anti-parallel to $\boldsymbol{k}$, plot for $[\pm]\sqrt{y + i2\tilde{\alpha}\rho_s\mathcal{G}}$.

$\omega(k)$ at the threshold point:

$$\begin{aligned}
\mathrm{Re}[\omega] &= \frac{1}{2}\left\{\pm\rho_s\mathcal{G} \mp \cos\left[\frac{1}{2}\arctan\left(\frac{2\tilde{\alpha}\rho_s\mathcal{G}}{y}\right)\right]\right\} \\
&= \frac{1}{2}\left\{\pm\rho_s\mathcal{G} \mp [y^2+4\tilde{\alpha}^2(\rho_s\mathcal{G})^2]^{\frac{1}{4}}\sqrt{\frac{1+y/\sqrt{y^2+4\tilde{\alpha}^2(\rho_s\mathcal{G})^2}}{2}}\right\} \\
&= \frac{1}{2}\left\{\pm\rho_s\mathcal{G} \mp \sqrt{y+\tilde{\alpha}^2}\right\} \\
&= \frac{1}{2}\left\{\pm\rho_s\mathcal{G} \mp \rho_s\mathcal{G}\right\} = 0, \qquad (3.78)
\end{aligned}$$

where $\cos\frac{\theta}{2} = \sqrt{\frac{1+\cos\theta}{2}}$ has been used. $\mathrm{Re}[\omega] = 0$ is true for any k at their corresponding critical points, which means the spin wave instability is not associated with propagating modes, but is in fact an instability towards the formation of *stationary* a spatial pattern with period $2\pi/k_0$. When an inhomogeneous spatial configuration is developed, exchange energy of the AF background is increased. Therefore, to sustain such a texture, energy of conduction electrons must be transferred continuously to the background moments. This may cause a sudden rise of the differential resistance $\mathrm{d}V/\mathrm{d}I$ at the threshold, which could be detected with high accuracy [45, 116–118]. We emphasis in passing that only the existence of the instability is predictable, the dynamics beyond the threshold point requires a separate treatment.

The critical condition Eq. (3.76) can be obtained by an alternative strategy. If the system develops a stationary spatial pattern at the threshold (see Eq. (3.78)), the background profile must be a solution of the *time-independent* version of Eq. (3.35), *viz.*,

$$c^2\boldsymbol{n}\times\nabla^2\boldsymbol{n} = \omega_0^2\boldsymbol{n}_\perp + \mathcal{G}(\boldsymbol{j}_s\cdot\nabla)\boldsymbol{n}. \qquad (3.79)$$

By substituting the spin wave ansatz, we obtain the eigenvalues of the solution

$$\lambda = \frac{1}{2}\left[\pm i\frac{\mathcal{G}j_s}{c^2}[\pm]\sqrt{4\left(\frac{\omega_0}{c}\right)^2 - \left(\frac{\mathcal{G}j_s}{c^2}\right)^2}\right]. \tag{3.80}$$

The eigenvalues are purely imaginary *if and only if* Eq. (3.76) is satisfied, which characterizes the stationary spatial waves with wave number $\pm\frac{\omega_0}{c}$.

Closing remark: In the previous and present chapters, the reciprocal picture of the coupled dynamics of conduction electrons and bulk AF textures is developed in great detail. The theory is purely general and applies to a broad class of AF metals. In the real world, however, AF materials are typically insulators, thus spintronic phenomena can hardly occur in the bulk. This motives us to generalize our investigation to AF insulators and turn to the interfacial phenomena, which will be presented in the next two chapters.

Chapter 4

Spin Pumping in Antiferromagnets

[1]A major task of spintronics is understanding the mutual control of spin transport and magnetic properties. This inspires intense studies in fundamental physics which opens new avenues in magnetic recording technologies. A new direction in this field aims at harnessing spin dynamics in materials with vanishing magnetization, such as antiferromagnets (AFs) with compensated magnetic moments on an atomic scale. As compared to ferromagnets (Fs), AFs operate at a much higher frequency in the Tera Hertz (THz) ranges [54, 55, 94, 130], which makes it possible to perform ultra fast information processing and communication. At the same time, since there are no stray fields in AFs, they are more robust against magnetic perturbations, an attractive feature of AFs for use in next-generation data storage material. However, to build a viable magnetic device using AF, it is vital to find observable effects induced by the rotation of the order parameter. The recent discovery of tunneling anisotropic magnetoresistance in AF may potentially fulfill this demand [67, 84, 126]. Nevertheless, in such experiments, the AF is dragged

[1]The contents of this chapter are based on the article: R. Cheng, J. Xiao, Q. Niu, and A. Brataas, *Spin Pumping and Spin-Transfer Torques in Antiferromagnets*, Phys. Rev. Lett. **113**, 057601 (2014).

passively by an adjacent F, which is rotated by a magnetic field. This motivates us to ask: will an AF interact directly with (spin) currents without the inclusion of F or magnetic field?

Partial answers are available from recent investigations. While the observation of current-induced change of the exchange bias on a F/AF interface indicates spin-transfer torques (STTs) in AFs [122, 128], theoretical models of STT have been developed in a variety of contexts [20, 32–34, 39, 40, 61, 76, 92, 102, 103, 120, 135]. To achieve a general understanding of spintronics based on AFs, we recall a crucial insight from well-established ferromagnetic spintronics: STT and spin pumping are two reciprocal processes intrinsically connected [12, 88]; they are derivable from each other [65]. To the best our knowledge, all existing studies on AF have focused on STT, whereas spin pumping has received no attention because it seems to be naively believed that the vanishing magnetization spoils any spin pumping in AF.

Spin pumping is the generation of spin currents by the a precessing magnetization [65, 111, 113]. When the magnetization $\boldsymbol{m}$ of a F varies in time, a spin current proportional to $\boldsymbol{m} \times \dot{\boldsymbol{m}}$ is pumped into an adjacent normal (N) metal. In contrast, $\boldsymbol{m}$ vanishes in equilibrium in homogeneous AFs and is small even when the system is driven out-of-equilibrium. Instead, the staggered field (or Néel order) $\boldsymbol{n}$ characterizes the system. A natural question arises: does the motion of $\boldsymbol{n}$ lead to any pumping effect?

In the following sections, we first argue heuristically that spin pumping from the compensated magnetization of the two sublattices constructively add

up rather than cancel. We confirm this anticipation by exploring electron scattering across a N/AF interface, and derive analytically the pumped spin and staggered spin currents [21]. To complete the reciprocal picture, we finally derive the STT due to an applied spin voltage.

4.1 Antiferromagnetic Resonance

We consider an AF with two sublattices and an easy axis along $\hat{\boldsymbol{z}}$ [51,56]. The directions of the magnetic moments are denoted by two unit vectors $\boldsymbol{m}_1$ and $\boldsymbol{m}_2$. The precession of $\boldsymbol{m}_1$ and $\boldsymbol{m}_2$ are driven by the exchange interaction, the anisotropy, and a magnetic field assumed to be in the $\hat{\boldsymbol{z}}$-direction. In units of frequency, they are represented by ω_E, ω_A, and $\omega_H = \gamma H_0$ (γ is the gyromagnetic ratio), respectively.

The three ingredients determine the eigen-frequency of the AF precession. When the frequency of a driving electromagnetic wave matches the eigen-frequency, antiferromagnetic resonance (AFMR) occurs. We start with the equations of motion

$$\dot{\boldsymbol{m}}_1 = \boldsymbol{m}_1 \times [\omega_E \boldsymbol{m}_2 - (\omega_A + \omega_H)\hat{\boldsymbol{z}}], \tag{4.1a}$$

$$\dot{\boldsymbol{m}}_2 = \boldsymbol{m}_2 \times [\omega_E \boldsymbol{m}_1 + (\omega_A - \omega_H)\hat{\boldsymbol{z}}], \tag{4.1b}$$

where additional damping terms will be discussed later when necessary. We add up the above two equations

$$\dot{\boldsymbol{m}} = \omega_A \hat{\boldsymbol{z}} \times \boldsymbol{n} + \hat{\boldsymbol{z}} \times (\omega_A \boldsymbol{n} + \omega_H \boldsymbol{m}), \tag{4.2}$$

and subtract them to obtain

$$\dot{\boldsymbol{n}} = 2\omega_E \boldsymbol{n} \times \boldsymbol{m} + \hat{\boldsymbol{z}} \times (\omega_A \boldsymbol{m} + \omega_H \boldsymbol{n}). \tag{4.3}$$

Take the time derivative of Eq. (4.3), we have

$$\ddot{\boldsymbol{n}} = 2\omega_E(\dot{\boldsymbol{n}} \times \boldsymbol{m} + \boldsymbol{n} \times \dot{\boldsymbol{m}}) + \hat{\boldsymbol{z}} \times (\omega_A \dot{\boldsymbol{m}} + \omega_H \dot{\boldsymbol{n}}). \tag{4.4}$$

Plugging Eq. (4.2) into Eq. (4.4) yields

$$\begin{aligned} \ddot{\boldsymbol{n}} =& 2\omega_E[\dot{\boldsymbol{n}} \times \boldsymbol{m} + \omega_A(n^2 \hat{\boldsymbol{z}} - n_z \boldsymbol{n}) - \omega_H(\hat{\boldsymbol{z}} \cdot \boldsymbol{n})\boldsymbol{m}] \\ &+ \omega_A^2(n_z \hat{\boldsymbol{z}} - \boldsymbol{n}) + \omega_H \omega_A \hat{\boldsymbol{z}} \times (\hat{\boldsymbol{z}} \times \boldsymbol{m}) + \omega_H \hat{\boldsymbol{z}} \times \dot{\boldsymbol{n}}. \end{aligned} \tag{4.5}$$

In AFMR, the deviation of $\boldsymbol{n}$ from $\hat{\boldsymbol{z}}$-axis is small, so $n_z \approx 1$; the amplitudes of the two sublattices are nearly the same, thus the canting is small $|\boldsymbol{m}| \ll 1$, and $n^2 \approx 1$. Apply the vector product of $\boldsymbol{n}$ on both sides of Eq. (4.5), taking into account that $\boldsymbol{m} \cdot \boldsymbol{n} = 0$, we have

$$\boldsymbol{n} \times \ddot{\boldsymbol{n}} = (2\omega_E \omega_A + \omega_A^2)\boldsymbol{n} \times \hat{\boldsymbol{z}} - \omega_H[(\omega_A + 2\omega_E)\boldsymbol{n} \times \boldsymbol{m} - \dot{\boldsymbol{n}}]. \tag{4.6}$$

To eliminate $\boldsymbol{m}$, we resort to Eq. (4.3) and apply the vector product of $\boldsymbol{n}$ on both sides, and obtain the expression

$$\boldsymbol{m} = \frac{1}{\omega_A + 2\omega_E}[\omega_H \boldsymbol{n} \times (\hat{\boldsymbol{z}} \times \boldsymbol{n}) - \boldsymbol{n} \times \dot{\boldsymbol{n}}], \tag{4.7}$$

from which we read of: (i) precessions of $\boldsymbol{m}$ and $\boldsymbol{n}$ have a π phase difference; (ii) the magnitude of $\boldsymbol{m}$ is smaller than that of $\boldsymbol{n}$ by a factor $\frac{\omega}{\omega_A + 2\omega_E}\theta$ where θ is the cone angle of $\boldsymbol{n}$. Substitute Eq. (4.7) into Eq. (4.6), we obtain

$$\boldsymbol{n} \times \ddot{\boldsymbol{n}} = (2\omega_E \omega_A + \omega_A^2)\boldsymbol{n} \times \hat{\boldsymbol{z}} - \omega_H[\dot{\boldsymbol{n}} + \omega_H(\boldsymbol{n} \times \hat{\boldsymbol{z}})]. \tag{4.8}$$

If we decompose $\boldsymbol{n}$ by the ansatz

$$\boldsymbol{n} = \hat{\boldsymbol{z}} + e^{i\omega t}\begin{pmatrix} n_x \\ n_y \end{pmatrix} \quad \text{with } n_x, n_y \ll 1, \tag{4.9}$$

it is straightforward to compute the resonance frequency

$$\omega = \pm\gamma H_0 \pm \sqrt{\omega_A(\omega_A + 2\omega_E)}, \tag{4.10}$$

where the two $\pm$ are independent, so it seems that there are four different eigenmodes. However, we will show that the number of distinguishable modes is two. Practically, ω_E overwhelms ω_A by orders of magnitude, thus we could take $\omega \approx \pm\omega_H \pm \sqrt{2\omega_A\omega_E}$.

4.1.1 Eigenmodes

In linear response regime, we decompose $\boldsymbol{m}_1$ and $\boldsymbol{m}_2$ into equilibrium and oscillating parts

$$\boldsymbol{m}_1 = \hat{\boldsymbol{z}} + e^{i\omega t}\begin{pmatrix} m_{1x} \\ m_{1y} \end{pmatrix}, \qquad \boldsymbol{m}_2 = -\hat{\boldsymbol{z}} + e^{i\omega t}\begin{pmatrix} m_{2x} \\ m_{2y} \end{pmatrix}, \tag{4.11}$$

and assume $|\boldsymbol{m}_\perp| \ll 1$. In the base $(m_{1x},\ m_{2x},\ m_{1y},\ m_{2y})$, the resonance frequencies are the eigenvalues of the matrix

$$\mathcal{M} = \begin{bmatrix} 0 & 0 & -i\alpha & i\beta \\ 0 & 0 & -i\beta & -i\lambda \\ i\alpha & -i\beta & 0 & 0 \\ i\beta & i\lambda & 0 & 0 \end{bmatrix}, \tag{4.12}$$

where $\alpha = \omega_H - (\omega_A + \omega_E)$, $\beta = \omega_E$, and $\lambda = \omega_H + (\omega_A + \omega_E)$. The eigenvalues of $\mathcal{M}$ can be easily derived as

$$\omega_a = -\omega_a' = \omega_H + \sqrt{\omega_A(\omega_A + 2\omega_E)}, \tag{4.13a}$$

$$\omega_b = -\omega_b' = \omega_H - \sqrt{\omega_A(\omega_A + 2\omega_E)}, \tag{4.13b}$$

which reproduces Eq. (4.10) that are obtained in a non-rigorous way. In the order of $\omega_a,\ \omega_a,\ \omega_b,\ \omega_b'$, the eigenvectors of $\mathcal{M}$ are collected in a matrix

$$\mathcal{N} = \begin{bmatrix} 1 & 1 & 1 & 1 \\ -1/\eta & -1/\eta & -\eta & -\eta \\ i & -i & i & -i \\ -i/\eta & i/\eta & -i\eta & i\eta \end{bmatrix} \tag{4.14}$$

as its four columns, respectively, where the coefficient

$$\eta = 1 + \frac{\omega_A}{\omega_E} + \sqrt{\frac{\omega_A(\omega_A + 2\omega_E)}{\omega_E^2}} \approx \left[1 + \sqrt{\frac{\omega_A}{\omega_E}}\right]^2 \tag{4.15}$$

determines the ratio between the amplitudes of $\boldsymbol{m}_1$ and $\boldsymbol{m}_2$, and it is independent of ω_H. From Eq. (4.13) and (4.14), we know that ω_a and ω_a' are NOT different modes but are redundant representation of the same mode; so are ω_b and ω_b'. The two distinguishable modes are

$$\omega = \omega_H \pm \omega_R = \omega_H \pm \sqrt{\omega_A(\omega_A + 2\omega_E)}, \tag{4.16}$$

which are characterized by different chiralities and are depicted in Fig. 4.1. From a bird's eye view along $-\hat{\boldsymbol{z}}$ of the left-handed (right-handed) mode, both $\boldsymbol{m}_1$ and $\boldsymbol{m}_2$ undergo a circular clockwise (counterclockwise) precession with π phase difference. In the absence of magnetic field, *viz.* $\omega_H = 0$, the two modes are degenerate. In contrast to ferromagnetic resonance, AFMR does not require the magnetic field.

4.1.2 Susceptibility and Damping

AFMR is marked by the peak of susceptibility in response to an external electromagnetic wave with matching frequencies. To derive the susceptibility,

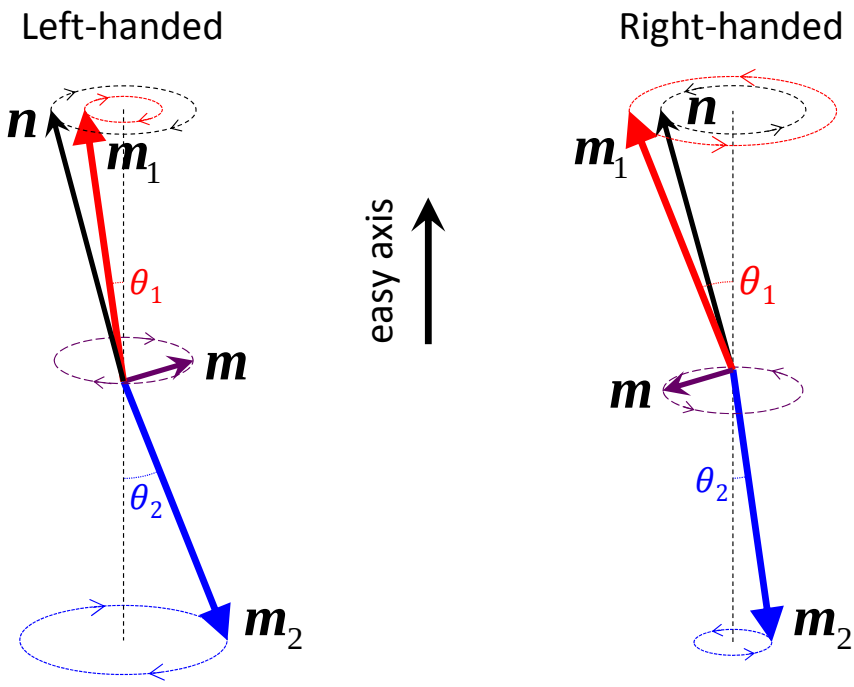

Figure 4.1: The two eigenmodes of Eq. (4.16) have opposite chiralities and opposite ratios between the cone angles of $\boldsymbol{m}_1$ and $\boldsymbol{m}_2$. A magnetic field along the easy axis breaks the degeneracy of the two modes.

we add a small oscillating part to the external magnetic field so that $\boldsymbol{H} = H_0\hat{\boldsymbol{z}} + \boldsymbol{h}_\perp$, and Gilbert damping terms to Eq. (4.1) (it is easy to show that the Landau-Lifshitz damping will do the same job), which yield

$$\dot{\boldsymbol{m}}_1 = \boldsymbol{m}_1 \times [\omega_E \boldsymbol{m}_2 - (\omega_H + \omega_A)\hat{\boldsymbol{z}} - \gamma \boldsymbol{h}_\perp] + \alpha_1 \boldsymbol{m}_1 \times \dot{\boldsymbol{m}}_1, \tag{4.17a}$$

$$\dot{\boldsymbol{m}}_2 = \boldsymbol{m}_2 \times [\omega_E \boldsymbol{m}_1 - (\omega_H - \omega_A)\hat{\boldsymbol{z}} - \gamma \boldsymbol{h}_\perp] + \alpha_2 \boldsymbol{m}_2 \times \dot{\boldsymbol{m}}_2, \tag{4.17b}$$

where α_1 and α_2 can be different in general. Define complex vectors $\tilde{h}_\pm = h_x \pm i h_y$ and $\tilde{m}_\pm = m_x \pm i m_y$, where $+(-)$ stands for the right-handed (left-handed) polarization [35]. Some straightforward algebra lead us to

$$[\omega(1 - i\alpha_1) - (\omega_H + \omega_E + \omega_A)]\tilde{m}_{1\pm} - \omega_E \tilde{m}_{2\pm} = -\gamma \tilde{h}_\pm, \tag{4.18}$$

$$\omega_E \tilde{m}_{1\pm} + [\omega(1 + i\alpha_2) - (\omega_H - \omega_E - \omega_A)\tilde{m}_{2\pm} = \gamma \tilde{h}_\pm, \tag{4.19}$$

from which we solve the transverse magnetic components in terms of the oscillating magnetic field

$$\begin{bmatrix} \tilde{m}_{1\pm} \\ \tilde{m}_{2\pm} \end{bmatrix} = \frac{\gamma \tilde{h}_\pm}{\mathcal{D}} \begin{bmatrix} \omega_H - \omega - \omega_A - i\alpha_2\omega \\ -\omega_H + \omega - \omega_A - i\alpha_1\omega \end{bmatrix}, \tag{4.20}$$

where the denominator reads

$$\begin{aligned} \mathcal{D} =& (\omega - \omega_H)^2 + \alpha_1\alpha_2\omega^2 - \omega_A(\omega_A + 2\omega_E) \\ & - i\omega[(\alpha_1 - \alpha_2)(\omega - \omega_H) + (\alpha_1 + \alpha_2)(\omega_A + \omega_E)]. \end{aligned} \tag{4.21}$$

If $\alpha_1 = \alpha_2 = 0$, $\mathcal{D} = (\omega - \omega_H)^2 - \omega_A(\omega_A + 2\omega_E)$ diverges at both ω_a and ω_b, which has been expected ny the previous analysis. Since $\boldsymbol{m}_1$ and $\boldsymbol{m}_2$ come from identical magnetic atoms and the system anisotropy is uniaxial, α_1 and α_2 have

essentially the same magnitude. If $\alpha_1 = -\alpha_2$, the two moments are damped towards $\hat{\boldsymbol{z}}$ and $-\hat{\boldsymbol{z}}$, respectively, in mode ω_a; in mode ω_b, however, they will experience anti-damping and slip towards the equator, which is unphysical. So we must have $\alpha_1 = \alpha_2$, where *the two moments are damped towards their effective magnetic fields rather than the easy axis.* We illustrate this in Fig. 4.2, the damping torque on the moment with larger cone angle tends to diminish its amplitude, while the damping torque on the moment with smaller cone angle drives it to be antiparallel with the other moment. With $\alpha_1 = \alpha_2 = \alpha$, and recall $\omega_R = \sqrt{\omega_A(\omega_A + 2\omega_E)}$, Eq. (4.21) becomes

$$\mathcal{D} = [(\omega - \omega_H)^2 + \alpha^2\omega^2 - \omega_R^2] - 2i\alpha\omega(\omega_A + \omega_E). \tag{4.22}$$

In the calculation of spin pumping below, we need the susceptibilities of $\boldsymbol{m}$ and $\boldsymbol{n}$ fields, which are defined as

$$\chi_\pm = \frac{\tilde{m}_{1\pm} + \tilde{m}_{2\pm}}{2\tilde{h}_\pm} = \frac{-\gamma(\omega_A + i\alpha\omega)}{\mathcal{D}}, \tag{4.23a}$$

$$\mathscr{X}_\pm = \frac{\tilde{m}_{1\pm} - \tilde{m}_{2\pm}}{2\tilde{h}_\pm} = \frac{-\gamma(\omega - \omega_H)}{\mathcal{D}}, \tag{4.23b}$$

for $\alpha \ll 1$ and $\omega_A \ll \omega_E$, the magnitude of $\chi_\pm$ at resonance is much smaller than that of $\mathscr{X}_\pm$ ($|m_\pm| \ll |n_\pm|$), which are approximately

$$|\mathscr{X}_\pm^R| \approx \frac{\gamma}{\alpha(\omega_R \pm \omega_H)}\sqrt{\frac{\omega_A}{\omega_E}}. \tag{4.24}$$

Comparing with the FMR susceptibility $|\chi_{_F}| \approx \frac{\gamma}{\alpha|\omega_H|}$ [35], we see that $\mathscr{X}_\pm^R$ is suppressed by a factor of $\sqrt{\frac{\omega_A}{\omega_E}}$. However, in some AF such as FeF_2, $\omega_A \approx 0.36\omega_E$, thus the factor is roughly 0.6, not small in any sense [78, 79]. If the

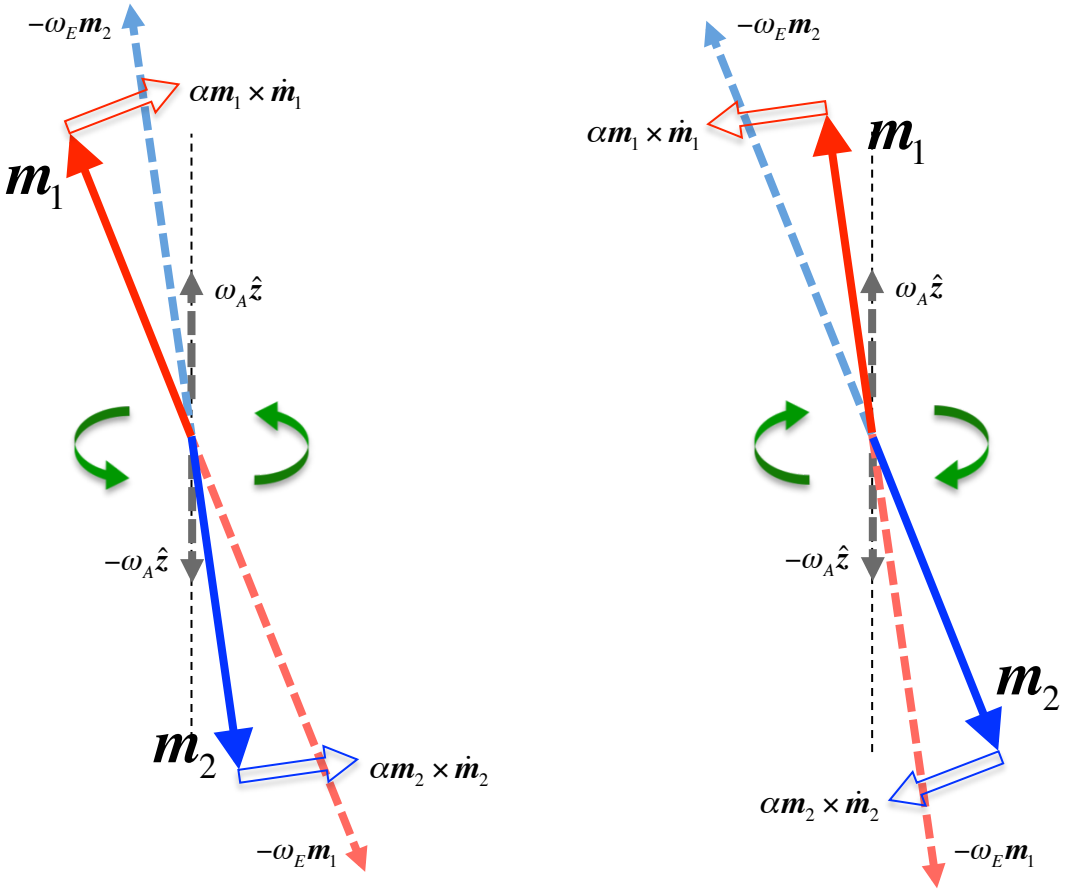

Figure 4.2: In both mode ω_a (left) and ω_b (right), the damping torque pushes the moment with the larger amplitude towards the easy axis because the effective field (dotted arrows) it feels resides inside its precessing cone, whereas the moment with the smaller amplitude is dragged by the damping torque towards the antiparallel direction of the other moment since the effective field is located outside its precessing cone.

static magnetic field H_0 is applied along $+\hat{\boldsymbol{z}}$ ($-\hat{\boldsymbol{z}}$) direction, *i.e.*, ω_H is positive (negative), $\mathscr{X}_-^R$ ($\mathscr{X}_+^R$) will be enhanced. In fact, the resonance susceptibility is inversely proportional to the resonance frequency, what the magnetic field does is bringing down the resonance frequency ω_b (ω_a) thus enhancing the absorption rate of the left-handed (right-handed) mode.

For very strong magnetic field, the system experiences spin-flop transition at $\omega_H \sim \omega_R$ [50], where the sublattice magnetic moments suddenly become perpendicular to the easy-axis. The resonance susceptibility diverges at this critical point, but in real experiment, an infinitesimal deviation of the magnetic field from the easy axis direction cures the divergence [90]; a finite temperature causes nonzero $\chi_{//}$ which renders the AFMR to be Ferrimagnetic resonance [127] and the divergence is circumvented. Therefore, while the resonance susceptibility peaks in the neighborhood of spin-flop transition, the absorption rate of microwave in a real system may not be large if $\omega_A \ll \omega_E$. Using materials with large ω_A/ω_E ratio should be a thumb rule.

Having sufficient knowledge of AFMR, we are able to anticipate the spin pumping by AFMR. A heuristic way to grasp the essential feature of this issue is to consider $\boldsymbol{m}_1$ and $\boldsymbol{m}_2$ as two independent F subsystems. Then spin currents pumped from them will be proportional to $\boldsymbol{m}_1 \times \dot{\boldsymbol{m}}_1$ and $\boldsymbol{m}_2 \times \dot{\boldsymbol{m}}_2$, respectively. From Fig. 4.1 we see that $\boldsymbol{m}_1 \approx -\boldsymbol{m}_2$ and $\dot{\boldsymbol{m}}_1 \approx -\dot{\boldsymbol{m}}_2$, thus the contributions from the two are basically the same and add up constructively. As a result, the total spin current is roughly proportional to $\boldsymbol{n} \times \dot{\boldsymbol{n}}$ where $\boldsymbol{n} = (\boldsymbol{m}_1 - \boldsymbol{m}_2)/2$ denotes the staggered field. In a strict sense, however, due

to the difference of the cone angles of $\boldsymbol{m}_1$ and $\boldsymbol{m}_2$, a small magnetization $\boldsymbol{m}$ will always be induced, as is shown in Fig. 4.1.

Furthermore, scattering channels associated with different sublattices on a N/AF interface will mix, thus an AF is not equivalent to two Fs. To what extent the above naive picture survives is ultimately determined by the interface scattering of electrons.

4.2 Interface Scattering

Typical AF materials are insulators [36, 47, 78, 79] and incident electrons from the normal metal cannot penetrate far. Consequently, only a single atomic layer of AF directly connected to N suffices to describe the dominant contribution to interface scattering. Therefore, the essential physics is captured by modeling the N/AF interface as being semi-infinite system in the transport direction and infinite in the transverse direction. As illustrated in Fig. 4.10, the interface is compensated, where neighboring magnetic moments are located at different sublattices. The case of an uncompensated interface is analogous to N/F(insulator) interface.

This section involves substantial amount of tedious mathematical manipulations. To make it more understandable, we start from a simple one dimensional chain, and use two standard approaches to solve the scattering matrix: the wave function matching method, and the Fisher-Lee formalism based on the interface Green's function [24, 25]. From the latter, we prove quantitatively that a normal metal—magnetic insulator interface can well be

modeled as being semi-infinite system in the transport direction. Base on this fact, we are able to perform the cumbersome calculation of spin-dependent electron scattering problems in higher dimensions.

4.2.1 One Dimension

(1) Single semi-infinite 1-d chain:

In case (I) of Fig. 4.3, the end atomic site has a magnetic moment $\boldsymbol{m}$. For current normalization, the incident and reflected plane waves are

$$\psi^{in} = \sqrt{\frac{\hbar}{t \sin ka}} \begin{bmatrix} \vdots \\ e^{-2ika} \\ e^{-ika} \\ 1 \end{bmatrix} |s\rangle, \quad \psi^{re} = r_{s's} \sqrt{\frac{\hbar}{t \sin ka}} \begin{bmatrix} \vdots \\ e^{+2ika} \\ e^{+ika} \\ 1 \end{bmatrix} |s'\rangle, \tag{4.25}$$

where s denotes the spin index. The wave function should satisfy

$$-t\psi_{-1} + [(U - E) - J\boldsymbol{m} \cdot \boldsymbol{\sigma}]\psi_0 = 0, \tag{4.26}$$

where $U = 2t$ and $E = 2t(1 - \cos ka)$, and t and J represent the hopping integral and the exchange coupling strength, respectively. From Eq. (4.25),

$$\psi_{-1} = \sqrt{\frac{\hbar}{t \sin ka}} \left[e^{-ika}|s\rangle + e^{ika} r_{s's}|s'\rangle \right], \tag{4.27a}$$

$$\psi_0 = \sqrt{\frac{\hbar}{t \sin ka}} \left[|s\rangle + r_{s's}|s'\rangle \right], \tag{4.27b}$$

substitute them into Eq. (4.26), and project the equation onto $\langle s''|$, we obtain

$$te^{-ika}\delta_{s''s} + te^{ika} r_{s''s} + J\boldsymbol{m} \cdot \boldsymbol{\sigma}_{s''s'}[\delta_{s's} + r_{s's}] = 2t \cos ka[\delta_{s''s} + r_{s''s}]. \tag{4.28}$$

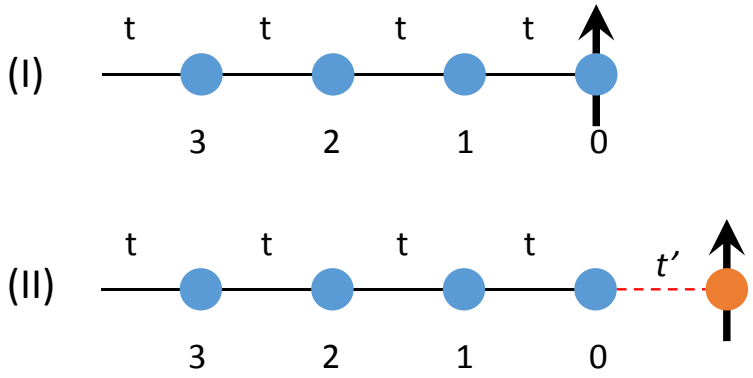

Figure 4.3: Case (II) differs from case (I) in that the magnetic atom is distinct.

Define $\lambda = J/t$, Eq. (4.28) in matrix form is $(e^{-ika}\mathrm{I} - \lambda \boldsymbol{m}\cdot\boldsymbol{\sigma})r = \lambda \boldsymbol{m}\cdot\boldsymbol{\sigma} - e^{ika}\mathrm{I}$. Decompose the reflection matrix r by the Pauli matrices, it is solved as

$$r = \frac{1-\lambda^2}{\lambda^2 - e^{-2ika}}\mathrm{I} + \frac{2i\lambda \sin ka}{\lambda^2 - e^{-2ika}}\boldsymbol{m}\cdot\boldsymbol{\sigma}. \tag{4.29}$$

When $\lambda \to 0$, the second term vanishes, and $r \to -e^{2ika}\mathrm{I}$. Denote $r \equiv r_0\mathrm{I} + \Delta S \boldsymbol{m}\cdot\boldsymbol{\sigma}$ where ΔS determines spin-pumping, it can be expressed as

$$\Delta S = \frac{2i\lambda \sin ka}{\lambda^2 - e^{-2ika}} = \frac{2\lambda \sin ka[\sin 2ka + i(\lambda^2 - \cos 2ka)]}{(\lambda^2 - \cos 2ka)^2 + \sin^2 ka}, \tag{4.30}$$

where k is determined by the Fermi energy: $ka = \arccos(1 - E_f/2t)$.

If the magnetic atom is different from the rest, as depicted by case (II) of Fig. 4.3, hopping to that atom is t'. We define $\xi = t'/t$, then

$$-t\psi_{-1} + (U-E)\psi_0 - t'\psi_M = 0, \tag{4.31a}$$

$$-t'\psi_0 + [(U-E) - J\boldsymbol{m}\cdot\boldsymbol{\sigma}]\psi_M = 0, \tag{4.31b}$$

where ψ_M is the wave function of the magnetic atom. Denote $C_{s's}$ as the probability of an electron being in spin state $|s'\rangle$ on the magnetic atom when

the incident wave is in state $|s\rangle$. Then ψ_M can be decomposed by

$$\psi_M = \sqrt{\frac{\hbar}{t \sin ka}} C_{s's} |s'\rangle. \tag{4.32}$$

Similar to (I), Eq. (4.31) yield two matrix equations

$$e^{ika}\mathrm{I} + e^{-ika} r - \xi C = 0, \tag{4.33}$$

$$\xi(\mathrm{I} + r) = [-\lambda \boldsymbol{m} \cdot \boldsymbol{\sigma} + 2\cos ka] C, \tag{4.34}$$

where the $s''s$ element of the product $\boldsymbol{m} \cdot \boldsymbol{\sigma} C$ is $\boldsymbol{m} \cdot [\boldsymbol{\sigma}]_{s''s'} [C]_{s's}$. Eliminate matrix C and decompose r by Pauli matrices, we obtain the solution

$$r = A\mathrm{I} + B\boldsymbol{m} \cdot \boldsymbol{\sigma}, \tag{4.35}$$

$$A = \frac{(\xi^4 - \lambda^2) + 4(1 - \xi^2)\cos^2 ka}{\lambda^2 e^{-2ika} - (2e^{-ika}\cos ka - \xi^2)^2}, \tag{4.36}$$

$$B = \frac{2i\lambda\xi^2 \sin ka}{\lambda^2 e^{-2ika} - (2e^{-ika}\cos ka - \xi^2)^2}, \tag{4.37}$$

where A can be written in a more suggestive form

$$A = -e^{2ika} + e^{ika} \frac{2i\xi^2 \sin ka (2e^{-ika}\cos ka - \xi^2)}{\lambda^2 e^{-2ika} - (2e^{-ika}\cos ka - \xi^2)^2}. \tag{4.38}$$

If $\xi \to 0$, $A \to -e^{2ika}$ and $B \to 0$, as expected. If $\xi = 1$, we have

$$r = e^{2ika} \left[\frac{1 - \lambda^2}{\lambda^2 - e^{-2ika}} \mathrm{I} + \frac{2i\lambda \sin ka}{\lambda^2 - e^{-2ika}} \boldsymbol{m} \cdot \boldsymbol{\sigma} \right], \tag{4.39}$$

which differs from Eq. (4.29) only by a phase factor e^{2ika}. This is because the plane wave basis incorporate the magnetic atom if $t' = t$. If $\xi \ll 1$ but $\lambda \gg 1$,

$$A \approx e^{2ika}[-1 + i\frac{2\xi^2}{\lambda^2} \sin 2ka], \quad B \approx i\frac{2\xi^2}{\lambda} e^{2ika} \sin ka, \tag{4.40}$$

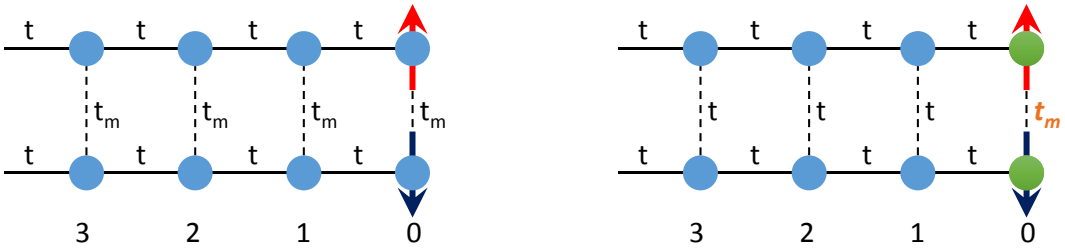

Figure 4.4: Left: all connections between the two chains are t_m; Right: only the magnetic atoms are connected via t_m while all other links are t.

where the factor ξ^2/λ can be regraded as coming from a second order hopping process between the chain and the magnetic atom. For ξ of order one, however, the two cases above are NOT qualitatively different. Thus in the following discussions, without jeopardizing the essential physics, we assume $\xi = 1$ to simplify the calculation unless otherwise stated.

(2) Double semi-infinite 1-d chain:

We extend the 1-d model to a double chain where the magnetic atoms are aligned anti-parallel in Fig. 4.4. In the left panel, all connections joining the two chains are t_m, denote $\alpha = t_m/t$; in the right panel, only the magnetic atoms are joined by t_m whereas all other links are t. For the former, the wave function satisfies

$$-t(\phi_{n-1} + \phi_{n+1}) - t_m\hat{\tau}_1\phi_n = (E - U)\phi_n, \tag{4.41}$$

where $\hat{\tau}_1$ acts on the sublattice space, and $U = 2(t+t_m)$. Define $\varepsilon = (E-U)/t$ and $\lambda = J/t$, the band structure is easily obtained

$$\varepsilon = -2\cos ka - \tau\alpha, \quad \text{with } |\tau\rangle \equiv \phi_\tau = \frac{1}{\sqrt{2}}\begin{bmatrix}1\\ \tau\end{bmatrix},\ \tau = \pm. \tag{4.42}$$

Let $R^{\tau' \tau}_{s' s}$ denote the amplitude for an incident state $|\tau\rangle|s\rangle$ to be reflected into $|\tau'\rangle|s'\rangle$, by which the wave function (of the n-th atom pair) becomes

$$\psi_n = \sqrt{\frac{\hbar}{t \sin k^\tau a}} e^{-ink^\tau a}|\tau\rangle|s\rangle + R^{\tau' \tau}_{s' s} \sqrt{\frac{\hbar}{t \sin k^{\tau'} a}} e^{ink^{\tau'} a}|\tau'\rangle|s'\rangle, \tag{4.43}$$

where k^τ satisfies $\varepsilon = -2\cos k^\tau a - \tau\alpha$. One the boundary,

$$-t\psi_{-1} + [-J\tau_3 \otimes (\boldsymbol{n} \cdot \boldsymbol{\sigma}) - t_m \hat{\tau}_1]\psi_0 = (E - U)\psi_0. \tag{4.44}$$

Similar to the 1-d case, we project the whole equation onto the $\langle\tau''|\langle s''|$ state. Notice that in the $|\tau\rangle \otimes |s\rangle$ representation,

$$\tau_1^{\tau'' \tau} = \frac{1}{2}(1,\ \tau'') \begin{pmatrix} 0 & 1 \\ 1 & 0 \end{pmatrix} \begin{pmatrix} 1 \\ \tau \end{pmatrix} = \begin{pmatrix} 1 & 0 \\ 0 & -1 \end{pmatrix} = \tau'' \delta^{\tau'' \tau}, \tag{4.45a}$$

$$\tau_3^{\tau'' \tau} = \frac{1}{2}(1,\ \tau'') \begin{pmatrix} 1 & 0 \\ 0 & -1 \end{pmatrix} \begin{pmatrix} 1 \\ \tau \end{pmatrix} = \begin{pmatrix} 0 & 1 \\ 1 & 0 \end{pmatrix} = \delta^{\tau'', -\tau}, \tag{4.45b}$$

from which we obtain

$$\begin{aligned} e^{-ik^\tau a}\delta^{\tau'' \tau}_{s'' s} + R^{\tau'' \tau}_{s'' s} \sqrt{\frac{\sin k^\tau a}{\sin k^{\tau''} a}} e^{ik^{\tau''} a} \\ + \lambda \delta^{\tau'', -\tau} (\boldsymbol{n} \cdot \boldsymbol{\sigma})_{s'' s} + \lambda (\boldsymbol{n} \cdot \boldsymbol{\sigma})_{s'' s'} R^{-\tau'', \tau}_{s' s} \sqrt{\frac{\sin k^\tau a}{\sin k^{-\tau''} a}} \\ = [2\cos k^\tau a + \alpha(\tau - \tau'')] \left[\delta^{\tau'' \tau}_{s'' s} + R^{\tau'' \tau}_{s'' s} \sqrt{\frac{\sin k^\tau a}{\sin k^{\tau''} a}} \right]. \end{aligned} \tag{4.46}$$

Scattering at a N/AF interface has four channels: (τ, s) where $\tau = +, -$ and $s = \uparrow, \downarrow$. Haney and MacDonald [40] have argued that spin-flip scattering occurs if and only if the sublattice state is also flipped between $|+\rangle$ and $|-\rangle$, which follows from the invariance of the AF Hamiltonian under the combined operations of sublattice interchange and time reversal. Therefore, the spin

dependence of the reflection coefficients are

$$R^{\pm,\pm}_{s',s} = r^{\pm,\pm}\delta_{s',s}, \quad R^{\pm,\mp}_{s',s} = r^{\pm,\mp}(\boldsymbol{n}\cdot\boldsymbol{\sigma}_{s',s}). \tag{4.47}$$

For fixed energy $\varepsilon_+ = \varepsilon_- = \varepsilon_f$, Eq. (4.42) requires

$$2\alpha = e^{ik_x^- a} + e^{-ik_x^- a} - (e^{ik_x^+ a} + e^{-ik_x^+ a}), \tag{4.48}$$

which can be used to eliminate α. After some tedious calculation, we finally obtain the reflection coefficients

$$r^{+,+} = \frac{e^{i(k^+-k^-)a} - \lambda^2}{\lambda^2 - e^{-i(k^++k^-)a}}, \tag{4.49}$$

$$r^{-,-} = \frac{e^{i(k^--k^+)a} - \lambda^2}{\lambda^2 - e^{-i(k^++k^-)a}}, \tag{4.50}$$

$$r^{+,-} = r^{-,+} = \frac{2i\lambda\sqrt{\sin k^+ a \sin k^- a}}{\lambda^2 - e^{-i(k^++k^-)a}}. \tag{4.51}$$

When $\alpha \to 0$, the chains become decoupled and $k^+ = k^- = k$, so $r^{+,+} = r^{-,-} = \frac{1-\lambda^2}{\lambda^2 - e^{-2ika}}$, and $r^{+,-} = r^{-,+} = \frac{2i\lambda \sin ka}{\lambda^2 - e^{-2ika}}$. This is consistent with the 1-d result Eq. (4.29). The entire reflection matrix can be written as

$$R = \begin{bmatrix} r^{++}\sigma_0 & r^{+-}(\boldsymbol{n}\cdot\boldsymbol{\sigma}) \\ r^{-+}(\boldsymbol{n}\cdot\boldsymbol{\sigma}) & r^{--}\sigma_0 \end{bmatrix}, \tag{4.52}$$

which will be used frequently in the following sections.

If only the magnetic atoms are communicated through t_m as illustrated by the right panel of Fig. 4.4, it renders the magnetic atoms different from others, thus the plane wave retains only to non-magnetic sites. The wave function of the magnetic atoms is

$$\psi_M = C^{\tau'\tau}_{s's}\sqrt{\frac{\hbar}{t\sin k^{\tau'}a}}|\tau'\rangle|s'\rangle, \tag{4.53}$$

and this time we need to solve two equations

$$-t[\psi_{-1} + \hat{Q}\psi_0 + \psi_M] = (E-U)\psi_0, \tag{4.54a}$$

$$-t\psi_0 + [-J\sigma_3 \otimes (\boldsymbol{n}\cdot\boldsymbol{\sigma}) - t_m\hat{Q}]\psi_M = (E-U)\psi_M, \tag{4.54b}$$

where ψ_n is defined in Eq. (4.43). Again, set $\lambda = J/t$ and $\alpha = t_m/t$, we obtain

$$\begin{aligned} &e^{-ik^\tau a}\delta^{\tau''\tau}_{s''s} + \sqrt{\frac{\sin k^\tau a}{\sin k^{\tau''} a}}[R^{\tau''\tau}_{s''s}e^{ik^{\tau''}a} + C^{\tau''\tau}_{s''s}] \\ &\qquad = [2\cos k^\tau a + (\tau - \tau'')]\left[\delta^{\tau''\tau}_{s''s} + R^{\tau''\tau}_{s''s}\sqrt{\frac{\sin k^\tau a}{\sin k^{\tau''}a}}\right], \end{aligned} \tag{4.55a}$$

$$\begin{aligned} &\delta^{\tau''\tau}_{s''s} + R^{\tau''\tau}_{s''s}\sqrt{\frac{\sin k^\tau a}{\sin k^{\tau''}a}} + \lambda(\boldsymbol{n}\cdot\boldsymbol{\sigma})_{s''s'}C^{-\tau'',\tau}_{s's}\sqrt{\frac{\sin k^\tau a}{\sin k^{-\tau''}a}} \\ &\qquad = [2\cos k^\tau a + (\tau - \alpha\tau'')]C^{\tau''\tau}_{s's}\sqrt{\frac{\sin k^\tau a}{\sin k^{\tau''}a}}. \end{aligned} \tag{4.55b}$$

Adopt Eq. (4.52) for the R matrix, we obtain after a lengthy algebra:

$$r^{++} = e^{2ik^+a}\frac{[e^{ik^+a} + (1-\alpha)][e^{-ik^-a} - (1-\alpha)] - \lambda^2}{\lambda^2 - [e^{-ik^+a} + (1-\alpha)][e^{-ik^-a} - (1-\alpha)]}, \tag{4.56}$$

$$r^{--} = e^{2ik^-a}\frac{[e^{-ik^+a} + (1-\alpha)][e^{ik^-a} - (1-\alpha)] - \lambda^2}{\lambda^2 - [e^{-ik^+a} + (1-\alpha)][e^{-ik^-a} - (1-\alpha)]}, \tag{4.57}$$

$$r^{+-} = r^{-+} = \frac{2i\lambda e^{i(k^+ + k^-)a}\sqrt{\sin k^+ a \sin k^- a}}{\lambda^2 - [e^{-ik^+a} + (1-\alpha)][e^{-ik^-a} - (1-\alpha)]}. \tag{4.58}$$

If $\alpha \to 1$, these results reduce to the previous result up to a phase factor.

4.2.2 Fisher-Lee Solutions

In Fig. 4.5, a normal metal chain is connected to an ferromagnetic chain through t', the lattice spacing of the two sides are not necessarily identical. We can use similar wave function matching techniques to handle this problem,

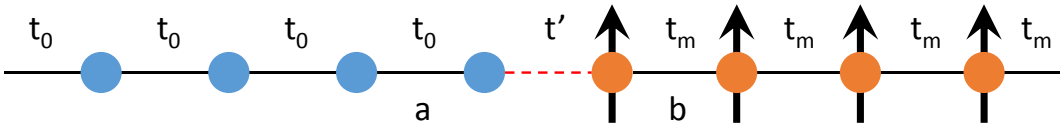

Figure 4.5: A 1-d normal metal chain with hopping t_0 and lattice spacing a is connected via t' to a 1-d AF chain with hopping t_m and lattice spacing b.

but it becomes extremely complicated when generalizing into 3-d. So in the following, we adopt the Green's function approach (Fisher-Lee formalism) to solve the metallic case. The central issue of this approach is the derivation of self-energy Σ_N and Σ_F for the normal metal and ferromagnet, respectively.

(1) Green's function of the normal metal:

The Green's function $G = [\omega \mathrm{I} - H_0]^{-1}$ of the semi-infinite normal metal is defined as

$$G = \begin{bmatrix} E & t_0 & 0 & \cdots & \cdots \\ t_0 & E & t_0 & \cdots & \cdots \\ 0 & t_0 & E & t_0 & \\ \vdots & 0 & t_0 & E & \ddots \\ \vdots & \vdots & & \ddots & \ddots \end{bmatrix}^{-1}, \tag{4.59}$$

where $E = \omega - 2t_0 = 2t_0 \cos ka$ is the shifted energy. This is an infinite matrix, we set its dimensionality to be N and take the $N \to \infty$ limit at the end. However, only the first element G_{00} is relevant to the interface scattering [24, 25], thus what we actually need is

$$G_{00} = \lim_{N\to\infty} \frac{D_{N-1}}{D_N}, \tag{4.60}$$

where D_N is the determinant of the $N \times N$ dimensional matrix. By a straight-

forward manipulation, we obtain the recursion relation

$$D_N = ED_{N-1} - t_0^2 D_{N-2}. \tag{4.61}$$

We can solve it by solving its characteristic equation

$$r^2 - Er + t_0^2 = 0, \tag{4.62}$$

when $-2t_0 \leq E \leq 2t_0$, it has two complex roots:

$$r_1 = \frac{1}{2}[E + i\sqrt{4t_0^2 - E^2}], \qquad r_2 = \frac{1}{2}[E - i\sqrt{4t_0^2 - E^2}], \tag{4.63a}$$

when $E < -2t_0$ or $E > 2t_0$, it has two real roots:

$$r_1 = \frac{1}{2}[E + \sqrt{4t_0^2 - E^2}], \qquad r_2 = \frac{1}{2}[E - \sqrt{4t_0^2 - E^2}]. \tag{4.64a}$$

The general expression for D_N is

$$D_N = ar_1^N + br_2^N, \tag{4.65}$$

where the coefficients a and b can be fixed by the initial condition $D_1 = E$ and $D_2 = E^2 - t_0^2$.

(i) For $-2t_0 \leq E \leq 2t_0$, we obtain

$$a = \frac{1}{2}\left[1 - i\frac{E}{\sqrt{4t_0^2 - E^2}}\right], \qquad b = \frac{1}{2}\left[1 + i\frac{E}{\sqrt{4t_0^2 - E^2}}\right]. \tag{4.66}$$

Define $R = \frac{2t_0}{\sqrt{4t_0^2 - E^2}}$ and $\varphi = \arccos\frac{E}{2t_0}$, D_N can be expressed as

$$\begin{aligned} D_N =& \frac{1}{2^{N+1}}\left\{\left[1 - i\frac{E}{\sqrt{4t_0^2 - E^2}}\right]\left[E + i\sqrt{4t_0^2 - E^2}\right]^N \right. \\ &\left. + \left[1 + i\frac{E}{\sqrt{4t_0^2 - E^2}}\right]\left[E - i\sqrt{4t_0^2 - E^2}\right]^N\right\} \\ =& \pm R\, t_0^N \sin(N+1)\varphi, \end{aligned} \tag{4.67}$$

with $+(-)$ for $E > 0 (E < 0)$. The Green's function we are looking for is

$$G_{00} = \frac{1}{t_0} \lim_{N\to\infty} \frac{\sin[N\varphi]}{\sin[(N+1)\varphi]}. \tag{4.68}$$

To get an unambiguous limit, we need to add an infinitesimal imaginary part to the energy: $E \to E + i\eta^+$ (we only consider the retarded Green's function; the advanced solution refers to η^-). Then

$$\varphi = \arccos\frac{E}{2t_0} - i\frac{\eta^+}{\sqrt{1-(\frac{E}{2t_0})^2}} + \mathcal{O}(\eta^{+2}), \tag{4.69}$$

in the $N \to \infty$ limit, the factor $e^{-iN\varphi}$ dies out, thus we have

$$\begin{aligned} G_{00} &= \frac{1}{t_0} \lim_{N\to\infty} \frac{e^{iN\varphi} - e^{-iN\varphi}}{e^{i(N+1)\varphi} - e^{-i(N+1)\varphi}} \\ &= \frac{1}{t_0} e^{-i\varphi} = \frac{1}{t_0} e^{-i\arccos\frac{E}{2t_0}}. \end{aligned} \tag{4.70}$$

In view of the band structure, we have $ka = \arccos(1 - \frac{\varepsilon}{2t_0})$, the final form of the retarded Green's function reads

$$G_{00} = -\frac{1}{t_0} e^{ika}, \quad \text{with } k = k(\varepsilon). \tag{4.71}$$

(ii) For $E < -2t_0$ or $E > 2t_0$, we obtain

$$a = \frac{1}{2}\left[1 + \frac{E}{\sqrt{4t_0^2 - E^2}}\right], \qquad b = \frac{1}{2}\left[1 - \frac{E}{\sqrt{4t_0^2 - E^2}}\right], \tag{4.72}$$

thus the Green's function becomes

$$\begin{aligned} G_{00} &= \frac{1}{t_0} \lim_{N\to\infty} \frac{D_{N-1}}{D_N} \\ &= 2\frac{(E + \sqrt{E^2 - 4t_0^2})^N - (E - \sqrt{E^2 - 4t_0^2})^N}{(E + \sqrt{E^2 - 4t_0^2})^{N+1} - (E - \sqrt{E^2 - 4t_0^2})^{N+1}}, \end{aligned} \tag{4.73}$$

if $E < -2t_0$, we have

$$G_{00} = \frac{1}{2t_0^2}\left[E + \sqrt{E^2 - 4t_0^2}\right]; \tag{4.74}$$

if $E > 2t_0$, we have

$$G_{00} = \frac{1}{2t_0^2}\left[E - \sqrt{E^2 - 4t_0^2}\right]. \tag{4.75}$$

When $E \neq 0$ is fixed, and let $t_0 \to 0$, $G_{00} \to 1/E$.

(2) Green's function of the ferromagnet:

To compute the Green's function for the ferromagnet, spin degree of freedom has to be considered, which renders the Green's function matrix

$$G^N = \begin{bmatrix} \omega \mathrm{I} - H_0 & -T & 0 & \cdots \\ -T^\dagger & \omega \mathrm{I} - H_0 & -T & \cdots \\ 0 & -T^\dagger & \omega \mathrm{I} - H_0 & \cdots \\ \vdots & \vdots & \vdots & \ddots \end{bmatrix}^{-1}_{N\times N}, \tag{4.76}$$

where $H_0 = -J\boldsymbol{m}\cdot\boldsymbol{\sigma} + 2t_m\sigma_0$ and $T = -t_m\sigma_0$, where τ_0 is the identity matrix. From linear algebra, the inversion of a blocked matrix is

$$\begin{bmatrix} R_{n\times n} & P_{n\times m} \\ Q_{m\times n} & S_{m\times m} \end{bmatrix}^{-1} = \begin{bmatrix} (R - PS^{-1}Q)^{-1} & -(R - PS^{-1}Q)^{-1}PS^{-1} \\ -S^{-1}Q(R - PS^{-1}Q)^{-1} & S^{-1} + S^{-1}Q(R - PS^{-1}Q)^{-1}PS^{-1} \end{bmatrix}. \tag{4.77}$$

If we identify $R = \omega\mathrm{I} - H_0$ and $P = Q^\dagger = [T\ 0\ 0\ \cdots\ 0]$, then S is nothing but G^{N-1} that represents the Green's function for a ferromagnetic chain with the leftmost atom removed. The upper left block of the right hand side of Eq. (4.77) tells us that

$$(\omega\mathrm{I} - H_0)G_{00}^N - TG_{00}^{N-1}T^\dagger G_{00}^N = \mathrm{I}, \tag{4.78a}$$

$$G_{00}^N(\omega\mathrm{I} - H_0) - G_{00}^N T G_{00}^{N-1}T^\dagger = \mathrm{I}, \tag{4.78b}$$

which indicates $[H_0, G_{00}^N] = 0$ since $T = T^\dagger$. This commutation relation will play a crucial rule in the following calculations. As $N \to \infty$, we must have $G_{00}^N \approx G_{00}^{N-1}$, for simplicity we denote $g = \lim_{N\to\infty} G_{00}^N$. Then Eq. (4.78) provides us with a matrix equation of g

$$(\omega \mathrm{I} - H_0)g - t_m^2 g^2 = \mathrm{I}. \tag{4.79}$$

To solve Eq. (4.79), we take the z-axis in the spin space to be $\boldsymbol{m}$, thus $H_0 = -J\sigma_3 + 2t_m\sigma_0$. Decompose g by the Pauli matrices

$$g = A\sigma_0 + B\sigma_1 + C\sigma_2 + D\sigma_3, \tag{4.80}$$

the commutation relation $[H_0, G_{00}^N] = 0$ requires $B = C = 0$, and coefficients A and D can be solved by Eq. (4.79). *This will be our standard procedure of solving Green's functions throughout this section.* Define $\alpha = A + D$ and $\beta = A - D$, and set the Fermi energy $E_F = \omega - 2t_m = 0$:

(i) If $J < 2t_m$, the ferromagnet is metallic, and the retarded solution is

$$\alpha = \frac{1}{2t_m^2}\left[-J - i\sqrt{4t_m^2 - J^2}\right], \quad \beta = \frac{1}{2t_m^2}\left[J - i\sqrt{4t_m^2 - J^2}\right]. \tag{4.81}$$

(ii) If $J > 2t_m$, the ferromagnet is insulating, and the retarded solution is

$$\alpha = \frac{1}{2t_m^2}\left[-J + \sqrt{J^2 - 4t_m^2}\right], \quad \beta = \frac{1}{2t_m^2}\left[J - \sqrt{J^2 - 4t_m^2}\right]. \tag{4.82}$$

Finally, the self-energy of the ferromagnet is

$$\Sigma_F = \frac{t'^2}{2}[(\alpha + \beta)\sigma_0 + (\alpha - \beta)\sigma_3], \tag{4.83}$$

where σ_3 will be replaced by $\boldsymbol{m}\cdot\boldsymbol{\sigma}$ at the end to dismiss the influence of the special gauge chosen to simplify our calculations (similar trick has been adopted in Chapter two).

(3) Electron reflection:

According to the Fisher-Lee equation, the reflection coefficient is

$$r = -1 + (2it_0 \sin ka)\mathcal{G}, \tag{4.84}$$

where $\mathcal{G}$ is the Green's function for the "system", which is taken to be the last atom on the normal metal side. When the Fermi energy is set to be zero, $ka = \pi/2$, and the Green's function is

$$\mathcal{G} = [0 - \Sigma_N - \Sigma_F]^{-1}, \tag{4.85}$$

where $\Sigma_N = -it_0$ is the self-energy of the normal metal. Scale $\lambda = J/t_0$, $\xi = t'/t_0$, and $\alpha = t_m/t_0$ as what has been done before; consider Eq. (4.83), (4.84), and (4.85), we solve the reflection coefficient

$$r = \frac{\left[4\alpha^4 - \xi^4(\lambda - \sqrt{\lambda^2 - 4\alpha^2})^2\right]\sigma_0 + 4i\alpha^2\xi^2(\lambda - \sqrt{\lambda^2 - 4\alpha^2})\sigma_3}{4\alpha^4 + \xi^4(\lambda - \sqrt{\lambda^2 - 4\alpha^2})^2} \quad \text{for } \alpha < \frac{\lambda}{2}, \tag{4.86}$$

$$r = \frac{(\alpha^2 - \xi^4)\sigma_0 + i\lambda\xi^2\sigma_3}{\alpha^2 + \xi^4 + \xi^2\sqrt{4\alpha^2 - \lambda^2}} \quad \text{for } \alpha > \frac{\lambda}{2}. \tag{4.87}$$

We notice that Eq. (4.86) satisfies $|r|^2 = 1$. If $\alpha \to 0$, Eq. (4.86) becomes

$$r = \frac{\lambda^2 - \xi^4}{\lambda^2 + \xi^4}\sigma + \frac{2i\lambda\xi^2}{\lambda^2 + \xi^4}\boldsymbol{m}\cdot\boldsymbol{\sigma}, \tag{4.88}$$

which reproduces Eq. (4.35), (4.36) and (4.37) for $ka = \pi/2$. We plot Eq. (4.86) and (4.87) as functions of α and ξ in Fig. 4.6, where we find that

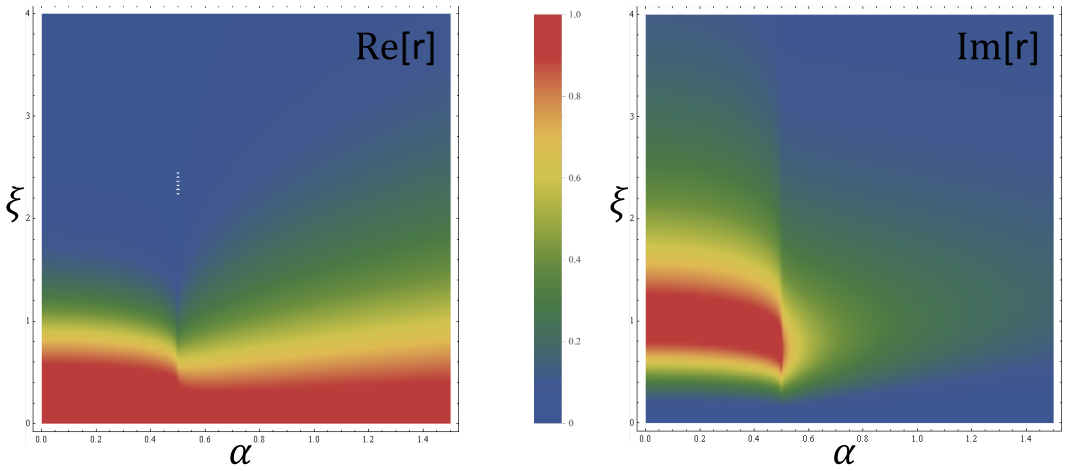

Figure 4.6: Density plot of the real and imaginary parts of r versus α and ξ, where $\lambda = 1$. For $\alpha < \lambda/2$, the α dependence of r is weak.

for the insulating case ($\alpha < \lambda/2$), the α dependence is quite weak. In other word, *the increasing penetration depth of the evanescent wave does NOT alter r significantly.* This fact justifies the validity of the semi-infinite mode we adopted in the previous section where only one magnetic atom is considered.

(4) 1-d infinite normal metal—antiferromagnet chain:

With the Fisher-Lee solution above, we take one step further towards the spin-dependent scattering of an antiferromagnetic interface. Consider a 1-d N/AF chain as illustrated in Fig. 4.7. The magnetic atoms (red and blue) are described by the Hamiltonians

$$H_1 = 2t_m\sigma_0 - J\sigma_3, \quad H_2 = 2t_m\sigma_0 + J\sigma_3, \tag{4.89}$$

in an alternating pattern. However, since $H_1 \neq H_2$, the iteration scheme of solving the Green's function previously developed has to be generalized. The

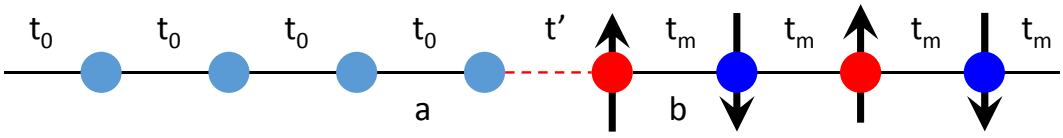

Figure 4.7: Replace the ferromagnet in Fig. 4.5 with antiferromagnet, all parameters are the same.

Green's function matrix is now

$$G = \begin{bmatrix} E-H_1 & t_m\sigma_0 & 0 & \cdots & \cdots \\ t_m\sigma_0 & E-H_2 & t_m\sigma_0 & \cdots & \cdots \\ 0 & t_m\sigma_0 & E-H_1 & t_m\sigma_0 & \\ \vdots & 0 & t_m\sigma_0 & E-H_2 & \ddots \\ \vdots & \vdots & & \ddots & \ddots \end{bmatrix}^{-1}. \tag{4.90}$$

Since $G_{00}^N \approx G_{00}^{N-2}$ when $N \to \infty$, we have to do the matrix reduction twice in order to eliminate G_{00}^{N-1}. After some algebra, we obtain

$$h_2 h_1 g - t_m^2 g h_1 g = h_2, \tag{4.91a}$$

$$g h_1 h_2 - t_m^2 g h_1 g = h_2, \tag{4.91b}$$

where $g = \lim_{N\to\infty} G_{00}^N = \lim_{N\to\infty} G_{00}^{N-2}$, and $h_{1(2)} = E - H_{1(2)}$.

Different from that of a ferromagnet, we obtain a generalized commutation relation $h_2 h_1 g = g h_1 h_2$. Decompose the Green's function as

$$g = \mathcal{A}\sigma_0 + \mathcal{B}\sigma_1 + \mathcal{C}\sigma_2 + \mathcal{D}\sigma_3, \tag{4.92}$$

it automatically satisfies the generalized commutation relation. Substitute Eq. (4.92) into Eq. (4.91), we obtain $\mathcal{B} = \mathcal{C} = 0$; denote $\Omega = E - 2t_m$, then $\mathcal{A}$ and $\mathcal{D}$ satisfy either $J\mathcal{A} + \Omega\mathcal{D} = 0$, or $(J^2 - \Omega^2) + 2t_m^2(\mathcal{A}\Omega + \mathcal{D}J) = 0$. If the

former is true, the solution is

$$\mathcal{A} = \frac{\Omega}{2t_m^2}\left[1 \pm \sqrt{1 - \frac{4t_m^2}{\Omega^2 - J^2}}\right], \tag{4.93a}$$

$$\mathcal{D} = \frac{J}{2t_m^2}\left[-1 \mp \sqrt{1 - \frac{4t_m^2}{\Omega^2 - J^2}}\right]. \tag{4.93b}$$

If the latter is true, the solution is

$$\mathcal{A} = \frac{\Omega}{2t_m^2}\left[1 \pm \frac{J}{\Omega}\sqrt{1 - \frac{4t_m^2}{\Omega^2 - J^2}}\right], \tag{4.94a}$$

$$\mathcal{D} = \frac{J}{2t_m^2}\left[-1 \mp \frac{\Omega}{J}\sqrt{1 - \frac{4t_m^2}{\Omega^2 - J^2}}\right]. \tag{4.94b}$$

But we know that the physical solution should reduce to the normal metal case ($\mathcal{D} \to 0$) when $J \to 0$, thus only the former survives. If we set the Fermi energy to be zero ($\Omega = 0$), the system is always insulating for arbitrary finite J. So the solution becomes

$$\mathcal{A} = 0, \quad \mathcal{D} = \frac{1}{2t_m^2}\left[-J + \sqrt{J^2 + 4t_m^2}\right]. \tag{4.95}$$

Substitute them into the Green's function:

$$\mathcal{G} = [0 - \Sigma_N - \Sigma_F]^{-1} = [it_0\sigma_0 - t'^2\mathcal{D}\sigma_3]^{-1} = \frac{-it_0\sigma_0 - t'^2\mathcal{D}\sigma_3}{t_0^2 + t'^4\mathcal{D}^2}, \tag{4.96}$$

scale $\alpha = t_m/t_0$, $\lambda = J/t_0$, and $\xi = t'/t_0$, and identify σ_3 by $\boldsymbol{n}\cdot\boldsymbol{\sigma}$ as what it would be in a general frame, the reflection coefficient is obtained

$$\begin{aligned} r &= r_0\sigma_0 + \Delta r(\boldsymbol{n}\cdot\boldsymbol{\sigma}) = -1 + 2it_0\mathcal{G} \\ &= \frac{\left[4\alpha^4 - \xi^4(\lambda - \sqrt{\lambda^2 + 4\alpha^2})^2\right]\sigma_0 + 4i\alpha^2\xi^2(\lambda - \sqrt{\lambda^2 + 4\alpha^2})\boldsymbol{n}\cdot\boldsymbol{\sigma}}{4\alpha^4 + \xi^4(\lambda - \sqrt{\lambda^2 + 4\alpha^2})^2}. \end{aligned} \tag{4.97}$$

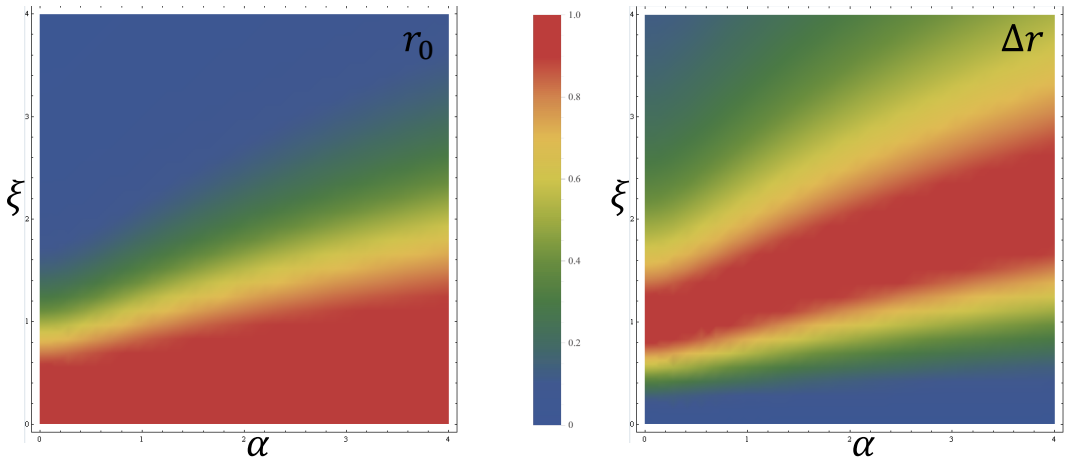

Figure 4.8: Density plot of the r_0 and Δr in Eq. (4.97) as functions of α and ξ with $\lambda = 1$.

When $\alpha \to 0$, Eq. (4.97) reduces to

$$r = \frac{\lambda^2 - \xi^4}{\lambda^2 + \xi^4}\sigma - \frac{2i\lambda\xi^2}{\lambda^2 + \xi^4}\boldsymbol{n} \cdot \boldsymbol{\sigma}, \tag{4.98}$$

which is the same as Eq. (4.35)-(4.37) for $ka = \pi/2$ ($E_F = 0$). The only difference is that $\boldsymbol{m}$ is replaced by the staggered order $\boldsymbol{n} = (\boldsymbol{m}_1 - \boldsymbol{m}_2)/2$.

From Eq. (4.97), we see that Δr has a maximum value 1 regardless of α and ξ. We plot r_0 and Δr in Fig. 4.8, which shows that as α increases, the maximum Δr occurs at increasing ξ. We read off an important information from this fact: *for 1-d insulating AF chain, spin-pumping into the normal metal is determined by the end magnetic moment as if the system is a N/F chain; tunneling into the bulk AF (evanescent waves) only modifies the optimal value of* ξ. As will become clear later, this justifies that for an uncompensated N/AF interface in higher dimensions, spin-pumping has no qualitative difference from that in ferromagnetic systems.

4.2.3 Higher Dimensions

Comparing to the Fisher-Lee formalism, wave function matching is more transparent and straightforward, thus we will adopt the latter in this section and generalize the 1-d result into higher dimensions.

– **Two dimension**:

We consider two cases for two dimensions in analogy to the 1-d double chain. Depicted in the left panel of Fig. 4.9, we simply stack 1-d chains of Fig. 4.3 in staggered order, and assume the hopping along y direction is t_m for all sites. While translational symmetry is preserved along y, the coupling to the magnetic atoms yields the folding of BZ. So the wave function is

$$\psi(\boldsymbol{r}) = e^{ik_y y}\phi(x) = e^{ik_y y}\phi_n = e^{ik_y(2ma)} \begin{bmatrix} \phi_n^A \\ \phi_n^B \end{bmatrix}, \tag{4.99}$$

where n and m are integers labeling the atomic sites. The eigen-equation reads

$$E\phi_n = U\phi_n - t(\phi_{n-1} + \phi_{n+1}) - t_m\hat{Q}\phi_n, \tag{4.100}$$

where the operator $\hat{Q}$ acts on the pseudo-spin space, it takes the form

$$\hat{Q} = \begin{bmatrix} 0 & 2\cos k_y a \\ 2\cos k_y a & 0 \end{bmatrix} = 2\cos k_y a \tau_1. \tag{4.101}$$

One should note that valid choices of $\hat{Q}$ are not restricted to Eq. (4.101), thanks to the gauge freedom of the Bloch wave. For bulk normal metal, Eq. (4.100) can be easily solved. Define $\varepsilon = (E-U)/t$ and $\alpha = t_m/t$, we obtain

$$\varepsilon = -2[\cos k_x a + \alpha\tau\cos k_y a], \quad \text{with } |\tau\rangle \equiv \phi_\tau = \frac{1}{\sqrt{2}} \begin{bmatrix} 1 \\ \tau \end{bmatrix}, \tag{4.102}$$

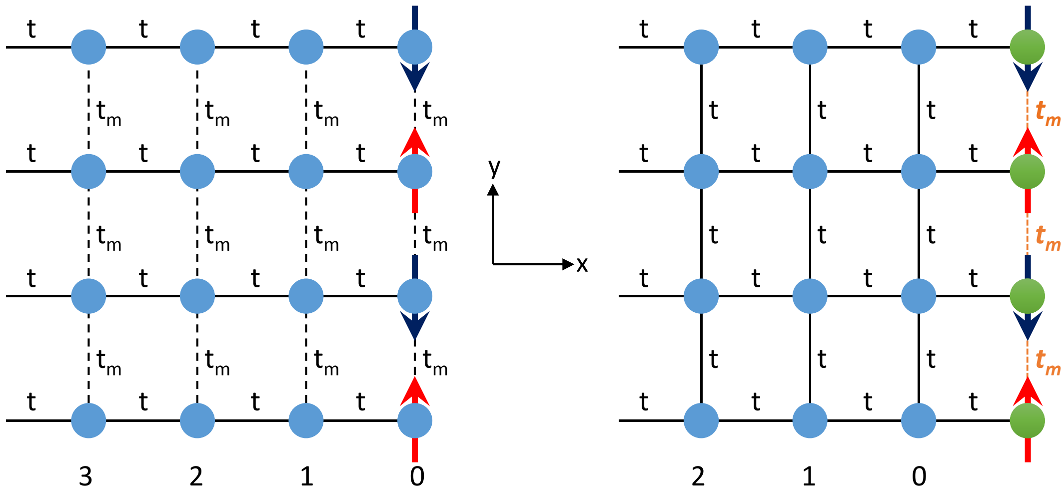

Figure 4.9: Left: a simple stack of 1-d chains, hopping along y is assumed to be t_m for all sites. Right: t_m refers only to the hopping between magnetic atoms, all other hoppings are t.

where $\tau = \pm$ represent the two bands in the shrunk BZ. We notice that the case of double chain amounts to set $2\cos k_y a = 1$.

Again assume $R^{\pm,\pm}_{s',s} = r^{\pm,\pm}\delta_{s',s}$ and $R^{\pm,\mp}_{s',s} = r^{\pm,\mp}(\boldsymbol{n}\cdot\boldsymbol{\sigma}_{s',s})$; the band structure also provides a relation $4\cos k_y a = e^{ik_x^- a} + e^{-ik_x^- a} - (e^{ik_x^+ a} + e^{-ik_x^+ a})$. Following a similar procedure as the double-chain case, we obtain

$$r^{+,+} = \frac{e^{i(k_x^+ - k_x^-)a} - \lambda^2}{\lambda^2 - e^{-i(k_x^+ + k_x^-)a}}, \qquad r^{+,-} = \frac{2i\lambda\sqrt{\sin k_x^+ a \sin k_x^- a}}{\lambda^2 - e^{-i(k_x^+ + k_x^-)a}}, \tag{4.103}$$

$$r^{-,+} = \frac{2i\lambda\sqrt{\sin k_x^- a \sin k_x^+ a}}{\lambda^2 - e^{-i(k_x^+ + k_x^-)a}}, \qquad r^{-,-} = \frac{e^{i(k_x^- - k_x^+)a} - \lambda^2}{\lambda^2 - e^{-i(k_x^+ + k_x^-)a}}, \tag{4.104}$$

which is exactly the same form as the double chain case. However, k_x^+ and k_x^- are now dependent on k_y: for $\varepsilon_f = 0$ we have $k_x^\pm a = \arccos[\mp\alpha\cos k_y a]$, which gives $(k_x^+ + k_x^-)a = \pi$ and $\sin k_x^+ a = \sin k_x^- a = \sqrt{1 - \alpha^2\cos^2 k_y a}$.

Now we turn to the right panel of Fig. 4.9 where only magnetic atoms

are connected via t_m. Following a similar procedure as the double chain case, we finally obtain

$$r^{++} = e^{2ik_x^+ a} \frac{[e^{ik_x^+ a} + 2(1-\alpha)\cos k_y a][e^{-ik_x^- a} - 2(1-\alpha)\cos k_y a] - \lambda^2}{\lambda^2 - [e^{-ik_x^+ a} + 2(1-\alpha)\cos k_y a][e^{-ik_x^- a} - 2(1-\alpha)\cos k_y a]}, \tag{4.105}$$

$$r^{--} = e^{2ik_x^- a} \frac{[e^{-ik_x^+ a} + 2(1-\alpha)\cos k_y a][e^{ik_x^- a} - 2(1-\alpha)\cos k_y a] - \lambda^2}{\lambda^2 - [e^{-ik_x^+ a} + 2(1-\alpha)\cos k_y a][e^{-ik_x^- a} - 2(1-\alpha)\cos k_y a]}, \tag{4.106}$$

$$r^{+-} = r^{-+} = \frac{2i\lambda e^{i(k_x^+ + k_x^-)a}\sqrt{\sin k_x^+ a \sin k_x^- a}}{\lambda^2 - [e^{-ik_x^+ a} + 2(1-\alpha)\cos k_y a][e^{-ik_x^- a} - 2(1-\alpha)\cos k_y a]}, \tag{4.107}$$

If $\alpha \to 1$, these results reduce to the previous case where hopping along y is the same for all sites.

– Three dimension

Depicted in Fig. 4.10, situation in 3-d is similar to the latter case of 2-d, where only magnetic atoms are connected via $-t_m$ while all other links have the same hopping $-t$. This simple model represents a real interface of normal metal/AF insulator.

We choose $[0, 1, 1]$ and $[0, \bar{1}, 1]$ as our y and z directions, the merit of which is that only two atoms are grouped into a unit cell, thus we are able to take advantage of the 2-d approach. What we need to modify are: $U = 6t$,

$$\hat{Q} = 4\cos\frac{k_y a}{\sqrt{2}}\cos\frac{k_z a}{\sqrt{2}}\ \hat{\tau}_1, \tag{4.108}$$

and the band structure $\varepsilon_\pm = -2\cos k_x^\pm \mp 4\cos\frac{k_y a}{\sqrt{2}}\cos\frac{k_z a}{\sqrt{2}}$. For linear response, only electrons on the Fermi surface contribute, thus in the following calculation

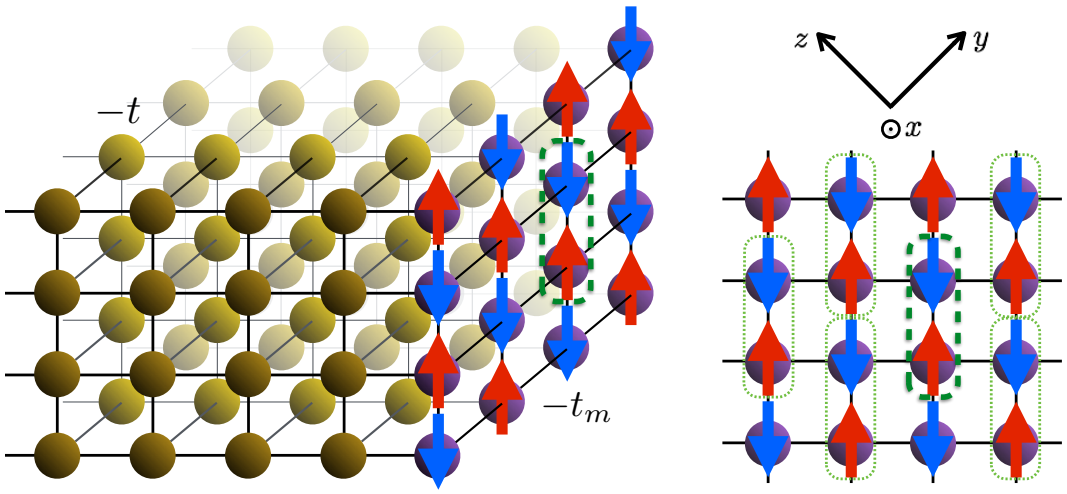

Figure 4.10: A compensated N/AF interface with cubic lattice. The interface normal is along $\hat{\boldsymbol{x}}$. Unit cells (dotted Green circles) are periodic in the $[0,1,1]$ and $[0,\bar{1},1]$ directions, which are labeled by $\hat{\boldsymbol{y}}$ and $\hat{\boldsymbol{z}}$, respectively.

we assume $\varepsilon_+ = \varepsilon_- = \varepsilon_f$. The result should be of the same form as Eq. (4.105)–Eq. (4.107) except that $\cos k_y a$ is replaced by $2\cos\frac{k_y a}{\sqrt{2}}\cos\frac{k_z a}{\sqrt{2}}$, especially,

$$r^{+,-} = \frac{2i\lambda e^{i(k_x^+ + k_x^-)a}\sqrt{\sin k_x^+ a \sin k_x^- a}}{\lambda^2 - [e^{-ik_x^+ a} + 4(1-\alpha)\cos\frac{k_y a}{\sqrt{2}}\cos\frac{k_z a}{\sqrt{2}}][e^{-ik_x^- a} - 4(1-\alpha)\cos\frac{k_y a}{\sqrt{2}}\cos\frac{k_z a}{\sqrt{2}}]}. \tag{4.109}$$

When $\varepsilon_f = 0$, we have $k_x^+ + k_x^- = \pi/a$. As only $k_x > 0$ states will be considered ($k_x < 0$ states will never reach the interface), we know

$$k_x^+ a = \pi - \arccos[2\cos\frac{k_y a}{\sqrt{2}}\cos\frac{k_z a}{\sqrt{2}}], \qquad k_x^- a = \arccos[2\cos\frac{k_y a}{\sqrt{2}}\cos\frac{k_z a}{\sqrt{2}}],$$

so that the module square of ΔS can be simplified as

$$|r^{+,-}|^2 = \frac{4\lambda^2[1 - 4\cos^2\frac{k_y a}{\sqrt{2}}\cos^2\frac{k_z a}{\sqrt{2}}]}{\left[\lambda^2 + 1 + 16\alpha(\alpha-1)\cos^2\frac{k_y a}{\sqrt{2}}\cos^2\frac{k_z a}{\sqrt{2}}\right]^2}. \tag{4.110}$$

Eq. (4.110) is what we are going to use in calculating the spin-mixing conductance in the following section.

4.2.4 Spin-mixing Conductance

As discussed in previous chapters, in the exchange limit we have $|\boldsymbol{m}| \ll 1$ and $|\boldsymbol{n}| \approx 1$. It can be shown that to linear order in the small $\boldsymbol{m}$, Eq. (4.52) is only slightly modified by adding a term proportional to $\boldsymbol{m}$. The coefficient of the added term is approximately $r^{+,-}$. For the sake of mathematical clarity, we turn back to the A-B sublattice representation ($\hat{\tau}_1$ and $\hat{\tau}_3$ interchange), where the scattering matrix is

$$S = S_0 + S_w \hat{\tau}_1 \hat{\sigma}_0 + \Delta S[\hat{\tau}_3(\boldsymbol{n} \cdot \hat{\boldsymbol{\sigma}}) + \hat{\tau}_0(\boldsymbol{m} \cdot \hat{\boldsymbol{\sigma}})], \tag{4.111}$$

where $\hat{\boldsymbol{\sigma}}$ and $\hat{\tau}_{1,2,3}$ are spin and pseudo-spin Pauli matrices, and $\hat{\tau}_0$ and $\hat{\sigma}_0$ are identity matrices. The last two terms of Eq. (4.111) with a common coefficient ΔS are spin-dependent and represent the Umklapp and normal scatterings, respectively. In the Umklapp process, an electron acquires π/a momentum in the transverse direction during the scattering. The coefficient ΔS, in our insulating AF case, is just $r^{+,-}$ obtained in Eq. (4.109).

The term $\hat{\tau}_2[(\boldsymbol{n} \times \boldsymbol{m}) \cdot \boldsymbol{\sigma}]$ is also allowed by symmetry. But its coefficient is much smaller than ΔS. Meanwhile, it does not contribute to the mixing conductance upon integration over the Fermi surface.

As will become clear in the following, pumping effects are related to the coefficients in Eq. (4.111) through the spin-mixing conductance $G_{\text{mix}} =$

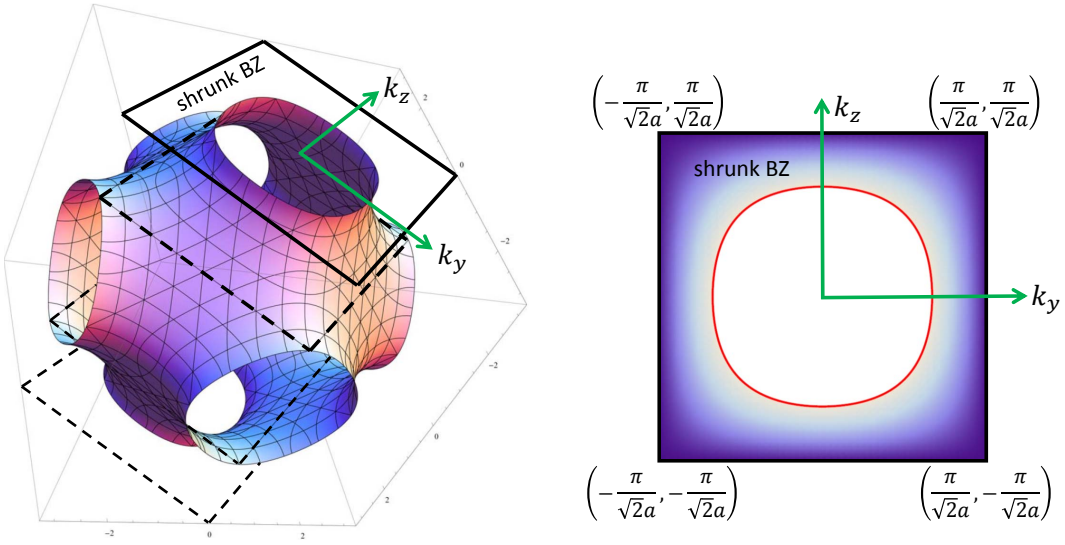

Figure 4.11: The left panel depicts the Fermi surface $\varepsilon_f = 0$. Integration over k_y and k_z is restricted to the region where $0 < 2\cos\frac{k_y a}{\sqrt{2}}\cos\frac{k_z a}{\sqrt{2}} < 1$ is satisfied. From a bird's eye view, it is just the shaded area of the right panel.

$G_r + iG_i$, where

$$G_r = \frac{e^2\mathcal{A}}{h\pi^2}\iint |\Delta S|^2 dk_y dk_z, \tag{4.112}$$

$$G_i = \frac{e^2\mathcal{A}}{h\pi^2}\iint \mathrm{Im}[S_0^*\Delta S] dk_y dk_z, \tag{4.113}$$

where k_y and k_z are the transverse momenta and $\mathcal{A}$ the interface cross section. Similar to their counterparts in F, G_r typically overwhelms G_i by orders of magnitude within practical parameter ranges, thus G_r is more pertinent to our discussions.

The integrations of Eq. (4.112) and (4.113) are performed over the Fermi surface. As shown in Fig. 4.11, the shrunk BZ is marked by $k_y \in (-\frac{\pi}{\sqrt{2}a}, \frac{\pi}{\sqrt{2}a}) \cap k_z \in (-\frac{\pi}{\sqrt{2}a}, \frac{\pi}{\sqrt{2}a})$, within which $2\cos\frac{k_y a}{\sqrt{2}}\cos\frac{k_z a}{\sqrt{2}}$ is always positive.

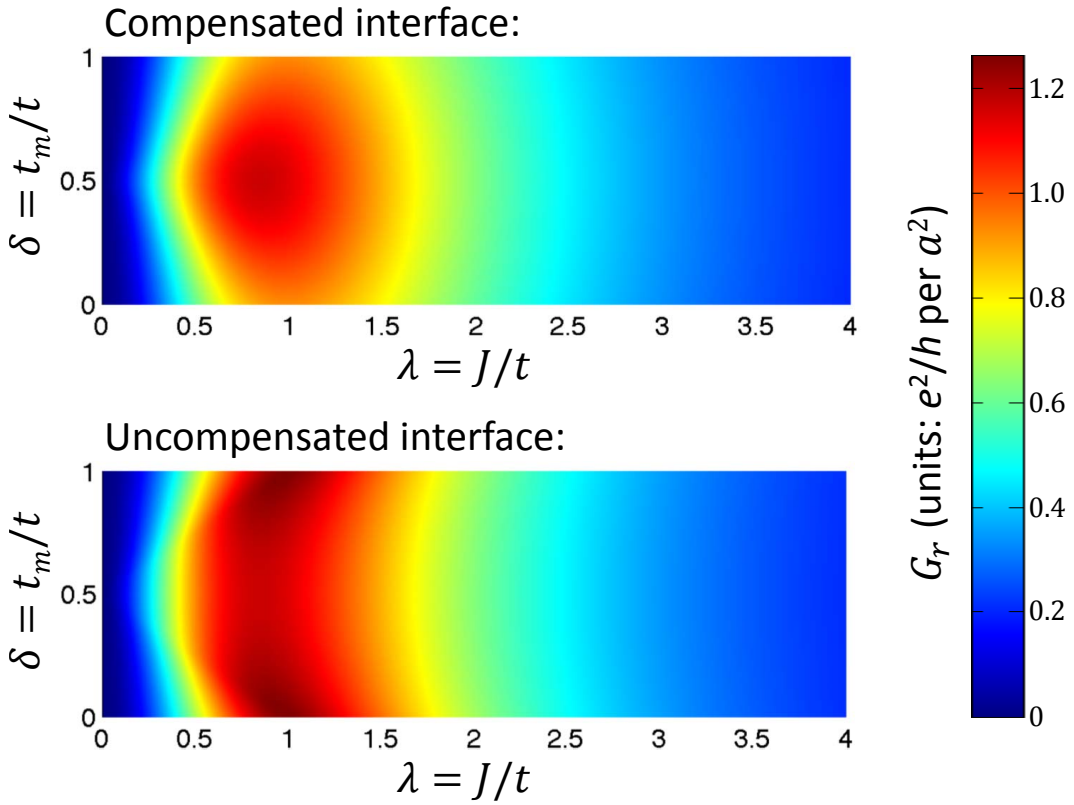

Figure 4.12: (Color online) Spin mixing conductance G_r as a function of λ and δ in units of e^2/h per a^2 (a is lattice constant) for compensated and uncompensated N/AF interfaces.

But the integration over (k_y, k_z)-plane should be restricted to the region where $0 < 2\cos\frac{k_y a}{\sqrt{2}}\cos\frac{k_z a}{\sqrt{2}} < 1$, which corresponds to the shaded area in the right panel of Fig. 4.11. An analytical result is not available due to the complicated shape of the Fermi surface, so we numerically perform the integration.

We define the dimensionless energies $\lambda = J/t$ and $\delta = t_m/t$. The result $G_r = G_r(\lambda, \delta)$ is plotted in the upper panel of Fig. 4.12, where G_r reaches the maximum at $\lambda = 0.86$ and $\delta = 0.5$. To elucidate how spin scattering is affected

by the staggered field, we also calculate G_r for an uncompensated interface as a representative for N/F and plot the result in the lower panel of Fig. 4.12. Clearly, the two cases are similar in magnitude [2], implying that spin transfer on a compensated N/AF interface is as efficient as that on N/F for the case of insulating magnets. With the current insight of AF dynamics, this feature is consistent with the expectations in Ref. [46] of "no difference for the spin absorbed by a fully ordered interface with a large net magnetic moment or a compensated one."

4.3 Spin Pumping

Although the AF resonance frequency reaches the THz region ($1 \sim 10$ meV), the motion of the staggered field remains adiabatic as evidenced by comparing ($\hbar$ times) the resonance frequency with two characteristic energy scales: (i) the Fermi energy in N is a few eV; (ii) the exchange coupling between conduction electron spins and magnetic moments can be as large as eV. As a result, the spin eigenstates and the scattering matrix Eq. (4.111) adiabatically adapt to the instantaneous configuration of AF.

Consequently, spin-pumping can be studied from the perspective of adiabatic pumping, which was first introduced in a closed system by Thouless [110] and was later generalized to open systems [146]. The seminal work

[2] Within tight-binding model, a bipartite AF is always insulating at half filling for finite J, regardless of t_m. But comparing to t in N, t_m is in general much smaller, thus $\delta = t_m/t$ is customarily taken to be close to zero. For $\delta \to 0$, the maxima of G_r appear at $\lambda = 1$ for both compensated and uncompensated interfaces.

by Brouwer [13] has developed the idea of adiabatic pumping to a general equation applicable to any type of pumping due to slowly changing parameters. The Brouwer's equation was later identified as the non-Abelian Berry phase for open systems [147], which has upgraded the pumping problem on an equal footing as the effective gauge coupling discussed in Chapter two.

4.3.1 Brouwer's Equation

When a system Hamiltonian depends on a set of parameters $\{X_i\}$, the total time derivative is expressed by $\frac{\mathrm{d}}{\mathrm{d}t} = \sum_i \frac{\mathrm{d}X_i}{\mathrm{d}t}\frac{\partial}{\partial X_i}$. As a result, a geometric phase is accumulated by the wave function after a closed path of traveling in the parameter space,

$$\gamma = 2i \iint \mathrm{d}\boldsymbol{s} \cdot \mathrm{Im}\langle\nabla\psi| \times |\nabla\psi\rangle, \tag{4.114}$$

known as the Berry's phase [9], where $\mathrm{d}\boldsymbol{s}$ is the differential area along surface normal in the region subtended by the closed path.

When generalized to open systems [146,147], it is the scattering matrix that replaces the wave function. Denote the probability amplitude of scattering from m to n channels by S_{nm}, then the Berry phase of the n-th channel upon one period of parameter change is

$$\gamma_n = 2i \sum_m \iint \mathrm{d}\boldsymbol{s} \cdot \mathrm{Im}\nabla S^\dagger_{nm} \times \nabla S_{mn}, \tag{4.115}$$

where ∇ represents gradient in the parameter space. In the electron scattering problem, the Berry phase associated with the n-th channel determines the

emissivity of that channel. Specifically, the net charge flowing into the channel is $Q_n = \frac{e}{2\pi}\gamma_n$. As a result, the average current is $I_n = Q_n/T$ where T is the period of parameter change. Due to charge conservation, the current is subject to the constraint $\sum_n I_n = 0$, which is the open-system counterpart of the constraint on the Berry phase.

If the scattering channels are spin-dependent, we will also get pumped spin currents. As mentioned just now, the magnetic resonance frequency is much smaller than the exchange interaction, thus the magnetic precession naturally serves as the parametric adiabatic motion, and the spin current pumped into channel α can be formally expressed as [13, 65, 111, 113]

$$\boldsymbol{I}_\alpha^{(s)}(t) = e\sum_i \frac{\partial \boldsymbol{R}}{\partial X_i}\frac{\mathrm{d}X_i}{\mathrm{d}t}, \tag{4.116}$$

$$\frac{\partial \boldsymbol{R}}{\partial X_i} = \frac{1}{2\pi}\sum_\beta \sum_{mn}\sum_{ss'}\sum_\sigma \frac{\partial S_{\alpha\beta}^{(ms,n\sigma),*}}{\partial X_i}\hat{\sigma}^{ss'}S_{\beta\alpha}^{(ms',n\sigma)}, \tag{4.117}$$

where $\sum_{mn}$ stands for summations over channels of transverse momenta. The above equations are purely general and does not distinguish AF from ferromagnet in priori. In fact, if the summation incorporates sub-lattice channels (or pseudo-spin), the AF spin pumping will be put on an equal footing with ferromagnetic spin pumping.

The Brower's equation is purely general and applies to other pumped currents as well. According to what appears in the position of $\hat{\sigma}$, corresponding pumped current is obtained.

4.3.2 Pumped Spin and Staggered Spin Currents

Regarding the staggered field $\boldsymbol{n}$ and magnetization $\boldsymbol{m}$ as two independent adiabatic parameters, and taking into account the following identities

$$\mathrm{Tr}[\tau_i\tau_j] = \mathrm{Tr}[\sigma_i\sigma_j] = 2\delta_{ij}, \tag{4.118}$$

$$\mathrm{Tr}[\tau_i\tau_j\tau_k] = \mathrm{Tr}[\sigma_i\sigma_j\sigma_k] = 2i\varepsilon_{ijk}, \tag{4.119}$$

$$\varepsilon_{ijk}\varepsilon_{kmn} = \delta_{im}\delta_{jn} - \delta_{in}\delta_{jm}, \tag{4.120}$$

$$\varepsilon_{ijk}\varepsilon_{jab}\varepsilon_{kmn} = \delta_{im}\varepsilon_{nab} - \delta_{in}\varepsilon_{mab}, \tag{4.121}$$

we obtain the pumped spin current by substituting the scattering matrix S in Eq. (4.111) into Eq. (4.116). The result is [21]

$$\frac{e}{\hbar}\boldsymbol{I}_s = G_r(\boldsymbol{n}\times\dot{\boldsymbol{n}} + \boldsymbol{m}\times\dot{\boldsymbol{m}}) - G_i\dot{\boldsymbol{m}}, \tag{4.122}$$

where $\boldsymbol{I}_s$ is measured in units of an electrical current. Since $\boldsymbol{n} = (\boldsymbol{m}_1 - \boldsymbol{m}_2)/2$ and $\boldsymbol{m} = (\boldsymbol{m}_1 + \boldsymbol{m}_2)/2$, Eq. (4.122) can indeed be interpreted as arising from a coherent sum of two independent F spin pumping contributions by $\boldsymbol{m}_1$ and $\boldsymbol{m}_2$, which justifies the naive result envisioned at the beginning. However, the spin-mixing conductance G_r and G_i are *different* from those of F due to the mixing of scattering channels from different sublattices. Moreover, AF dynamics is much faster than ferromagnets thus a stronger spin pumping is expected from AF.

By taking a time average of Eq. (4.122) over one period of oscillation, only the first two terms survive and contribute to the dc component of spin current I_s^{dc}. Despite that $|\boldsymbol{m}| \ll |\boldsymbol{n}|$, the contribution of $\boldsymbol{m}\times\dot{\boldsymbol{m}}$ to I_s^{dc} can be

comparable to that of $\boldsymbol{n}\times\dot{\boldsymbol{n}}$. This is because I_s^{dc} is proportional to θ^2 (θ labels the cone angle of precession) and the cone angle associated with the staggered field is much smaller than the one associated with the magnetization, $\theta_n \approx 0$ but $\theta_m \approx \pi/2$, as shown in Fig. 4.1.

Consider now the AF motion is generated by a microwave with oscillating magnetic field $\boldsymbol{h}_\perp$ perpendicular to the easy axis, then

$$\begin{aligned} I_s^{dc} \approx & G_r|\tilde{h}_+|^2\omega\left[|\chi_+(\omega)|^2+|\mathscr{X}_+(\omega)|^2\right] \\ = & \frac{G_r\gamma^2|\tilde{h}_+|^2\omega\left[(\omega_A^2+\alpha^2\omega^2)+(\omega-\omega_H)^2\right]}{\left[(\omega-\omega_H)^2+\alpha^2\omega^2-\omega_R^2\right]^2+4\alpha^2\omega^2(\omega_A+\omega_E)^2}, \end{aligned} \tag{4.123}$$

where χ_+ and $\mathscr{X}_+$ are susceptibilities defined in Eq. (4.23a) and Eq. (4.23b), respectively. Here, we stick to the + convention, while allow ω to be both positive and negative in order to represent the right-handed mode and the left-handed mode, respectively.

If the microwave is circularly polarized, only the mode with matching polarization depicted in Fig. 4.1 is driven into resonance at certain frequency. When the magnetic field vanishes, I_s^{dc} is an odd function of ω and is plotted in the upper panel of Fig. 4.13, where the peak (dip) for positive (negative) ω corresponds to the resonance of right-handed (left-handed) mode. Hence an important consequence is implied: the direction of dc spin current is linked to the circular polarization of the driving microwave.

Since the sublattice degree of freedom is involved in the AF dynamics, we can also derive a staggered spin pumping. A staggered spin current represents the imbalance between the spin current carried by the two sublattices. It

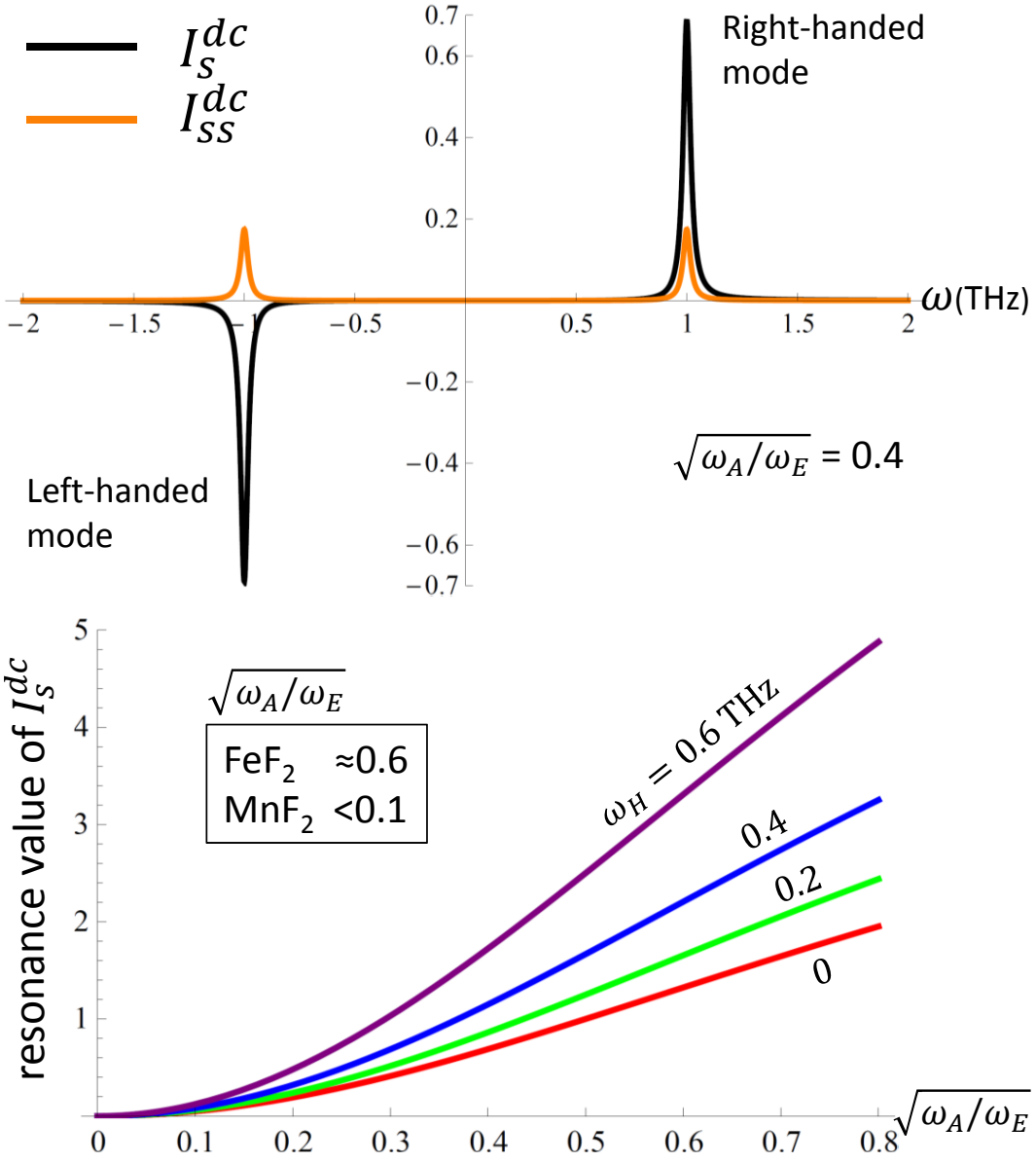

Figure 4.13: (Color online) Upper panel: dc components of spin and staggered spin currents as functions of ω in units of $\frac{\hbar}{e}G_r(\gamma h_\perp)^2$·ns. Parameters: $\omega_H = 0$, $\omega_R = 1$THz, $\sqrt{\omega_A/\omega_E} = 0.4$, and Gilbert damping $\alpha = 0.01$. Lower panel: for fixed microwave power, the resonance value of I_s^{dc} (in the same unit as above) increases with increasing $\sqrt{\omega_A/\omega_E}$; it is also improvable by increasing ω_H ($-\omega_H$) when the right-handed (left-handed) mode is excited.

has three components $\boldsymbol{I}_{ss}^{(1)}$, $\boldsymbol{I}_{ss}^{(2)}$, $\boldsymbol{I}_{ss}^{(3)}$ associated with three pseudo-spin Pauli matrices. In a similar manner as spin pumping,

$$\frac{e}{\hbar}\boldsymbol{I}_{ss}^{(3)} = G_r(\boldsymbol{n}\times\dot{\boldsymbol{m}} + \boldsymbol{m}\times\dot{\boldsymbol{n}}) - G_i\dot{\boldsymbol{n}}, \tag{4.124}$$

and $\frac{e}{\hbar}\boldsymbol{I}_{ss}^{(1)} = -\mathrm{Im}[G_w]\dot{\boldsymbol{m}}$ and $\frac{e}{\hbar}\boldsymbol{I}_{ss}^{(2)} = -\mathrm{Re}[G_w]\dot{\boldsymbol{n}}$, where

$$G_w = \frac{e^2\mathcal{A}}{h\pi^2}\iint S_w^*\Delta S dk_y dk_z, \tag{4.125}$$

results from spin-dependent Umklapp scattering that is unique to AF. When we take the time average, $\boldsymbol{I}_{ss}^{(1)}$ and $\boldsymbol{I}_{ss}^{(2)}$ drop out, only $\boldsymbol{I}_{ss}^{(3)}$ survives. The dc component I_{ss}^{dc} is

$$\begin{aligned} I_{ss}^{dc} &\approx 2G_r\omega\left|\chi_+(\omega)\mathscr{X}_+(\omega)^*\right|\left|\tilde{h}_+\right|^2 \\ &\approx \frac{2G_r\gamma^2|\tilde{h}_+|^2\omega(\omega-\omega_H)\sqrt{\omega_A^2+\alpha^2\omega^2}}{\left[(\omega-\omega_H)^2+\alpha^2\omega^2-\omega_R^2\right]^2+4\alpha^2\omega^2(\omega_A+\omega_E)^2}, \end{aligned} \tag{4.126}$$

whih is an even function of ω in the absence of static magnetic field, and is plotted in Fig. 4.13 (upper panel).

We emphasis that elastic spin scattering in the normal metal will destroy any staggered spin accumulation, which decays on the time scale of $\hbar/t$. Therefore, the staggered spin current can only be defined within a distance of the mean free path away from the interface.

As a matter of fact, four possible combinations can be studied in the adiabatic regime: charge pumping, spin pumping, pseudo-spin pumping, and staggered spin pumping. However, one can easily shown that the charge pumping and the pseudo-spin pumping all vanish because of symmetry. While a

collinear AF breaks time reversal symmetry, the combined symmetry of time reversal with sublattice interchange is preserved [89].

4.4 Materials and Experiments

When a spin current is injected into a heavy metal with strong spin-orbit coupling, it will be converted into a measurable transverse voltage via the inverse spin Hall effect [2, 73, 93]. This effect has been widely used in the detection of spin pumping by F resonance, and we expect to verify our prediction with the same technique. However, in a recent experiment using Pt/MnF_2 [90], no apparent signal is found at a similar level of microwave power as in conventional Pt/YIG. To explain this null observation, we resort to the efficiency of the microwave absorption at resonance point, which is proportional to $\sqrt{\omega_A/\omega_E}$ in AF, whereas no such factor exists in F. To see it more explicitly, we plot in Fig. 4.13 (lower panel) the resonance value of I_s^{dc} versus $\sqrt{\omega_A/\omega_E}$. In MnF_2 [36, 47], $\sqrt{\omega_A/\omega_E}$ is only few percent, which we believe is responsible for the suppression of the signals. Fortunately, there are better candidates, *e.g.*, FeF_2 has the same crystal and magnetic structures as MnF_2, but the ratio $\sqrt{\omega_A/\omega_E} \approx 0.6$ is extraordinarily large [78, 79]. Thus, we expect a sizable microwave-driven spin pumping using Pt/FeF_2 heterostructure.

In addition, the microwave absorption can also be enhanced by reducing the resonance frequency with a strong magnetic field, as illustrated by the lower panel of Fig. 4.13. But this brings about a dilemma that it is hard to take full advantage of the high frequency (THz) and the high microwave absorption

efficiency simultaneously. One way out of this dilemma is to detect the spin pumping by observing the enhancement of Gilbert damping. An alternative cure is to drive the AF dynamics by spin-transfer torques via spin Hall effect instead of microwaves.

Small grains are unavoidable in large area N/AF interfaces since the typical grain size is below μm. As the optimal microwave absorption occurs only when the local easy axis is perpendicular to the oscillating magnetic field, the non-collinearity of the anisotropy fields of individual grains will somewhat reduce the net spin pumping upon averaging over the entire interface. However, progress in fabrication of N/AF heterostructure and reduced cross sections should lead to improved surface quality with less disorder in the form of grains.

We note that the majority of transition metal oxides, such as NiO and MnO [98], belong to the class of easy-plane AF. The resonance mode of such materials, however, does not have definite chirality. The two sublattice moments rotate the opposite way, and spin pumping is essentially canceled out. Another possible candidate Cr_2O_3 [26, 29, 87] has very high $T_N \approx 308$ K above room temperature, it exhibits corundum structure and is an easy-axis AF. However, experimental data indicates that the anisotropy energy of Cr_2O_3 is quite small, which reduces the susceptibility at resonance.

Chapter 5

Spin-transfer Torques in Antiferromagnets

[1]In this chapter, we derive the reciprocal effect of spin pumping on a N/AF heterostructure, which consists of the back-action of an incident spin current from the normal metal that exerts on the interfacial AF magnetic moments. It is expressed as spin-transfer torques (STT). In principle, we should also include the torque arising from staggered spin current. However, as stated in the previous chapter, staggered spin accumulation decays very fast and is extremely difficult to generate. Therefore, for practical purposes, we only study spin current induced torques in the following.

5.1 Onsager Reciprocity Relations

In linear response regime, the microscopic reversibility of thermodynamic processes sets important constraints on macroscopic transport coefficients, which results in equalities of certain ratios between flows and thermodynamic forces, known as the Onsager reciprocity relations [60, 80, 81]. Consider multiple pairs of current (flow) $\dot{X}_i$ and driving force Y_i that are related by

[1]The contents of this chapter are based on the article: R. Cheng, J. Xiao, Q. Niu, and A. Brataas, *Spin Pumping and Spin-Transfer Torques in Antiferromagnets*, Phys. Rev. Lett. **113**, 057601 (2014).

linear response: $\dot{X}_i = L_{ij} Y_j$, where summation over repeated index is implied. The rate of change of the free energy, or the entropy production rate, is

$$\dot{F} = L_{ij} \dot{X}_i Y_j, \tag{5.1}$$

the Onsager reciprocity relation requires that $L_{ij}(\boldsymbol{H}, \boldsymbol{m}) = \epsilon_i \epsilon_j L_{ji}(-\boldsymbol{H}, -\boldsymbol{m})$, where $\epsilon_i = 1$ ($\epsilon_i = -1$) if X_i is even (odd) under time reversal.

For example, if a magnetic system is subject to both an electric field and a magnetic field, the two driving forces lead to electric current and magnetization dynamics. The linear response relation is expressed as

$$\begin{bmatrix} M_s \mathcal{V} \dot{\boldsymbol{m}} \\ \boldsymbol{I}^s \end{bmatrix} = \begin{bmatrix} L^{mm} & L^{ms} \\ L^{sm} & L^{ss} \end{bmatrix} \begin{bmatrix} \boldsymbol{H} \\ \boldsymbol{V}^s \end{bmatrix}, \tag{5.2}$$

where $\boldsymbol{I}^s$ is the spin current, $\boldsymbol{H}$ is the effective magnetic field, and $\boldsymbol{V}^s$ is the vector of spin voltage. The coefficient L^{ms} represents the spin-transfer torque induced by the current flow, while L^{sm} represents spin pumping from magnetization precession. The Onsager relation $L^{sm}_{ij}(\boldsymbol{m}, \boldsymbol{H}) = L^{ms}_{ji}(-\boldsymbol{m}, -\boldsymbol{H})$ enables us to derive either one of the two effects by the other.

The dimension of the driving forces are usually different under different conventions. However, the dimensionality of the off-diagonal transport coefficients are always equal. Specifically, if only the β-th driving force is present, the α-th current is $\dot{X}_\alpha = L_{\alpha\beta} Y_\beta$ (no summation over β); similarly, $\dot{X}_\beta = L_{\beta\alpha} Y_\alpha$ if only the α-th driving force exists. The dimension of $L_{\alpha\beta}$ and $L_{\beta\alpha}$ are $[L_{\alpha\beta}] = [X_\alpha]/([Y_\beta][T])$ and $[L_{\beta\alpha}] = [X_\beta]/([Y_\alpha][T])$, respectively. Since $[X_\alpha][Y_\alpha] = [X_\beta][Y_\beta] = [F]$, hence $[Y_\beta]/[X_\alpha] = [Y_\alpha]/[X_\beta]$, and we immediately

have $[L_{\alpha\beta}] = [L_{\beta\alpha}]$. Therefore, we are free to choose the dimension of currents and driving forces arbitrarily (in order to simplify calculation), and the dimension of off-diagonal transport coefficients will be compatible automatically.

If the system is antiferromagnetic, however, Eq. (5.2) must be generalized to incorporate both spin and staggered spin currents

$$\begin{bmatrix} \dot{\boldsymbol{m}} \\ \dot{\boldsymbol{n}} \\ \boldsymbol{I}^s \\ \boldsymbol{I}^a \end{bmatrix} = \begin{bmatrix} L^{mm} & L^{mn} & L^{ms} & L^{ma} \\ L^{nm} & L^{nn} & L^{ns} & L^{na} \\ L^{sm} & L^{sn} & L^{ss} & L^{sa} \\ L^{am} & L^{an} & L^{as} & L^{aa} \end{bmatrix} \begin{bmatrix} \boldsymbol{f}_m \\ \boldsymbol{f}_n \\ \boldsymbol{V}_s \\ \boldsymbol{V}_a \end{bmatrix}, \tag{5.3}$$

where $\boldsymbol{I}_a$ and $\boldsymbol{V}_a$ are staggered spin current and voltage, respectively. The effective magnetic field in Eq. (5.2) is generalized into two thermodynamic forces $\boldsymbol{f}_m$ and $\boldsymbol{f}_n$ acting on the magnetization and the staggered field. The Onsager relation is now

$$L_{ij}(\boldsymbol{H}, \boldsymbol{m}, \boldsymbol{n}) = \epsilon_i \epsilon_j L_{ji}(-\boldsymbol{H}, -\boldsymbol{m}, -\boldsymbol{n}), \tag{5.4}$$

where $\boldsymbol{n}$ is odd under time reversal.

5.2 Current-induced Torques

The symmetry allowed free energy of an AF material can be constructed by symmetry considerations [39, 60]. In the exchange limit, the free energy is invariant under the interchange of the two sublattices, *i.e.*, $F[\boldsymbol{m}, \boldsymbol{n}] = F[\boldsymbol{m}, -\boldsymbol{n}]$. The leading order free energy that respects the symmetry requirements is $F = \int \mathrm{d}\boldsymbol{r}[\mathcal{A}\boldsymbol{m}^2/2 + \mathcal{B}\sum_{i=x,y,z}(\partial \boldsymbol{n})^2/2 - \boldsymbol{H}\cdot\boldsymbol{m}]$, where $\mathcal{A}$ and $\mathcal{B}$ are the homogeneous and inhomogeneous exchange constants, respectively [39, 120]. To simply the following calculations and to be consistent with

our conventions in the previous chapter, we scale every term by frequency, and the free energy becomes

$$F = \int \mathrm{d}\mathcal{V}[\frac{\hbar\omega_0}{2a^3}\boldsymbol{m}^2 + \frac{\hbar\omega_n}{2a}\sum_{i=x,y,z}(\partial_i \boldsymbol{n})^2 - \frac{\hbar\omega_H}{a^3}\boldsymbol{m}\cdot\hat{H}], \tag{5.5}$$

where a is the lattice constant; $\boldsymbol{m}$, $\boldsymbol{n}$, and $\hat{H}$ are all *dimensionless* unit vectors that can be spatially inhomogeneous. The corresponding thermodynamic forces acting on $\boldsymbol{m}$ and $\boldsymbol{n}$ are

$$\boldsymbol{f}_m = -\frac{\delta F}{\delta \boldsymbol{m}}, \qquad \boldsymbol{f}_n = -\frac{\delta F}{\delta \boldsymbol{n}}, \tag{5.6}$$

they are extensive variables and assumes the energy dimension. Regarding the invariance under sublattice interchange, and $\boldsymbol{m}\cdot\boldsymbol{n} = 0$ and $|\boldsymbol{n}|^2 \approx 1$, the symmetry allowed Landau-Lifshitz equations are [39]

$$\hbar\dot{\boldsymbol{m}} = \frac{a^3}{\mathcal{V}}[\boldsymbol{f}_n \times \boldsymbol{n} + \boldsymbol{f}_m \times \boldsymbol{m}], \tag{5.7a}$$

$$\hbar\dot{\boldsymbol{n}} = \frac{a^3}{\mathcal{V}}\boldsymbol{f}_m \times \boldsymbol{n}, \tag{5.7b}$$

where the gyro-magnetic ratio has been absorbed by the thermodynamic forces upon scaling, and the damping terms are ignored.

From Eq. (5.5) and Eq. (5.6), we know $\boldsymbol{f}_m = -\hbar\omega_0\boldsymbol{m}\frac{\mathcal{V}}{a^3}$ for $\omega_H = 0$, thus a simple manipulation of Eq. (5.7b) reveals that

$$\boldsymbol{m} = -\frac{1}{\omega_0}\boldsymbol{n}\times\dot{\boldsymbol{n}}. \tag{5.8}$$

Comparing Eq. (5.8) with Eq. (4.7) for $\omega_H = 0$, we have

$$\omega_0 = \omega_A + 2\omega_E. \tag{5.9}$$

Inserting Eq. (5.7a) and Eq. (5.7b) into Eq. (4.122) gives the response of the spin current to $\boldsymbol{f}_m$ and $\boldsymbol{f}_n$. By invoking the Onsager relation Eq. (5.4), we derive the response of $\boldsymbol{m}$ and $\boldsymbol{n}$ to a given spin voltage $\boldsymbol{V}_s$ in the normal metal, which is identified as two STT terms $\boldsymbol{\tau}_m$ and $\boldsymbol{\tau}_m$. To linear order in $\boldsymbol{m}$, the two torques are expressed in frequency dimensions as [21]

$$\boldsymbol{\tau}_m = -\frac{a^3}{e\mathcal{V}} G_r \boldsymbol{n} \times (\boldsymbol{n} \times \boldsymbol{V}_s), \tag{5.10a}$$

$$\boldsymbol{\tau}_n = -\frac{a^3}{e\mathcal{V}} [G_r \boldsymbol{n} \times (\boldsymbol{m} \times \boldsymbol{V}_s) - G_i \boldsymbol{n} \times \boldsymbol{V}_s], \tag{5.10b}$$

which are consistent with the proposed phenomenological model [32–34]. They are supposed to be added back to Eq. (5.7a) and Eq. (5.7b).

In solving the AF dynamics, it is instructive to eliminate $\boldsymbol{m}$ and derive a closed equation of motion in terms of $\boldsymbol{n}$ alone [20, 39, 103]. To linear order in the small $\boldsymbol{m}$, the second term of Eq. (5.7a) can be neglected. And the dynamics of the system is now expressed by

$$\dot{\boldsymbol{m}} = \frac{1}{\hbar} \frac{a^3}{\mathcal{V}} \boldsymbol{f}_n \times \boldsymbol{n} + \boldsymbol{\tau}_m, \tag{5.11a}$$

$$\dot{\boldsymbol{n}} = \frac{1}{\hbar} \frac{a^3}{\mathcal{V}} \boldsymbol{f}_m \times \boldsymbol{n} + \boldsymbol{\tau}_n, \tag{5.11b}$$

from Eq. (5.11b) we know $\omega_0 \boldsymbol{m} = \boldsymbol{n} \times \boldsymbol{\tau}_n - \boldsymbol{n} \times \dot{\boldsymbol{n}}$, which gives

$$\dot{\boldsymbol{m}} = \frac{1}{\omega_0} [\frac{\mathrm{d}}{\mathrm{d}t} (\boldsymbol{n} \times \boldsymbol{\tau}_n) - \boldsymbol{n} \times \ddot{\boldsymbol{n}}]. \tag{5.12}$$

Substitute Eq. (5.12) into Eq. (5.11a) we obtain

$$\boldsymbol{n} \times \ddot{\boldsymbol{n}} + \omega_0 \omega_n a^2 \nabla^2 \boldsymbol{n} + \omega_0 \boldsymbol{\tau}_m = \frac{\mathrm{d}}{\mathrm{d}t} (\boldsymbol{n} \times \boldsymbol{\tau}_n), \tag{5.13}$$

which is purely general. The right hand side of Eq. (5.13) involves time derivative on $\boldsymbol{\tau}_n$, it is regarded as a higher order term. To prove rigorously that $\boldsymbol{\tau}_n$ is indeed a higher order torque, we eliminate $\boldsymbol{m}$ by virtue of Eq. (5.10b) and Eq. (5.11b), which yields

$$\boldsymbol{\tau}_n \times \boldsymbol{n} + \frac{G_r}{e\omega_0}(\boldsymbol{n}\cdot\boldsymbol{V}_s)\boldsymbol{\tau}_n = \frac{G_r}{e\omega_0}\dot{\boldsymbol{n}}. \tag{5.14}$$

Eq. (5.14) can be solved exactly, but for simplicity, it suffices to keep the solution up to linear order in $G_r/e\omega_0$,

$$\boldsymbol{\tau}_n = \frac{G_r}{e\omega_0}(\boldsymbol{n}\cdot\boldsymbol{V}_s)\boldsymbol{n}\times\dot{\boldsymbol{n}}. \tag{5.15}$$

Therefore, the effect of $\frac{\mathrm{d}}{\mathrm{d}t}(\boldsymbol{n}\times\boldsymbol{\tau}_n)$ term in Eq. (5.13) is of order $\omega_A(G_rV_s/e)$, comparing with the $\omega_0\boldsymbol{\tau}_m$ term that is of order $\omega_0(G_rV_s/e)$. In view of Eq. (5.9) we know $\omega_0 \approx 2\omega_E \gg \omega_A$, thus the $\boldsymbol{\tau}_m$ torque is the dominant term whereas. In a strict sense, however, their contributions also depend on the relative orientation between $\boldsymbol{n}$ and $\boldsymbol{V}_s$.

Finally, we resume the Gilbert damping as well as the easy axis anisotropy, the effective dynamics to linear order in $\boldsymbol{V}_s$, $\boldsymbol{m}$, and $\dot{\boldsymbol{n}}$ becomes

$$\boldsymbol{n}\times(\ddot{\boldsymbol{n}} + \alpha\omega_0\dot{\boldsymbol{n}} + \omega_R^2\boldsymbol{n}_\perp) = \frac{\omega_0 a^3}{e\mathcal{V}}G_r\boldsymbol{n}\times(\boldsymbol{n}\times\boldsymbol{V}_s). \tag{5.16}$$

where $\boldsymbol{n}_\perp$ are perpendicular components of $\boldsymbol{n}$ with respect to the easy axis. As the STT only acts on the interface and we consider a thin AF and disregard a possible non-uniform motion, otherwise a term $\omega_0\omega_n a^2\boldsymbol{n}\times\nabla^2\boldsymbol{n}$ should be included in Eq. (5.16). For thick metallic AF where electrons propagate into the bulk, Eq. (5.16) should be replaced by its bulk counterpart [20, 39].

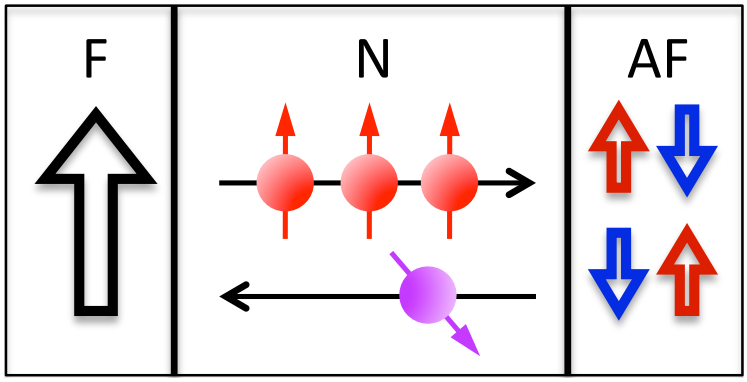

Figure 5.1: Spin-polarized electrons incident on the N/AF interface get reflected, by which angular momentum is transfered to the magnetic atoms.

5.3 Spin Wave Excitations

As an example, we consider the uniform AF dynamics driven by STT. Assume the spin voltage $\boldsymbol{V}_s$ is collinear with the easy axis, the spectrum of Eq. (5.16) is solved as

$$\frac{\omega}{\omega_0} = \frac{1}{2}\left[-i\alpha \pm \sqrt{-\alpha^2 + \frac{4}{\omega_0}\left(\omega_A + i\frac{a^3 G_r V_s}{e\mathcal{V}}\right)}\right]. \tag{5.17}$$

For small V_s, ω has a negative imaginary part so that any perturbed motion will decay exponentially in time and the system is stable. However, a sufficiently large V_s will flip the sign of $\mathrm{Im}[\omega]$, which yields the system unstable and marks the onset of uniform AF excitation.

By setting $\mathrm{Im}[\omega] = 0$, we obtain the threshold spin voltage

$$V_s^{\mathrm{th}} = \pm\frac{e\mathcal{V}}{a^3}\left(\frac{\alpha\omega_R}{G_r}\right), \tag{5.18}$$

where $+(-)$ corresponds to the excitation of right-handed (left-handed) mode. The chirality selection by the sign of spin voltage is just consistent with the

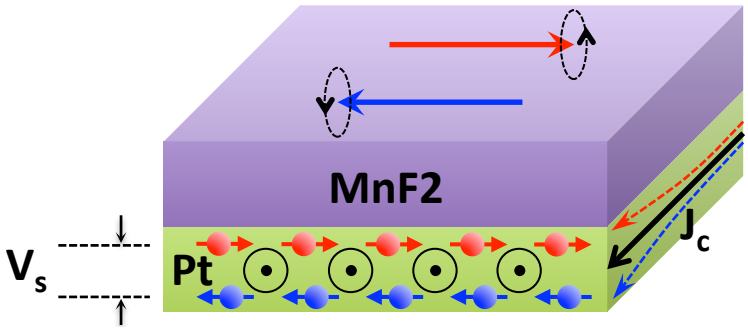

Figure 5.2: A spin-Hall nano-oscillator based on a Pt/MnF_2 bilayer. The current flowing in the bottom Pt layer generates a spin voltage vertical to the plane, which drives the dynamics of /MnF_2 through STT.

direction control of spin pumping by the microwave polarization. Since G_r scales linearly with the interface area, V_s^{th} scales linearly with the thickness of the AF layer.

In real experiments, a challenge arises from the large ω_R, but we can still get reasonable V_s^{th} by reducing the layer thickness. For MnF_2 and FeF_2 of few nm thick, the threshold spin voltage is estimated to be 10-100 μV. The STT-driven AF dynamics suggests the feasibility of building a spin-torque nano-oscillator (STNO) using AF, which generates THz signal from a dc input without the need of static magnetic field. However, as typical AF materials are insulators, a spin-valve like STNO is impossible. We notice that in recent experiments [62,63], people have successfully excite magnetic resonance by spin Hall effect, which works for both metallic and insulating magnetic materials. We expect to build such a spin Hall nano-oscillator based on antiferromagnetic materials with similar techniques, as schematically depicted in Fig. 5.2.

Chapter 6

Conclusions

6.1 Summary and Conclusions

We are now in a good position to conclude the long journey of antiferromagnetic spintronics. Motivated by the anticipation that the adiabatic motion of the staggered field, the order parameter of antiferromagnets, should lead to non-trivial response of conduction electrons in a similar but not the same sense as that in ferromagnets, we have solved the coupled dynamics of the staggered field and conduction electrons in both bulk antiferromagnetic textures and N/AF heterostructures.

In bulk antiferromagnetic metals where the staggered field exhibits smooth spatial modulation and slow time variation, the behavior of conduction electrons can well be captured by a non-Abelian gauge theory, which generalizes the established Abelian gauge theory in ferromagnetic metals. The spin dependent electron transport is significantly affected by the spin-motive force originating from the non-Abelian version of the Lorentz force. Different from its counterpart in ferromagnets, the spin-motive force in antiferromagnets generates pure spin voltage instead of charge voltage across the sample.

As a reverse effect, the dynamics of the staggered field strongly depends

on the motion of conduction electrons. Different from the (adiabatic) spin transfer torque in ferromagnets, a spin current drives the second order time derivative of the staggered field by spin forcing, which fosters new possibility to realize high domain wall velocity with low current density. Thanks to the linear dispersion of spin waves, the spin-current induced magnon emission in antiferromagnets resembles the Cherenkov radiation of photons in a media with reduced speed of light.

On the interface of compensated antiferromagnets with normal metals, spin scattering is found to be not far from the naive picture where the staggered field is split up into two independent ferromagnetic orders, but the mixing of scattering channels do renders the naive picture non-strict. For collinear antiferromagnets with easy axis anisotropy, a non-trivial spin pumping has been derived based on the simple two-sublattice model. Unique to antiferromagnets, the pumped staggered spin currents also exist in theory, but it is quite difficult to detect as the staggered spin accumulation decays very fast away from the interface.

As a reciprocal effect, the spin-transfer torques are derived from spin pumping via the Onsager relations. When a spin voltage is applied on the interface of an antiferromagnet, it drives the coupled dynamics of the staggered field and the small magnetization. In an effort to eliminate the magnetization, we found a similar equation of motion in terms of the staggered field alone as that in bulk antiferromagnets. While the current-induced torques have quite similar forms as their ferromagnetic counterparts, it is $\boldsymbol{n} \times \partial_t^2 \boldsymbol{n}$ that replaces

what should otherwise be $\partial_t \boldsymbol{m}$. As typical antiferromagnets are insulators, a spin-Hall nano-oscillator is proposed to verify the prediction.

All the above conclusions are summarized in Tab. 6.1 in a comparative manner with their counterparts in ferromagnets.

6.2 Outlook and Perspectives

Investigations throughout the dissertation are based on the single electron approximation where many body physics has been completely ignored. In addition, the theory is valid in the adiabatic limit, where non-adiabatic effects can not be described *analytically* by the effective theory in principle. Phenomenological models do captures the non-adiabatic corrections, but a microscopic derivation is still in need.

The spin-orbit coupling may play an essential role, but we have omitted it from the very beginning. What can be simply anticipated from spin-orbit coupling is that the momentum space Berry curvature should be non-zero, and electron scattering on the interface does not preserve spin. Those features can lead to significant deviations from current predictions, hence they are good candidates for future studies.

Besides, recent attentions have been aroused on the magnon-driven dynamics of antiferromagnets, which applies to insulating materials in particular. It is quite important to formulate an effective theory of magnon transport in antiferromagnets with slowly-varying staggered field.

Ferromagnets	Antiferromagnets
non-degenerate band $\xi = \langle A\|B\rangle = 1$	doubly degenerate band $\xi(\boldsymbol{k}) = \langle A\|B\rangle \in (0,1)$
$\boldsymbol{s} = \boldsymbol{n}$	$\dot{\boldsymbol{s}} = (1-\xi^2)(\boldsymbol{s}\cdot\boldsymbol{n})\dot{\boldsymbol{n}}$
U(1) Abelian Berry phase: $\gamma(\Gamma) = \oint_C \mathcal{A}_\mu dr_\mu$ Dirac monopole	SU(2) non-Abelian Berry phase: $U(\Gamma) = \mathcal{P}\exp[-i\oint_C \boldsymbol{\mathcal{A}}^r_\mu \cdot \boldsymbol{\tau} dr_\mu]$ 't Hooft-Polyakov monopole
$\dot{\boldsymbol{k}} = \boldsymbol{E} + \dot{\boldsymbol{r}} \times \boldsymbol{B}$ $\dot{\boldsymbol{r}} = -\partial_{\boldsymbol{k}}\varepsilon$	$\dot{\boldsymbol{k}} = (1-\xi^2)(\boldsymbol{s}\cdot\boldsymbol{n})(\boldsymbol{E} + \dot{\boldsymbol{r}} \times \boldsymbol{B})$ $\dot{\boldsymbol{r}} = -\partial_{\boldsymbol{k}}\varepsilon - \frac{1}{2}(\boldsymbol{s}\times\boldsymbol{n})\cdot\dot{\boldsymbol{n}}\ \partial_{\boldsymbol{k}}\ln\xi$
$\partial_t \boldsymbol{m}$ subjects to: adiabatic $\quad(\boldsymbol{j}_s\cdot\nabla)\boldsymbol{m}$ non-adiabatic $\quad\beta\boldsymbol{m}\times(\boldsymbol{j}_s\cdot\nabla)\boldsymbol{m}$	$\boldsymbol{n}\times\partial_t^2\boldsymbol{n}$ subjects to: adiabatic $\quad(1-\xi^2)(\boldsymbol{j}_s\cdot\nabla)\boldsymbol{n}$ non-adiabatic $\quad\beta(1-\xi^2)\boldsymbol{n}\times(\boldsymbol{j}_c\cdot\nabla)\boldsymbol{n}$
$\boldsymbol{I}_s:\ G_r\boldsymbol{m}\times\dot{\boldsymbol{m}} - G_i\dot{\boldsymbol{m}}$ $\boldsymbol{I}_c:\ 0$ $\boldsymbol{I}_{ss}$: not applicable $\boldsymbol{I}_{ps}$: not applicable	$\boldsymbol{I}_s:\ G_r(\boldsymbol{n}\times\dot{\boldsymbol{n}} + \boldsymbol{m}\times\dot{\boldsymbol{m}}) - G_i\dot{\boldsymbol{m}}$ $\boldsymbol{I}_c:\ 0$ $\boldsymbol{I}_{ss}:\ G_r(\boldsymbol{n}\times\dot{\boldsymbol{m}} + \boldsymbol{m}\times\dot{\boldsymbol{n}}) - G_i\dot{\boldsymbol{n}}$ $\boldsymbol{I}_{ps}:\ 0$
$L_{ij}(\boldsymbol{H},\boldsymbol{m}) = L_{ji}(-\boldsymbol{H},-\boldsymbol{m})$	$L_{ij}(\boldsymbol{H},\boldsymbol{m},\boldsymbol{n}) = L_{ji}(-\boldsymbol{H},-\boldsymbol{m},-\boldsymbol{n})$
$\boldsymbol{\tau}_m:\ G_r\boldsymbol{m}\times(\boldsymbol{m}\times\boldsymbol{V}_s)$ $\boldsymbol{\tau}_n$: not applicable	$\boldsymbol{\tau}_m:\ G_r\boldsymbol{n}\times(\boldsymbol{n}\times\boldsymbol{V}_s)$ $\boldsymbol{\tau}_n:\ G_r\boldsymbol{n}\times(\boldsymbol{m}\times\boldsymbol{V}_s) - G_i\boldsymbol{n}\times\boldsymbol{V}_s$
$(\partial_t\boldsymbol{m}) \sim \boldsymbol{\tau}_m$	$(\boldsymbol{n}\times\partial_t^2\boldsymbol{n}) \sim \boldsymbol{\tau}_m + \partial_t(\boldsymbol{n}\times\boldsymbol{\tau}_n)$

Table 6.1: A full comparison of the major results of ferromagnetic and antiferromagnetic spintronics. Upper panels: bulk magnetic textures with slowly varying order parameters. Lower panels: heterostructures of magnetic materials with normal metals. Symbols are chosen in the same convention as those used in previous chapters.

As one of the first explorations of antiferromagnetic spintronics in the community, our study guides through a variety of ways to realize novel functioning of antiferromagnetic materials in different situations. However, to achieve a similar level of understanding of antiferromagnets as ferromagnets, there is still a long way to go.

Appendix

Appendix 1

Equivalence of O(3) NLSM and CP^1 model

A striking property of the CP^1 model is the gauge field minimally coupled to the CP^1 field acquires the Maxwell dynamics in the long wave length limit [86], which mediates attractive interaction between conduction electrons of opposite spins.

We provide a simple but rigid proof of the equivalence between O(3) NLSM and the CP^1 model via path integral approach. We write down explicitly the amplitude for the O(3) NLSM:

$$\mathcal{Z}_1 = \int \mathscr{D}^3\hat{n}\delta(\hat{n}^2-1)e^{-\frac{1}{4g}\int \mathrm{d}x\partial_\mu\hat{n}\cdot\partial_\mu\hat{n}}, \tag{1.1}$$

and the amplitude for the CP^1 model:

$$\mathcal{Z}_2 = \int \mathscr{D}^4z\mathscr{D}A_\mu\delta(|z|^2-1)e^{-\frac{1}{g}\int \mathrm{d}x|(\partial_\mu - iA_\mu)z|^2}. \tag{1.2}$$

Proof of the equivalence is nothing but to show $\mathcal{Z}_1$ is proportional to $\mathcal{Z}_2$ under the Hopf map $\hat{n} = z^\dagger\hat{\sigma}z$. Express the CP^1 field as $z = (z_1, z_2)^T = (re^{i\alpha}, se^{i\beta})^T$, it is easy to check that $r^2 + s^2 = 1$ due to $\hat{n}^2 = |z|^2 = |z_1|^2 + |z_2|^2 = 1$. This means that the CP^1 field is constrained on a unit complex sphere. In terms of r, s, α, and β, the action in $\mathcal{Z}_1$ can be written as

$$\frac{1}{4g}\int \mathrm{d}x\partial_\mu\hat{n}\cdot\partial_\mu\hat{n} = \frac{1}{g}\int \mathrm{d}x[r^2s^2(\partial_\mu\alpha - \partial_\mu\beta)^2 + (\partial_\mu r)^2 + (\partial_\mu s)^2]. \tag{1.3}$$

Next, we integrate out the gauge field in $\mathcal{Z}_2$ which is Gaussian, and then express the action also in terms of the new variables r, s, α, and β:

$$\begin{aligned}
\mathcal{Z}_2 &= \int \mathscr{D}^4 z \mathscr{D} A_\mu \delta(|z|^2 - 1) e^{-\frac{1}{g}\int \mathrm{d}x |(\partial_\mu - iA_\mu) z|^2} \\
&= \int \mathscr{D}^4 z \mathscr{D} A_\mu \delta(|z|^2 - 1) e^{-\frac{1}{g}\int \mathrm{d}x \partial_\mu z^\dagger \partial_\mu z} e^{-\frac{1}{g}\int \mathrm{d}x [A_\mu^2 + iA_\mu (z^\dagger \partial_\mu z - z \partial_\mu z^\dagger)]} \\
&= (\pi g)^2 \int \mathscr{D}^4 z \delta(|z|^2 - 1) e^{\frac{1}{g}\int \mathrm{d}x (r^2 \partial_\mu \alpha + s^2 \partial_\mu \beta)^2} \\
&\qquad\qquad e^{-\frac{1}{g}\int \mathrm{d}x [r^2 (\partial_\mu \alpha)^2 + s^2 (\partial_\mu \beta)^2 + (\partial_\mu r)^2 + (\partial_\mu s)^2]}.
\end{aligned} \tag{1.4}$$

Considering $r^4 = r^2(1 - s^2)$ and $s^4 = s^2(1 - r^2)$, it is straightforward to show that the action in the above path integral just equals the action obtained in Eq. (1.3). Put it another way, while the two path integrals have different variables, their integrands (the actions) are equal:

$$\mathcal{Z}_1 = \int \mathscr{D}^3 \hat{n} \delta(\hat{n}^2 - 1) e^{-S_1[\hat{n}]} \tag{1.5}$$

$$\mathcal{Z}_2 = (\pi g)^2 \int \mathscr{D}^4 z \delta(|z|^2 - 1) e^{-S_2[\hat{n}(z)]} \tag{1.6}$$

$$\text{with} \quad S_1[\hat{n}] = S_2[\hat{n}(z)] = S[r, s, \alpha, \beta]$$

To proceed, we have to show that the entire amplitudes of Eq. (1.5) and Eq. (1.6) are proportional, i.e., the equality:

$$\int \mathscr{D}^4 z \delta(|z|^2 - 1) e^{-S[\hat{n}(z)]} = c \int \mathscr{D}^3 \hat{n} \delta(\hat{n}^2 - 1) e^{-S[\hat{n}]} \tag{1.7}$$

where c is an overall constant that can be eliminated by proper normalization.

By virtue of the selection rule of the δ function and the Hopf map $\hat{n} = z^\dagger \hat{\sigma} z$ we used above, we are able to rewrite the left hand side of Eq. (1.7)

in the form:

$$\int \mathscr{D}^4 z \delta(|z|^2-1) e^{-S[\hat{n}(z)]} = \int \mathscr{D}^4 z \delta(|z|^2-1) \int \mathscr{D}^3 \hat{n} \delta^3(\hat{n} - z^\dagger \hat{\sigma} z) e^{-S[\hat{n}]}, \tag{1.8}$$

thus the equality of Eq. (1.7) would be proved if we can show

$$\int \mathscr{D}^4 z \delta^3(\hat{n} - z^\dagger \hat{\sigma} z) \delta(|z|^2-1) = c\ \delta(\hat{n}^2 - 1). \tag{1.9}$$

In other words, the proof of the equivalence between the two models is now a matter of demonstrating Eq. (1.9). To prove Eq. (1.9), we first clarify the meaning of $\mathscr{D}^4 z$ by

$$\mathscr{D}^4 z = \prod_{x_\mu, j=1,2} \mathrm{dRe}z_j(x_\mu) \mathrm{dIm}z_j(x_\mu), \tag{1.10}$$

and then carry out the integral in the r, s, α, β coordinates. Since $\mathrm{Re}z_1 = r\cos\alpha$, $\mathrm{Im}z_1 = r\sin\alpha$, $\mathrm{Re}z_2 = s\cos\beta$, and $\mathrm{Im}z_2 = s\sin\beta$, the Jacobian of the coordinate transformation reads

$$J = \frac{\partial(\mathrm{Re}z_1, \mathrm{Im}z_1, \mathrm{Re}z_2, \mathrm{Im}z_2)}{\partial(r, \alpha, s, \beta)} = rs. \tag{1.11}$$

Then the left hand side of Eq. (1.9) becomes:

$$\begin{aligned}
\text{L.H.S.} = & \int_0^\infty r dr \int_0^\infty s ds \int_0^{2\pi} d\alpha \int_0^{2\pi} d\beta\ \delta(r^2+s^2-1) \\
& \delta(n_x - 2rs\cos(\alpha-\beta))\delta(n_y + 2rs\sin(\alpha-\beta))\delta(n_z - (r^2-s^2)) \\
= & \frac{1}{16} \int_0^\infty dR \int_0^\infty dS \int_0^{4\pi} d\theta \int_{-2\pi}^{2\pi} d\phi \delta(R+S-1) \\
& \delta(n_x - 2\sqrt{RS}\cos(\phi))\delta(n_y + 2\sqrt{RS}\sin(\phi))\delta(n_z - (R-S)),
\end{aligned} \tag{1.12}$$

where simple transformation of variables has been used. Integrating in the order dR, dθ, and dS, we obtain

$$\begin{aligned}\text{L.H.S.} =& \frac{\pi}{4}\int_0^\infty dS \int_{-2\pi}^{2\pi} d\phi \delta(n_x - 2\sqrt{(1-S)S}\cos(\phi)) \\ & \delta(n_y + 2\sqrt{(1-S)S}\sin(\phi))\delta(n_z - (1-2S)) \\ =& \frac{\pi}{8}\int_{-2\pi}^{2\pi} d\phi\ \delta(n_x - \sqrt{1-{n_z}^2}\cos(\phi))\delta(n_y + \sqrt{1-{n_z}^2}\sin(\phi)). \quad (1.13)\end{aligned}$$

The last integration over $d\phi$ is somehow tricky. Define the function $f(\phi) = \sqrt{1-{n_z}^2}\cos\phi - n_x$, it has two zero points at $\phi_0 = \pm\arccos\frac{n_x}{\sqrt{1-{n_z}^2}}$ and the absolute value of its derivative at these points is

$$|f'(\phi_0)| = \sqrt{1-{n_z}^2}\sin\phi_0 = \sqrt{1-n_x^2-n_z^2}, \quad (1.14)$$

using the properties of the δ function, Eq. (1.13) becomes

$$\begin{aligned}\text{L.H.S.} =& \frac{\pi}{8}\int_{-2\pi}^{2\pi} \mathrm{d}\phi\ \delta(n_y + \sqrt{1-{n_z}^2}\sin(\phi)) \\ & \frac{\delta(\phi - \arccos\frac{n_x}{\sqrt{1-{n_z}^2}}) + \delta(\phi + \arccos\frac{n_x}{\sqrt{1-{n_z}^2}})}{\sqrt{1-n_x^2-n_z^2}} \\ =& \frac{\pi}{8\sqrt{1-n_x^2-n_z^2}}[\delta(n_y - \sqrt{1-n_x^2-n_z^2}) + \delta(n_y + \sqrt{1-n_x^2-n_z^2})] \\ =& \frac{\pi}{4}\delta(n_x^2+n_y^2+n_z^2-1) = \frac{\pi}{4}\delta(\hat{n}^2-1). \quad (1.15)\end{aligned}$$

Therefore, Eq. (1.9), hence Eq. (1.7) is proved.

In conclusion, the CP^1 model is equivalent to the NLSM under the Hubbard-Stratonovich transformation

$$\begin{aligned}\int \mathscr{D}^4 z \mathscr{D} A_\mu \delta(|z|^2-1)\ e^{-\frac{1}{g}\int \mathrm{d}x|(\partial_\mu - iA_\mu)z|^2} \\ = \frac{\pi^3 g^2}{4}\int \mathscr{D}^3\hat{n}\delta(\hat{n}^2-1)e^{-\frac{1}{4g}\int \mathrm{d}x \partial_\mu\hat{n}\cdot\partial_\mu\hat{n}}. \quad (1.16)\end{aligned}$$

Bibliography

[1] Yakir Aharonov and Ady Stern. Origin of the geometric forces accompanying berry's geometric potentials. *Physical review letters*, 69(25):3593, 1992.

[2] Kazuya Ando, Saburo Takahashi, Junichi Ieda, Yosuke Kajiwara, Hiroyasu Nakayama, Tatsuro Yoshino, Kazuya Harii, Yasunori Fujikawa, M Matsuo, S Maekawa, et al. Inverse spin-hall effect induced by spin pumping in metallic system. *Journal of Applied Physics*, 109(10):103913, 2011.

[3] Assa Auerbach. *Interacting electrons and quantum magnetism*. Springer, 1994.

[4] S. E. Barnes and S. Maekawa. Current-spin coupling for ferromagnetic domain walls in fine wires. *Phys. Rev. Lett.*, 95:107204, Sep 2005.

[5] S. E. Barnes and S. Maekawa. Generalization of faraday's law to include nonconservative spin forces. *Physical review letters*, 98(24):246601, 2007.

[6] Ya B. Bazaliy, B. A. Jones, and Shou-Cheng Zhang. Modification of the landau-lifshitz equation in the presence of a spin-polarized current

in colossal-and giant-magnetoresistive materials. *Physical Review B*, 57(6):R3213, 1998.

[7] G. S. D. Beach, M. Tsoi, and J. L. Erskine. Current-induced domain wall motion. *Journal of magnetism and magnetic materials*, 320(7):1272–1281, 2008.

[8] L. Berger. Emission of spin waves by a magnetic multilayer traversed by a current. *Phys. Rev. B*, 54:9353–9358, Oct 1996.

[9] Michael V Berry. Quantal phase factors accompanying adiabatic changes. *Proceedings of the Royal Society of London. A. Mathematical and Physical Sciences*, 392(1802):45–57, 1984.

[10] M. Bode, E. Y. Vedmedenko, K. Von Bergmann, A. Kubetzka, P. Ferriani, S. Heinze, and R. Wiesendanger. Atomic spin structure of antiferromagnetic domain walls. *Nature materials*, 5(6):477–481, 2006.

[11] Matthias Bode, M. Heide, K. Von Bergmann, P. Ferriani, S. Heinze, G. Bihlmayer, A. Kubetzka, O. Pietzsch, S Blügel, and R. Wiesendanger. Chiral magnetic order at surfaces driven by inversion asymmetry. *Nature*, 447(7141):190–193, 2007.

[12] Arne Brataas, Andrew D Kent, and Hideo Ohno. Current-induced torques in magnetic materials. *Nature materials*, 11(5):372–381, 2012.

[13] P. W. Brouwer. Scattering approach to parametric pumping. *Phys. Rev. B*, 58:R10135–R10138, Oct 1998.

[14] P. Bruno, V. K. Dugaev, and M. Taillefumier. Topological hall effect and berry phase in magnetic nanostructures. *Physical review letters*, 93(9):096806, 2004.

[15] C. Burrowes, A. P. Mihai, D. Ravelosona, J.-V. Kim, C. Chappert, L. Vila, A. Marty, Y. Samson, F. Garcia-Sanchez, L. D. Buda-Prejbeanu, et al. Non-adiabatic spin-torques in narrow magnetic domain walls. *Nature Physics*, 6(1):17–21, 2010.

[16] Ming-Che Chang and Qian Niu. Berry phase, hyperorbits, and the hofstadter spectrum: Semiclassical dynamics in magnetic bloch bands. *Physical Review B*, 53(11):7010, 1996.

[17] Ming-Che Chang and Qian Niu. Berry curvature, orbital moment, and effective quantum theory of electrons in electromagnetic fields. *Journal of Physics: Condensed Matter*, 20(19):193202, 2008.

[18] Ran Cheng and Qian Niu. Electron dynamics in slowly varying antiferromagnetic texture. *Physical Review B*, 86:245118, 2012.

[19] Ran Cheng and Qian Niu. Microscopic derivation of spin-transfer torque in ferromagnets. *Phys. Rev. B*, 88:024422, Jul 2013.

[20] Ran Cheng and Qian Niu. Dynamics of antiferromagnets driven by spin current. *Physical Review B*, 89:081105(R), 2014.

[21] Ran Cheng, Jiang Xiao, Qian Niu, and Arne Brataas. Spin pumping and spin-transfer torques in antiferromagnets. *Phys. Rev. Lett.*, 113:057601, Jul 2014.

[22] Dimitrie Culcer, Yugui Yao, and Qian Niu. Coherent wave-packet evolution in coupled bands. *Phys. Rev. B*, 72:085110, Aug 2005.

[23] Jean Dalibard, Fabrice Gerbier, Gediminas Juzeliūnas, and Patrik Öhberg. Colloquium. *Rev. Mod. Phys.*, 83:1523–1543, Nov 2011.

[24] Supriyo Datta. *Electronic transport in mesoscopic systems*. Cambridge university press, 1997.

[25] Supriyo Datta. *Quantum transport: atom to transistor*. Cambridge University Press, 2005.

[26] Edward S. Dayhoff. Antiferromagnetic resonance in cr2o3. *Phys. Rev.*, 107:84–91, Jul 1957.

[27] R. A. Duine. Effects of nonadiabaticity on the voltage generated by a moving domain wall. *Phys. Rev. B*, 79:014407, Jan 2009.

[28] Karin Everschor, Markus Garst, R. A. Duine, and Achim Rosch. Current-induced rotational torques in the skyrmion lattice phase of chiral magnets. *Physical Review B*, 84(6):064401, 2011.

[29] Simon Foner. High-field antiferromagnetic resonance in cr2o3. *Phys. Rev.*, 130:183–197, Apr 1963.

[30] Eduardo Fradkin. *Field theories of condensed matter systems*, volume 7. Addison-Wesley Redwood City, 1991.

[31] Ion Garate, K. Gilmore, M. D. Stiles, and A. H. MacDonald. Nonadiabatic spin-transfer torque in real materials. *Phys. Rev. B*, 79:104416, Mar 2009.

[32] E. V. Gomonay and V. M. Loktev. Spintronics of antiferromagnetic systems (review article). *Low Temperature Physics*, 40(1), 2014.

[33] Helen V. Gomonay, Roman V. Kunitsyn, and Vadim M. Loktev. Symmetry and the macroscopic dynamics of antiferromagnetic materials in the presence of spin-polarized current. *Phys. Rev. B*, 85:134446, Apr 2012.

[34] Helen V. Gomonay and Vadim M. Loktev. Spin transfer and current-induced switching in antiferromagnets. *Phys. Rev. B*, 81:144427, Apr 2010.

[35] Alexander G. Gurevich and Gennadii A. Melkov. *Magnetization oscillations and waves*. CRC Press, 1996.

[36] M. Hagiwara, K. Katsumata, I. Yamada, and H. Suzuki. Antiferromagnetic resonance in over wide ranges of frequency and magnetic field. *Journal of Physics: Condensed Matter*, 8(39):7349, 1996.

[37] F. D. M. Haldane. Nonlinear field theory of large-spin heisenberg antiferromagnets: Semiclassically quantized solitons of the one-dimensional easy-axis néel state. *Phys. Rev. Lett.*, 50:1153–1156, Apr 1983.

[38] F. D. M. Haldane. O(3) nonlinear σ model and the topological distinction between integer- and half-integer-spin antiferromagnets in two dimensions. *Phys. Rev. Lett.*, 61:1029–1032, Aug 1988.

[39] Kjetil M. D. Hals, Yaroslav Tserkovnyak, and Arne Brataas. Phenomenology of current-induced dynamics in antiferromagnets. *Physical review letters*, 106(10):107206, 2011.

[40] Paul M. Haney and A. H. MacDonald. Current-induced torques due to compensated antiferromagnets. *Physical review letters*, 100(19):196801, 2008.

[41] Masamitsu Hayashi, Jun'ichi Ieda, Yuta Yamane, Jun-ichiro Ohe, Yukiko K. Takahashi, Seiji Mitani, and Sadamichi Maekawa. Time-domain observation of the spinmotive force in permalloy nanowires. *Phys. Rev. Lett.*, 108:147202, Apr 2012.

[42] L. Heyne, J. Rhensius, D. Ilgaz, A. Bisig, U. Rüdiger, M. Kläui, L. Joly, F. Nolting, L. J. Heyderman, J. U. Thiele, and F. Kronast. Direct determination of large spin-torque nonadiabaticity in vortex core dynamics. *Phys. Rev. Lett.*, 105:187203, Oct 2010.

[43] Gerard Hooft. Magnetic monopoles in unified gauge theories. *Nuclear Physics B*, 79(2):276–284, 1974.

[44] R. Jaramillo, T. F. Rosenbaum, E. D. Isaacs, O. G. Shpyrko, P. G. Evans, G. Aeppli, and Z. Cai. Microscopic and macroscopic signatures of antiferromagnetic domain walls. *Physical review letters*, 98(11):117206, 2007.

[45] Y. Ji, C. L. Chien, and M. D. Stiles. Current-induced spin-wave excitations in a single ferromagnetic layer. *Phys. Rev. Lett.*, 90:106601, Mar 2003.

[46] Xingtao Jia, Kai Liu, Ke Xia, and Gerrit E. W. Bauer. Spin transfer torque on magnetic insulators. *EPL (Europhysics Letters)*, 96(1):17005, 2011.

[47] Fred M. Johnson and Arthur H. Nethercot. Antiferromagnetic resonance in mnf2. *Phys. Rev.*, 114:705–716, May 1959.

[48] F. Jonietz, S. Mühlbauer, C. Pfleiderer, A. Neubauer, W. Münzer, A. Bauer, T. Adams, R. Georgii, P. Böni, R. A. Duine, et al. Spin transfer torques in mnsi at ultralow current densities. *Science*, 330(6011):1648–1651, 2010.

[49] T. Jungwirth, V. Novák, X. Martí, M. Cukr, F. Máca, A. B. Shick, J. Mašek, P. Horodyská, P. Němec, V. Holý, J. Zemek, P. Kužel, I. Němec,

B. L. Gallagher, R. P. Campion, C. T. Foxon, and J. Wunderlich. Demonstration of molecular beam epitaxy and a semiconducting band structure for i-mn-v compounds. *Phys. Rev. B*, 83:035321, Jan 2011.

[50] F. Keffer and H. Chow. Dynamics of the antiferromagnetic spin-flop transition. *Phys. Rev. Lett.*, 31:1061–1063, Oct 1973.

[51] F. Keffer and C. Kittel. Theory of antiferromagnetic resonance. *Phys. Rev.*, 85:329–337, Jan 1952.

[52] S. Khmelevskyi, A. B. Shick, and P. Mohn. Element-specific analysis of the magnetic anisotropy in mn-based antiferromagnetic alloys from first principles. *Phys. Rev. B*, 83:224419, Jun 2011.

[53] Joo-Von Kim and R. L. Stamps. Hysteresis from antiferromagnet domain-wall processes in exchange-biased systems: Magnetic defects and thermal effects. *Phys. Rev. B*, 71:094405, Mar 2005.

[54] A. V. Kimel, B. A. Ivanov, R. V. Pisarev, P. A. Usachev, A. Kirilyuk, and Th Rasing. Inertia-driven spin switching in antiferromagnets. *Nature Physics*, 5(10):727–731, 2009.

[55] A. V. Kimel, A. Kirilyuk, P. A. Usachev, R. V. Pisarev, A. M. Balbashov, and Th Rasing. Ultrafast non-thermal control of magnetization by instantaneous photomagnetic pulses. *Nature*, 435(7042):655–657, 2005.

[56] Charles Kittel. On the theory of ferromagnetic resonance absorption. *Phys. Rev.*, 73:155–161, Jan 1948.

[57] Minhyea Lee, W. Kang, Y. Onose, Y. Tokura, and N. P. Ong. Unusual hall effect anomaly in mnsi under pressure. *Physical review letters*, 102(18):186601, 2009.

[58] S. Lepadatu, J. S. Claydon, C. J. Kinane, T. R. Charlton, S. Langridge, A. Potenza, S. S. Dhesi, P. S. Keatley, R. J. Hicken, B. J. Hickey, and C. H. Marrows. Domain-wall pinning, nonadiabatic spin-transfer torque, and spin-current polarization in permalloy wires doped with vanadium. *Phys. Rev. B*, 81:020413, Jan 2010.

[59] Z. Li and S. Zhang. Domain-wall dynamics and spin-wave excitations with spin-transfer torques. *Phys. Rev. Lett.*, 92:207203, May 2004.

[60] E. M. Lifshitz and L. P. Pitaevskii. Statistical physics part 2, landau and lifshitz course of theoretical physics, 1980.

[61] Jacob Linder. Controllable spin-transfer torque on an antiferromagnet in a dual spin-valve. *Phys. Rev. B*, 84:094404, Sep 2011.

[62] Luqiao Liu, Takahiro Moriyama, D. C. Ralph, and R. A. Buhrman. Spin-torque ferromagnetic resonance induced by the spin hall effect. *Phys. Rev. Lett.*, 106:036601, Jan 2011.

[63] R. H. Liu, W. L. Lim, and S. Urazhdin. Spectral characteristics of the microwave emission by the spin hall nano-oscillator. *Phys. Rev. Lett.*, 110:147601, Apr 2013.

[64] A. H. MacDonald and M. Tsoi. Antiferromagnetic metal spintronics. *Philosophical Transactions of the Royal Society A: Mathematical, Physical and Engineering Sciences*, 369(1948):3098–3114, 2011.

[65] Sadamichi Maekawa, Sergio O. Valenzuela, Eiji Saitoh, and Takashi Kimura. *Spin Current*, volume 17. Oxford University Press, 2012.

[66] A. Manchon and S. Zhang. Theory of nonequilibrium intrinsic spin torque in a single nanomagnet. *Phys. Rev. B*, 78:212405, Dec 2008.

[67] X. Martí, B. G. Park, J. Wunderlich, H. Reichlová, Y. Kurosaki, M. Yamada, H. Yamamoto, A. Nishide, J. Hayakawa, H. Takahashi, and T. Jungwirth. Electrical measurement of antiferromagnetic moments in exchange-coupled irmn/nife stacks. *Phys. Rev. Lett.*, 108:017201, Jan 2012.

[68] D. Mauri, H. C. Siegmann, P. S. Bagus, and E. Kay. Simple model for thin ferromagnetic films exchange coupled to an antiferromagnetic substrate. *Journal of Applied Physics*, 62(7), 1987.

[69] C. Alden Mead. Molecular kramers degeneracy and non-abelian adiabatic phase factors. *Phys. Rev. Lett.*, 59:161–164, Jul 1987.

[70] Guido Meier, Markus Bolte, René Eiselt, Benjamin Krüger, Dong-Hyun Kim, and Peter Fischer. Direct imaging of stochastic domain-wall motion driven by nanosecond current pulses. *Phys. Rev. Lett.*, 98:187202, May 2007.

[71] I. M. Miron, P.-J. Zermatten, G. Gaudin, S. Auffret, B. Rodmacq, and A. Schuhl. Domain wall spin torquemeter. *Phys. Rev. Lett.*, 102:137202, Mar 2009.

[72] John Moody, A. Shapere, and Frank Wilczek. Realizations of magnetic-monopole gauge fields: Diatoms and spin precession. *Phys. Rev. Lett.*, 56:893–896, Mar 1986.

[73] O. Mosendz, J. E. Pearson, F. Y. Fradin, G. E. W. Bauer, S. D. Bader, and A. Hoffmann. Quantifying spin hall angles from spin pumping: Experiments and theory. *Phys. Rev. Lett.*, 104:046601, Jan 2010.

[74] A. Neubauer, C. Pfleiderer, B. Binz, A. Rosch, R. Ritz, P. G. Niklowitz, and P Böni. Topological hall effect in the a phase of mnsi. *Physical review letters*, 102(18):186602, 2009.

[75] F. Nolting, A. Scholl, J. Stöhr, Jin Won Seo, J. Fompeyrine, H. Siegwart, J. P. Locquet, S. Anders, J. Lüning, E. E. Fullerton, et al. Direct observation of the alignment of ferromagnetic spins by antiferromagnetic spins. *Nature*, 405(6788):767–769, 2000.

[76] Alvaro S. Núnez, R. A. Duine, Paul Haney, and A. H. MacDonald. Theory of spin torques and giant magnetoresistance in antiferromagnetic metals. *Physical Review B*, 73(21):214426, 2006.

[77] Katsunori Obata and Gen Tatara. Current-induced domain wall motion in rashba spin-orbit system. *Phys. Rev. B*, 77:214429, Jun 2008.

[78] R. C. Ohlmann. Dissertation: Antiferromagnetic resonance in fef2 infrared frequencies, university of california, june 1960.

[79] R. C. Ohlmann and M. Tinkham. Antiferromagnetic resonance in fef2 at far-infrared frequencies. *Physical Review*, 123(2):425, 1961.

[80] Lars Onsager. Reciprocal relations in irreversible processes. i. *Phys. Rev.*, 37:405–426, Feb 1931.

[81] Lars Onsager. Reciprocal relations in irreversible processes. ii. *Phys. Rev.*, 38:2265–2279, Dec 1931.

[82] N. Papanicolaou. Antiferromagnetic domain walls. *Phys. Rev. B*, 51:15062–15073, Jun 1995.

[83] N. Papanicolaou. Dynamics of domain walls in weak ferromagnets. *Phys. Rev. B*, 55:12290–12308, May 1997.

[84] B. G. Park, J. Wunderlich, X. Marti, V. Holỳ, Y. Kurosaki, M. Yamada, H. Yamamoto, A. Nishide, J. Hayakawa, H. Takahashi, et al. A spin-valve-like magnetoresistance of an antiferromagnet-based tunnel junction. *Nature materials*, 10(5):347–351, 2011.

[85] Frédéric Piéchon and André Thiaville. Spin transfer torque in continuous textures: Semiclassical boltzmann approach. *Phys. Rev. B*, 75:174414, May 2007.

[86] Alexander M. Polyakov et al. Gauge fields and strings. 1987.

[87] Marko Patrick John Punkkinen, K. Kokko, H. Levämäki, M. Ropo, Song Lu, Lorand Delczeg, HL Zhang, Erna Krisztina Delczeg-Czirjak, Börje Johansson, and Levente Vitos. Adhesion of the iron–chromium oxide interface from first-principles theory. *Journal of Physics: Condensed Matter*, 25(49):495501, 2013.

[88] D. C. Ralph and Mark D. Stiles. Spin transfer torques. *Journal of Magnetism and Magnetic Materials*, 320(7):1190–1216, 2008.

[89] Revaz Ramazashvili. Kramers degeneracy in a magnetic field and zeeman spin-orbit coupling in antiferromagnetic conductors. *Phys. Rev. Lett.*, 101:137202, Sep 2008.

[90] M .P. Ross. Dissertation: Spin dynamics in an antiferromagnet, technische universitat munchen, 2013.

[91] Subir Sachdev. *Quantum phase transitions*. Wiley Online Library, 2007.

[92] Hamed Ben Mohamed Saidaoui, Aurelien Manchon, and Xavier Waintal. Spin transfer torque in antiferromagnetic spin valves: From clean to disordered regimes. *Phys. Rev. B*, 89:174430, May 2014.

[93] C. W. Sandweg, Y. Kajiwara, A. V. Chumak, A. A. Serga, V. I. Vasyuchka, M. B. Jungfleisch, E. Saitoh, and B. Hillebrands. Spin pumping by parametrically excited exchange magnons. *Phys. Rev. Lett.*, 106:216601, May 2011.

[94] Takuya Satoh, Sung-Jin Cho, Ryugo Iida, Tsutomu Shimura, Kazuo Kuroda, Hiroaki Ueda, Yutaka Ueda, B. A. Ivanov, Franco Nori, and Manfred Fiebig. Spin oscillations in antiferromagnetic nio triggered by circularly polarized light. *Phys. Rev. Lett.*, 105:077402, Aug 2010.

[95] Norman L. Schryer and Laurence R. Walker. The motion of 180 domain walls in uniform dc magnetic fields. *Journal of Applied Physics*, 45(12):5406–5421, 2003.

[96] T. Schulz, R. Ritz, A. Bauer, M. Halder, M. Wagner, C. Franz, C. Pfleiderer, K. Everschor, M. Garst, and A. Rosch. Emergent electrodynamics of skyrmions in a chiral magnet. *Nature Physics*, 8(4):301–304, 2012.

[97] Yakov M Shnir. *Magnetic monopoles*. Springer, 2005.

[98] A. J. Sievers and M. Tinkham. Far infrared antiferromagnetic resonance in mno and nio. *Phys. Rev.*, 129:1566–1571, Feb 1963.

[99] John C. Slonczewski. Current-driven excitation of magnetic multilayers. *Journal of Magnetism and Magnetic Materials*, 159(1):L1–L7, 1996.

[100] Julian Sonner and David Tong. Scheme for building a 't hooft˘polyakov monopole. *Phys. Rev. Lett.*, 102:191801, May 2009.

[101] Ganesh Sundaram and Qian Niu. Wave-packet dynamics in slowly perturbed crystals: Gradient corrections and berry-phase effects. *Physical Review B*, 59(23):14915, 1999.

[102] A. C. Swaving and R. A. Duine. Current-induced torques in continuous antiferromagnetic textures. *Physical Review B*, 83(5):054428, 2011.

[103] A. C. Swaving and R. A. Duine. Influence of a transport current on a domain wall in an antiferromagnetic metal. *Journal of Physics: Condensed Matter*, 24(2):024223, 2012.

[104] Saburo Takahashi and Sadamichi Maekawa. Spin current in metals and superconductors. *Journal of the Physical Society of Japan*, 77(3):031009, 2008.

[105] Tomohiro Taniguchi, Jun Sato, and Hiroshi Imamura. Theory of spin accumulation and spin-transfer torque in a magnetic domain wall. *Phys. Rev. B*, 79:212410, Jun 2009.

[106] Gen Tatara and Peter Entel. Calculation of current-induced torque from spin continuity equation. *Phys. Rev. B*, 78:064429, Aug 2008.

[107] Gen Tatara and Hiroshi Kohno. Theory of current-driven domain wall motion: Spin transfer versus momentum transfer. *Phys. Rev. Lett.*, 92:086601, Feb 2004.

[108] A. Thiaville, Y. Nakatani, J. Miltat, and Y. Suzuki. Micromagnetic understanding of current-driven domain wall motion in patterned nanowires. *EPL (Europhysics Letters)*, 69(6):990, 2005.

[109] A. A. Thiele. Steady-state motion of magnetic domains. *Phys. Rev. Lett.*, 30:230–233, Feb 1973.

[110] D. J. Thouless. Quantization of particle transport. *Phys. Rev. B*, 27:6083–6087, May 1983.

[111] Yaroslav Tserkovnyak, Arne Brataas, and Gerrit E. W. Bauer. Enhanced gilbert damping in thin ferromagnetic films. *Phys. Rev. Lett.*, 88:117601, Feb 2002.

[112] Yaroslav Tserkovnyak, Arne Brataas, and Gerrit E. W. Bauer. Theory of current-driven magnetization dynamics in inhomogeneous ferromagnets. *Journal of Magnetism and Magnetic Materials*, 320(7):1282–1292, 2008.

[113] Yaroslav Tserkovnyak, Arne Brataas, Gerrit E. W. Bauer, and Bertrand I. Halperin. Nonlocal magnetization dynamics in ferromagnetic heterostructures. *Rev. Mod. Phys.*, 77:1375–1421, Dec 2005.

[114] Yaroslav Tserkovnyak, Hans Joakim Skadsem, Arne Brataas, and Gerrit E. W. Bauer. Current-induced magnetization dynamics in disordered itinerant ferromagnets. *Phys. Rev. B*, 74:144405, Oct 2006.

[115] Yaroslav Tserkovnyak and Clement H. Wong. Theory of spin magnetohydrodynamics. *Physical Review B*, 79(1):014402, 2009.

[116] M. Tsoi, A. G. M. Jansen, J. Bass, W.-C. Chiang, M. Seck, V. Tsoi, and P. Wyder. Excitation of a magnetic multilayer by an electric current. *Phys. Rev. Lett.*, 80:4281–4284, May 1998.

[117] M. Tsoi, A. G. M. Jansen, J. Bass, W.-C. Chiang, M. Seck, V. Tsoi, and P. Wyder. Excitation of a magnetic multilayer by an electric current. *Phys. Rev. Lett.*, 80:4281–4284, May 1998.

[118] M. Tsoi, V. Tsoi, J. Bass, A. G. M. Jansen, and P. Wyder. Current-driven resonances in magnetic multilayers. *Phys. Rev. Lett.*, 89:246803, Nov 2002.

[119] Alexei M. Tsvelik. *Quantum field theory in condensed matter physics*. Cambridge university press, 2006.

[120] Erlend G. Tveten, Alireza Qaiumzadeh, O. A. Tretiakov, and Arne Brataas. Staggered dynamics in antiferromagnets by collective coordinates. *Phys. Rev. Lett.*, 110:127208, Mar 2013.

[121] R. Y. Umetsu, M. Miyakawa, K. Fukamichi, and A. Sakuma. Pseudogap in the density of states and the highest néel temperature of the l10-type mnir alloy system. *Phys. Rev. B*, 69:104411, Mar 2004.

[122] Sergei Urazhdin and Nicholas Anthony. Effect of polarized current on the magnetic state of an antiferromagnet. *Physical review letters*, 99(4):046602, 2007.

[123] A. Vanhaverbeke and M. Viret. Simple model of current-induced spin torque in domain walls. *Phys. Rev. B*, 75:024411, Jan 2007.

[124] G. E. Volovik. Linear momentum in ferromagnets. *Journal of Physics C: Solid State Physics*, 20(7):L83, 1987.

[125] Xavier Waintal and Michel Viret. Current-induced distortion of a magnetic domain wall. *EPL (Europhysics Letters)*, 65(3):427, 2004.

[126] Y. Y. Wang, C. Song, B. Cui, G. Y. Wang, F. Zeng, and F. Pan. Room-temperature perpendicular exchange coupling and tunneling anisotropic magnetoresistance in an antiferromagnet-based tunnel junction. *Phys. Rev. Lett.*, 109:137201, Sep 2012.

[127] Roald K. Wangsness. Magnetic resonance in ferrimagnetics. *Phys. Rev.*, 93:68–71, Jan 1954.

[128] Z. Wei, A. Sharma, A. S. Nunez, P. M. Haney, R. A. Duine, J. Bass, A. H. MacDonald, and M. Tsoi. Changing exchange bias in spin valves with an electric current. *Physical review letters*, 98(11):116603, 2007.

[129] X. G. Wen and A. Zee. Spin waves and topological terms in the mean-field theory of two-dimensional ferromagnets and antiferromagnets. *Phys. Rev. Lett.*, 61:1025–1028, Aug 1988.

[130] S. Wienholdt, D. Hinzke, and U. Nowak. Thz switching of antiferromagnets and ferrimagnets. *Phys. Rev. Lett.*, 108:247207, Jun 2012.

[131] R. Wieser, E. Y. Vedmedenko, and R. Wiesendanger. Indirect control of antiferromagnetic domain walls with spin current. *Physical review letters*, 106(6):067204, 2011.

[132] Clement H. Wong and Yaroslav Tserkovnyak. Hydrodynamic theory of coupled current and magnetization dynamics in spin-textured ferromagnets. *Physical Review B*, 80(18):184411, 2009.

[133] Di Xiao, Ming-Che Chang, and Qian Niu. Berry phase effects on electronic properties. *Reviews of modern physics*, 82(3):1959, 2010.

[134] Jiang Xiao, A. Zangwill, and M. D. Stiles. Spin-transfer torque for continuously variable magnetization. *Phys. Rev. B*, 73:054428, Feb 2006.

[135] Yuan Xu, Shuai Wang, and Ke Xia. Spin-transfer torques in antiferromagnetic metals from first principles. *Physical review letters*, 100(22):226602, 2008.

[136] Y. Yamane, K. Sasage, T. An, K. Harii, J. Ohe, J. Ieda, S. E. Barnes, E. Saitoh, and S. Maekawa. Continuous generation of spinmotive force in a patterned ferromagnetic film. *Phys. Rev. Lett.*, 107:236602, Nov 2011.

[137] F. Y. Yang and C. L. Chien. Spiraling spin structure in an exchange-coupled antiferromagnetic layer. *Phys. Rev. Lett.*, 85:2597–2600, Sep 2000.

[138] Shengyuan A Yang, Geoffrey S Beach, Carl Knutson, Di Xiao, Qian Niu, Maxim Tsoi, and James L Erskine. Universal electromotive force

induced by domain wall motion. *Physical review letters*, 102(6):067201, 2009.

[139] Shengyuan A Yang, Geoffrey SD Beach, Carl Knutson, Di Xiao, Zhenyu Zhang, Maxim Tsoi, Qian Niu, AH MacDonald, and James L Erskine. Topological electromotive force from domain-wall dynamics in a ferromagnet. *Physical Review B*, 82(5):054410, 2010.

[140] Jinwu Ye, Yong Baek Kim, A. J. Millis, B. I. Shraiman, P. Majumdar, and Z. Tešanović. Berry phase theory of the anomalous hall effect: application to colossal magnetoresistance manganites. *Physical review letters*, 83(18):3737, 1999.

[141] Jiadong Zang, Maxim Mostovoy, Jung Hoon Han, and Naoto Nagaosa. Dynamics of skyrmion crystals in metallic thin films. *Phys. Rev. Lett.*, 107:136804, Sep 2011.

[142] Anthony Zee. *Quantum field theory in a nutshell*. Princeton university press, 2010.

[143] Qi Zhang and Biao Wu. General approach to quantum-classical hybrid systems and geometric forces. *Phys. Rev. Lett.*, 97:190401, Nov 2006.

[144] S. Zhang and Z. Li. Roles of nonequilibrium conduction electrons on the magnetization dynamics of ferromagnets. *Phys. Rev. Lett.*, 93:127204, Sep 2004.

[145] Shufeng Zhang and Steven S.-L. Zhang. Generalization of the landau-lifshitz-gilbert equation for conducting ferromagnets. *Phys. Rev. Lett.*, 102:086601, Feb 2009.

[146] F. Zhou, B. Spivak, and B. Altshuler. Mesoscopic mechanism of adiabatic charge transport. *Phys. Rev. Lett.*, 82:608–611, Jan 1999.

[147] Huan-Qiang Zhou, Sam Young Cho, and Ross H. McKenzie. Gauge fields, geometric phases, and quantum adiabatic pumps. *Phys. Rev. Lett.*, 91:186803, Oct 2003.

[148] Igor Žutić, Jaroslav Fabian, and S Das Sarma. Spintronics: Fundamentals and applications. *Reviews of modern physics*, 76(2):323, 2004.

[149] B. Zygelman. Non-abelian geometric phase and long-range atomic forces. *Phys. Rev. Lett.*, 64:256–259, Jan 1990.

Vita

Ran Cheng was born in Shenyang, China in 1985. He received the Bachelor of Science degree in Applied Physics in 2008 from the Huazhong University of Science and Technology (HUST), Wuhan, China. He started graduate studies specializing in condensed matter physics in the University of Texas at Austin in September, 2008.

Permanent address: (e-mail) crrcrrc@gmail.com

This dissertation was typeset with LaTeX[†] by the author.

[†]LaTeX is a document preparation system developed by Leslie Lamport as a special version of Donald Knuth's TeX Program.